LATVIJAS UNIVERSITĀTE

PROMOCIJAS DARBS

LATVIJAS UNIVERSITĀTE

ĶĪMIJAS FAKULTĀTE

Aina Semjonova

ORGANISKU VIELU POLIMORFISMA KONTROLE, IZMANTOJOT KRISTALIZĀCIJAS PIEDEVAS

PROMOCIJAS DARBS

Zinātnes doktora (Ph.D.) zinātniskā grāda iegūšanai
dabaszinātnēs (ķīmijas nozarē)

Apakšnozare: Fizikālā ķīmija

Darba vadītājs:
asoc. prof., *Dr. chem*. Agris Bērziņš

Promocijas darbs izstrādāts Latvijas Universitātes Ķīmijas fakultātes Fizikālās ķīmijas katedrā laika posmā no 2020. gada līdz 2023. gadam.

LATVIJAS UNIVERSITĀTE

NACIONĀLAIS ATTĪSTĪBAS PLĀNS 2020

EIROPAS SAVIENĪBA
Eiropas Sociālais fonds

I E G U L D Ī J U M S   T A V Ā   N Ā K O T N Ē

Darbs sastāv no kopsavilkuma latviešu un angļu valodā un no četrām zinātniskajām publikācijām. Darba forma: publikāciju kopa ķīmijā, fizikālās ķīmijas apakšnozarē.

Darba vadītājs: asoc. prof., *Dr. chem.* **Agris Bērziņš**

Darba recenzenti:
1) asoc. prof., *Dr. chem.* **Guntars Vaivars** (Latvijas Universitāte);
2) *Dr. chem.* **Raitis Bobrovs** (Latvijas Organiskās sintēzes institūts);
3) asoc. prof., *Dr. chem.* **Dejans-Krešimirs Bučars** (Londonas Universitātes koledža).

Promocijas darba aizstāvēšana notiks 2024. gada 12. septembrī, plkst. 16.00, Latvijas Universitātes Ķīmijas nozares promocijas padomes atklātā sēdē, Latvijas Universitātes Akadēmiskā centra Dabas mājā, 2017. auditorijā, Jelgavas ielā 1, Rīgā.

Ar promocijas darbu un tā kopsavilkumu var iepazīties Latvijas Universitātes bibliotēkā Rīgā, Raiņa bulvārī 19.

Latvijas Universitātes Ķīmijas zinātņu nozares promocijas padomes:

priekšsēdētājs: prof., *Dr. chem.* **Edgars Sūna**

sekretāre: asoc. prof., *Dr. chem.* **Vita Rudoviča**

ANOTĀCIJA

Promocijas darbā pētīta vairāku modeļvielu, 2,6-dimetoksibenzoskābes, 2,6-dimetoksifenil-borksābes un izonikotīnamīda, kristalizācija. Modeļvielas izvēlētas pamatojoties uz to spēju kristalizācijā veidot polimorfās formas ar dažādiem molekulārajiem sintoniem, t.i., dimēru un ķēžu struktūras. Izpētīta šo modeļvielu kristālisko fāžu daudzveidība, veicot modeļvielu kristalizāciju no dažādiem šķīdinātājiem ar dažādām kristalizācijas metodēm. Iegūtās kristāliskās fāzes raksturotas ar rentgendendifraktometriju un termiskās analīzes metodēm. Stabilākajām formām noteikta šķīdība un relatīvā stabilitāte. Veikta kristalizācija dažāda veida kristalizācijas piedevu – polimēru, virsmaktīvo vielu un strukturāli līdzīgu savienojumu – klātienē. Izpētīta kristalizācijas piedevu ietekme uz stabilāko polimorfo formu šķīdību un relatīvo stabilitāti. No pulvera un monokristāla rentgendifrakcijas datiem noteiktas kristāliskās struktūras četrām jaunām fāzēm. Veikta modeļvielu kristālisko struktūru ģeometrijas optimizācija un aprēķinātas to kristālrežģa enerģijas, kā arī veikta kristālrežģa enerģijas tīkla un asimetriskajā vienībā esošo molekulu Hiršfelda virsmu un iespējamo mijiedarbību analīze un morfoloģijas simulācijas, lai izskaidrotu iespējamo kristalizācijas piedevu ietekmi uz polimorfisma kontroles mehānismu.

Atslēgvārdi: polimorfisms, kristalizācija, kristalizācijas piedevas, kristāliskās struktūras analīze, pulvera rentgendifraktometrija, termiskā analīze.

Saturs / Content

APZĪMĒJUMU SARAKSTS

AA   etiķskābe;
BA   sviestskābe;
BFDH   Bravē–Fridela–Donneja–Harkera;
Btriol   benzola-1,2,3-triols;
CSD   Kembridžas struktūru datubāze;
CSP   kristālu struktūras prognozēšana;
DSC   diferenciali skenējošā kalorimetrija;
FA   skudrskābe;
FAM   formamīds;
FAV   farmaceitiski aktīvā viela
FIM   mijiedarbību karte;
INA   izonikotīnamīds;
IPA   izopropanols;
HPC   hidroksipropilceluloze;
MPBA   2,6-dimetoksifenilborskābe;
MD   molekulārā dinamika;
NA   nikotīnskābe;
ND   naftalin-1,5-diols;
OGP   oktil β-D-glukopiranozīds;
PA   propionskābe;
PEG   polietilēnglikols;
PhGlu   floroglucinols;
Poly80   polisorbāts 80;
PXRD   pulvera rentgendifrakcija;
SAM   pašorganizējošie monoslāņi;
SCXRD   monokristāla rentgendifrakcija;
SMPT   šķīdinātāja veicinātā fāžu pāreja;
Span 20   sorbitānlaurāts;
$S_{šķīdinātājs}$ solvāts;
TFE   2,2,2-trifluoroetanols;
TG   termogravimetrija;
THF   tetrahidrofurāns;
Tween 20   polisorbāts 20;
VAV   virsmaktīvās vielas;
2PA   2-pikolīnskābe;
4CPBA   4-karboksifenilborskābe;
5OH2NBA   5-hidroksi-2-nitrobenzoskābe;
2,6MeOBA   2,6-dimetoksibenzoskābe.

IEVADS

Liela daļa farmaceitiski aktīvo vielu (FAV) var kristalizēties dažādās kristāliskajās formās.[1] Kristāliskajai formai, kuru izmanto medikamentu ražošanā, ir jāatbilst references prasībām, tāpēc to kontrole ražošanas procesā ir obligāta prasība.[2] Tomēr samērā bieži kristalizācijā no šķīduma iegūst dažādu formu maisījumu,[3] kas tālāk var ietekmēt FAV šķīdību[4] un biopieejamību[5] vai citas fizikālās īpašības. Šāda nevēlama polimorfo formu maisījumu veidošanās ir novērota vairākām zāļu vielām.[3] Tāpat bieži ļoti līdzīgos apstākļos iespējams iegūt dažādas polimorfās formas,[6] kas negarantē selektivitāti kristalizācijā un nenodrošina atkārtojamību, līdz ar to nenodrošina industrijas prasību ievērošanu.

Farmaceitiskajā ražošanā lietošanai gatavajā zāļu formā drošāk ir izvēlēties stabilāko polimorfo formu, jo tai piemīt zemākā enerģija, līdz ar to tā būs stabila visos ražošanas posmos. Tomēr, ja vielas šķīdība ir zema, problēmas var sagādāt fakts, ka stabilākajai formai ir zemākā šķīdība. Šī iemesla dēļ reizēm gatavajā zāļu formā tiek lietota metastabilā forma, šādu izvēli balstot uz labāku šķīdību[7] vai dažkārt arī stabilākās formas patentaizsardzības dēļ.[8] Metastabilo formu iegūšanas procesā kā piemaisījums bieži veidojas termodinamiski stabilākā forma.[3] To ir praktiski neiespējami atdalīt vai pārvērst vajadzīgajā formā, turklāt šāds piemaisījums uzglabāšanas laikā var veicināt fāžu pāreju uz stabilāko formu.[6] Iepriekš minēto iemeslu dēļ ir nepieciešams optimizēt un kontrolēt kristalizācijas, ražošanas un gatavā produkta uzglabāšanas procesus.[9] Viens no kristalizācijas optimizācijas variantiem ir piedevu izmantošana.[10]

Kristalizācijas procesa kontrole, izmantojot kristalizācijas piedevas, arī mūsdienās joprojām ir empīriska metode.[10] Izmantojot pieejamos FAV molekulu iespējamo mijiedarbības aprēķinus, kā arī enerģijas izmaiņas konformācijas maiņas rezultātā, jau tagad, izmantojot kristāliskās struktūras prognozēšanas (CSP) metodi, ir iespējams paredzēt, kādas ir FAV visstabilākās kristāliskās struktūras. Tomēr pašlaik nav rīku, kas ļautu noteikt konkrētas kristāliskās formas iegūšanas iespējamību, jo īpaši, ja kristāliskās formas iznākums ir atkarīgs no kristalizācijas apstākļiem. Nav arī zināmas pieejas, lai novērtētu, kā kāda konkrēta piedeva izmainītu konkrētas polimorfās formas iegūšanas iespējamību. Šī iemesla dēļ katrai FAV ilgstošos eksperimentālos pētījumos tiek izstrādāta selektīva metode konkrētas kristāliskas formas iegūšanai.[11] Lai varētu izstrādāt piedevu kontrolētu konkrētas kristāliskās formas kristalizāciju, ir nepieciešama molekulāra līmeņa izpratne par kristalizācijas procesu un piedevas lomu tajā.[10] Lai gan šķīdumā esošie vielu asociāti dažkārt tiek saistīti ar iegūto polimorfo formu,[12] ir pierādīts, ka citos gadījumos tie neietekmē kristalizācijas iznākumu.[13] Zinātniskajā literatūrā ir atrodama informācija par piedevu (tādu kā Lengmīra monoslāņu[14] un pašorganizējošo monoslāņu (SAM)[15]) izmantošanu vairāku FAV un modeļa vielu

kristalizācijas procesa kontrolei,[16] bet bieži vien piedevas ir dārgas vai tās nav iespējams atdalīt no FAV kristāliem. Turklāt tās bieži vien nenodrošina vienas vēlamās polimorfās formas selektīvu kristalizāciju, bet tikai veicina tās veidošanos. Tā kā kristalizācijas polimorfo formu iznākumu noteicošie faktori ir sarežģīti un līdz galam neizprasti, pat mūsdienās teorētiskie aprēķini nesniedz skaidru pieeju, kā atrast izvēlētās kristāliskās formas kristalizācijas apstākļus. Tāpat nav skaidri zināmas molekulārās dinamikas (MD) pieejas simulāciju veikšanai, lai noteiktu kristālisko struktūru, kas veidotos kristalizācijā no šķīduma.

Promocijas darba mērķis ir iegūt izpratni par kristalizācijas iespējamo mehānismu piedevu klātienē, kuru varētu izmantot FAV kristalizācijā iegūtās polimorfās formas kontrolei. No šī mērķa izriet šādi darba **uzdevumi:**

1. Izpētīt modeļvielu 2,6-dimetoksibenzoskābes, 2,6-dimetoksifenilborskābes un izonikotīnamīda kristalizācijā iegūto polimorfo formu, izmantojot dažādas kristalizācijas metodes, apstākļus un šķīdinātājus;

2. Ar rentgendifrakcijas un termiskās analīzes metodēm raksturot iegūtās jaunās kristāliskās formas un noteikt to struktūru no monokristāla vai pulvera rentgendifrakcijas datiem;

3. Izpētīt dažādu veidu kristalizācijas piedevu ietekmi uz modeļvielu kristalizācijā iegūto polimorfo formu;

4. Identificēt piedevas, kas potenciāli spēj selektīvi ietekmēt modeļvielu kristalizācijā iegūto polimorfo formu, un veikt eksperimentus, lai novērtētu apstākļu un citu faktoru ietekmi uz kristalizācijā iegūto polimorfo formu šo piedevu klātbūtnē;

5. Noteikt izvēlētu piedevu ietekmi uz modeļvielu stabilāko polimorfo formu šķīdību un relatīvo termodinamisko stabilitāti;

6. Veikt iegūto fāžu kristālisko struktūru kristalogrāfisko analīzi un teorētiskos aprēķinus, lai noteiktu iespējamo kristalizācijas mehānismu piedevu klātbūtnē.

Zinātniskā novitāte un praktiskā nozīme

- Pētījuma laikā tika izstrādāta metode, kas kristalizācijas kontrolē ļauj izmantot izmaksu efektīvas kristalizācijas piedevas (SAM izmaksas var pārsniegt vairākus simtus eiro par katru laboratorijas mēroga kristalizācijas eksperimentu, turpretī šajā pētījumā izmantotās vielas maksā zem desmit eiro par gramu), kuras ir viegli atdalāmas vai kuras var iekļaut zāļu formās, piemēram, virsmaktīvās vielas un polimērus.

- Pētījumā iegūtas zināšanas par faktoriem, kas nodrošina selektīvu kristalizāciju, tostarp par piedevām, kas nodrošina kristalizācijā iegūtās polimorfās formas kontroli. Iegūtos

rezultātus var izmantot, izstrādājot vispārīgas vadlīnijas vai kristalizācijas procesa kontroles modeli.

- Kristalogrāfiskā analīze un teorētisko aprēķinu izmantošana sniedza informāciju par kristālisko formu atšķirībām, kas ļāva izskaidrot iespējamo kristalizācijā iegūtās polimorfās formas maiņas mehānismu, izmantojot kristalizācijas piedevas. Turklāt teorētisko aprēķinu un eksperimentālo rezultātu kombinācija veicināja izpratni par mijiedarbībām molekulārā līmenī, kas kopumā nosaka kristalizācijas rezultātu.

- Izstrādāto kristalizācijas kontroles metodi ir potenciāls izmantot farmācijas rūpniecībā, lai kontrolētu dažādu strukturāli līdzīgu FAV kristalizāciju, piemēram, FAV, kas atbilst mazmolekulārām benzoskābēm, kuras veido polimorfus, kuru struktūrā ietilpst ūdeņraža saišu dimēri un ķēdes – pētīto savienojumu veidotajiem līdzīgi ūdeņraža saišu motīvi.

PUBLICĒTIE REZULTĀTI

Publikācijas

1.   **Semjonova, A.**, Bērziņš, A. Controlling the Polymorphic Outcome of 2,6-Dimethoxybenzoic Acid Crystallization Using Additives. *Crystals,* **2022**, *12*, 1161. (IF$_{2022}$ = 2,67)

A. Semjonova izstrādāja 100% no eksperimentālā darba apjoma, sniedza ieguldījumu publikācijas rakstīšanā (80%), noformēja pētījuma rezultātus atbilstoši žurnāla prasībām, kā arī sagatavoja atbildes uz recenzentu jautājumiem un aizrādījumiem.

2.   **Semjonova, A.,** Bērziņš, A. Surfactant Provided Control of Crystallization Polymorphic Outcome and Stabilization of Metastable Polymorphs of 2,6-Dimethoxyphenylboronic Acid. *Crystals*, **2022**, *12*, 1738. (IF$_{2022}$ = 2,67)

A. Semjonova izstrādāja 100% no eksperimentālā darba apjoma, sniedza ieguldījumu publikācijas rakstīšanā (80%), noformēja pētījuma rezultātus atbilstoši žurnāla prasībām, kā arī sagatavoja atbildes uz recenzentu jautājumiem un aizrādījumiem.

3.   **Semjonova, A**., Bērziņš, A. Crystallization of metastable isonicotinamide polymorphs and preventing concomitant crystallization by additives. *Crystal Growth & Design,* **2023**, *23* (12), 8584-8596. (IF$_{2023}$ = 3,80)

A. Semjonova izstrādāja 100% no eksperimentālā darba apjoma, sniedza ieguldījumu publikācijas rakstīšanā (80%), noformēja pētījuma rezultātus atbilstoši žurnāla prasībām, kā arī sagatavoja atbildes uz recenzentu jautājumiem un aizrādījumiem.

4.   **Semjonova, A**., Kons, A., Belyakov, S., Mishnev, A., Bērziņš, A. Diversity and Similarity in Isonicotinamide Two-Component Phases with Alkyl Carboxylic Acids: Focus on Solvates. *Crystal Growth & Design,* **2024,** *24* (5), 2082-2093. (IF$_{2023}$ = 3,80)

A. Semjonova izstrādāja 90% no eksperimentālā darba apjoma, sniedza ieguldījumu publikācijas rakstīšanā (80%), noformēja pētījuma rezultātus atbilstoši žurnāla prasībām, kā arī sagatavoja atbildes uz recenzentu jautājumiem un aizrādījumiem.

Konferences

- **Semjonova, A.,** Kons, A., Belyakovs, S., Mishnev, A., Bērziņš, A. A New Solvates of Isonicotinamide and Alkyl Carboxylic Acids. *University of Latvia 82nd conference,* Rīga, Latvija, **2024.**

- **Semjonova, A.,** Bērziņš, A. Surfactant Provided Control of Crystallization Polymorphic Outcome and Stabilization of Metastable Polymorphs of 2,6-Dimethoxyphenylboronic Acid. *12th Bologna's convention on crystal forms*, Boloņa, Itālija, **2023.**

- **Semjonova, A.,** Bērziņš, A. Effect of structurally related additives on crystallization control of a highly polymorphous isonicotinamide. *BCA Spring meeting 2023*, Šefīlda, Apvienotā Karaliste, **2023**

- **Semjonova, A.,** Bērziņš, A. Controlling the polymorphic outcome of 2,6-dimethoxybenzoic acid crystallization using additives. *14th International Conference on Crystal Growth of Organic Materials*, Brisele, Beļģija, **2022.**

- **Semjonova, A.,** Bērziņš, A. Effect of crystallization additives on the crystallization of isonicotinicamide polymorphs. *14th International Conference on Crystal Growth of Organic Materials*, Brisele, Beļģija, **2022.**

- **Semjonova, A.,** Bērziņš, A. Effect of Crystallization Additives on Crystallization of 2,6-Dimethoxybenzoic Acid Polymorphs and Their Stability. *Understanding Crystallisation: Faraday Discussion*, Jorka, Apvienotā Karaliste (tiešsaiste), **2022.**

- **Semjonova, A.,** Bērziņš, A. Control possibilities of 2,6-dimetohxybenzoic acid conformational polymorphism using crystallization additives. *University of Latvia 80th conference,* Rīga, Latvija (tiešsaiste), **2022.**

- **Semjonova, A.,** Bērziņš, A. Polymorphic outcome control in crystallization and stabilization of metastable forms using surfactants. *Materials Science and Applied Chemistry 2021,* Rīga, Latvija (tiešsaiste), **2021.**

- **Semjonova, A.,** Bērziņš, A. Crystallization and stabilization of 2,6-dimethoxyphenylboronic acid metastable polymorph using surfactants. *EcoBalt 2021,* Rīga, Latvija (tiešsaiste), **2021.**

- **Semjonova, A.;** Bērziņš, A. Characterization of 2,6-Dimethoxybenzoic Acid Polymorphs and Crystallization Control Possibilities with Crystallization Additives. *11th Crystal Forms @Bologna: Walking the walk of polymorphs, co-crystals and solvates,* Boloņa, Itālija (tiešsaiste), **2021.**

- **Semjonova, A.**, Bērziņš, A. Screening of Crystallization Additives for Polymorph Control of 2,6-Dimethoxybenzoic Acid. *University of Latvia 79th conference,* Rīga, Latvija (tiešsaiste), **2021.**
- **Semjonova, A.**, Bērziņš, A. Influence of Crystallization Additives on Morphology of Selected Benzoic Acids – a Molecular Dynamics (MD) Simulation Study. The *2nd International Online Conference on Crystals,* tiešsaiste, **2020.**
- **Semjonova, A.**, Bērziņš, A. Influence of Crystallization Additives on Morphology of Selected Benzoic Acids – a Molecular Dynamics (MD) Simulation Study. *Materials Science and Applied Chemistry 2020,* Rīga, Latvija (tiešsaiste), **2020.**

Darbā neiekļautās publikācijas

- **Semjonova, A.**; Bērziņš, A. Influence of Crystallization Additives on Morphology of Selected Benzoic Acids – a Molecular Dynamics (MD) Simulation Study. *Key Engineering Materials*, **2021**, 903, 22-27.
- Bērziņš, A.; **Semjonova, A.**; Actiņš, A.; Salvalaglio, M. Speciation of substituted benzoic acids in solution: evaluation of spectroscopic and computational methods for the identification of associates and their role in crystallization. *Crystal Growth & Design*, **2021**, 21, 9, 4823–4836.

1. LITERATŪRAS APSKATS

1.1. Farmaceitiski aktīvo vielu polimorfisms

Polimorfisms ir vielu spēja kristalizēties dažādās kristāliskajās struktūrās (skat. 1.1. att.).[9] Polimorfi ir kristāliskās struktūras ar identisku ķīmisko sastāvu, taču dažādu molekulu pakojumu vai konformāciju. Solvātu struktūra sastāv no neitrālas vielas molekulām ar stehiometrisku vai mainīgu šķīdinātāja daudzumu. Hidrāti ir solvātu apakšveids, kuru kristālrežģī iekļautais šķīdinātājs ir ūdens. Kokristāli turpretī sastāv no divām vai vairāk neitrālām molekulām stehiometriskās attiecībās, bet sāļi sastāv no divām jonizētām molekulām.[17] Cietvielām ar dažādām kristāliskajām struktūrām var piemist dažādas fizikālās īpašības, piemēram, šķīdība,[4] šķīšanas ātrums,[18] stabilitāte[19] un biopieejamība.[20] Šo iemeslu dēļ kristālinženierija paver jaunas iespējas iegūt FAV ar labākām fizikālām īpašībām.[21] Solvātiem un kokristāliem var piemist labāka šķīdība un šķīšanas ātrums nekā tīrām FAV polimorfajām formām, kā rezultātā var uzlabot medikamentu biopieejamību un efektivitāti,[22] radīt sinerģētisku efektu un samazināt nepieciešamo medikamenta devu,[21] vai arī iegūt kristālisko struktūru ar ražošanas procesam piemērotākām īpašībām.[23] Papildu tam, izmaiņas kristāliskajā struktūrā var uzlabot FAV ķīmisko stabilitāti.[24]
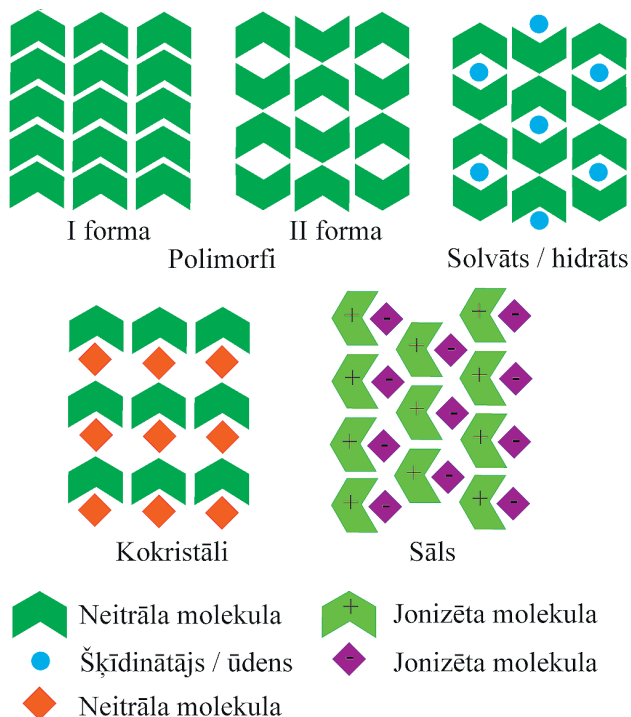
1.1. att. **Shematisks farmaceitiski aktīvo vielu veidoto dažādu fāžu attēlojums.**

Balstoties uz polimorfu kristāliskās struktūru atšķirībām, polimorfismu var iedalīt:[25]

- konformācijas polimorfismā – polimorfajās formās atšķiras molekulu konformācija;[26,27]

- sintonu jeb ūdeņraža saišu polimorfisms – polimorfo formu struktūrās ir atšķirīgi ūdeņraža saišu sintoni;[25,28]
- konfigurācijas polimorfisms – piemīt vielām, kuru dažādās konfigurācijas vai tautomēri spēj veidot dažādas kristāliskās struktūras;[25]
- pakojuma polimorfisms – polimorfajās formās molekulu konformācija ir vienāda, bet atšķiras to pakojums.[29]

Kristālisko fāžu kontrole ir viens no izaicinošākajiem soļiem zāļu ražošanas procesā farmācijas industrijā.[30] Pirms gatavās zāļu formas attīstīšanas ir svarīgi apzināt visas iespējamās kristāliskās formas un raksturot to īpašības, jo zāļu formas izvēle, nepieciešamās palīgvielas un pašas FAV deva ir atkarīga no kristāliskās formas fizikālajām īpašībām.[31]

Vienlaicīga kristalizācija ir vismaz divu dažādas struktūras polimorfu vienlaicīga veidošanās kristalizācijā.[32] Šī parādība ir novērojama dažādu polimorfo formu konkurējošas nukleācijas un augšanas ātrumu dēļ.[33] Vienlaicīga kristalizācija ir saistīta ar dažādiem kinētiskiem un termodinamiskiem faktoriem.[34] Visbiežāk vairāku formu maisījumu pakļaujot šķīdinātāja veicinātai fāžu pārejai (SMPT) gala produktā novēro tikai stabilāko formu.[3] Turklāt ir jāpārbauda izvēlētās kristāliskās fāzes stabilitāte ilgstošas uzglabāšanas laikā. Vēsturiski ir bijuši vairāki gadījumi,[35] kuros jauns, stabilāks polimorfs ir atklāts vairākus gadus pēc medikamenta izstrādes, un tas ir radījis dažādas problēmas pacientiem, sākot no zemākas medikamenta efektivitātes līdz par medikamenta izņemšanai no tirgus.[36]

Pie klasiskajām kristālisko fāžu kontroles metodēm pieder šķīduma atdzesēšana, ietvaicēšana, izgulsnēšana, tvaika difūzija, piesēšana u.c. Kristalizācijā iegūtā fāze ir atkarīga no izmantotā šķīdinātāja, atdzesēšanas vai ietvaicēšanas ātruma, atdzesēšanas sākuma un beigu temperatūrām, šķīduma koncentrācijas (vielas pārsātinājuma) un citiem faktoriem.[9] Diemžēl klasiskās kristalizācijas metodes ne vienmēr spēj nodrošināt tīras polimorfās formas iegūšanu. Šādos gadījumos piesēšana ir visizplatītākā pieeja, lai nodrošinātu iegūtā polimorfa kontroli, taču arī tā ne vienmēr nodrošina vēlamās kristāliskās formas veidošanos. Alternatīvi iespējams izmantot arī citas kristalizācijas metodes: kristalizācija ar ultraskaņas palīdzību,[37] lāzera ierosinātā nukleācija,[38] kristalizācija gelos[39] vai kristalizācija piedevu[16] un templātu[40] klātbūtnē.

1.2. Kristalizācijas piedevu izmantošana polimorfisma kontrolei

Kristalizācijas piedevu vai templātu izmantošana ir empīriska metode, kuru var izmantot polimorfisma kontrolei. Pastāv vairāki veidi kristalizācijas piedevu izmantošanai:[41]
- kristalizācija, izmantojot nešķīstošas piedevas vai templātus:
  - Lengmīra monoslāņus (*Langmuir monolayers)*;[14]

- o pašorganizējošos monoslāņus (*self-assambled monolayers,* SAM);[15]
- o polimērus;[42]
- o nešķīstošu savienojumu virsmas kā templātus;[43]
- kristalizācija, izmantojot šķīstošas piedevas.[44]

Lengmīra monoslāņi un SAM ir efektīvi templāti kristalizācijā iegūtā polimorfa kontrolei, taču katras kristāliskās struktūras iegūšanai tos nepieciešams speciāli dizainēt, pēc katras kristalizācijas tos ir nepieciešams reģenerēt, kā arī ne vienmēr iegūtos kristālus var attīrīt no SAM materiāla piemaisījumiem.[45] Šķīstošas piedevas var būt dažāda veida savienojumi: gan strukturāli līdzīgi kristalizējamajam savienojumam, gan arī atšķirīgi. Homogēnās piedevas ir vienkāršāk atdalīt no kristāliem, taču tās var integrēties kristāla struktūrā.[46] Strukturāli līdzīgas piedevas ir izmantotas, piemēram, lai iegūtu paracetamola,[11] *para*-aminobenzoskābes,[47] benzamīda,[48] u.c. savienojumu metastabilās formas. Taču strukturāli līdzīgām piedevām var būt arī farmakoloģiska vai toksiska iedarbība, turklāt līdzīgās struktūras dēļ tās var iekļauties iegūtajos kristālos, piemēram, veidojot cieto šķīdumu.[49] Līdz ar to ne visas strukturāli līdzīgas piedevas var izmantot, lai stabilizētu farmaceitisko preparātu polimorfās formas. Kā kristalizācijas piedevas var izmantot arī farmācijā atļautās zāļu formu palīgvielas,[44] jo šādas palīgvielas nebūtu nepieciešams atdalīt no iegūtas FAV, jo potenciālie zāļu vielas piemaisījumi ir atļauti izmantošanai zāļu formā, piemēram, polimēri un VAV.[50]

Kristalizācijas piedevu izmantošana var novērst vienlaicīgu polimorfo formu kristalizāciju, stabilizēt metastabilās formas,[51] veicināt to nukleāciju,[46] mainīt polimorfu relatīvo stabilitāti[52] vai novērst stabilās formas nukleāciju. Kristalizāciju piedevu klātienē plaši izmanto dabas un rūpniecības procesos, sākot no biomineralizācijas līdz materiālu sintēzei.[53]

Pastāv vairākas teorijas par kristalizācijas piedevu iespējamo mehānismu, ļaujot tām nodrošināt polimorfisma kontroli, piemēram:

- piedevas var darboties kā nukleācijas centri;[10]
- piedevas var selektīvi adsorbēties uz konkrētām kristāla plaknēm, inhibējot šo kristālu un arī attiecīgi šī polimorfa augšanu;[54]
- piedevas var orientēt kristalizējamo vielu noteiktā veidā, ļaujot iegūt vēlamo polimorfu;[55]
- piedevas var pazemināt nukleācijas aktivācijas enerģiju.[34]

Tomēr precīzs piedevu kontroles mehānisms vairumā gadījumu joprojām nav zināms.

1.3. Kristalogrāfiskā analīze un teorētiskie aprēķini

Mūsdienās kristālisko struktūru salīdzināšanai un kristalizācijas iznākuma pamatošanai ir pieejami un tiek izmantoti dažāda veida kristalogrāfiskās analīzes rīki un teorētiskie aprēķini.

Konformeru stabilitāte ietekmē polimorfu stabilitāti kā arī nosaka to, kādā konformācijā molekulas pastāv šķīdumā, tāpēc ir nepieciešams noteikt, kuri ir stabilākie konformēri, un kādā ir kristāliskajās struktūrās ietilpstošo konformēru stabilitāte. Konformēru stabilitātes noteikšanai nepieciešams veikt atsevišķu molekulu ģeometrijas optimizāciju un enerģijas aprēķinu vakuumā vai nepārtrauktā šķīdinātāja vidē. Pamatā mūsdienās to veic ar kādu no blīvuma funkcionāļu teorijas metodēm vai elektronu korelācijas *ab initio* metodēm, kurās izmanto kvantu mehānikas pieeju.[56]

Ne mazāk būtisks faktors, kas ietekmē polimorfu stabilitāti, ir kristāliskajā struktūrā esošās starpmolekulārās mijiedarbības.[57–59] Šim aprēķinam nepieciešams veikt periodiskās kristāliskās struktūras ģeometrijas optimizāciju, ko mūsdienās iespējams veikt ar blīvuma funkcionāļu teorijas metodēm. Tālāk aprēķinot mijiedarbības enerģiju starp struktūrā esošajām molekulām iespējams noteikt kopējo starpmolekulāro mijiedarbību enerģiju, kam izmanto vai nu empīriskas,[60] pusempīriskas[61,62] vai *ab initio*[63] metodes. Polimorfu stabilitāti raksturojošo kristālrežģa enerģiju iespējams aprēķināt vai nu summējot kopējo starpmolekulāro mijiedarbību enerģiju un relatīvo konformēru enerģiju, vai vienkārši kā starpību starp kristāliskās struktūras enerģiju un izolētu globālajam enerģijas minimumam atbilstošas ģeometrijas molekulu enerģiju gāzes fāzē. Jāņem gan vērā, ka kristālrežģa enerģija neiekļauj termisko efektu ietekmi un līdz ar to sniedz informāciju par polimorfu relatīvo stabilitāti 0 K temperatūrā.[64]

Kristālisko struktūru salīdzināšanai tiek izmantoti tādi rīki kā enerģētiskie tīkli (*energy frameworks*), Hiršfelda virsmas un to 2D pirkstu nospiedumu grafiki un mijiedarbības kartes (skat. 1.2.att.).
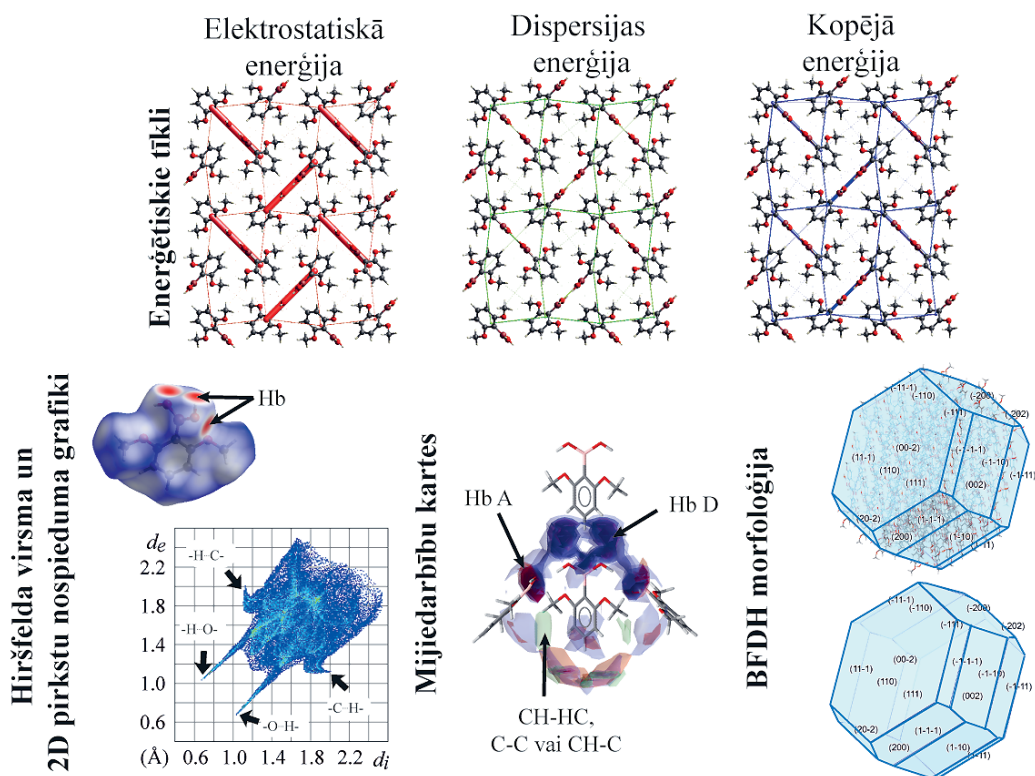
1.2. att. **Kristogrāfisko analīžu metožu grafisks atspoguļojums. Hb – ūdeņraža saite; Hb A – ūdeņraža saites akceptors; Hb D – ūdeņraža saites donors.**

Enerģētiskie tīkli vizualizē starpmolekulāro mijiedarbību enerģiju polimorfu kristāliskajās struktūrās, papildus demonstrējot kristālrežģa enerģijas sadalījumu starp dažādiem enerģijas ieguldījumiem (elektrostatiskā, dispersijas un kopējā).[65] Hiršfelda virsmas sniedz informāciju par starpmolekulārajām mijiedarbībām un elektronu blīvumu struktūrā, ļaujot labāk izprast atšķirības struktūrās esošajās ūdeņraža saitēs un citās mijiedarbībās, kā arī pakojumā.[66,67] Hiršfelda virsmu 2D pirkstu nospiedumu grafiki sniedz dziļāku ieskatu par mijiedarbībām kristāliskajā struktūrā un konkrētu mijiedarbību veidu ieguldījumu.

Mijiedarbības kartes (*full-interaction maps*, FIM) vizualizē reģionus ap molekulu, kuros, pamatojoties uz programmā *IsoStar* iepriekš iegūtiem starpmolekulāro mijiedarbību datiem Kembridžas struktūru datubāzē (*Cambridge Structural Database,* CSD) ietilpstošajās struktūrās,[68] ir sagaidāma starpmolekulārā mijiedarbība, ļaujot novērtēt, vai struktūrā ir izpildītas mijiedarbības preferences. Pierādīts, ka FIM analīze ļauj novērtēt polimorfu stabilitāti.[69,70]

Daudzas kristālu fizikālās īpašības ir atkarīgas no to morfoloģijas. Pastāv vairāki modeļi kristāla morfoloģijas prognozēšanai, bet visbiežāk izmantotais ir **B**ravē-**F**rīdela-**D**onnaja-**H**arkera (BFDH) modelis, jo, salīdzinājumā ar citiem modeļiem, morfoloģijas noteikšana pēc tā ir vieglāk īstenojama. Šis modelis izmanto apgriezti proporcionālu sakarību starp starpplakņu attālumu un augšanas ātrumu, taču neņem vērā kinētiskos faktorus un šķīdinātāja vai piedevu lomu kristāla augšanā.[71] Tā kā var pieņemt, ka, ja struktūrā ir apgabali, kuros, balstoties uz

FIM, nav apmierinātas starpmolekulārās mijiedarbības, tad piedevu nodrošinātās papildu mijiedarbības var stabilizēt attiecīgo polimorfu. Tomēr šāds efekts var parādīties tikai uz kristālu virsmas, līdz ar to tiek izmantotas uz BFDH morfoloģijas projicētas FIM. Neraugoties uz minēto BFDH modeļa neprecizitāti, FIM analīze apvienojumā ar BFDH morfoloģiju var paredzēt potenciālās piedevu molekulu adsorbcijas vietas.[68]

1.4. Pētītās sistēmas

Promocijas darbā tika pētītas trīs modeļvielas: 2,6-dimetoksibenzoskābe (2,6MeOBA), 2,6-dimetoksifenilborskābe (MPBA) un izonikotīnamīds (INA) (skat. 1.3. att.).
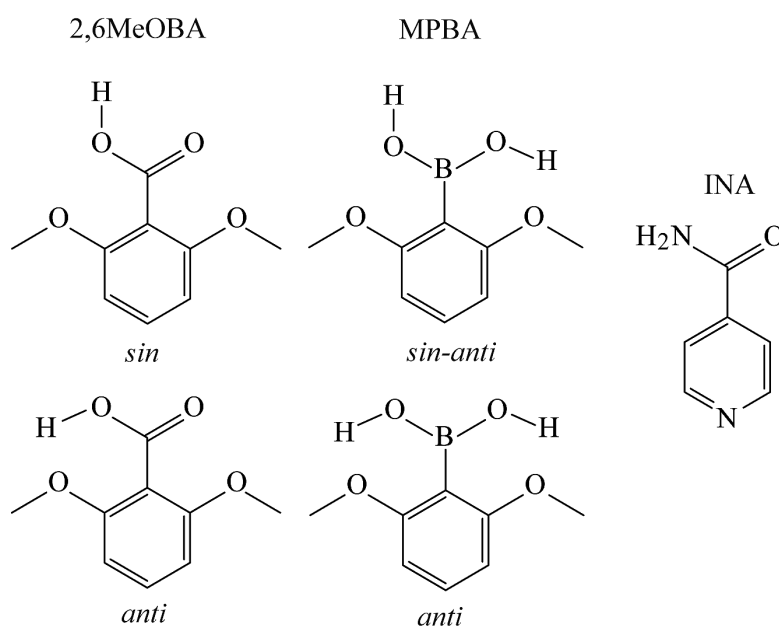
1.3. att. **Promocijas darbā izmantoto modeļvielu struktūrformulas un to konformācijas.**

Visām trim modeļvielām CSD ir publicētas vismaz divu polimorfu kristāliskās struktūras, kurās veidojas dažādi molekulārie sintoni (dimēri un ķēdes, shematisku sintonu atšķirību skat. 1.4. att.). Modeļvielu izvēle veikta balstoties tieši uz spēju veidot polimorfus ar atšķirīgiem molekulārajiem sintoniem, jo, pieņemot, ka kontroles mehānismā būtiska loma varētu būt starpmolekulārajām mijiedarbībām, secināts, ka kristalizācijā piedevu klātienē lielākas iespējas būs kontrolēt tādu polimorfu kristalizāciju, kuros molekulārie sintoni ir atšķirīgi.

Dimēri   Ķēdes
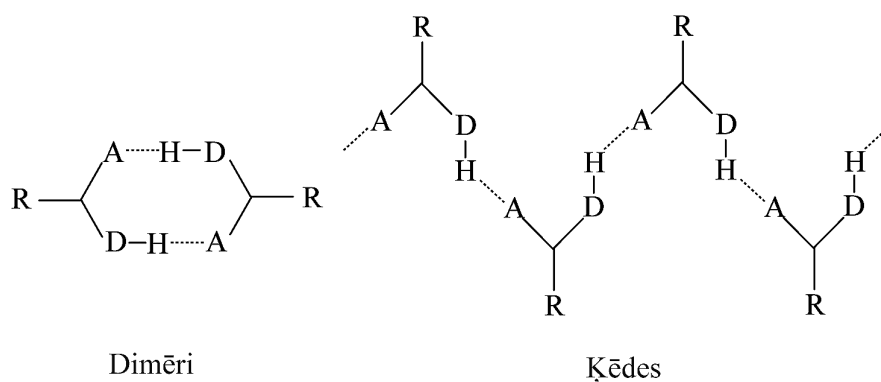
1.4.att. **Visu modeļvielu kristāliskajās struktūrās novēroto dimēru un ķēžu molekulāro sintonu shematisks attēlojums. A – ūdeņraža saites akceptors; D – ūdeņraža saites donors.**

Zināms, ka 2,6MeOBA kristalizējas trīs polimorfo formu veidā,[26,72–74] no kurām termodinamiski stabilākā ir I forma.[26,74] Tajā 2,6MeOBA molekulas ieņem *anti*-planāru konformāciju, un ir saistītas ar ūdeņraža saišu ķēdēm, veidojot katemērus.[72,75] Turpretī II un III formā 2,6MeOBA molekulas ieņem *syn*-planāru konformāciju un veido karbonskābju homodimērus.[26,73,74] Iepriekšējos pētījumos II formas iegūšana veikta kristalizācijas piedevas fenilborskābes klātienē.[73]

MPBA kristalizējas divās polimorfajās formās.[76] Termodinamiski stabilākā no tām ir I forma. Tās struktūra satur borskābes homodimērus un borskābe ieņem *syn-anti*-konformāciju. Turpretī II forma satur netipisku ar ūdeņraža saitēm saistītu sintonu, ko veido trīs MPBA molekulas.

INA veido sešas polimorfās formas,[77–80] divus monohidrātus[81] un dažus solvātus: etiķskābes,[28] skudrskābes,[82] propionskābes[83] un formamīda[84] solvātus. Termodinamiski stabilākā forma normālos apstākļos ir I forma,[77,79] kas satur amīda grupas veidotus homodimērus.[78] Turpretī visas pārējās INA polimorfās formas satur dažādu INA ķēžu sintonus, kas veidojas no amīda grupas un piridīna slāpekļa atoma veidotajām ūdeņraža saitē.[77–80] Lai gan literatūrā ir pieejami pētījumi par INA polimorfo formu kontroli, izmantojot kristalizācijas piedevas, šajos pētījumos nav izdevies panākt selektīvu un atkārtojamu polimorfo formu kontroli.[43,79,80]

2. EKSPERIMENTĀLĀ DAĻA

Kristālisko fāžu raksturošana un struktūru noteikšana

Fāžu identifikācija veikta ar *Bruker D8 Advance* pulvera rentgendifraktometru (PXRD) ar 1D pozīcijas jutīgo *LynxEye* detektoru, izmantojot vara anoda (Cu K$_\alpha$) rentgenstarojumu. Paraugi analizēti iepresēti stikla kivetēs. Rentgendifraktogrammas uzņemtas 2θ intervālā no 3° līdz 35°, izmantojot skenēšanas ātrumu 0,2 s / 0,02°. Lai novērstu INA solvātu desolvatāciju, analīzes laikā paraugi tika pārklāti ar 10 μm polietilēna plēvi. Polimorfo formu kvantificēšana tika ar Ritvelda metodi programmā Profex 4.3.6.

Pulvera rentgendifraktogrammas kristāliskās struktūras noteikšanai uzņemtas ar *Bruker D8 Discover* pulvera rentgendifraktometru ar 1D pozīcijas jutīgo *LynxEye* detektoru, izmantojot caustarojošo ģeometriju un vara anoda (Cu K$_\alpha$) rentgenstarojumu. Paraugi analizēti, ievietojot tos borosilikāta stikla kapilārā ar iekšējo diametru 0,5 mm (Hilgenberga stikls Nr. 10), kapilāru aizkausējot un ievietot goniometra statīvā un uzņemšanas laikā rotējot ar ātrumu 60 apgr./min. Rengendifraktogrammas uzņemtas 2θ intervālā no 3° līdz 70° , izmantojot skenēšanas ātrumu 36 s / 0,01. Indeksēšana, telpiskās grupas noteikšana un kristāliskās struktūras noteikšana no iegūtajām rentgendifraktogrammām veikta datorprogrammā *EXPO2014*. Labākajam struktūras modelim veikta Ritvelda optimizācija datorprogrammā *TOPAS5*.

Kristālisko struktūru noteikšana no monokristālu paraugiem tika veikta, difraktogrammas uzņemot ar *Rigaku XtaLAB Synergy-S dualflex* difraktometru (SCXRD) ar *HyPix6000* detektoru, izmantojot vara anoda (Cu K$_\alpha$) rentgenstarojumu. Monokristāli analizēti, nofiksējot tos ar eļļu magnētiskā *CryoCap* neilona cilpā, kas novietota uz goniometra galviņas. Struktūru noteikšana veikta ar datorprogrammā *ShelXT*, un optimizācija tika veikta datorprogrammu *SHELXL*, izmantojot mazāko kvadrātu metodi. (analīzes veiktas Latvijas Organiskās sintēzes institūtā, Rīgā, Latvijā)

Jaunisegūto kristālisko fāžu analīze un solvātu stehiometrijas noteikšana veikta, izmantojot diferenciāli skenējošās kalorimetrijas/termogravimetrijas (DSC/TG) analīzi ar iekārtu *Mettler Toledo TGA/DSC2*. Paraugi karsēti no 25 līdz 200 °C slāpekļa atmosfērā ar karsēšanas ātrumu 10 °C min^{-1}. Paraugu DSC analīze veikta ar kalorimetru *TA DSC 25*. Paraugi karsēti no 25 līdz 200 °C slāpekļa atmosfērā ar karsēšanas ātrumu 10 °C·min^{-1} vai 2 °C·min^{-1}.

Šķīdinātāja un kristalizācijas piedevu izvēle

Dzesēšanas un ietvaicēšanas kristalizācijai izvēlēti plaši lietoti organiskie šķīdinātāji no dažādām šķīdinātāju klasēm. Papildus INA kristalizācijai izvēlētas arī alkilkarbonskābes un daži citi netipiski šķīdinātāji, jo iepriekš veiktos pētījumos ir iegūti INA etiķskābes solvāts (S_{AA}) un propionskābes disolvāts (S_{dPA}). Pēc kristalizācijas rezultātu izvērtēšanas, tālākiem pētījumiem, lai novērtētu pārsātinājuma un atdzesēšanas ātruma ietekmi uz kristalizācijā iegūto polimorfo formu, tika izvēlēti daži šķīdinātāji. Šķīdinātāji tika izvēlēti pēc sekojošiem kritērijiem:

- Modeļvielas šķīdība tajā ir starp 5 un 50 mg mL^{-1};
- Ir iespējams iegūt vēlamo metastabilo polimorfu kopā ar stabilās formas piemaisījumu (2,6MeOBA);
- Ir iespējams iegūt tika stabilo polimorfo formu (MPBA);
- Kristalizācijā vienlaicīgi veidojās vairāku polimorfo formu maisījums (INA).

Tad dažos no šķīdinātājiem tika pētīts dažādu kristalizāciajss piedevu ietekme uz kristalizācijā iegūto polimorfo formu. Kā kristalizācijas piedevas tika izvēlētas VAV, polimēri un dažādi molekulārie savienojumi ar spēju veidot dažādas starpmolekulārās mijiedarbības. No pētītajām piedevām tālākiem detalizētiem pētījumiem tika atlasītas tikai dažas piedevas, kuras uzrādīja augstāko potenciālu veicināt metastabilās formas kristalizāciju (2,6MeOBA un MPBA) vai novērst vienlaicīgu kristalizāciju un veicināt metastabilā polimorfa kristalizāciju (INA).

Kristalizācijas eksperimenti

Kristalizācijas un fāžu pārejas eksperimenti šķīdinātāja klātienē (SMPT) kontrolētos apstākļos, kā arī šķīdības noteikšana veikta ar automātiskās kristalizācijas iekārtu *Technobis Crystal16*. Eksperimentiem tika izmantots temperatūru intervāls no 5 līdz 100°, karsēšanas un dzesēšanas ātrums no 0,1 līdz 20 °C min^{-1} un maisīšanas ātrumu no 0 līdz 1250 apgriez./min.

Teorētiskie aprēķini

CSD analīze un struktūru meklēšana tika veikta ar ConQuest 2022.2.0., izmantojot CSD versiju 5.43. Kristālisko struktūru ģeometrijas optimizācija tika veikta programmā Quantum Espresso 6.4.1, bet molekulu ģeometrijas optimizācija programmā Gaussian09 Revision D.01. Pēc ģeometrijas optimizācijas augstākā struktūras simetrija tika noteikta, izmantojot ISOCIF rīku (versija 3.1.0). Kristālrežģa enerģijas aprēķināšana un Hiršfelda virsmu un to 2D pirkstu nospiedumu karšu iegūšana tika veikta programmā CrystalExplorer21. Ūdeņraža saišu identifikācija, pilnās mijiedarbības karšu (FIM) iegūšana un kristāla morfoloģijas simulācija

pēc Bravē–Fridela–Donneja–Harkera (BFDH) metodes tika veikta programmā Mercury2020.3.0. Polimorfu molekulārā pakojuma salīdzināšana tika veikta CrystalCMP programmā, izmantojot CSD datubāzē ievietotās kristāliskās struktūras. Šķīdības temperatūras atkarība tika aprakstīta ar van't Hofa vienādojumu, izmantojot lineārās regresijas analīzi Microsoft Excel Linest funkcijā.

3. REZULTĀTI UN DISKUSIJA

3.1. Kristalizācija no tīriem šķīdinātājiem

Pirmais, ko nepieciešams noteikt, ir kāda katra modeļvielas polimorfā forma tiek iegūta, izmantojot dažādas kristalizācijas metodes un pētījumam izvēlētos šķīdinātājus. Katrai modeļvielai tika veikts plašs polimorfo formu skrīnings, veicot atdzesēšanas un ietvaicēšanas kristalizāciju dažādās temperatūrās no dažādiem šķīdinātājiem. Katrai modeļvielai kristalizācijā izmantotie šķīdinātāji tika izvēlēti balstoties uz iepriekš kristalizācijā iegūtajām fāzēm, vielas šķīdību un šķīdinātāju pieejamību laboratorijā.

Lielākajā daļā veikto 2,6MeOBA atdzesēšanas kristalizāciju tika iegūta I forma, lai gan dažkārt novēroja arī III formas piemaisījumus (skat. 3.1. tab.). Ietvaicēšanas kristalizācijas eksperimentos bija novērojama korelācija starp iegūto polimorfo formu un temperatūru: zemākā temperatūrā (5 °C) lielākajā daļā eksperimentu tika iegūta I forma, bieži ar nelielu III formas piemaisījumu, bet augstākā temperatūrā (50 °C) tika iegūta III forma ar I formas piemaisījumiem.

Turpretī, gandrīz visās MPBA kristalizācijās, īpaši no aprotoniem šķīdinātājiem, tika iegūta tīra I forma (skat. 3.1. tab.). Savukārt no polāriem protoniem šķīdinātājiem (izopropanola (IPA), metanola un izobutanola) bija iespējams iegūt metastabilo MPBA II formu. Papildus jau zināmajiem polimorfiem tika iegūts jauns MPBA polimorfs (III forma). Tā kristalizējās kopā ar II formu ietvaicēšanas kristalizācijā no izopropanola un heptanola. Diemžēl mēģinājumi noteikt III formas kristālisko struktūru bija neveiksmīgi, jo netika iegūti piemēroti kristāli SCXRD analīzei, bet pulvera paraugs saturēja II formas piemaisījumu (skat. 3.1. att.).

INA kristalizācijas rezultāti pilnībā atšķīrās no pārējo divu modeļvielu kristalizācijas rezultātiem (skat. 3.1. tab.). Lielākajā daļā apstākļu iegūtajos kristalizācijas produktos bija sastopami vairākas INA polimorfās formas, kas saskan ar citos pētījumos iegūtajiem rezultātiem.[80,85] Parasti II un VI forma vai II un IV forma kristalizējās kopā, bet no dažiem šķīdinātājiem tika iegūts visu šo trīs formu maisījums. Turklāt, lai gan ir noteikts, ka I forma ir termodinamiski stabilākais polimorfs,[77,79,85] kristalizācijā I forma tika iegūta reti, savukārt II forma (stabilākā forma augstākās temperatūrās) bija visbiežāk iegūtais kristalizācijas produkts. Kristalizācijā no etiķskābes (AA) un formamīda (FAM), tika iegūti jau zināmie INA solvāti.[28,84] Turklāt atdzesēšanas kristalizācijā no skudrskābes (FA), propionskābes (PA), sviestskābes (BA) un 2,2,2-trifluoretanola (TFE) tika iegūti kristalizācijas produkti ar atšķirīgām PXRD ainām (skat. 3.1. att.), kas neatbilst jau zināmajiem INA polimorfiem vai solvātiem. Iegūtās jaunās fāzes analizēja ar DSC/TG kā arī noteica to struktūru. Iegūtie rezultāti

liecina, ka šīs formas ir solvāti (skat. 3.2. nodaļu). Visām modeļvielām jauniegūtās kristāliskās formas 3.1. tabulā ir atzīmētas ar zvaigznīti.
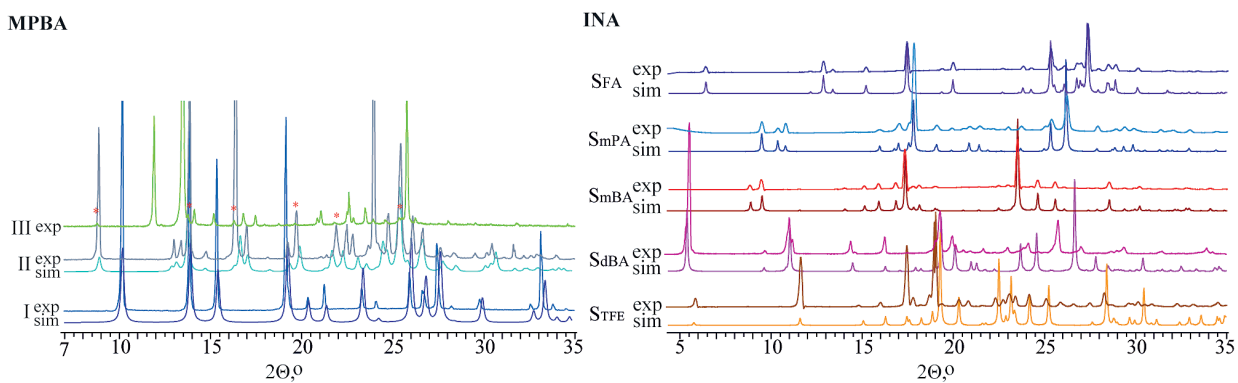
3.1. attēls. **MPBA polimorfu un INA solvātu eksperimentālās un no kristāliskajām struktūrām simulētās PXRD ainas. MPBA II formas piemaisījums III formas paraugā ir atzīmēts ar sarkanām zvaigznītēm.**

Tālākiem detalizētākiem atdzesēšanas ātruma ietekmes uz kristalizācija iegūto polimorfo formu pētījumiem tika izvēlēti daži šķīdinātāji:

- Ūdens (2,6MeOBA);
- Toluols (MPBA);
- IPA, 1,4-dioksāns, nitrometāns, acetons (INA).

Kopsavilkums par modeļvielu kristalizācijā no tīriem šķīdinātājiem iegūto polimorfo formu.

Šķīdinātājs	Atdzesēšana 2,6MeOBA	Atdzesēšana MPBA	Atdzesēšana INA	Ietvaicēšana 5 °C 2,6MeOBA	Ietvaicēšana 25 °C 2,6MeOBA	Ietvaicēšana 25 °C MPBA	Ietvaicēšana 25 °C INA	Ietvaicēšana 50 °C 2,6MeOBA	Ietvaicēšana 50 °C MPBA	Ietvaicēšana 50 °C INA
1,4-Dioksāns	I + III↓	I	III	III	I + III	I	II + VI	III	I	II
Metanols	I + III↓	II	II + IV	III	I↓ + II + III	II	II + IV + VI	I	I	II + IV
Acetons	I	I	I	I + III	I	I	II + IV + VI	III	I	II + IV + VI
Tetrahidrofurāns (THF)	I	I	II + VI	I + III	I + III	I	II + III	I↓ + III	I	II + IV + VI
Izopropanols (IPA)	I	I	II + IV + III + VI	I	I + III↓	II + III	III	III	I + II	II + III
Acetonitrils	I	I	II + IV + VI	I + III↓	I + III	I	I + II + IV	I / III	I	II + IV
4-Metil-2-pentanons	I	I	II + VI	I	I + III↓	I	II + IV	I + III	I	II + IV
Metilacetāts	I	N/A	N/A	I + III↓	I + III	N/A	N/A	I↓ + III	N/A	N/A
terc-Butilmetilēteris	I	I	II + VI	I	I	I	IV + VI	I + III	I	IV + VI
Ūdens	I	I	N/A	I	I	I	N/A	I	I + II	N/A
Toluols	I	I	N/A	N/A	I + III	I	N/A	N/A	I	N/A
Hloroforms	I	I	II + IV	N/A	I + III↓	I	II + IV + VI	N/A	I	IV + VI
Dihlorometāns	I + III↓	I	N/A	N/A	I + III↓	I	N/A	N/A	I	N/A
Etilacetāts	I	I	N/A	N/A	I	I	N/A	N/A	I	N/A
Skudrskābe (FA)	I	N/A	S_{FA}	N/A	I	N/A	N/A	N/A	N/A	N/A
Nitrometāns	I	I	II + IV	N/A	I	I	II + IV	N/A	I	II + IV
o-Ksilols	N/A	I	N/A	N/A	N/A	I	N/A	N/A	I	N/A
Dietilkarbonāts	N/A	I	II + IV + VI	N/A	N/A	I	II + IV + VI	N/A	I	II + IV + VI
Cikloheksanols	N/A	I	N/A	N/A	N/A	I	N/A	N/A	I	N/A
2,2,2-Trifluoroetanols (TFE)	N/A	I	S_{TFE}*	N/A	N/A	I	N/A	N/A	I + II	N/A
Heptanols	N/A	I	N/A	N/A	N/A	II + III	N/A	N/A	I	N/A
Izopentanols	N/A	I	N/A	N/A	N/A	I + II	N/A	N/A	I	N/A
n-Butilacetāts	N/A	N/A	II + IV	N/A	N/A	N/A	IV + VI	N/A	N/A	II + IV + VI
Etiķskābe (AA)	N/A	N/A	S_{AA}	N/A	N/A	N/A	N/A	N/A	N/A	N/A
Formamīds (FAM)	N/A	N/A	S_{FAM}	N/A	N/A	N/A	N/A	N/A	N/A	N/A
Propionskābe (PA)	N/A	N/A	S_{mPA}* (5 °C); S_{dlPA} (-10 °C)	N/A	N/A	N/A	N/A	N/A	N/A	N/A
Sviestskābe (BA)	N/A	N/A	S_{dlBA}*	N/A	N/A	N/A	N/A	N/A	N/A	N/A

Atkārtota 2,6MeOBA kristalizācija no tīra ūdens ar tūlītēju parauga nofiltrēšanu un iegūto kristālu analīze apstiprināja, ka kristalizācijā veidojas I un III formas maisījums, kam gadījumā, ja kristāli paliek ilgstoši šķīdumā, seko fāžu pāreja šķīdinātāja klātienē (SMPT) par I formu. Šī iemesla dēļ iepriekšējos kristalizācijas eksperimentos tika novērota tikai I forma. Kristalizējot no koncentrēta ūdens šķīduma ar vislielāko dzesēšanas ātrumu ieguva visu trīs polimorfo formu maisījumu (skat. 3.2. att.), savukārt visos paraugos ar vismazāko dzesēšanas ātrumu veidojās III forma, par spīti tam, ka pie mazākā dzesēšanas ātruma bija sagaidāma termodinamiski stabilākās I formas veidošanās. Šajos eksperimentos fāžu pāreju uz I formu novērsa tas, ka kristāli veidojās tuvu ūdens virsmai lielu aglomerātu veidā. Turpretī MPBA kristalizācijā no toluola dzesēšanas ātrums neietekmēja iegūto polimorfo formu, un vienmēr tika iegūta I forma.

INA kristalizācijas eksperimentos, izmantojot dažādu dzesēšanas ātrumu, tika iegūta atšķirīga polimorfā forma. Tīra III forma tika iegūta no 1,4-dioksāna, izmantojot vislielāko dzesēšanas ātrumu, bet dzesēšanas ātruma samazināšana veicināja stabilāku formu (II un VI) veidošanos.[85] Kristalizācijā no IPA izmantojot vislielāko dzesēšanas ātrumu tika iegūti dažādi III formu saturoši polimorfo formu maisījumi, bet eksperimentos ar mazāku dzesēšanas ātrumu tika iegūtas stabilākas formas. Turpretī III forma veidošanos no nitrometāna vai acetona nenovēroja.

Kopumā šie rezultāti, izņemot MPBA iegūtos, saskan ar Ostvalda stadiju likumu:[86] tā vietā, lai veidotos stabilākās formas kristālu aizmetņi, veidojas tās polimorfās formas aizmetņi, kuras enerģija ir tuvākā.
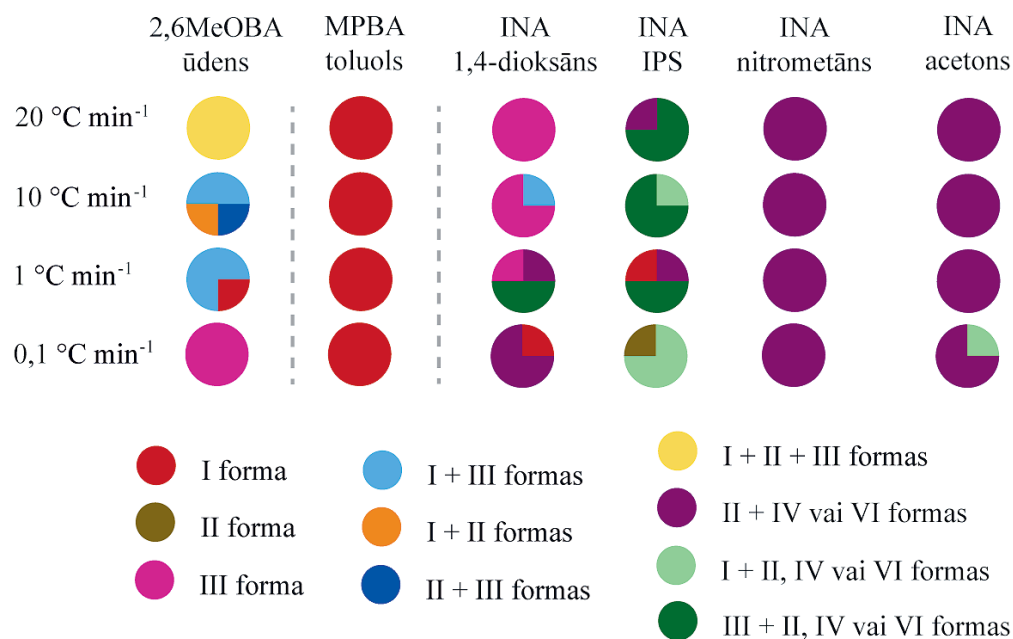
3.2. att. **Kristalizācijā iegūtā polimorfā forma, izmantojot dažādus dzesēšanas ātrumus un maisīšanas ātrumu 900 apgriez./min. Katra ¼ no sektoru diagrammas atspoguļo vienu paralēlo eksperimentu.**

3.2. Izonikotīnamīda solvātu daudzveidība un līdzība

Šajā pētījumā tika iegūti četri jauni INA solvāti: PA monosolvāts (S_{mPA}); BA monosolvāts (S_{mBA}) un disolvāts (S_{dBA}); TFE solvāts (S_{TFE}). Tāpat tika iegūti un analizēti arī FA solvāts (S_{FA}),[82] FAM solvāts (S_{FAM}), AA solvāts (S_{AA}) un PA disolvāts (S_{dPA}). Bez tam tika noteikta arī S_{FA} kristāliskā struktūra, jo tā nav pieejama CSD. Glabājot laboratorijas temperatūrā, visi solvāti desolvatējās, veidojot INA II, IV un VI formu maisījumu. Visi INA solvāti kristalizējas vai nu monoklīnā vai triklīnā singonijā, skat. 3.2. tabulu.
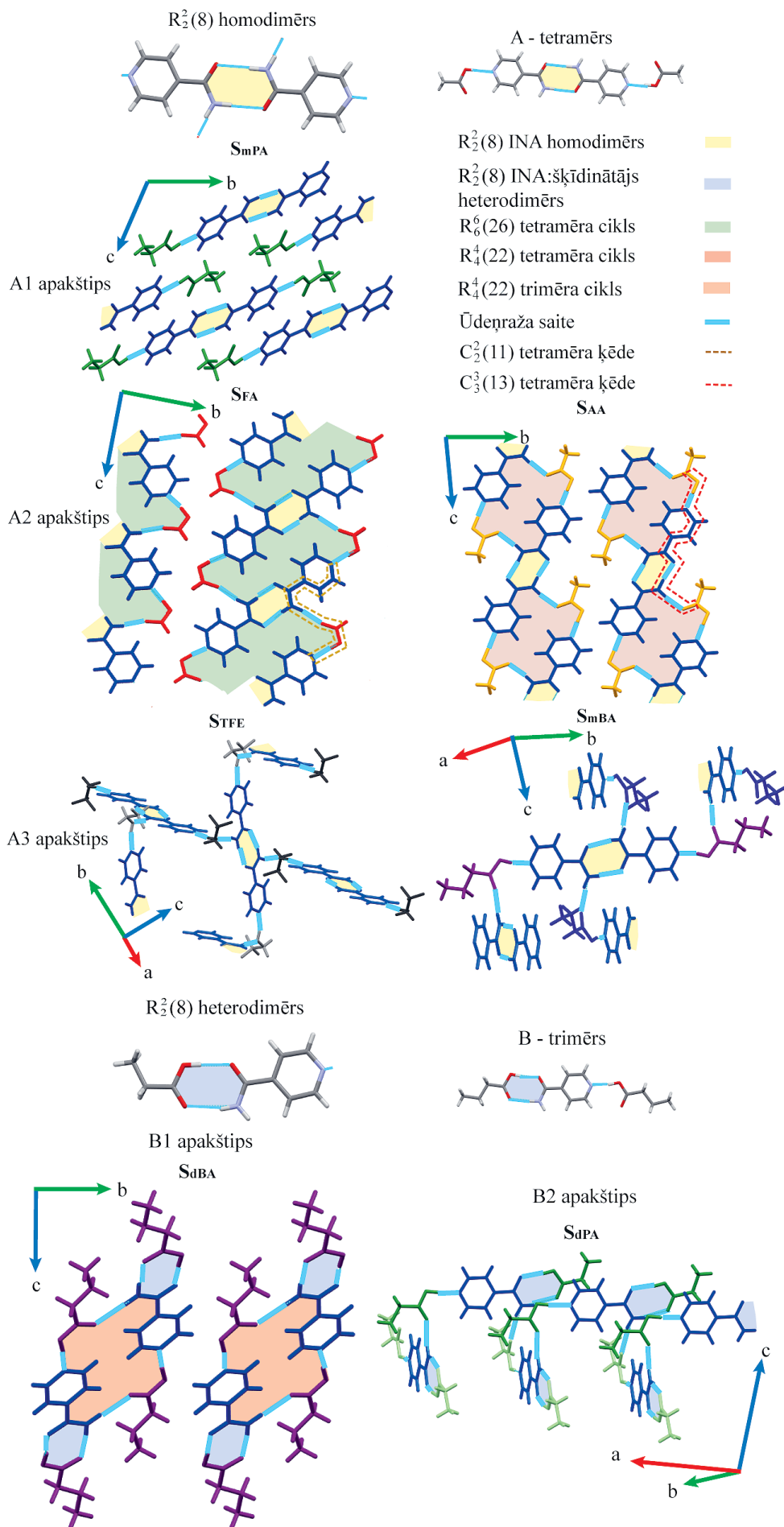
3.2. tabula

Pētījumā noteiktie INA solvātu kristalogrāfiskie dati

	S_{FA}	S_{mPA}	S_{mBA}	S_{dBA}	S_{TFE}
CSD identifikators	2236716	2236717	2236718	2302845	2237737
Formula	$C_6H_6N_2O \cdot CH_2O_2$	$C_6H_6N_2O \cdot C_3H_6O_2$	$C_6H_6N_2O \cdot C_4H_8O_2$	$C_6H_6N_2O \cdot 2C_4H_8O_2$	$C_6H_6N_2O \cdot C_2H_3F_3O$
Struktūras noteikšanas metode	Pulveris	Pulveris	Pulveris	Mono-kristāls	Mono-kristāls
Telpiskā grupa	*P2$_1$/c*	*P$\bar{1}$*	*C2/c*	*P$\bar{1}$*	*P2$_1$/c*
a, Å	3,8177(16)	5,88988	21,806(15)	5,24839(10)	15,2031(9)
b, Å	27,480(11)	9,685489	10,505(7)	9,28144(13)	5,3244(12)
c, Å	7,565(3)	10,19433	11,190(8)	16,3015(3)	11,7225(7)
α, grādi	90	112,4861	90	89,7515(12)	90
β, grādi	95,1158(12)	93,0070	114,2902(17)	89,8978(14)	91,303(6)
γ, grādi	90	105,726	90	80,7138(14)	90

INA solvātos var novērot divus atšķirīgus ūdeņraža saišu motīvu tipus, kurus, balstoties uz papildus ūdeņraža saitēm un to izvietojuma, var iedalīt piecos apakštipos. Pirmais ūdeņraža saites motīvs satur tipiskus INA $R_2^2(8)$ homodimērus (skat. 3.4. att.), kas ar šķīdinātāja molekulām veido tetramēru šķīdinātājs····INA dimērs····šķīdinātājs. S_{mPA} struktūrā ietilpst izolēti tetramēri, kas klasificēti kā A1 apakštips. Citu solvātu struktūrās novērojamas ūdeņraža saites starp tetramēriem šķīdinātājs·····INA dimērs···šķīdinātājs. Ja šādi saistītie tetramēri atrodas vienā plaknē, kā novēro S_{FA} un S_{AA}, tos klasificē A2 apakštipā, bet, ja saistītie tetramēri atrodas perpendikulāri viens otram, veidojot perpendikulāru molekulāro pakojumu, kā novēro S_{mBA} un arī S_{TFE}, tad tos klasificē A3 apakštipā. A2 apakštipa (S_{FA} un S_{AA}) tetramēri ir savstarpēji paralēli un veido tetramēru slāņus. Turklāt INA un šķīdinātāja molekulu atšķirīgā relatīvā novietojuma dēļ tetramēros FA····INA dimērs····FA fragmenti ir saistīti ar $C_2^2(11)$ ķēdēm, veidojot $R_6^6(26)$ ciklus, bet AA···INA dimērs···AA fragmenti saistās ar $C_3^3(13)$ ķēdēm,

veidojot $R_4^4(22)$ ciklus. A3 apakštipam piederošajos S_{TFE} un S_{mBA} katrs tetramērs ir saistīts ar gandrīz perpendikulāri novietotiem blakus esošiem tetramēriem.

Otrā veida jeb B tipa motīvi ir būtiski atšķirīgi, jo tos neveido INA $R_2^2(8)$ homodimēri. Abos B apakštipos INA veido $R_2^2(8)$ heterodimēru ar karbonskābi (skat. 3.4. att.), un šis dimērs veido ūdeņraža saiti ar citu šķīdinātāja molekulu, veidojot trimēru šķīdinātājs····INA:šķīdinātājs. B1 apakštipa solvāta S_{dBA} gadījumā šķīdinātājs····INA:šķīdinātājs trimērs ir saistīts ar ūdeņraža saitēm ar blakus esošu caur simetrijas centru saistītu trimēru, un veido $R_4^4(22)$ ciklu. Savukārt B2 apakštipa struktūrā S_{dPA} trimēri ar ūdeņraža saitēm ir saistīti ar diviem citiem perpendikulāri novietotiem trimēriem, tādējādi veidojot līdzīgu pakojumu, kāds novērots A3 apakštipa struktūrās.

$R_2^2(8)$ homodimērs

A - tetramērs

S_{mPA}

A1 apakštips

S_{FA}

A2 apakštips

S_{TFE}

A3 apakštips

$R_2^2(8)$ INA homodimērs

$R_2^2(8)$ INA:šķīdinātājs heterodimērs

$R_6^6(26)$ tetramēra cikls

$R_4^4(22)$ tetramēra cikls

$R_4^4(22)$ trimēra cikls

Ūdeņraža saite

$C_2^2(11)$ tetramēra ķēde

$C_3^3(13)$ tetramēra ķēde

S_{AA}

S_{mBA}

$R_2^2(8)$ heterodimērs

B - trimērs

B1 apakštips

S_{dBA}

B2 apakštips

S_{dPA}

3.4. att. **A un B tipa INA solvātos novērotās ūdeņraža saites.**

Ūdeņraža saišu motīvi S$_{FAM}$ atšķiras no citiem INA solvātiem (skat. 3.5. att.). Šajā struktūrā INA un FAM veido divus dažādus $R_2^2(8)$ homodimērus, kas savstarpēji saistīti ar ūdeņraža saitēm. Rezultātā veidojas molekulārais pakojums, kurā FAM homodimēri savieno INA molekulu slāni.

R$_2^2$(8) INA homodimēri   R$_2^2$(8) FAM homodimēri
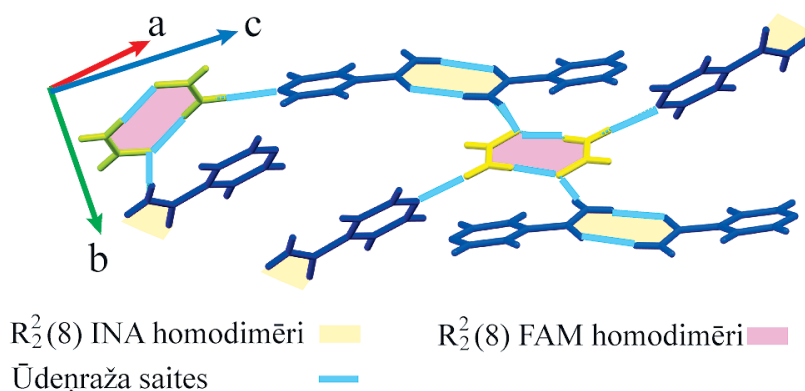
Ūdeņraža saites

3.5. att. **Ūdeņraža saites S$_{FAM}$.**

Kopumā visos INA solvātos novēro līdzīgus ūdeņraža saišu motīvus. Analizēto struktūru kopas paplašināšana, iekļaujot arī INA kokristālus (detalizēti rezultāti un to apraksts dots IV publikācijā), ļāva secināt, ka gandrīz visi INA alkilkarbonskābju solvāti un kokristāli kristalizējas struktūrās ar ļoti līdzīgiem ūdeņraža saišu motīviem, kas varētu ļaut prognozēt starpmolekulārās mijiedarbības un molekulāro pakojumu jauniem INA solvātiem/kokristāliem ar strukturāli līdzīgiem šķīdinātājiem/koformēriem.

3.3. Kristalizācija piedevu klātbūtnē

Kristalizācijas iznākumu piedevu klātbūtnē ietekmē sarežģītas un ne pilnībā raksturotas mijiedarbības starp kristalizējamo savienojumu, šķīdinātāju un piedevām, kā arī kristalizācijas apstākļi (piemēram, pārsātinājums, dzesēšanas un maisīšanas ātrumu). Iegūto polimorfo formu var izmainīt, mainot jebkuru no šiem aspektiem. Šajā pētījumā tika pētīta kristalizācija piedevu klātbūtnē, mainot kristalizācijas apstākļus, lai labāk izprastu piedevas lomu uz kristalizācijā iegūto polimorfo formu.

Šie pētījumi ir iepriekš aprakstīto eksperimentu turpinājums, un to mērķis ir noteikt, kuras piedevas ļautu kristalizācijā iegūt metastabilo polimorfo formu. Līdz ar to katrai modeļvielai tika pārbaudīti vismaz divi šķīdinātāji, kas tika izvēlēti balstoties uz iepriekšējiem kristalizācijas eksperimentiem, un vairāk nekā 10 piedevas ar iespējām veidot dažādas starpmolekulārās mijiedarbības (skatīt 3.3. tabulu).

Kopsavilkums par katrai modeļvielai izmantotajām kristalizācijas piedevām un šķīdinātāju.

Kristalizācijas piedeva	2,6MeOBA			MPBA		INA	
	THF	acetonitrils	ūdens	toluols	ūdens	1,4-dioksāns	IPA
Polietilēnglikols (PEG) 6000	√	√	√	√	√	√	√
Hidroksipropilceluloze (HPC)			√	√	√	√	
MPBA			√				
Oktil β-D-glukopiranozīds (OGP)	√	√	√	√	√	√	√
Polisorbāts 80 (Poly80)	√	√	√	√		√	√
Sorbitāna laurāts (Span 20); Polisorbāts 20 (Tween 20)	√	√		√		√	√
4-Karboksifenilborskābe (4CPBA)			√		√	√	√
2-Pikolīnskābe (2PA)				√		√	√
Naftalin-1,5-diols (ND)						√	√
Benzola-1,2,3-triols (Btriol)					√	√	√
1,3,5-Trihidroksibenzols (PhGlu); Nikotīnskābe (NA); 5-Hidroksi-2-nitrobenzoskābe (5OH2NBA).						√	√
Polikaprolaktons	√	√				√	√
Polivinilhlorīds	√	√				√	
Bis(2-hidroksietil)amino-tris(hidroksimetil)metāns			√		√	√	√
trans-Stilbēns				√		√	√
Poli(tetrahidrofurāns), Polipropilēnglikols				√		√	√
4-Jodfenilborskābe; Glicīns; NH$_4$Cl; Poli(akrilskābe); Poli(akrilamīds); Nātrija karboksimetilceluloze			√		√		
Celulozes acetāts			√			√	
Poli(metil metakrilāts)				√		√	
2,6MeOBA, Fenilborskābe				√	√		
PEG 200; Poliuretāns; 1,3-Difenilurea						√	√
Hidroksipropilmetilceluloze; Mikrokristāliskā celuloze			√				
PEG 600; Salicilskābe; Polietāns; Polistirols; 2-Hidroksifenilborskābe;				√			
Laktoze					√		
2-amino-2-(hidroksimetil) propān-1,3-diols							√

Plašākiem pētījumiem izvēlētās piedevas un šķīdinātāji, kā arī piedevas ietekme uz kristalizācijā iegūto polimorfo formu ir apkopota 3.4. tabulā, bet katrai modeļvielai izvēlēto piedevu molekulārās struktūras ir parādītas 3.6. attēlā.

Plašākiem pētījumiem izvēlētās piedevas, šķīdinātāji un kristalizācijas metode, kā arī piedevas ietekme uz kristalizācijā iegūto polimorfo formu.

	2,6MeOBA	MPBA	INA			
Šķīdinātājs	ūdens	toluols	IPA	1,4-dioksāns	nitrometāns	acetons
Kristalizācijas metode	atdzesēšana	ietvaicēšana	atdzesēšana			
Piedevas	PEG 6000, HPC, MPBA	OGP, Poly80, Span 20, Tween 20	4CPBA, 2PA, ND, Btriol, PhGlu, NA, 5OH2NBA	4CPBA, 2PA, ND		
Polimorfo formu iznākums	↑ III formu	II forma	↑ III forma	↑ III forma; ↓ polimorfo formu maisījumus	-	
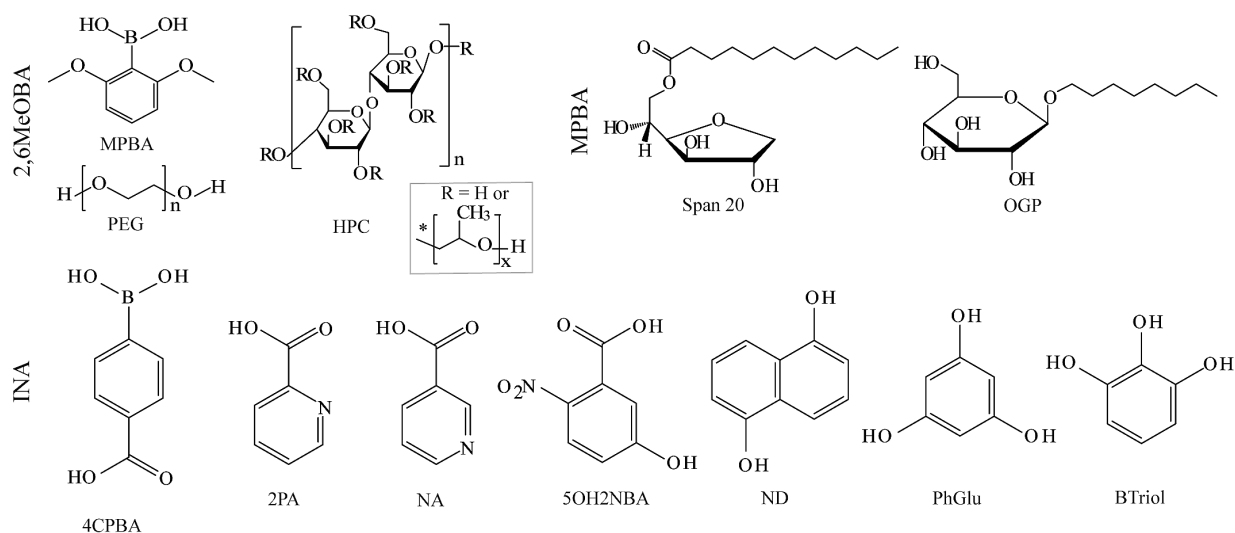
3.6. att. **Katrai modeļvielai izvēlēto piedevu molekulārās struktūrformulas.**

Detalizēti kristalizācijas eksperimenti, kas veikti piedevu klātbūtnē, tika izvēlēti, pamatojoties uz iegūtajiem rezultātiem, līdz ar ko katrai no modeļvielām tie bija atšķirīgi:

- Kristalizācija, izmantojot dažādu dzesēšanas ātrumu (2,6MeOBA, INA);
- Kristalizācija, izmantojot dažādu piedevu daudzumu (2,6MeOBA);
- Dažādu kristalizācijas metožu un šķīdinātāja izmantošana (MPBA);
- Kristalizācija, izmantojot dažādu maisīšanas ātrumu (INA).

3.3.1. 2,6-dimetoksibenzoskābes kristalizācijā iegūtā polimorfā forma

Kā piedevas izmantojot PEG un MPBA (skat. 3.7. att.), lielākajā daļā eksperimentu tika iegūts I un III formas maisījums. Turpretī, kā piedevu izmantojot HPC divās dažādās piedevu koncentrācijās, visbiežāk kristalizējās tīra III forma. Liels dzesēšanas ātrums veicināja III formas veidošanos. Pie vismazākā dzesēšanas ātruma piedevas veicināja I formas kristalizāciju. 0,5% HPC suspensijas izmantošana un 2,6MeOBA šķīdums ar mazu koncentrāciju (pārsātinājums apzīmēts kā c/c^*, kur c ir sākotnējā koncentrācija un c^* ir šķīdība 25 °C temperatūrā) III formas kristalizāciju veicināja vairāk, ja salīdzina ar kristalizāciju no 0,1% HPC šķīduma ar lielāku 2,6MeOBA koncentrāciju. Iespējams, ka šajā no apstākļiem notiekošajā heterogēnajā kristalizācijā vairāk HPC molekulu var mijiedarboties ar 2,6MeOBA molekulām un nukleācijas laikā stabilizēt *sin*-planāro konformāciju, kas kopumā ir līdzīgi Lin et al. pētījumā iegūtajiem rezultātiem.[87] Arī PEG ir potenciāls kontrolēt kristalizācijas iznākumu, izmantojot vidēju dzesēšanas ātrumu un augstu 2,6MeOBA koncentrāciju. Tomēr, pārbaudītās piedevas nenodrošina pilnīgi selektīvu kristalizāciju. Lai pārbaudītu piedevas daudzuma ietekmi uz kristalizācijas rezultātu, turpmākai izpētei tika izvēlēta kristalizācija PEG klātbūtnē ar dzesēšanas ātrumu 20 un 1°C min⁻¹ un HPC klātbūtnē ar dzesēšanas ātrumu 20 un 10 °C min⁻¹.
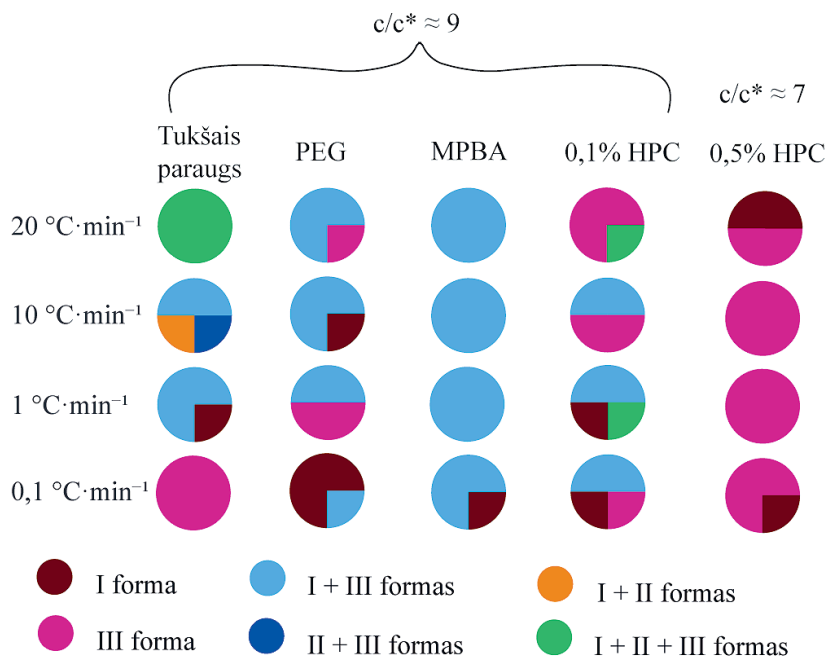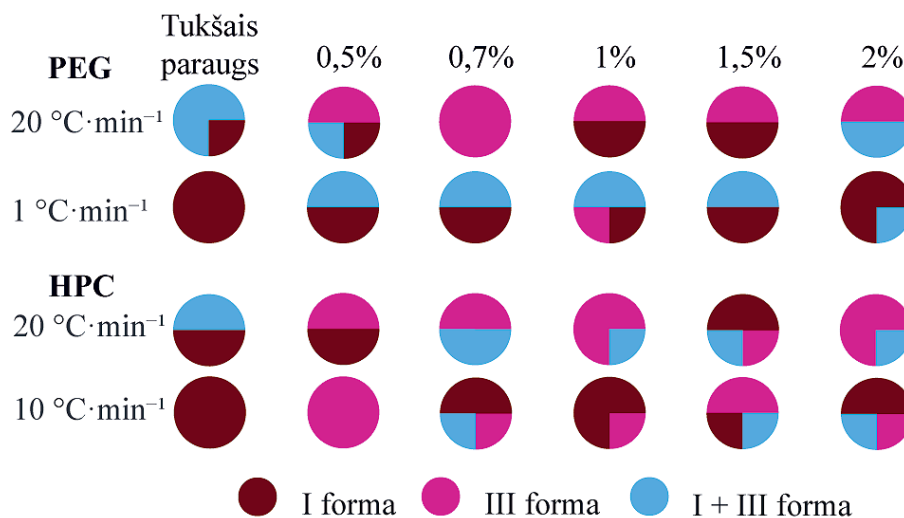

3.7. att. **Kristalizācijā iegūtā polimorfā forma 2,6MeOBA kristalizācijā no ūdens, izmantojot dažādas piedevas un dzesēšanas ātrumus. Katra ¼ no sektoru diagrammas attēlo vienu paralēlo eksperimentu.**

Lielākajā daļā kristalizāciju, izmantojot abas piedevas un vislielāko dzesēšanas ātrumu, tika iegūta III forma (skat. 3.8. att.). Arī šajā gadījumā piedevu klātbūtne nenodrošināja

polimorfo formu selektīvu kristalizāciju. HPC klātbūtnē abu polimorfo formu vienlaicīga kristalizācija gan bija retāka nekā PEG klātbūtnē. Netika novērota skaidra korelācija starp izvēlētās piedevas daudzumu un kristalizācijas rezultātu.

3.8. att. **Kristalizācijā iegūtā polimorfā forma 2,6MeOBA kristalizācijā no ūdens, izmantojot dažādu piedevu daudzumu. Katra ¼ no sektoru diagrammas attēlo vienu paralēlo eksperimentu.**

3.3.2. *2,6-dimetoksifenilborskābes kristalizācijā iegūtā polimorfā forma*

Atdzesēšanas kristalizācijā ar izvēlētajām piedevām tika iegūta gandrīz tikai I forma (skat. 3.9. att.). Turpretim II, III forma vai to maisījums tika iegūts ietvaicēšanas kristalizācijā Span 20, Tween 20 un OGP klātbūtnē. Tika novērots, ka Span 20 un OGP klātbūtne stabilizē II formu. Šo divu VAV klātbūtnē tā bija stabila līdz vienam mēnesim. Ietvaicēšana maisot novērsa metastabilo formu kristalizāciju. No pārbaudītajiem apstākļiem optimālākie metastabilo formu iegūšanai bija šķīdinātāja ietvaicēšana 50 °C temperatūrā bez maisīšanas. Šajos apstākļos sākumā tika ietvaicēts šķīdinātājs, iegūstot MPBA šķīdumu Span 20 vai OGP, tālāk iegūtais maisījums tika atdzesēts līdz istabas temperatūrai, un kristalizācija faktiski notika tikai pēc šīs atdzesēšanas. Šādi tika iegūti ļoti maza izmēra kristāli, un Span 20 un OGP klātbūtnē kristalizējās tīra III polimorfā forma.
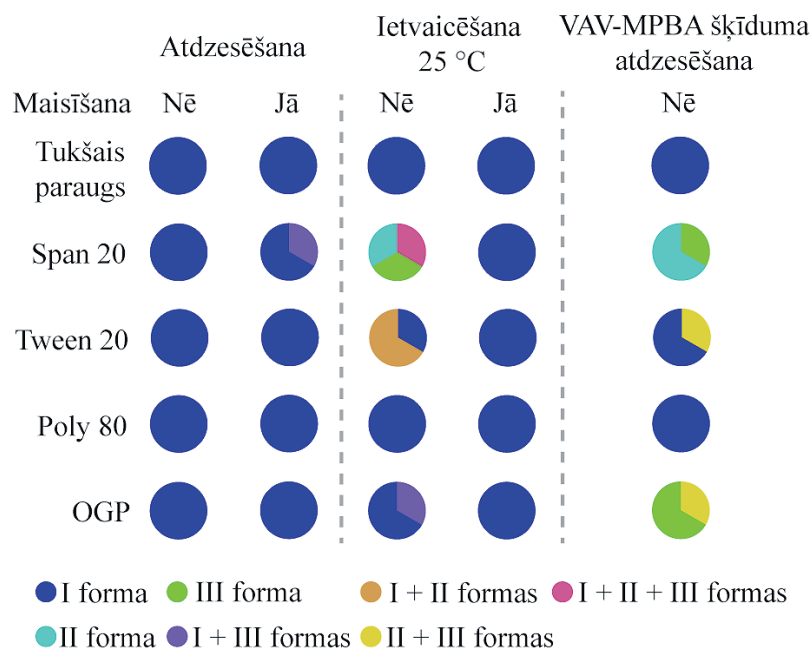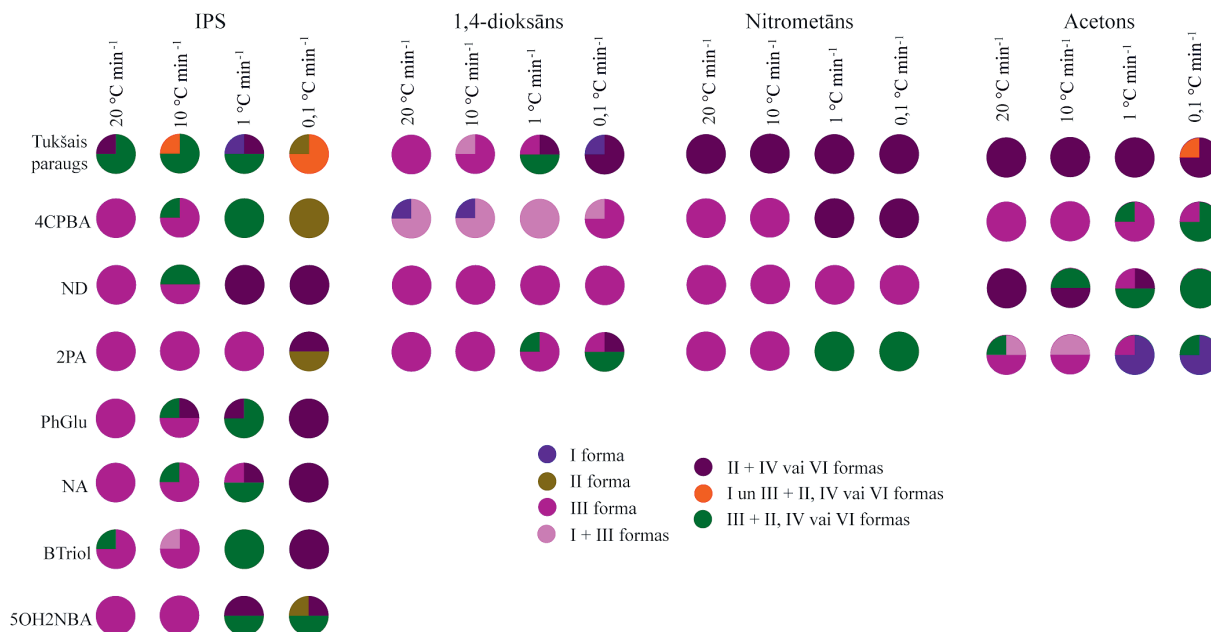
3.9. att. **Kristalizācijā iegūtā polimorfā forma MPBA kristalizācijā no toluola VAV klātbūtnē, izmantojot dažādas kristalizācijas metodes. Katra ⅓ no sektoru diagrammas attēlo vienu paralēlo eksperimentu.**

Lai noteiktu, vai sākotnējam šķīdinātājam ir nozīme šāda veida kristalizācijas procesā, MPBA-Span 20 šķīdums tika iegūts, izmantojot arī citus šķīdinātājus. Visos 15 eksperimentos, kuros kā šķīdinātājs tika izmantots acetons, IPA, THF, acetonitrils un toluols, tika iegūta tīra II forma, līdz ar to var secināt, ka II formas veidošanos šajos apstākļos nosaka tikai Span 20.

3.3.3. Izonikotīnamīda kristalizācijā iegūtā polimorfā forma

Gandrīz visas izvēlētās piedevas veicināja III formas kristalizāciju no IPA un 1,4-dioksāna, ja izmantoja lielākos dzesēšanas ātrumus (skat. 3.10. att.). Visaugstāko spēju nodrošināt III formas kristalizāciju no IPA uzrādīja 2PA, jo III forma tika iegūta arī izmantojot dzesēšanas ātrumu 1 °C min^{-1}, pie kura citu piedevu klātbūtnē galvenokārt tika iegūts II, IV un VI formas maisījums. ND uzrādīja visaugstāko spēju saglabāt kristalizācijā no 1,4-dioksāna iegūtu III formu pat pie maza dzesēšanas ātruma. 4CPBA veicināja I formas nukleāciju no 1,4-dioksāna. Jāatzīmē, ka iepriekš no šī šķīdinātāja gan šajā, gan arī citos pētījumos tika iegūtas tikai citas polimorfās formas.[78,85] Selektīvākās piedevas tika pārbaudītas arī kristalizācijā no acetona un nitrometāna, no kuriem iepriekšējos eksperimentos netika novērota III formas kristalizācija. 2PA un 4CPBA nodrošināja kristalizācijas kontroli arī no šiem šķīdinātājiem: 4CPBA veicināja III formas kristalizāciju, bet 2PA – I formas kristalizāciju. 2PA klātbūtnē ar vislielāko dzesēšanas ātrumu tika veicināta III formas kristalizācija, bet ar mazāku dzesēšanas ātrumu lielākoties tika iegūta tīra I forma. Kopumā rezultāti liecina, ka tīra stabilākās polimorfās formas (I formas) iegūšana tiešā kristalizācijā ir samērā sarežģīta. Visu trīs

pārbaudīto piedevu klātbūtnē nitrometānā tika veicināta tīras III formas veidošanās, izmantojot lielākos dzesēšanas ātrumus, savukārt ND nodrošināja tīras III formas veidošanos, izmantojot visus četrus dzesēšanas ātrumus.

3.10. att. **Kristalizācijā iegūtā polimorfā forma INA kristalizācijā izvēlēto piedevu klātbūtnē, izmantojot dažādus dzesēšanas ātrumus. Katra ¼ sektoru diagrammas attēlo vienu paralēlo eksperimentu.**

Tika pārbaudīta arī maisīšanas ātruma ietekme uz kristalizācijas iznākumu. Tika novērots, ka, izmantojot lielu dzesēšanas ātrumu un mazu maisīšanas ātrumu vai pat kristalizāciju bez maisīšanas, tika veicināta I formas veidošanās no IPA (skat. 3.11. att.). Savukārt III formas kristalizāciju veicināja testēto piedevu klātbūtne un lielāka dzesēšanas ātruma izmantošana. Kristalizācijas no 1,4-dioksāna iznākuma kontrole ar testētajām piedevām bija atkārtojamāka, īpaši izmantojot maisīšanu. Piedevu klātbūtne nodrošināja I un III formas maisījuma veidošanos, ja tika izmantots liels dzesēšanas ātrums bez maisīšanas. Visselektīvākā III formas kristalizācija tika panākta ND klātbūtnē, izmantojot mazu atdzesēšanas ātrumu, bet maisīšanas ātrums to neietekmēja. Eksperimentos, kuros izmantoja mazāko dzesēšanas ātrumu un kuros līdz ar to pēc kristalizācijas iegūto suspensiju maisīja ilgāku laiku, līdz tika sasniegta noteiktā beigu temperatūra 10 °C, tika iegūti par III formu stabilāki polimorfi (II, IV vai VI forma[85]). Līdz ar to, izmantojot dzesēšanas ātrumu 1 °C min⁻¹, gandrīz neviena no piedevām nespēja nodrošināt III vai I formas kristalizāciju.
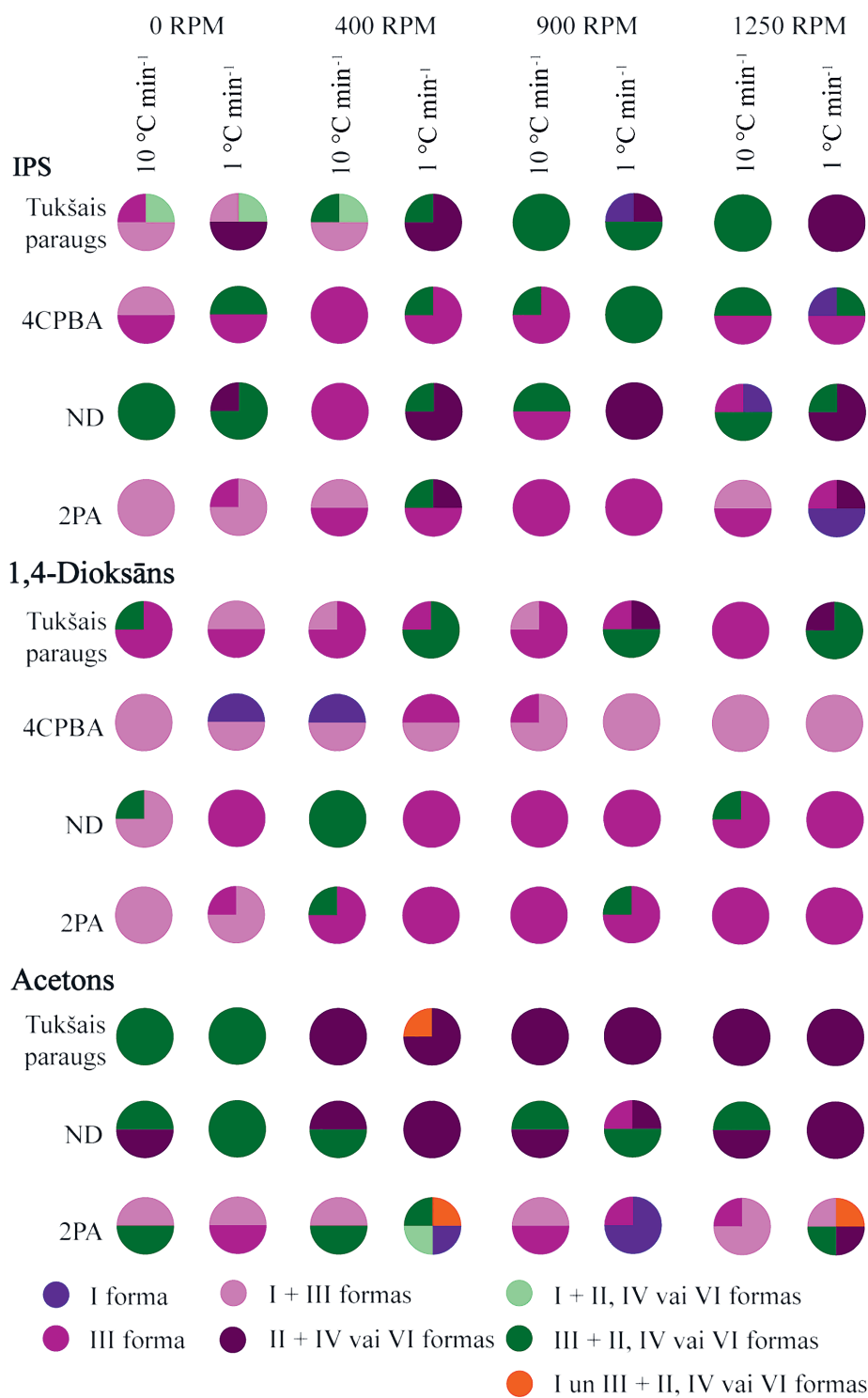
3.11. att. **Kristalizācijā iegūtā polimorfā forma INA kristalizācijā ar izvēlētajām piedevām, izmantojot divus atdzesēšanas ātrumus un dažādus maisīšanas ātrumus. Katra ¼ sektoru diagrammas attēlo vienu paralēlo eksperimentu.**

3.4. Kristalizācijas piedevu iespējamā ietekme uz nukleāciju un kristālu augšanu

3.3. nodaļā aprakstītie rezultāti skaidri parāda, ka kristalizācijas piedevas var veicināt metastabilo formu kristalizāciju, bet precīzs mehānisms, kā piedevas nodrošina kristalizācijā iegūtās polimorfās formas kontroli, nav zināms. Šajā pētījumā tika izmantotas dažādas pieejas, lai gūtu ieskatu faktoros, kas nosaka kristalizācijā iegūto polimorfo formu visām trim pētītajām modeļvielām. Šīs pieejas ietvēra eksperimentālo datu un teorētiskos aprēķinu izmantošanu:

- Šķīdības izmaiņu pētījums (2,6MeOBA);
- SMPT ietekmes pētījums (2,6MeOBA, INA);
- Kristāliskās struktūras raksturlielumu, tādu kā kristālrežģa enerģija, Hiršfelda virsmas un to 2D pirkstu nospiedumu kartes, FIM un BFDH morfoloģijas, salīdzināšana (MPBA, INA).

Piedevu ietekme uz šķīdību tika pētīta tikai 2,6MeOBA, jo pārējām vielām kristalizācijā bez piedevu klātbūtnes nebija iespējams iegūt tīras polimorfās formas. Tā kā 2,6MeOBA kristālrežģa enerģijas aprēķini un Hiršfelda virsmas un to 2D pirkstu nospiedumu karšu analīze jau ir publicēta,[74] šie raksturlielumi šī pētījuma ietvaros netika noteikti atkārtoti. Teorētiskie aprēķini tika veikti tikai tiem INA polimorfiem, kuri tika iegūti kristalizācijas eksperimentos, līdz ar ko V forma netika analizēta.

3.4.1. *Šķīdības pētījums*

Visstabilākajai formai ir viszemākā šķīdība, bet piedevu pievienošana šķīdumā var ietekmēt šķīdību, tādējādi palielinot metastabilo formu kristalizācijas varbūtību. Piemēram, ir pierādīts, ka piedevas samazina *p*-metilacetanilīda šķīdību, bet palielina kristālu rašanās un augšanas ātrumu.[88] 2,6MeOBA I formas šķīdību gandrīz neietekmē 1% PEG šķīduma izmantošana (skat. 3.12. att.). Temperatūrā līdz 30 °C šķīdība ir gandrīz identiska šķīdībai tīrā ūdenī, bet augstākā temperatūrā šķīdība nedaudz samazinājās. Turpretī III formas šķīdība PEG klātbūtnē nedaudz palielinās temperatūrā līdz 35 °C, bet augstākā temperatūrā šķīdība ir zemāka nekā tīrā šķīdinātājā. Abu formu ļoti līdzīgā šķīdība var izskaidrot gandrīz vienmēr novēroto vienlaicīgo kristalizāciju šīs piedevas klātbūtnē, kā tas novērots 3.3.1. apakšnodaļā aprakstītajos kristalizācijas eksperimentos. 1% PEG šķīdumā noteiktā termodinamiskā līdzsvara temperatūra ir par 8 °C zemāka nekā tīrā ūdenī (79 °C).
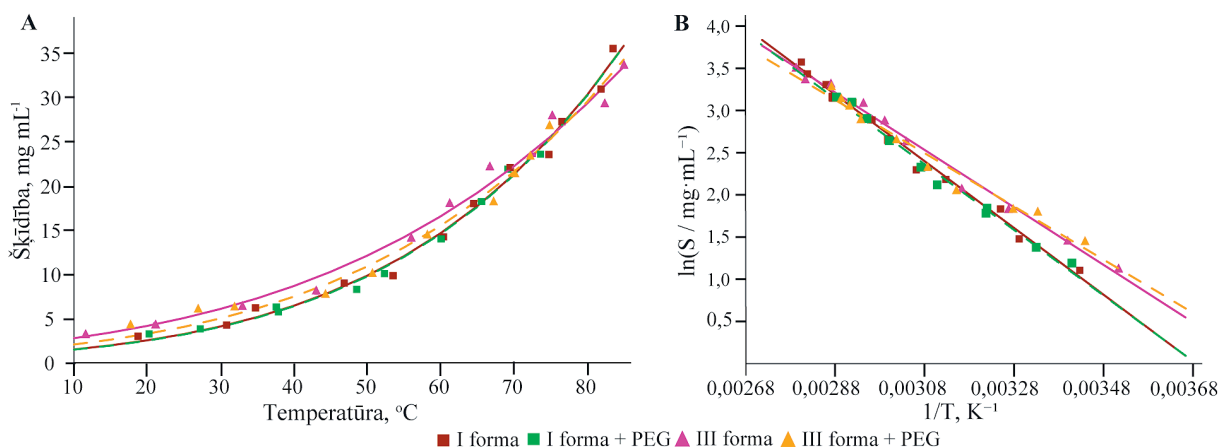
3.12. att. **2,6MeOBA I un III formu šķīdības līknes tīrā ūdenī un 1% PEG šķīdumā. A – eksponenciālais grafiks; B – linearizētais grafiks. Brūna nepārtraukta līnija – I forma tīrā ūdenī; zaļa raustīta līnija – I forma 1% PEG šķīdumā; rozā vienlaidu līnija – III forma tīrā ūdenī; oranža pārtraukta līnija – III forma 1% PEG šķīdumā. Trijstūri un kvadrāti attēlo eksperimentālos datus.**

3.4.2. *Šķīdinātāja veicinātu fāžu pāreju pētījums*

2,6MeOBA SMPT kinētikas mērījumi rāda, ka fāžu pārejas ātrums suspendēšanas eksperimentos ir ļoti liels (skat. 3.13. att.). Suspendējot I un III formas maisījumu visos pārbaudītajos šķīdinātājos un 1% PEG ūdens šķīdumā, tīra I forma tika iegūta mazāk nekā 15 min laikā, bet 0,1% HPC ūdens šķīdumā SMPT par I formu tika palēnināta. Pilnīga tīras III formas fāžu pāreja par tīru I formu ūdenī ir lēnāka. Šāda SMPT 1% PEG ūdens šķīdumā aizņem ilgāku laiku nekā suspendējot abu polimorfu maisījumu, savukārt 0,1% HPC ūdens šķīdumā SMPT tiek būtiski palēnināta, un I formas klātiene netika konstatēta pat pēc 24 h suspendēšanas.
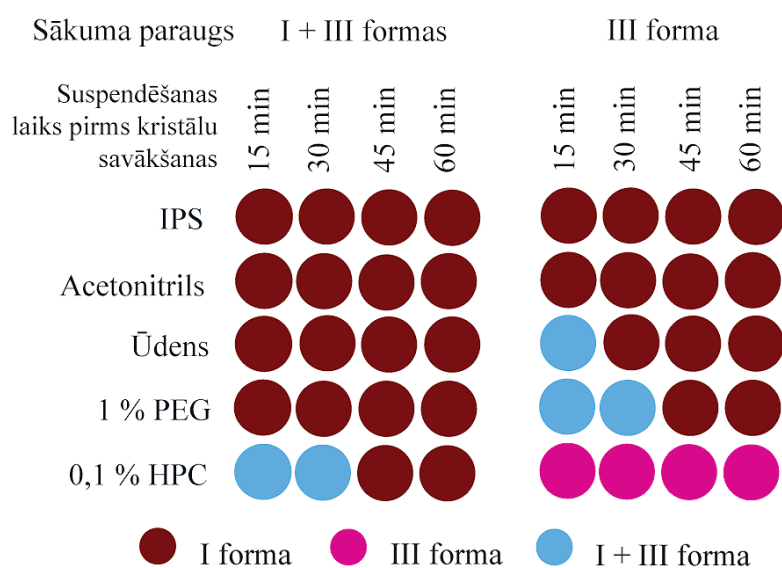
3.13. att. **Cietās fāzes sastāvs pēc suspendēšanas 25 °C temperatūrā.**

INA kristalizācijas piedevu klātbūtnē iegūtie rezultāti (skat. 3.3.3. apakšnodaļu) kopumā liecina par iespēju, ka vispirms veidojas III forma un pēc tam, maisot suspensiju, tā pāriet citās termodinamiski stabilākās formās SMPT rezultātā. SMPT eksperimentu rezultāti (skat. 3.14. att.) savukārt liecina, ka nevienas testētās piedevas klātbūtnē iegūtā kristāliskā forma 30 minūšu laikā pēc nukleācijas būtu būtiski mainījusies, kas ir saskaņā ar Kulkarni et al. veiktajam piesēšanas kristalizācijas pētījumam.[89] Līdz ar to atšķirības ar dažādu maisīšanas ātrumu iegūtajās INA polimorfajās formās nav saistīts ar SMPT, bet gan ar piedevu atšķirīgo spēju ietekmēt kristalizācijas iznākumu. Ja izmanto lielākus atdzesēšanas ātrumus, nukleācija notiek zemākā temperatūrā kad šķīdumā ir augstāks pārsātinājums, savukārt, ja izmanto lēnākus atdzesēšanas ātrumus, nukleācija notiek augstākā temperatūrā kad šķīdumā ir zemāks pārsātinājums. Piedevas pazemināja nukleācijas temperatūru, palielinot pārsātinājumu nukleācijas brīdī, un tas faktiski varētu būt viens no iespējamiem piedevu efektiem, kas var mainīt kristalizācijā iegūto polimorfo formu.
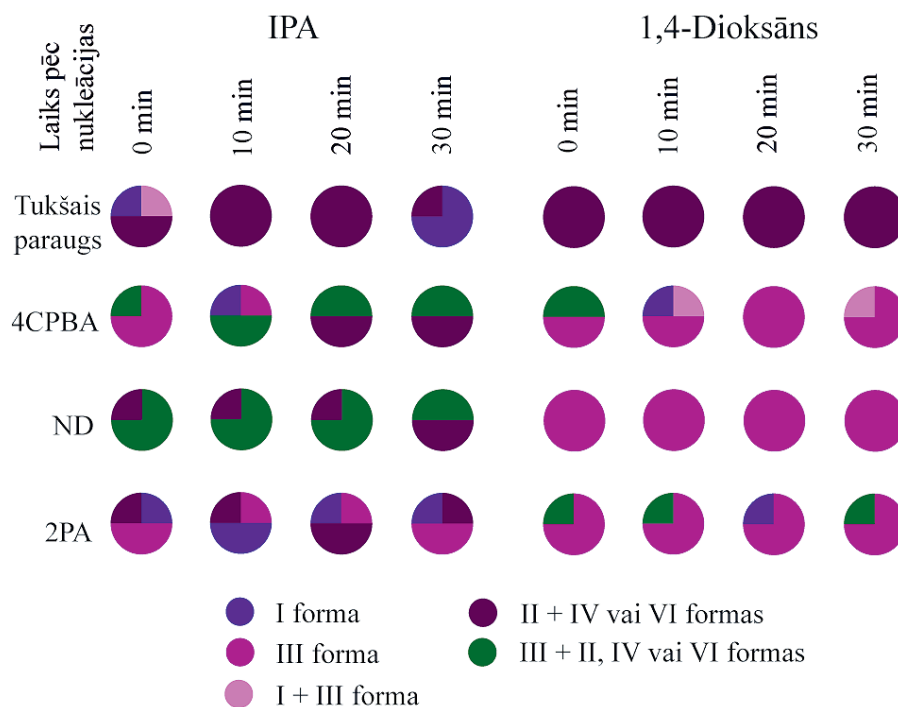
3.14. att. **Kristalizācijā iegūtā polimorfā forma INA kristalizācijā ar izvēlētām piedevām, izmantojot 1 °C min^{-1} atdzesēšanas ātrumu un dažādu laiku, kad kristāli tika savākti pēc nukleācijas. Katra ¼ sektora diagrammas attēlo vienu paralēlo eksperimentu**.

3.4.3. Kristalogrāfisks raksturojums

Tika noteikts, ka MPBA globālā enerģijas minimuma konformācija atbilst *anti*-konformeram, kurā ir divas iekšmolekulārās ūdeņraža saites starp borskābes hidroksilgrupām un metoksigrupām. INA molekulārās konformācijas analīze savukārt parādīja, ka visstabilākajā

konformācijā benzola gredzens un amīda grupa ir nedaudz novirzīti un torsijas leņķis starp šīm grupām ir 21,88°.

Starpmolekulārās enerģijas aprēķiniem tika izmantota MPBA I formas kristāliskā struktūra monoklīnajā *Pc* telpiskajā grupā bez ūdeņraža nesakārtotības dimēros, ko veido *sin-anti*-konformēri. Abu polimorfo formu režģa enerģija ir gandrīz identiska (skat. 3.5. tab.). Lai gan aprēķinātā relatīvā enerģija ir pretrunā ar to, ka I forma ir noteikta kā termodinamiski stabilākā forma, to visticamāk ietekmē tas, ka šajā formā ir iespējams dažāds ūdeņraža atomu izvietojums dimēros, kas varētu nodrošināt entropijas pieaugumu, tādejādi pazeminot I formas Gibsa enerģija. Salīdzinot INA polimorfus, viszemākā kristālrežģa enerģija ir INA I formai, nākošajai zemākajai esot INA II formas režģa enerģijai. Visu pārējo polimorfo formu režģa enerģija ir gandrīz identiska. Ļoti līdzīgās režģa enerģiju vērtības izskaidro eksperimentāli novēroto polimorfo formu vienlaicīgu kristalizāciju. Aprēķinātās polimorfo formu enerģiju atšķirības abām vielām atbilst tipiskai organisko vielu polimorfo formu enerģijas atšķirībai (<5 kJ mol^{-1}). [64,69]

3.5. tabula

MPBA un INA polimorfo formu kristalogrāfiskie, iekšmolekulārie, starpmolekulārie un režģa enerģijas dati.

Modeļviela	Polimorfā forma	CSD references kods	Z/Z'	E_{intra}, kJ mol^{-1}	E_{inter}, kJ mol^{-1}	$E_{lattice}$, kJ mol^{-1}
MPBA	I forma	UJACIT01 (oriģinālā $P\bar{4}n2$ struktūra)	4/0,5 ($P\bar{4}n2$); 4/2 (*Pc*)	15,2	-144,4	-129,2
	II forma	UJACIT	12/1,5	6,0	-135,9	-129,8
INA	I forma	EHOWIH01	4 / 1	0,46	-124,7	-124,3
	II forma	EHOWIH02	8 / 2	0,05	-122,2	-122,2
	III forma	EHOWIH03	8 / 1	0,51	-120,6	-120,1
	IV forma	EHOWIH04	6 / 3	0,12	-119,8	-119,7
	VI forma	EHOWIH06	8 / 2	0,04	-121,4	-121,4

Abu MPBA polimorfo formu izteiktās atšķirības ūdeņraža saitēs rada lielas atšķirības režģa enerģijas komponenšu ieguldījumā kopējā enerģijā un abu formu enerģijas tīklos (*energy frameworks*). I formā dominējošā režģa enerģijas komponente ir elektrostatiskā enerģija, ko var saistīt ar spēcīgu ūdeņraža saišu tīklu šajā struktūrā. Turpretī II formā elektrostatiskās enerģijas un dispersijas enerģijas ieguldījums režģa enerģijā ir ļoti līdzīgs, jo starpmolekulāro ūdeņraža saišu daudzums šajā struktūrā ir būtiski mazāks un aromātisko mijiedarbību, tostarp π-π mijiedarbību, nozīme ir lielāka. Rezumējot var secināt, ka, neraugoties uz kopumā efektīvākām

dispersijas mijiedarbībām II formas struktūrā, ievērojami spēcīgākās ūdeņraža saites I formas struktūrā ir iemesls augstākai šīs formas starpmolekulārajai enerģijai, kas varētu izskaidrot arī tās augstāko stabilitāti. Ūdeņraža saišu spēja nodrošināt kristāliskās struktūras stabilizāciju ir pierādīta jau agrāk, piemēram, pētījumos ar proteīniem[90,91] un ritonavīru.[92]

Kā sagaidāms pamatojoties uz ļoti līdzīgajām starpmolekulārajām mijiedarbībām un molekulāro pakojumu, visām INA polimorfajām formām, izņemot I formu, ir gandrīz identisks enerģētisko tīklu izkārtojums. Galvenajās mijiedarbībās, kas stabilizē visu formu kristālisko struktūru, dominē elektrostatiskās enerģijas komponente, un dispersijas enerģijas komponente ir ievērojami mazāk nozīmīga. I formas struktūrā visievērojamākā no mijiedarbībām, kurā dominē elektrostatiskās enerģijas komponente, ir starp dimēru veidojošajām molekulām. Turpretī visās pārējās INA polimorfajās formās ievērojamākās mijiedarbības, kurās dominē elektrostatiskā enerģijas komponente, ir starp molekulām, kas veido INA molekulu ķēdes divos telpiskos virzienos un tādējādi veido ar ūdeņraža saitēm saistītu INA molekulu slāņus. I un III formā mijiedarbības ar visizteiktāko dispersijas enerģiju ir starp tām pašām molekulām, kurām ir arī visizteiktākā elektrostatiskā enerģija. Turpretī II, IV un VI formā tās ir aromātiskās un π-π mijiedarbības starp pretēji orientētām molekulām no blakus esošiem INA molekulu slāņiem un mijiedarbības ar molekulām, kas veido ūdeņraža saites ar minētajām molekulām no blakus esošajiem slāņiem.

Abu MPBA formu starpmolekulāro mijiedarbību atšķirības un INA II, IV un VI formu līdzība ir skaidri redzama arī Hiršfelda virsmās un to 2D pirkstu nospiedumu kartēs, bet ievērojamas atšķirības novērotas starp INA I un III formām (skat. 3.15. att.). MPBA I formā var novērot ūdeņraža saites, kas veido borskābes dimērus un to ķēdes, un dažādas H⋯C mijiedarbības, kas ir galvenās novērojamās mijiedarbības šajā formā. Abām MPBA II formas simetriski neatkarīgajām molekulām ir tikai viens ass maksimums, kas atbilst tam, ka tās ir spēcīgas ūdeņraža saites donors (A molekula) vai akceptors (B molekula). MPBA II formas B molekulai novēro arī iezīmes, kas saistīta ar π-π mijiedarbībām veidošanos. INA I formas Hiršfelda virsmas pirkstu nospieduma analīzē ir divi asi maksimumi, kas atbilst CO⋯H$_2$N mijiedarbībai, savukārt visām pārējām formām šie maksimumi ir platāki un katrs atbilst divām mijiedarbībām: N$_{pyr}$⋯H$_2$N vai CO⋯H$_2$N. INA II, IV un VI formas pirkstu nospiedumu analīzē ir izteikts maksimums diagrammas vidū, kas atbilst CH⋯HC mijiedarbībai. Vēl viena atšķirība starp šo triju formu pirkstu nospiedumu kartēm, salīdzinot ar I un III formu, ir apgabalā, kas atbilst π-π mijiedarbībām diagrammas vidū.
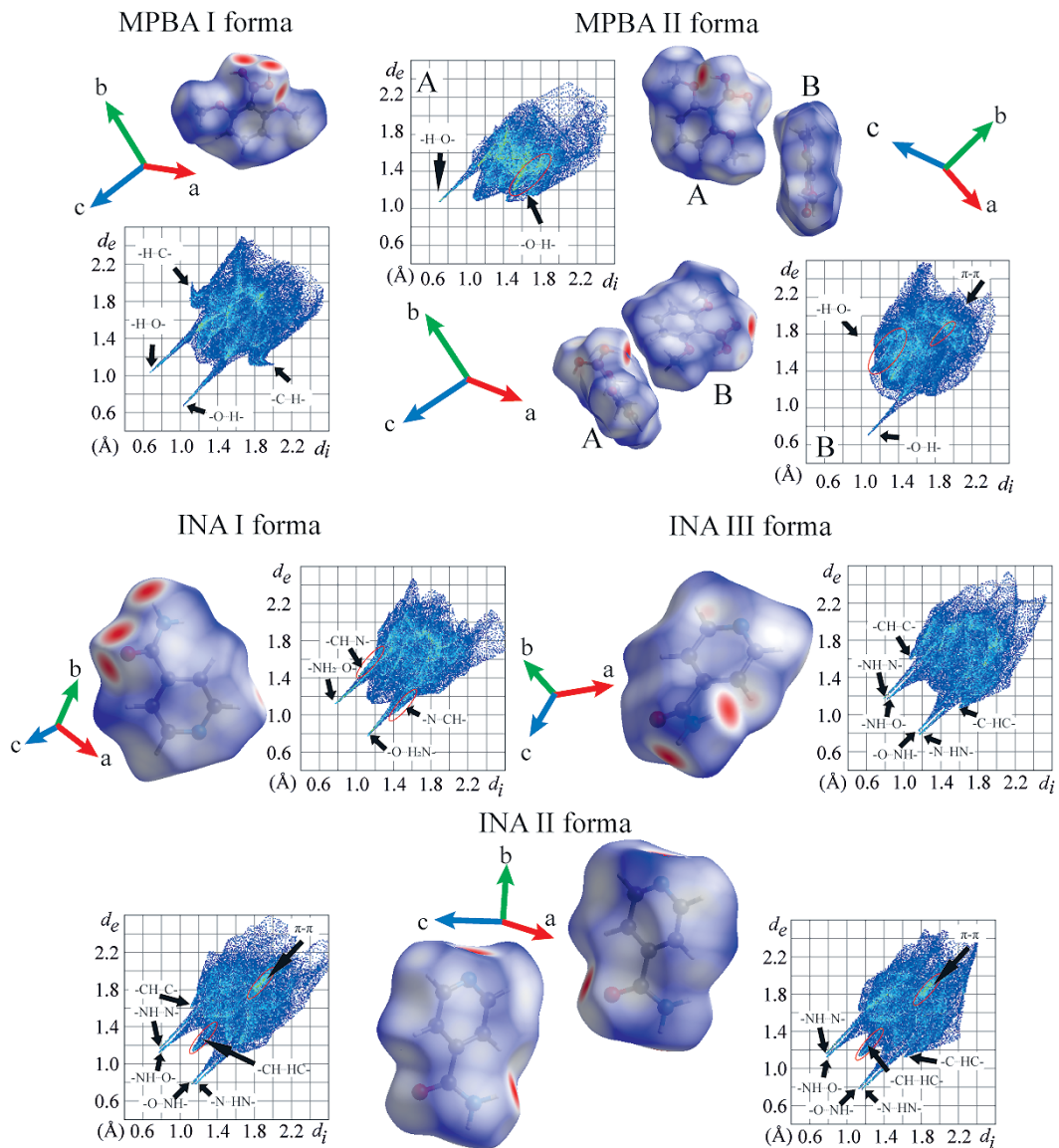
3.15. att. **Hiršfelda virsmas un to 2D pirkstu nospiedumu kartes MPBA I un II formai un INA I – III formai, norādot diagrammās novērotas raksturīgākās starpmolekulārās mijiedarbības.**

3.4.4. FIM un BFDH morfoloģijas analīze

MPBA I formā, kas veidota no homodimēriem, lielākā daļa potenciāli iespējamo starpmolekulāro mijiedarbību ir izveidojušās, turpretī II formā ir izveidojusies tikai puse no iespējamām ūdeņraža saišu mijiedarbībām. Līdz ar to MPBA II formā novērotās ūdeņraža saites neatbilst no CSD noteiktajam optimālajam ūdeņraža saišu skaitam un pozīcijām (trīs ūdeņraža saišu akceptori neveido ūdeņraža saites), kas varētu būt iemesls šīs formas zemajai stabilitātei un iespējai šo polimorfo formu iegūt tikai īpašos apstākļos. FIM analīze INA molekulām netika veikta, jo INA molekulas visos polimorfos ir tikpat kā identiskā konformācijā un visas potenciālās mijiedarbības ir izveidojušās.

Salīdzinot FIM, kas projicētas uz kristāla plaknēm, starp abiem MPBA polimorfiem ir būtiskas atšķirības (skat. 3.16. att.). Salīdzinājumā ar II formu, I formas kristāliem ir lielāka

varbūtība iesaistīties hidrofobajās mijiedarbībās un mijiedarbojas ar ūdeņraža saišu akceptoriem. Savukārt MPBA II formas kristālam, salīdzinot ar I formas kristālu, uz lielākajām plaknēm ir lielāka varbūtība mijiedarboties ar ūdeņraža saišu donoriem. Uz šīm plaknēm atrodas borskābes grupu skābekļa atomi *anti*-planārā konformācijā, un šīs plaknes aug, veidojoties ūdeņraža saitēm saistītiem trimēram, tāpēc uz plaknes ir atsegti ūdeņraža saišu akceptori, kas var veidot ūdeņraža saites ar donoriem. Šī iemesla dēļ VAV (ūdeņraža saišu donori) var vieglāk mijiedarboties ar šīm šķautnēm, salīdzinājumā ar I formu, kurai ūdeņraža saišu akceptoras grupas aizņem mazāku laukumu. Gan Span 20, gan OGP satur ūdeņraža saišu donoras grupas, kas var mijiedarboties ar MPBA borskābes grupu un stabilizēt II formas kristālus. Turklāt VAV hidrofobā daļa var palēnināt fāžu pāreju, veidojot micellas vai puslodes, un tādējādi novērst molekulu reorganizāciju, kas nepieciešama II formas pārejai par I formu.
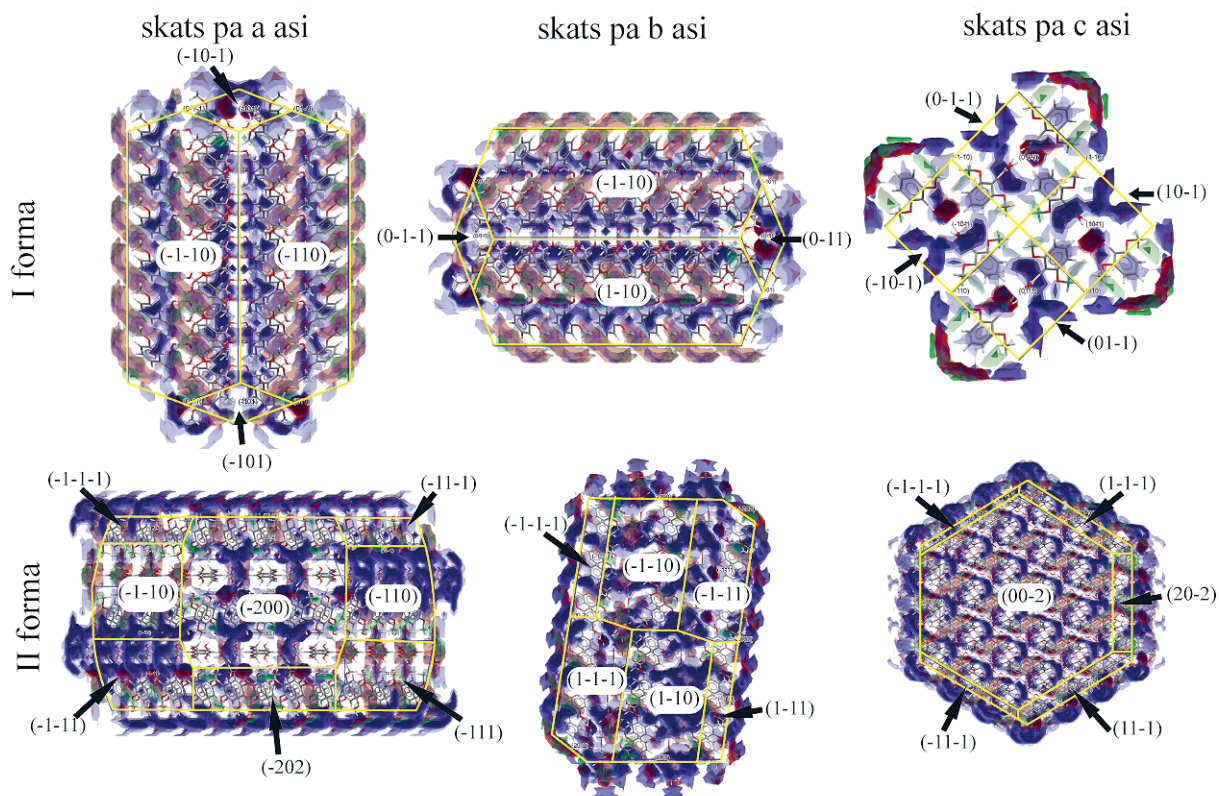
3.16. att. **FIM projekcijas uz MPBA I un II formas BFDH morfoloģijām. Ūdeņraža saišu donoru varbūtības apgabali ir parādīti zilā krāsā, ūdeņraža saišu akceptoru – sarkanā krāsā, bet hidrofobās mijiedarbības – zaļā krāsā.**

Ļoti līdzīgā molekulārā pakojuma dēļ arī BFDH morfoloģija un FIM, kas projicēts uz INA II, IV un VI formas kristāliskajām virsmām, ir ļoti līdzīgi (skat. 3.17. att.). Šo polimorfo formu lielākās kristāliskās plaknes aug, pievienojot molekulas, ko saista dažādas π-π un CH⋯π mijiedarbības, bet mazākās, ātrāk augošās plaknes, aug pievienojot molekulas, ko saista ūdeņraža saites. INA I un III formām uz lielākajām plaknēm ir atsegti ūdeņraža saišu akceptori un donori, un tāpēc tās ir to mijiedarbību vidū, kas veidojas šo plakņu augšanas laikā. I formas

plakņu grupa {100} aug, veidojoties amīdu $R_2^2 8$ homodimēriem, bet III formas plakņu grupas {111} un {002} aug, turpinoties $CO\cdots H_2N$ ķēdēm, tāpēc ūdeņraža saišu donori, piemēram, 2PA vai 4CPBA, var mijiedarboties ar šīm plaknēm vai veicināt šo polimorfo formu augšanu, aktivizējot atbilstošās augšanas vietas.
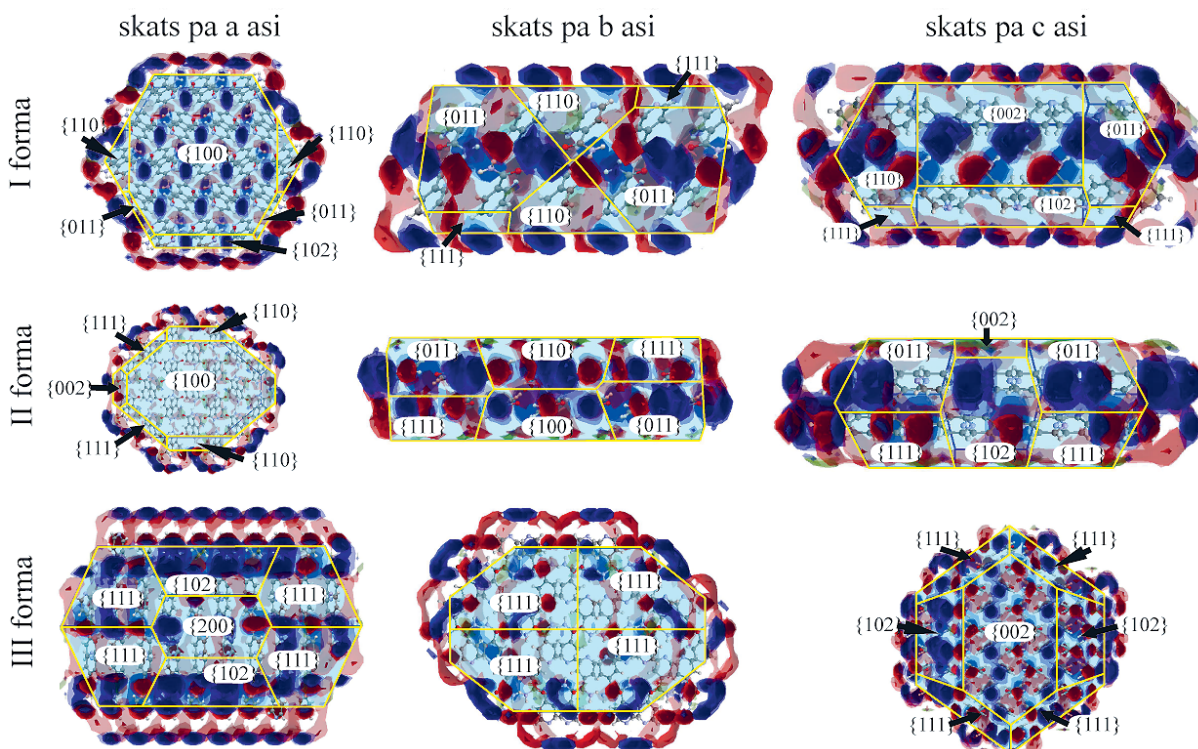
3.17. att. **FIM projekcijas uz INA I-III formas BFDH morfoloģijām. Ūdeņraža saišu donoru varbūtības apgabali ir attēloti zilā krāsā, ūdeņraža saišu akceptori – sarkanā krāsā, bet hidrofobās mijiedarbības – zaļā krāsā.**

SECINĀJUMI

1. Četru jauno (propionskābes monosolvāta, sviestskābes mono- un disolvāta, trifluoroetanola solvāta) un četru jau zināmo (skudrskābes, etiķskābes, formamīda solvāta un propionskābes disolvāta) izonikotīnamīda solvātu kristāliskajās struktūrās novēro līdzīgus ūdeņraža saišu motīvus, kas ļauj paredzēt līdzīgas starpmolekulārās mijiedarbības un molekulāro pakojumu jauniem solvātiem/kokristāliem ar strukturāli līdzīgiem šķīdinātājiem/ koformeriem.

2. Polietilēnglikols un hidroksipropilceluloze veicina 2,6-dimetoksibenzoskābes III formas kristalizāciju, taču kristalizācija piedevu klātienē nav pilnībā selektīvs, jo dažkārt iegūtā III forma satur I formas piemaisījumu.

3. Hidroksipropilceluloze kavē 2,6-dimeoksibenzoskābes šķīdinātāja veicinātu III formas fāžu pāreju par I formu, kas nodrošina III formas iegūšanu kristalizācijas procesā.

4. Sorbitāna laurāta (Span 20) un oktil β-D-glikopiranozīda klātbūtnē ir iespējams kristalizēt 2,6-dimetoksifenilborskābes II formu, un šīs kristalizācijas piedevas uzlabo 2,6-dimetoksifenilborskābes II formas stabilitāti, stabilizējot to līdz 1 mēnesim. Novērots, ka sorbitāna laurāta klātbūtnē šķīdinātājs neietekmē 2,6-dimetoksifenilborskābes kristalizācijā iegūto polimorfu.

5. Morfoloģijas un mijiedarbību karšu analīze ļāva noteikt, ka piedevas var adsorbēties uz 2,6-dimetoksifenilborskābes II formas kristālu plakņu {002} un {110} virsmas, un noteikt, ka piedevu sorbcija, visticamāk, novērš fāžu pāreju par I formu.

6. Izonikotīnamīda kristalizācija naftalin-1,5-diola klātbūtnē veicināja III formas kristalizāciju, bet 2-pikolīnskābe veicināja I formas kristalizāciju. Lielākā daļa izmantoto piedevu samazināja citu polimorfo formu saturu iegūtajos kristalizācijas produktos. Pie liela dzesēšanas ātruma (20 $^{\mathrm{o}}$C min^{-1}) kristalizācijas piedevas nodrošināja tīras izonikotīnamīda III formas kristalizāciju, bet, izmantojot mazu dzesēšanas ātrumu (0,1 $^{\mathrm{o}}$C min^{-1}), gandrīz visas piedevas zaudēja spēju nodrošināt kristalizācijas kontroli.

7. Izonikotīnamīda polimorfajām formām, kas kristalizējas vienlaicīgi (II, IV un VI forma), ir ļoti līdzīga kristālrežģa enerģija un starpmolekulārās mijiedarbības. Šī iemesla dēļ ir ļoti varbūtīgi, ka šo polimorfo formu nukleācijas enerģētiskā barjera un kristālu augšanas ātrums ir ļoti līdzīgi, savukārt piedevu klātbūtne, mainot kristalizācijas apstākļus, var panākt strukturāli atšķirīgāku formu kristalizāciju.

8. Morfoloģijas un mijiedarbību karšu analīze ļāva noteikt, ka piedevas var adsorbēties uz izonikotīnamīda I formas {100} un III formas {111} un {002} kristālu plakņu virsmas, un ir varbūtīgi, ka piedevu sorbcija ir saistīta ar šo augšanas vietu aktivizēšanu, nodrošinot vai veicinot I vai III formu veidošanos.

![University of Latvia logo]

UNIVERSITY
OF LATVIA

FACULTY OF CHEMISTRY

Aina Semjonova

STUDY OF POLYMORPHISM CONTROL OF ORGANIC SUBSTANCES USING CRYSTALLIZATION ADDITIVES

DOCTORAL THESIS

Submitted for the Degree of Doctor of Science (Ph. D.)
in Natural Sciences (in the field of Chemistry)

Subfield of Physical Chemistry

Scientific supervisor:
Assoc. prof., Dr. chem. Agris Bērziņš

Riga 2024

The Doctoral Thesis was caried out at the Chair of Physical Chemistry, Faculty of Chemistry, University of Latvia, Riga, Latvia from 2020 to 2023.

UNIVERSITY OF LATVIA

The thesis contains a summary in Latvian and English and four scientific articles. Form of the thesis: collection of scientific articles in Chemistry, Physical Chemistry.

Scientific supervisor: assoc. prof., Dr. chem. **Agris Bērziņš**.

Reviewers:
1) Assoc. prof., Dr. chem. **Guntars Vaivars** (University of Latvia);
2) Dr. chem. **Raitis Bobrovs** (Latvian Institute of Organic Synthesis);
3) Assoc. prof., Dr. chem. **Dejan-Kresimir Bucar** (University College London).

The thesis will be defended in a public session of the Promotional Committee of Chemistry, University of Latvia, at 16.00 on September 12th, 2024 at the University of Latvia Academic centre, House of Nature, Room 217. Jelgavas iela 1, Rīga.

The summary of the thesis is available at the Library of the University of Latvia, Raiņa bulv. 19.

University of Latvia Promotional Committee of Chemistry:

Chairman: Prof., Dr. chem. **Edgars Sūna**;

Secretary: Assoc. Prof., Dr. chem. **Vita Rudoviča**.

ABSTRACT

Crystallization of several model compounds, namely 2,6-dimethoxybenzoic acid, 2,6-dimethoxyphenylboronic acid and isonicotinamide, were studied in the thesis. The model compounds were chosen based on their ability to form polymorphs with different hydrogen bonding synthons, i.e., structures containing hydrogen bonded dimers and chains, in the crystallization. The formation of different crystalline phases of these model compounds in crystallization from different solvents with different crystallization methods has been studied. The obtained crystalline phases were characterised by X-ray diffraction and thermal analysis. For the most stable polymorphs the solubility and relative thermodynamic stability were also determined. Crystallization was performed by testing the effect of different types of crystallization additives – polymers, surfactants, and structurally similar compounds, on the polymorphic outcome. The effect of crystallization additives on the solubility and relative stability of the most stable polymorphs was also investigated. Crystal structures of four new phases of the studied compounds were determined from powder and single crystal X-ray diffraction. Crystallographic and computational analysis of all the relevant crystal structures of the model compounds were performed to provide a possible mechanism for the observed control of the crystallization polymorphic outcome by the most efficient crystallization additives.

Keywords: polymorphism, crystallization, crystallization additives, crystal structure analysis, powder X-ray diffraction, thermal analysis.

ABBREVIATIONS

AA	acetic acid;
API	active pharmaceutical ingredient;
BA	butyric acid;
BFDH	Bravais–Friedel–Donnay–Harker
Btriol	benzene-1,2,3-triol;
CSD	Cambridge Structural Database
CSP	crystal structure prediction;
DSC	differential scanning calorimetry;
FA	formic acid;
FAM	formamide;
FIM	full interaction map;
INA	isonicotinamide;
IPA	isopropanol;
HPC	hydroxypropyl cellulose;
MPBA	2,6-dimethoxyphenylboronic acid;
MD	molecular dynamic;
NA	nicotinic acid;
ND	naphthalene-1,5-diol;
OGP	octyl β-D-glucopyranoside;
PA	propionic acid;
PEG	polyethylene glycol;
PhGlu	phloroglucinol;
Poly80	polysorbate 80;
PXRD	powder X-ray diffraction;
SAM	self-assembled monolayers;
SCXRD	single crystal X-ray diffraction;
SMPT	solvent-mediated phase transition;
Span 20	sorbitan laurate;
$S_{solvent}$	solvate;
TFE	2,2,2-trifluoroethanol;
TG	thermogravimetry;
THF	tetrahydrofuran;
Tween 20	polysorbate 20;
2PA	2-picolinic acid;
4CPBA	4-carboxyphenylboronic acid;
5OH2NBA	5-hydroxy-2-nitrobenzoic acid;
2,6MeOBA	2,6-dimethoxybenzoic acid.

INTRODUCTION

The vast majority of active pharmaceutical ingredients (APIs) can crystallize in different crystalline forms.[1] In the pharmaceutical manufacturing the crystalline form obtained must meet the reference requirements, so the control of the obtained crystalline form is a mandatory requirement.[2] Often a mixture of different forms is obtained in a crystallization from solution,[3] which can further affect solubility,[4] bioavailability[5] or other physical properties of the API. Such undesired formation of polymorph mixtures has been observed in crystallization of multiple APIs.[3] Moreover, more than one polymorph can often be obtained under very similar conditions,[6] which does not guarantee selectivity in the crystallization and does not ensure repeatability, thus does not meet the requirements of the industry.

In the pharmaceutical production, it is safer to choose the most stable polymorphs for the finished dosage form, as it has the lowest energy, and thus is stable at all stages of the production. However, if the solubility of the compound is low, the fact that the most stable form has the lowest solubility can cause problems. For this reason, sometimes metastable polymorphs are preferred because of their better solubility.[7] Alternatively, they can be selected because the more stable polymorphs are patent protected.[8] In the process of obtaining a metastable polymorph, the thermodynamically stable polymorph is often formed as an impurity.[3] In such cases it is practically impossible to separate them or convert the mixture into the required polymorph, moreover, during storage a phase transition to the most stable polymorph is promoted by the presence of this phase in the mixture.[6] For the reasons mentioned above, it is necessary to optimize and control the processes of crystallization, production and storage of the finished product.[9] One of the options for ensuring that a pure polymorph is obtained in the crystallization is the use of additives.[10]

The control of the crystallization process using additives is currently still empirical.[10] Employing the available computational description of the possible interactions between API molecules as well as the conformation energy penalty, it is already possible to predict what are the most stable crystal structures of an API using crystal structure prediction (CSP) technique. However, currently there are no tools that would allow determining the likelihood of crystallization of a crystal form with a given crystal structure, particularly if the crystal form outcome depends on the crystallization conditions. Moreover, there is neither a general method that would allow predicting the polymorphic outcome of the crystallization from pure solvents, nor approach for evaluating how any particular additive would alter it. Therefore, for each API, a selective method of obtaining a particular crystalline form is being developed in long-term experimental studies.[11] To achieve ability to design additive controlled crystallization of

particular crystalline form, a molecular level understanding of the crystallization process and the role of the additive in it is required.[10] The associates present in solution sometimes can be lined to the resulting polymorph,[12] but it has also been shown that in other cases they do not affect the crystallization outcome.[13] In the scientific literature, information on the use of additives (such as Langmuir monolayers[14] and self-assembled monolayers (SAM)[15]) to control the crystallization process can be found for several APIs and model substances,[16] but often the additives are expensive or impossible to separate from the API crystals. Moreover, they often do not ensure selective crystallization of one desired form, but only promote its formation. Due to the complexity of the factors determining the polymorphic outcome, even nowadays computational calculations does not provide a clear approach for finding a crystallization procedure to obtain a selected crystal form. There is also no clearly confirmed approach for performing MD simulations which would be able to determine the crystal structure obtained in the crystallization from solution.

The **aim** of the doctoral thesis is to gain an understanding of the possible mechanism of crystallization in the presence of additives, which could be applied to control the crystallization polymorphic outcome of APIs. The following **tasks** were set to achieve the goal:

1. To explore the crystallization polymorphic outcome of the model substances 2,6-dimethoxybenzoic acid, 2,6-dimethoxyphenylboronic acid and isonicotinamide using different crystallization approaches, conditions and solvents;

2. To characterize the newly obtained crystalline forms with X-ray diffraction and thermal analysis and determine their crystal structure using single crystal or powder X-ray diffraction data;

3. To explore the effect of various types of crystallization additives on the crystallization polymorphic outcome of the model substances;

4. To identify the additives potentially providing ability to selectively affect the crystallization polymorphic outcome and perform experiments to evaluate the effect of conditions and other factors on the polymorphic outcome of the crystallization in presence of these additives;

5. To determine the effect of the selected additives on the solubility and thermodynamic stability of the most stable polymorphs of model compounds;

6. To perform crystallographic and computational analysis of the crystal structures of the obtained solid phases to provide a possible mechanism of the crystallization in the presence of the additives.

Scientific Novelty and Practical Significance

- This research contributes to the development of an additive assisted crystallization method allowing use of cost-effective crystallization additives (SAM costs can exceed several hundred euros per laboratory-scale crystallization experiment, whereas the substances used in this study cost less than a ten euros per gram) that are either easily separable or can be included in the dosage forms, such as surfactants and polymers.

- Part of the results of the research are knowledge about the factors that ensure selective crystallization, including additives providing control of the crystallization outcome. These can be further used in the development of a general guidelines or model of crystallization process control.

- The use of crystallographic analysis and theoretical calculations provided information on the differences between the crystal forms which allowed to propose a mechanism explaining the additive assisted change of the polymorphic outcome of crystallization. Additionally, combination of theoretical calculations and experimental results contributed to the understanding of the interactions at the molecular level that overall determine the crystallization outcome.

- The crystallization control method developed employing this knowledge has potential to be used in the pharmaceutical industry to control the crystallization of various structurally similar APIs, for example, APIs corresponding to low molecular weight benzoic acids, which form polymorphs containing hydrogen bond dimers and chains – similar hydrogen bonded motifs to those formed by the studied compounds.

RESULTS PUBLISHED

Publications

1. **Semjonova, A.,** Bērziņš, A. Controlling the Polymorphic Outcome of 2,6-Dimethoxybenzoic Acid Crystallization Using Additives. *Crystals,* **2022**, *12*, 1161. (IF$_{2022}$ = 2.67)

   A. Semjonova carried out 100 % of the experimental work, contributed to writing the article (80%), prepared the experimental results according to the journal guidelines, as well as prepared the answers to the questions and remarks given by reviewers.

2. **Semjonova, A.,** Bērziņš, A. Surfactant Provided Control of Crystallization Polymorphic Outcome and Stabilization of Metastable Polymorphs of 2,6-Dimethoxyphenylboronic Acid. *Crystals*, **2022**, *12*, 1738. (IF$_{2022}$ = 2.67)

   A. Semjonova carried out 100 % of the experimental work, contributed to writing the article (80%), prepared the experimental results according to the journal guidelines, as well as prepared the answers to the questions and remarks given by reviewers.

3. **Semjonova, A**., Bērziņš, A. Crystallization of metastable isonicotinamide polymorphs and preventing concomitant crystallization by additives. *Crystal Growth & Design,* **2023**, *23* (12), 8584-8596*.* (IF$_{2023}$ = 3.80)

   A. Semjonova carried out 100 % of the experimental work, contributed to writing the article (80%), prepared the experimental results according to the journal guidelines, as well as prepared the answers to the questions and remarks given by reviewers.

4. **Semjonova, A**., Kons, A., Belyakov, S., Mishnev, A., Bērziņš, A. Diversity and Similarity in Isonicotinamide Two-Component Phases with Alkyl Carboxylic Acids: Focus on Solvates. *Crystal Growth &* Design, **2024**, *24* (5), 2082-2093. (IF$_{2023}$ = 3.80)

   A. Semjonova carried out 90 % of the experimental work, contributed to writing the article (80%), prepared the experimental results according to the journal guidelines, as well as prepared the answers to the questions and remarks given by reviewers.

Conferences

- **Semjonova, A.,** Kons, A., Belyakovs, S., Mishnev, A., Bērziņš, A. A New Solvates of Isonicotinamide and Alkyl Carboxylic Acids. *University of Latvia 82nd conference,* Riga, Latvia, **2024.**

- **Semjonova, A.,** Bērziņš, A. Surfactant Provided Control of Crystallization Polymorphic Outcome and Stabilization of Metastable Polymorphs of 2,6-Dimethoxyphenylboronic Acid. *12th Bologna's convention on crystal forms*, Bologna, Italy, **2023.**

- **Semjonova, A.,** Bērziņš, A. Effect of structurally related additives on crystallization control of a highly polymorphous isonicotinamide. *BCA Spring meeting 2023*, Sheffield, United Kingdom, **2023**

- **Semjonova, A.,** Bērziņš, A. Controlling the polymorphic outcome of 2,6-dimethoxybenzoic acid crystallization using additives. *14th International Conference on Crystal Growth of Organic Materials*, Brussels, Belgium, **2022.**

- **Semjonova, A.,** Bērziņš, A. Effect of crystallization additives on the crystallization of isonicotinicamide polymorphs. *14th International Conference on Crystal Growth of Organic Materials*, Brussels, Belgium, **2022.**

- **Semjonova, A.,** Bērziņš, A. Effect of Crystallization Additives on Crystallization of 2,6-Dimethoxybenzoic Acid Polymorphs and Their Stability. *Understanding Crystallisation: Faraday Discussion*, York, United Kingdom (online), **2022.**

- **Semjonova, A.,** Bērziņš, A. Control possibilities of 2,6-dimetohxybenzoic acid conformational polymorphism using crystallization additives. *University of Latvia 80th conference,* Riga, Latvia (online), **2022.**

- **Semjonova, A.,** Bērziņš, A. Polymorphic outcome control in crystallization and stabilization of metastable forms using surfactants. *Materials Science and Applied Chemistry 2021,* Riga, Latvia (online), **2021.**

- **Semjonova, A.,** Bērziņš, A. Crystallization and stabilization of 2,6-dimethoxyphenylboronic acid metastable polymorph using surfactants. *EcoBalt 2021,* Riga, Latvia (online), **2021.**

- **Semjonova, A.;** Bērziņš, A. Characterization of 2,6-Dimethoxybenzoic Acid Polymorphs and Crystallization Control Possibilities with Crystallization Additives. *11th Crystal Forms @Bologna: Walking the walk of polymorphs, co-crystals and solvates,* Bologna, Italy (online), **2021.**

- **Semjonova, A.**, Bērziņš, A. Screening of Crystallization Additives for Polymorph Control of 2,6-Dimethoxybenzoic Acid. *University of Latvia 79th conference,* Riga, Latvia (online), **2021.**

- **Semjonova, A.**, Bērziņš, A. Influence of Crystallization Additives on Morphology of Selected Benzoic Acids – a Molecular Dynamics (MD) Simulation Study. The *2nd International Online Conference on Crystals,* online, **2020.**

- **Semjonova, A.**, Bērziņš, A. Influence of Crystallization Additives on Morphology of Selected Benzoic Acids – a Molecular Dynamics (MD) Simulation Study. *Materials Science and Applied Chemistry 2020,* Riga, Latvia (online), **2020.**
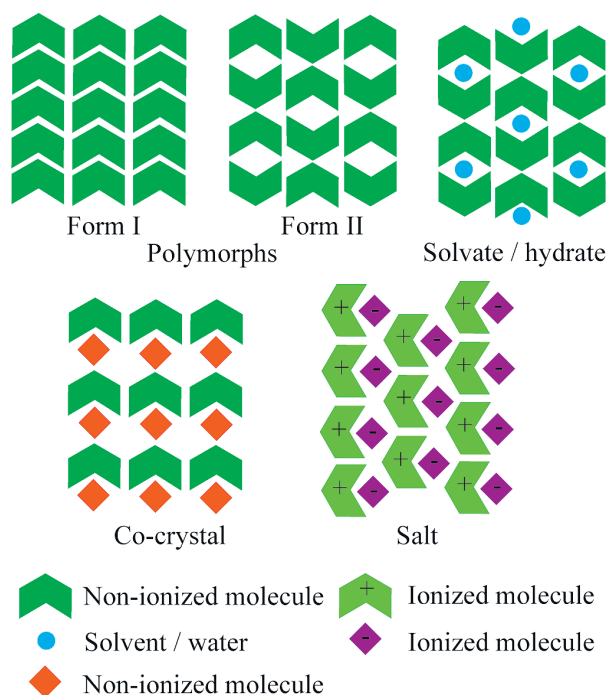
Other publications (not included in the work)

- **Semjonova, A.**; Bērziņš, A. Influence of Crystallization Additives on Morphology of Selected Benzoic Acids – a Molecular Dynamics (MD) Simulation Study. *Key Engineering Materials*, **2021**, 903, 22-27.

- Bērziņš, A.; **Semjonova, A.**; Actiņš, A.; Salvalaglio, M. Speciation of substituted benzoic acids in solution: evaluation of spectroscopic and computational methods for the identification of associates and their role in crystallization. *Crystal Growth & Design*, **2021**, 21, 9, 4823–4836.

1. THEORETICAL BACKGROUND

1.1. Polymorphism of active pharmaceutical ingredients

Polymorphism is the ability of a substances to crystallize in different crystal structures (see Figure 1.1.).[9] Polymorphs have identical chemical composition but differ by the molecule arrangement or conformation in the crystal structure. Solvate structure additionally contain stoichiometric or variable amounts of a solvent. Solvates containing water are named hydrates. Co-crystals are composed of two or more different non-ionized molecules in the same crystal structure in stoichiometric ratio, while the molecules in salts are ionized.[17] Solids with different crystal structures often have different physical properties, such as solubility,[4] dissolution rate,[18] stability[19] and bioavailability.[20] Therefore, crystal engineering opens new opportunities to obtain APIs with improved physicochemical properties.[21] Solvates and co-crystals often have better solubility and dissolution rate than phases formed by pure API and, therefore, increase bioavailability and drug efficacy,[22] synergistic effect and lower the necessary drug dose,[21] or just have more optimal properties for the manufacturing processes.[23] Change of the crystal form can also enhance the chemical stability of API.[24]

Form I   Form II
Polymorphs   Solvate / hydrate

Co-crystal   Salt

Non-ionized molecule   + Ionized molecule
Solvent / water   - Ionized molecule
Non-ionized molecule

Figure 1.1. **Schematic representation of different types of phases formed by active pharmaceutical ingredients.**

Polymorphic forms can be classified,[25] depending on differences in polymorphic structures:

- conformational polymorphism – polymorphs contain molecules with different molecular conformations; [26,27]

- synthon or hydrogen bond polymorphism – polymorphs have different hydrogen bond synthons in their structures; [25,28]

- configurational polymorphism – observed in substances whose different configurations or tautomers can form different crystal structures.[25]

- packing polymorphism – molecules in polymorphs have the same conformation, but different molecule packing.[29]

Control of the crystal phase is one of the most challenging steps in the drug production process in the pharmaceutical industry.[30] Before developing the finished dosage form, it is important to identify all possible crystalline forms and characterize their properties, because the choice of the dosage form, the required excipients and the dose of API itself depends on for the physical properties of the crystalline form.[31]

Concomitant crystallization occurs when at least two different polymorphs crystallize simultaneously.[32] This phenomenon is observed due to competing nucleation and growth rates of different polymorphs.[33] The concomitant crystallization are related to various kinetic and thermodynamic factors.[34] Most often, a mixture of different polymorphs is subjected for solvent-mediated phase transition (SMPT), and only the most stable polymorph can be observed in the final product.[3] In addition, it is required to check the stability of the selected crystalline phase in long-term storage. There have been several cases[35] where a new and more stable polymorph appeared many years after drug development. Such late appearance of a more stable polymorph often have caused problems for patients, from low drug efficacy to eventually disrupting the supply of medicines.[36]

Conventional crystal phase preparation methods are crystallization by cooling a solution, evaporation of a solution, precipitation, vapor diffusion etc. The obtained phase can depend on solvent used, cooling or evaporation rate, start and end temperature used for the cooling crystallization or evaporation temperature, concentration of solution (supersaturation) used and other variables.[9] Classical crystallization approaches, however, often do not provide crystallization of a pure polymorph. In such cases seeding is the most common approach to control the polymorph obtained, but also this does not always provide the desired crystalline form. Alternatively, other crystallization methods or approaches are introduced, for example, ultrasound-assisted crystallization,[37] laser-induced nucleation,[38] crystallization in gels[39] and in presence of additives[16] and templates.[40]

1.2. Crystallization additives for polymorphism control

Crystallization in presence of additives or templates is one of the empirical methods for controlling polymorphic outcomes. There are several approaches to crystallization with the presence of additives:[41]

- crystallization with insoluble additives or templates:
    - Langmuir monolayers;[14]
    - self-assembled monolayers (SAM);[15]
    - polymers;[42]
    - surfaces of other insoluble additives acting as templates;[43]
- crystallization with soluble additives.[44]

Langmuir monolayers and SAMs are efficient templates for control of the crystallization outcome but has to be designed for each specific crystal structure, and it is necessary to regenerate the monolayers after each crystallization, and often it is difficult to collect the obtained crystals without the impurities from the layer material.[45] Soluble additives can be divided in structurally similar (also known as tailor made additives) and structurally different from the compound which is being crystallized. Although it is easier to separate these additives from the crystals, sometimes they can integrate into the crystal structure.[46] Structurally related additives have been used to obtain metastable forms of paracetamol,[11] *para*-aminobenzoic acid,[47] benzamide,[48] etc. However, there are also risks in using structurally similar additives, as they can have pharmacological or even toxic effects, and because of the similar structure can incorporate in the obtained crystals, for example, by forming a solid solution.[49] Therefore, not all structurally related compounds can be used as additives to stabilize polymorphs of pharmaceutical products. Excipients used in the drug dosage forms can be employed as additives in the crystallization of the API,[44] as it would not be necessary to separate these additives after the crystallization because these additives (such as polymers, surfactants[50]) can be used in pharmaceutical products.

The use of crystallization additives may prevent concomitant crystallization and stabilize metastable forms,[51] promote their nucleation,[46] change the relative stability of polymorphs[52] or prevent nucleation of the stable form. Crystallization in presence of additives is widely used in natural crystallization and manufacturing processes, such as biomineralization, material synthesis.[53]

There are many possible mechanisms by which additives can control the outcomes of crystallization. For example:

- additives can work as nucleation sites;[10]

- additives can selectively adsorb to some of the crystal surface faces by inhibiting their growth and, therefore, the growth of this polymorph;[54]
- additives can also help to organize the crystallizable substance molecules to obtain the desired polymorph;[55]
- additives can lower the activation energy of nucleation.[34]

However, the exact mechanism for the control mechanism by the additives in most cases is still not explored.

1.3.   Crystallographic analysis and theoretical calculations

Nowadays, various crystallographic analysis tools and theoretical calculations are available and used to compare crystal structures and justify polymorphic outcome of crystallization.

The stability of conformers affects the stability of polymorphs and also determines the conformation in which molecules exist in solution, so it is necessary to determine which are the most stable conformers and what is the stability of conformers in crystalline structures. Determination of the stability of the conformers requires the geometry optimisation of individual molecules and energy calculations in vacuum or in a solvent continuum. This is nowadays normally done using a quantum mechanics approach by one of the density functional theory methods or *ab initio* electron correlation methods. [56]

An equally important factor affecting the stability of polymorphs is the intermolecular interactions present in the crystal structure.[57–59] This calculation requires the optimisation of the geometry of the periodic crystal structure, which is nowadays possible by density functional theory methods. Further calculation of the interaction energy between the molecules in the structure allows the determination of the total energy of the intermolecular interactions, for which either empirical,[60] semi-empirical [61,62] or *ab initio* [63] methods are used. The crystal lattice energy characterising the stability of polymorphs can be calculated either by summing the total intermolecular interaction energy and the relative conformer energy or simply as the difference between the crystal structure energy and the energy of isolated molecules in the gas phase adopting the global energy minimum geometry. Note, however, that the crystal lattice energy does not include the thermal effects and thus provides information on the relative stability of polymorphs at 0 K.[64]

Crystallographic analysis tools such as energy frameworks, Hirshfeld surfaces and their 2D fingerprint plots and full-interaction maps are used to compare crystalline structures (see Figure 1.2).
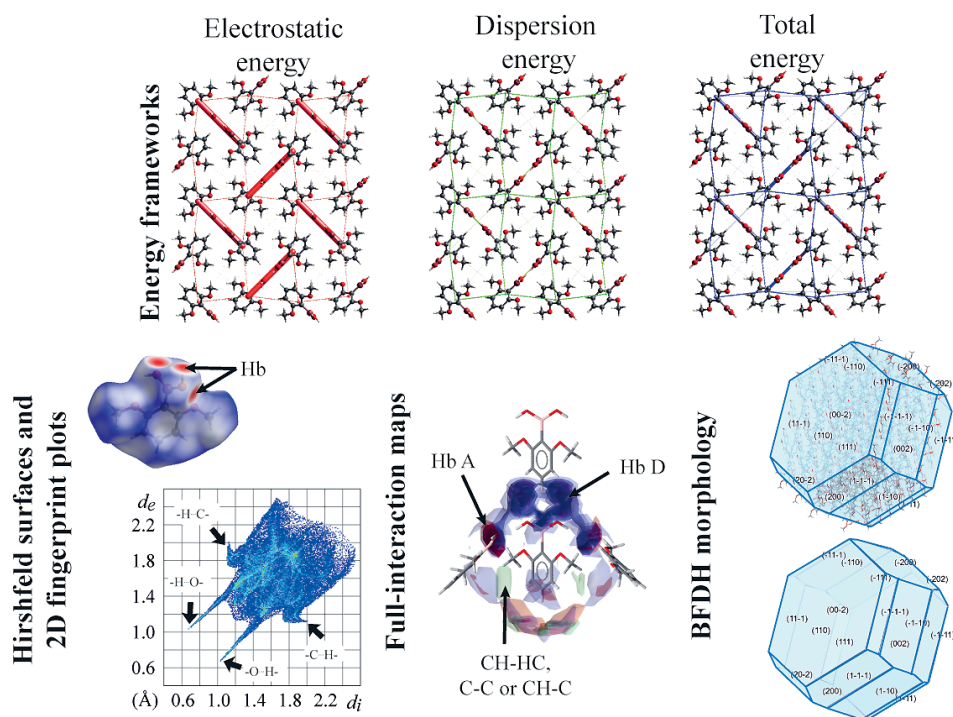
Figure 1.2. **Graphical representation of crystallographic analysis methods. Hb – hydrogen bond; Hb A – hydrogen bond acceptor; Hb D -hydrogen bond donor.**

Energy frameworks visualize the intermolecular interaction energy in crystal structures of polymorphs, further demonstrating the distribution of crystal lattice energy into different energy contributions (electrostatic and dispersion energy).[65] Hirshfeld surfaces provide information on intermolecular interactions and electron density in the structure, allowing a better understanding of differences in hydrogen bonding and other interactions in the structure, as well as in crystal packing.[66,67] Hirshfeld surface 2D fingerprint plots provide deeper insights into the interactions in the crystal structure and the contribution of specific interaction types.

Full-interaction maps (FIMs) visualize the regions around a molecule where, based on pre-extracted *IsoStar* interaction data from the Cambridge Structural Database (CSD),[68] intermolecular interactions are expected to occur, allowing to assess whether interaction preferences are satisfied in a structure. FIM analysis has been shown to allow the assessment of polymorph stability.[69,70]

Many physical properties of crystals depend on their morphology. Several models exist for predicting crystal morphology, but the most commonly used is the **B**ravais-**F**riedel-**D**onnay-**H**arker (BFDH) model, because of the easier approach used to predict the morphology compared to other models. This model uses an inversely proportional relationship between interplanar spacing and growth rate, but does not take into account kinetic factors and the role of solvent or additives on the crystal growth.[71] Since it can be assumed that if there are regions

in the structure where intermolecular interactions are not satisfied based on the FIM, then additional interactions provided by the additives may stabilize the polymorph. However, such an effect can only occur on the crystal surface, hence it is beneficial to use FIMs projected onto the BFDH morphology. Despite the overall inaccuracy of the BFDH model, FIM analysis combined with BFDH morphology can predict potential adsorption sites for additive molecules.[68]

1.4.   The studied compounds

In this study three model substances were investigated: 2,6-dimethoxybenzoic acid (2,6MeOBA), 2,6-dimethoxyphenylboronic acid (MPBA) and isonicotinamide (INA) (see Figure 1.3.).
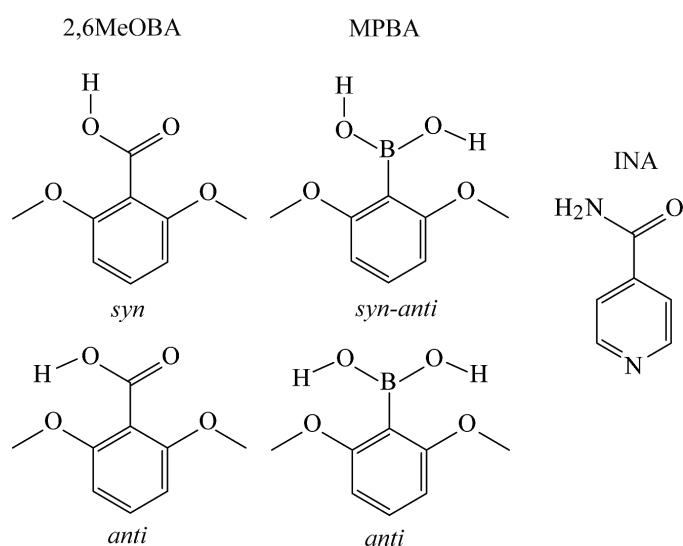

Figure 1.3. **Structural formulas and conformations of the model substances used in the study.**

For all three model substances, crystal structures of at least two polymorphs in which different supramolecular synthons are found (dimers and chains, see Figure 1.4. for schematic differences between these synthons) have been published in CSD. The existence of polymorphs containing different supramolecular synthons was used as a criteria for the choice of the model substances because the polymorphs containing different molecular synthons were expected to be more easily controllable by the additives assuming the importance of intermolecular interactions in the control mechanism.

Dimer   Chain
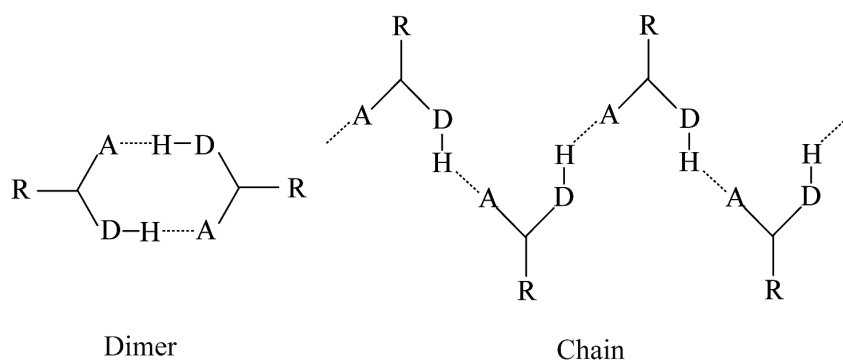
Figure 1.4. **Schematic representation of dimer and chain synthons observed in the crystal structures of all model substances. A – hydrogen bond acceptor; D – hydrogen bond donor.**

2,6MeOBA is reported to crystallize in three polymorphs.[26,72–74] Form I is the thermodynamically stable polymorph.[26,74] It contains 2,6MeOBA molecules in the *anti*-planar conformation linked by hydrogen-bonded chains forming catemer.[72,75] Form II and Form III contain 2,6MeOBA molecules in a *syn*-planar conformation that forms carboxylic acid homodimers.[26,73,74] Besides, phenylboronic acid was successfully used as an additive to crystallize the form II in one of the previous studies.[73]

MPBA has two known polymorphs.[76] Form I is the thermodynamically stable polymorph. Form I contains typical hydrogen bonded homodimers of boronic acid that adopts *syn-anti*-conformation, whereas Form II contains an unusual hydrogen-bonded boronic acid synthon formed by three molecules.

INA is reported to crystallize in six polymorphs,[77–80] two monohydrates[81] and few solvates: acetic,[28] formic,[82] and propionic[83] acid as well as formamide[84] solvates. Form I contains amide homodimers arranged in isolated corrugated sheets.[78] In contrast, all the other INA polymorphs contain hydrogen bonded chains formed by amide functionals and by amide and pyridine moieties.[77–80] Form I has been shown to be the stable polymorph in ambient conditions.[77,79] Although crystallization of INA in presence of additives and templates has been studied previously,[43,79,80] selective and repeatable crystallization was not achieved for any of the polymorphs

2. EXPERIMENTAL SECTION

Solid phase characterization and structure determination

Routine solid phase identification was performed on a *Bruker D8 Advance* powder X-ray diffractometer (PXRD) using copper radiation (Cu K$_\alpha$), equipped with a *LynxEye* position sensitive detector. The patterns were recorded from 3º to 35º on the 2θ scale using the scan speed of 0.2 s / 0.02º. To prevent the desolvation of INA solvates, during the analysis the samples were covered with a 10 μm polyethylene film. Quantification of polymorphic forms was performed with Rietveld refinement using Profex 4.3.6.

The PXRD patterns for crystal structure determination were measured on a *Bruker D8 Discover* diffractometer using copper radiation (Cu K$_\alpha$), equipped with a *LynxEye* position sensitive detector in transmission mode. Samples were sealed in rotating (60 rpm) borosilicate glass capillaries of 0.5 mm outer diameter (Hilgenberg glass No. 10), and a capillary sample stage with upper and lower knife edges were used. The diffraction patterns were collected using 36 s / 0.01° scanning speed from 3° to 70° on the 2θ scale. Indexing, space group determination, and structure solution from PXRD data were performed using *EXPO2014*. [The] best structure solution was then used for Rietveld refinement using *TOPAS5*.

Single crystals for structure determination were investigated on a *Rigaku XtaLAB Synergy-S dualflex* diffractometer (SCXRD) equipped with *HyPix6000* detector and a microfocus sealed X-ray tube with copper radiation (Cu K$_\alpha$). Single crystals were fixed with oil in a nylon loop of a magnetic *CryoCap* and set on a goniometer head. The structures were solved with the *ShelXT* program using Intrinsic Phasing and refined with the full-matrix least-squares method using *SHELXL*. (Latvian Institute of Organic Synthesis, Riga, Latvia)

The differential scanning calorimetry / thermogravimetry (DSC/TG) analysis to characterize the solid phases and to determine the stoichiometry of the solvent present in the solvates were performed with a *Mettler Toledo TGA/DSC2* instrument. The heating of the samples from 25 to 200 °C was carried out at a heating rate of 10 °C min^{-1} in nitrogen atmosphere. DSC analysis was performed using a *TA Instruments DSC 25* calorimeter. The heating of the samples from 25 to 200 °C was carried out at a heating rate of 10 °C·min^{-1} or 2 °C·min^{-1} in nitrogen atmosphere.

Selection of solvent and crystallization additives

Common organic solvents chosen from different solvent classes were selected for the cooling and evaporation crystallization of model substances. Additionally, alkyl carboxylic acids and few other uncommon solvents were selected for solid phase screening of INA because INA is reported to form acetic acid solvate (S$_{AA}$) and propionic acid disolvate (S$_{dPA}$). After

evaluation of the crystallization result few solvents were selected for further investigation of the effect of supersaturation and cooling rate on the crystallization outcome. They selection was based on the following criteria:

- model substance solubility is between 5 and 50 mg mL^{-1};
- for 2,6MeOBA: it is possible to obtain the desired metastable polymorph in a mixture with the stable polymorph;
- for MPBA: only the stable polymorph could be obtained;
- for INA: a mixture of several polymorphs could be obtained.

Then, in limited number of solvents, the effect of different crystallization additives on the polymorphic outcome was determined. Surfactants, polymers, and different molecular compounds with diverse possibilities to form intermolecular interactions were selected as additives. From all the tested additive, few additives showing the highest ability to promote the crystallization of the metastable polymorph (for 2,6MeOBA and MPBA) or preventing the concomitant crystallization and promoting the crystallization of metastable polymorph (for INA) were selected for extensive studies.

Crystallization experiments

Crystallization and solvent mediated phase transformation (SMPT) experiments under controlled conditions as well as solubility determination was carried out using the automatic crystallization equipment *Technobis Crystal16*. The temperature range from 5 to 100°C, heating and cooling rate from 0.1 to 20 °C min^{-1}, and stirring speed from 0 to 1250 rpm was used.

Theoretical calculations

ConQuest 2022.2.0 was used to perform crystal structure searches in the CSD (CSD version 5.43). Quantum Espresso 6.4.1 was used for the optimization of the crystal structure geometries, while the molecular geometry optimization was performed with Gaussian09 Revision D.01. The ISOCIF tool (version 3.1.0) was used to search for the highest symmetry of the geometry optimized crystal structures. Lattice energy calculation and construction of Hirshfeld surfaces and their 3D fingerprint plots were done using CrystalExplorer21. Mercury2020.3.0 was used for hydrogen bond identification and simulation of full interaction maps (FIM) and crystal morphologies by Bravais–Friedel–Donnay–Harker (BFDH) method. Molecular packaging of polymorphs was compared with CrystalCMP using crystal structures from the CSD database. The obtained solubility temperature dependence was described with the van't Hoff equation using the linear regression implemented in the Microsoft Excel Linest function.

3. RESULTS AND DISCUSSION

3.1. Crystallization from pure solvents

Initially for all the model substances it is necessary to determine which polymorphs can be obtained using different crystallization techniques and different solvents selected for the study. Therefore, each model substance underwent an extensive polymorph screening from a large range of solvents using cooling and evaporation crystallization methods under different temperatures. The list of used solvents for each model substance varies depending on the previously obtained phases, solubility, and availability in the laboratory.

In most of the performed 2,6MeOBA cooling crystallization experiments Form I was obtained, although impurity of Form III was sometimes present (see Table 3.1.). In the evaporation crystallization experiments the polymorph obtained correlated with the temperature: at lower temperature (5 °C) in most of the experiments Form I was obtained, frequently with some impurities of Form III. However, at higher temperature (50 °C) Form III with impurity of Form I was obtained.

In contrast, in almost all MPBA crystallization experiments, particularly from aprotic solvents, pure Form I was obtained (see Table 3.1.). However, from polar protic solvent (isopropanol (IPA), methanol, and isobutanol) it was possible to obtain the metastable MPBA Form II. Besides the already known polymorphs, a new MPBA polymorph, designated as Form III, was obtained. Form III crystallized together with Form II in evaporation crystallization from isopropanol and heptanol. Unfortunately, the attempts to determine the crystal structure of Form III were unsuccessful, as crystals suitable for SCXRD analysis were not obtained and the bulk sample contained an impurity of Form II (see Figure 3.1.).

Crystallization results of INA were completely different from the other two model substances (see Table 3.1.). In most of the conditions several INA polymorphs were present in the obtained crystallization products which agrees with the results from other studies.[80,85] Usually, Forms II and VI or Forms II and IV crystallized together, but from some solvents a mixture of all these three forms was obtained. Moreover, despite Form I is determined to be the stable polymorph,[77,79,85] it was rarely obtained in the crystallization, whereas Form II, the high temperature polymorph, was the most frequently obtained crystallization product. In crystallization from acetic acid (AA) and formamide (FAM) the already known INA solvates[28,84] were obtained. Additionally, crystallization products with distinct and from the known INA polymorphs or solvates differing PXRD patterns (see Figure 3.1.) were obtained in cooling crystallization from formic acid (FA), propionic acid (PA), butyric acid (BA), and 2,2,2-trifluoroethanol (TFE). The new crystalline forms obtained were analyzed by

DSC/TG and their structures were determined. The obtained results show that these forms are INA solvates (see section 3.2.). In Table 3.1. for all the model substances the newly obtained crystalline forms are market with an asterisk.
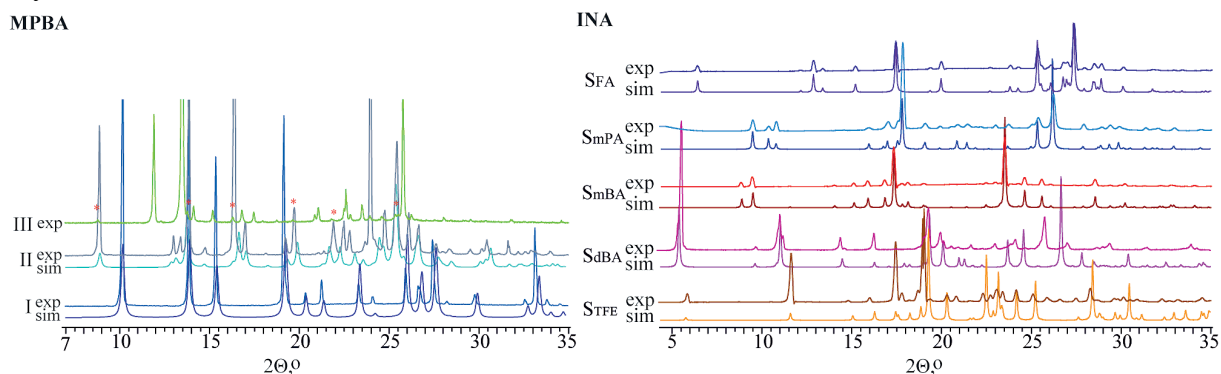
Figure 3.1. **Experimental and from crystal structures simulated PXRD patterns of MPBA polymorphs and INA solvates. For MPBA the Form II impurity in the Form III sample is marked with red asterisks.**

For more detailed investigation of the effect of cooling rate on the crystallization polymorphic outcome the below mentioned solvents were selected:

- water (for 2,6MeOBA);
- toluene (for MPBA);
- IPA, 1,4-dioxane, nitromethane, and acetone (for INA).

Table 3.1.

Summary of the crystallization polymorphic outcome of the model substances from pure solvents.

Solvent	Cooling			Evaporation						
				5 °C	25 °C			50 °C		
	2,6MeOBA	MPBA	INA	2,6MeOBA	2,6MeOBA	MPBA	INA	2,6MeOBA	MPBA	INA
1,4-Dioxane	I + III↓	I	III	III	I + III	I	II + VI	III	I	II
Methanol	I + III↓	II	II + IV	III	I↓ + II + III	II	II + IV + VI	I	I	II + IV
Acetone	I	I	I	I + III	I	I	II + IV + VI	III	I	II + IV + VI
Tetrahydrofuran (THF)	I	I	II + VI	I + III	I + III	I	II + III	I↓ + III	I	II + IV + VI
Isopropanol (IPA)	I	I	II + IV + III + VI	I	I + III↓	II + III	III	III	I + II	II + III
Acetonitrile	I	I	II + IV + VI	I + III↓	I + III	I	I + II + IV	I / III	I	II + IV
4-Methyl-2-pentanone	I	I	II + VI	I	I + III↓	I	II + IV	I + III	I	II + IV
Methyl acetate	I	N/A	N/A	I + III↓	I + III	N/A	N/A	I↓ + III	N/A	N/A
terc-Butyl methyl ether	I	I	II + VI	I	I	I	IV + VI	I + III	I	IV + VI
Water	I	I	N/A	I	I	I	N/A	I	I	N/A
Toluene	I	I	N/A	N/A	I + III	I	N/A	N/A	I	N/A
Chloroform	I	I	II + IV	N/A	I + III↓	I	II + IV + VI	N/A	I	IV + VI
Dichloromethane	I + III↓	I	N/A	N/A	I + III↓	I	N/A	N/A	I	N/A
Ethyl acetate	I	I	N/A	N/A	I	I	N/A	N/A	I	N/A
Formic acid (FA)	I	N/A	S_{FA}	N/A	I	N/A	N/A	N/A	N/A	N/A
Nitromethane	I	I	II + IV	N/A	I	I	II + IV	N/A	I	II + IV
o-Xylene	N/A	I	N/A	N/A	N/A	I	N/A	N/A	I	N/A
Diethyl carbonate	N/A	I	II + IV + VI	N/A	N/A	I	II + IV + VI	N/A	I	II + IV + VI
Cyclohexanol	N/A	I	N/A	N/A	N/A	I	N/A	N/A	I	N/A
2,2,2-Trifluoroethanol	N/A	I	S_{TFE}*	N/A	N/A	I	N/A	N/A	I + II	N/A
Heptanol	N/A	I	N/A	N/A	N/A	II + III	N/A	N/A	I	N/A
Isopentanol	N/A	I	N/A	N/A	N/A	I + II	N/A	N/A	I	N/A
n-Butyl acetate	N/A	N/A	II + IV	N/A	N/A	N/A	IV + VI	N/A	N/A	II + IV + VI
Acetic acid (AA)	N/A	N/A	S_{AA}	N/A	N/A	N/A	N/A	N/A	N/A	N/A
Formamide (FAM)	N/A	N/A	S_{FAM}	N/A	N/A	N/A	N/A	N/A	N/A	N/A
Propionic acid (PA)	N/A	N/A	S_{mPA}* (5 °C); S_{dPA} (-10 °C)	N/A	N/A	N/A	N/A	N/A	N/A	N/A
Butyric acid (BA)	N/A	N/A	S_{dBA}*	N/A	N/A	N/A	N/A	N/A	N/A	N/A

Repeated crystallizations of 2,6MeOBA from pure water with immediate filtration and analysis of the obtained crystals showed that a mixture of Forms I and III is obtained in the crystallization, followed by a SMPT to Form I if the crystallization product is kept in a suspension. Therefore, only Form I was observed in the above-described crystallization experiments. Mixture of all three polymorphs was obtained in crystallization from a highly concentrated pure water solution with the fastest cooling rate (see Figure 3.2.), while in all four experiments using the lowest cooling rate Form III was obtained, even though at a slower cooling rate the formation of the thermodynamically stable Form I was expected. The phase transition to Form I was prevented as the crystals formed near the water surface and formed large agglomerates. In contrast, in crystallization of MPBA from toluene the cooling rate did not affect the polymorphic outcome, and Form I was always obtained in the crystallization.

Different polymorphic outcomes were observed in crystallization of INA using different cooling rates. Pure Form III was obtained from 1,4-dioxane using the fastest cooling rate, but the decrease of the cooling rate facilitated formation of the more stable Forms II and VI.[85] Mixtures of different polymorphs containing Form III were obtained from IPA using the fastest cooling rates, but using lower cooling rates more stable forms were obtained. In contrast, Form III did not crystallize from nitromethane or acetone.

Overall, except for the MPBA, the obtained results agree with the Ostwald's rule of stages,[86] as instead of the nucleation of the most stable form the polymorph corresponding to the closest energy nucleates.
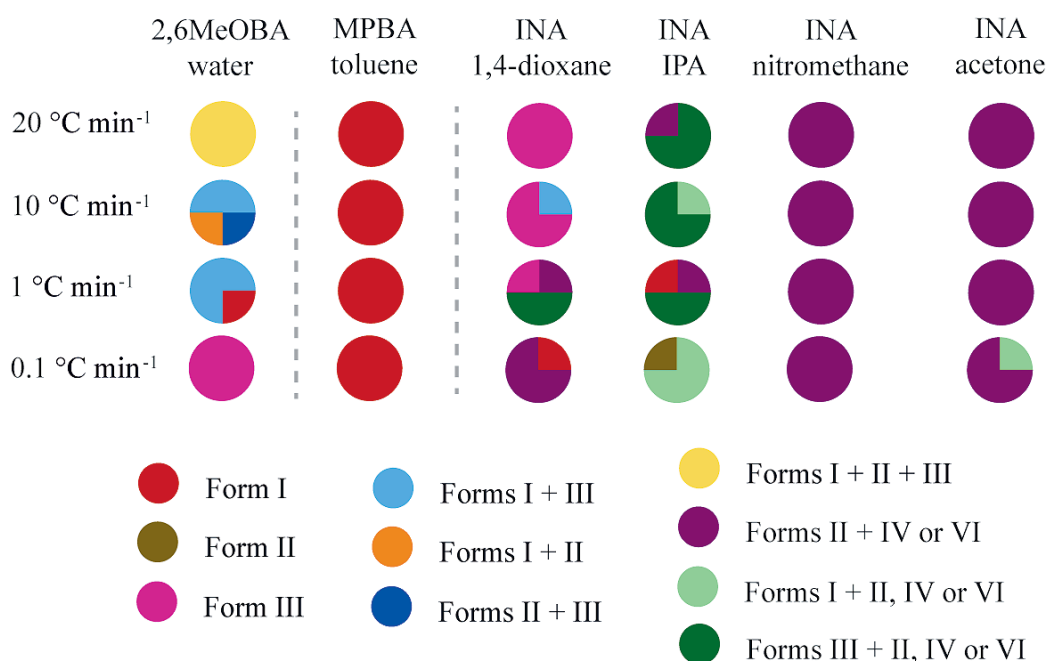
Figure 3.2. **Summary of polymorphs obtained using different cooling rates and a stirring rate of 900 RPM. Each ¼ of the pie chart represents one of the parallel experiments.**

3.2. Diversity and similarity in isonicotinamide solvates

Four new INA solvates were obtained as part of this study: PA monosolvate (S_{mPA}), BA monosolvate (S_{mBA}) and disolvate (S_{dBA}), and TFE solvate (S_{TFE}). In addition, the already known FA solvate (S_{FA}),[82] FAM solvate (S_{FAM}), AA solvate (S_{AA}) and PA disolvate (S_{dPA}) were obtained and analysed. The crystal structure of S_{FA} was also determined, as it is not deposited in the CSD.Click or tap here to enter text. Upon storage at ambient temperature all the solvates desolvate by forming a mixture of INA Forms II, IV and VI. All the INA solvates crystallize either in monoclinic or triclinic crystal system (see Table 3.2.)

Table 3.2.

Crystallographic data of INA solvates determined in this study.

	S_{FA}	S_{mPA}	S_{mBA}	S_{dBA}	S_{TFE}
CSD identifier	2236716	2236717	2236718	2302845	2237737
Formula	$C_6H_6N_2O \cdot$ CH_2O_2	$C_6H_6N_2O \cdot$ $C_3H_6O_2$	$C_6H_6N_2O \cdot$ $C_4H_8O_2$	$C_6H_6N_2O \cdot$ $2C_4H_8O_2$	$C_6H_6N_2O \cdot$ $C_2H_3F_3O$
Method of structure solution	Powder	Powder	Powder	Single crystal	Single crystal
Space group	$P2_1/c$	$P\bar{1}$	$C2/c$	$P\bar{1}$	$P2_1/c$
a, Å	3.8177(16)	5.88988	21.806(15)	5.24839(10)	15.2031(9)
b, Å	27.480(11)	9.685489	10.505(7)	9.28144(13)	5.3244(12)
c, Å	7.565(3)	10.19433	11.190(8)	16.3015(3)	11.7225(7)
α, deg	90	112.4861	90	89.7515(12)	90
β, deg	95.1158(12)	93.0070	114.2902(17)	89.8978(14)	91.303(6)
γ, deg	90	105.726	90	80.7138(14)	90

In INA solvates two distinct types of hydrogen bonding motifs are observed, which can further be divided into five subtypes based on additional hydrogen bonding and relative arrangement of the hydrogen bonded units. The first hydrogen bonding motif contains typical INA $R_2^2(8)$ homodimers (see Figure 3.4.), therefore, resulting in hydrogen bonded tetramers acid···INA dimer···acid. Isolated hydrogen bonded tetramers, as observed in S_{mPA}, is classified here as hydrogen bonding type A1. In other structures, however, the hydrogen bonded tetramers solvent···INA dimer···solvent are additionally linked to other tetramers by hydrogen bonds. The resulting hydrogen bonding is classified as type A2 if the linked tetramers lay in the same plane, as observed in S_{FA} and S_{AA}, or as type A3 if the linked tetramers are lying perpendicularly to each other by creating a packaging with adjacent molecule planes arranged perpendicular to each other, as observed in S_{mBA} and also S_{TFE}. In type A2 (S_{FA} and S_{AA}) the tetramers are essentially parallel to each other and form tetramer layers. Moreover, because of the different relative arrangement of INA molecules and acid molecules in the tetramers FA···INA dimer···FA fragments are linked by $C_2^2(11)$ chains and forms $R_6^6(26)$ rings, whereas

AA⋯INA dimer⋯AA fragments by $C_3^3(13)$ chains and forms $R_4^4(22)$ rings. In S_{TFE} and S_{mBA} (belonging to type A3) each tetramer is bonded to almost perpendicularly arranged adjacent tetramers.

The second motif type B is substantially different as INA homodimers $R_2^2(8)$ are not employed (see Figure 3.4.). In both subtypes of B INA forms $R_2^2(8)$ heterodimers with the carboxylic acid (see Figure 3.4.), and this dimer is linked to another carboxylic acid by a hydrogen bond resulting in a trimer acid⋯INA:acid. In hydrogen bonding type B1 (S_{dBA}) the solvent⋯INA:solvent trimer is linked with hydrogen bonds to an adjacent trimer related by the symmetry centre and forms $R_4^4(22)$ rings. In type B2, however, trimers are hydrogen bonded to two other perpendicularly aligned trimers as observed in S_{dPA}, thereby, resulting in similar packing to that observed in the structures containing type A3 motif.

$R_2^2(8)$ homodimers

S_{mPA}

A - tetramers

S_{AA}

Type A1

S_{FA}

$R_2^2(8)$ INA homodimers	
$R_2^2(8)$ INA:acid heterodimers	
$R_6^6(26)$ tetramer rings	
$R_4^4(22)$ tetramer rings	
$R_4^4(22)$ trimer rings	
Hydrogen bond	
$C_2^2(11)$ tetramer chain	
$C_3^3(13)$ tetramer chain	

Type A2

S_{TFE}

S_{mBA}

Type A3

$R_2^2(8)$ heterodimers

B - trimers

Type B1
S_{dBA}

Type B2
S_{dPA}

Figure 3.4. **Hydrogen bonding type A and type B as observed in INA solvates.**

72

The hydrogen bonding in S$_{FAM}$ is different from that in other INA solvates and, therefore, does not correspond to the described hydrogen bonding types (see Figure 3.5.). In this structure two different $R_2^2(8)$ homodimers are formed by INA and FAM, and these homodimers are linked to each other by hydrogen bonds. This results in a packing where FAM homodimers connect the layer of the INA molecules.

$R_2^2(8)$ INA homodimers $R_2^2(8)$ FAM homodimers
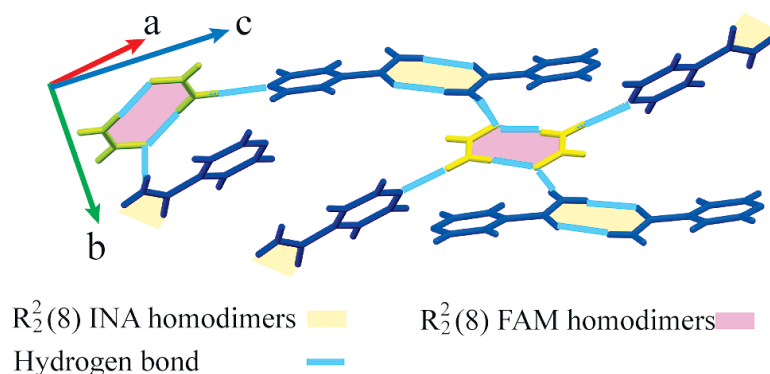
Hydrogen bond

Figure 3.5. **Hydrogen bonding in S$_{FAM}$.**

In summary, all of these solvates have similar hydrogen bond patterns. Extension of the set of the analysed structures by including also INA co-crystals (see the results and detailed discussion in publication IV) allowed to conclude that almost all INA alkyl carboxylic acid solvates and co-crystals crystallize in structures with highly similar hydrogen bond patterns, which in general could allow prediction of intermolecular interactions and molecular packaging for new solvates/co-crystals with structurally similar solvents/co-formers.

3.3. Polymorphic outcome in presence of crystallization additives

The polymorphic outcome of crystallization in the presence of additives is affected by complex and not fully understood interactions between the compound being crystallized, the solvent, and the additives, as well as by the crystallization conditions (e.g., supersaturation, cooling and stirring rate). The polymorphic outcome can be altered by changes in any of these aspects. In this study, crystallization in the presence of additives was investigated by changing the crystallization conditions to better understand the role of the additives on the crystallization polymorphic outcome.

This part of the research was a continuation of the previously described experiments aimed at identifying which additives would allow crystallization of the metastable forms. Therefore, for each model substance at least two solvents selected based on the preliminary crystallization experiments and more than 10 additives with different intermolecular interaction possibilities were tested (see Table 3.3.).

Table 3.3.

Summary of the crystallization additives and solvents used for each of the model substances.

Additive	2,6MeOBA			MPBA		INA	
	THF	acetonitrile	water	toluene	water	1,4-dioxane	IPA
Polyethylene glycol (PEG) 6000	√	√	√	√	√	√	√
Hydroxypropyl cellulose (HPC)			√	√	√	√	
MPBA			√				
Octyl β-D-glucopyranoside (OGP)	√	√	√	√	√	√	√
Polysorbate 80 (Poly80)	√	√	√	√		√	√
Sorbitan laurate (Span 20); Polysorbate 20 (Tween 20)	√	√		√		√	√
4-Carboxyphenylboronic acid (4CPBA)			√		√	√	√
2-Picolinic acid (2PA)				√		√	√
Naphthalene-1,5-diol (ND)						√	√
Benzene-1,2,3-triol (Btriol)					√	√	√
Pholoroglucinol (PhGlu); Nicotinic acid (NA); 5-Hydroxy-2-nitrobenzoic acid (5OH2NBA).						√	√
Polycaprolactone	√	√				√	√
Polyvinyl chloride	√	√				√	
Bis(2-hydroxyethyl)amino-tris(hydroxymethyl)methane			√		√	√	√
trans-Stilbene				√		√	√
Poly(tetrahydrofuran), Polypropylene glycol				√		√	√
4-Iodinephenylboronic acid; Glycine; NH_4Cl; Poly(acrylic acid); Poly(acrylic amide); Sodium carboxymethyl cellulose			√		√		
Cellulose acetate			√			√	
Poly(methyl methacrylate)				√		√	
2,6MeOBA, Phenylboronic acid				√	√		
PEG 200; Polyurethane; 1,3-Diphenylurea						√	√
Hydroxypropylmethyl cellulose; Microcrystalline cellulose			√				
PEG 600; Salicylic acid; Polyethene; Polystyrene 2-Hydroxyphenylboronic acid;				√			
Lactose					√		
2-Amino-2-(hydroxymethyl) propane-1,3-diol							√

The additives and solvents chosen for more extensive research along with the resulting effect on the polymorphic outcomes are summarized in Table 3.4., and the molecular structures of the selected additives for each model substance are shown in Figure 3.6.

Table 3.4.

The additives, solvents and crystallization methods chosen for more extensive research along with the resulting effect on the polymorphic outcome.

	2,6MeOBA	MPBA	INA			
Solvent	water	toluene	IPA	1,4-dioxane	nitromethane	acetone
Method	cooling	evaporation	cooling			
Additives	PEG 6000, HPC, MPBA	OGP, Poly80, Span 20, Tween 20	4CPBA, 2PA, ND, Btriol, PhGlu, NA, 5OH2NBA	4CPBA, 2PA, ND		
Polymorphic outcome	↑Form III	Form II	↑Form III	↑Form III; ↓polymorph mixtures	-	
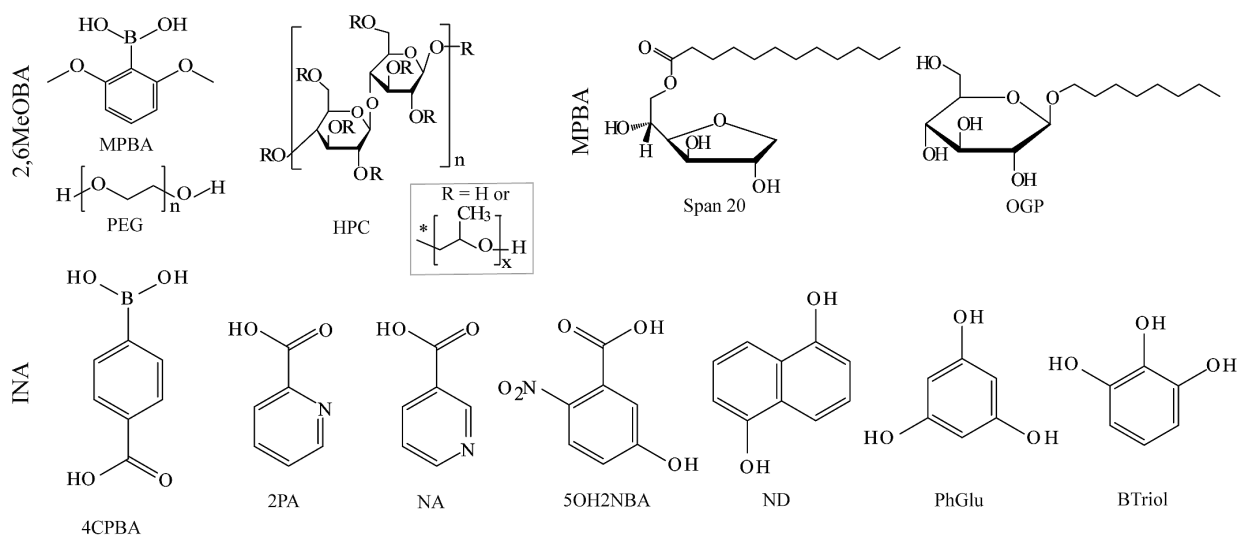
Figure 3.6. **Molecular structures of the selected additives for crystallization of the model substances.**

Detailed crystallization experiments performed in the presence of additives were selected based on the results obtained and therefore were different for each of the model substances:

- crystallization using various cooling speed (2,6MeOBA, INA);
- crystallization using various additive quantity (2,6MeOBA);
- use of various crystallization techniques and solvents (MPBA);
- crystallization using various stirring (agitation) rates (INA).

3.3.1. Polymorphic outcome of crystallization of 2,6-dimethoxybenzoic acid

In most of the crystallizations by using PEG and MPBA (see Figure 3.7.) as additives, a mixture of Forms I and III was obtained. In contrast, pure Form III was the most frequent crystallization product by using HPC as an additive at both additive concentrations. The formation of Form III was facilitated by the fastest cooling rates. Interestingly, at the slowest cooling rate, additives promoted crystallization of Form I. Use of 0.5% HPC suspension and 2,6MeOBA solution with lower concentration (supersaturation is designed as c/c^*, where c is the initial concentration and c^* is the solubility at 25 °C) promoted crystallization of Form III more clearly if compared to the crystallization experiments using 0.1% HPC solution and a higher concentration of 2,6MeOBA. It is possible that under the former conditions more HPC molecules could interact with 2,6MeOBA in heterogeneous crystallization and stabilize the *syn* conformation during nucleation, which in general is similar to the findings of Lin et al.[87] Also PEG has the potential to control the crystallization outcome, if a highly concentrated solution is crystallized using a moderately slow cooling rate. In general, however, the tested additives do not provide fully selective crystallization. Crystallizations in the presence of PEG with a cooling rate of 20 and 1 °C·min⁻¹ and in the presence of HPC with 20 and 10 °C·min⁻¹ were selected for further studies to test the effect of the amount of additive on the crystallization outcome.
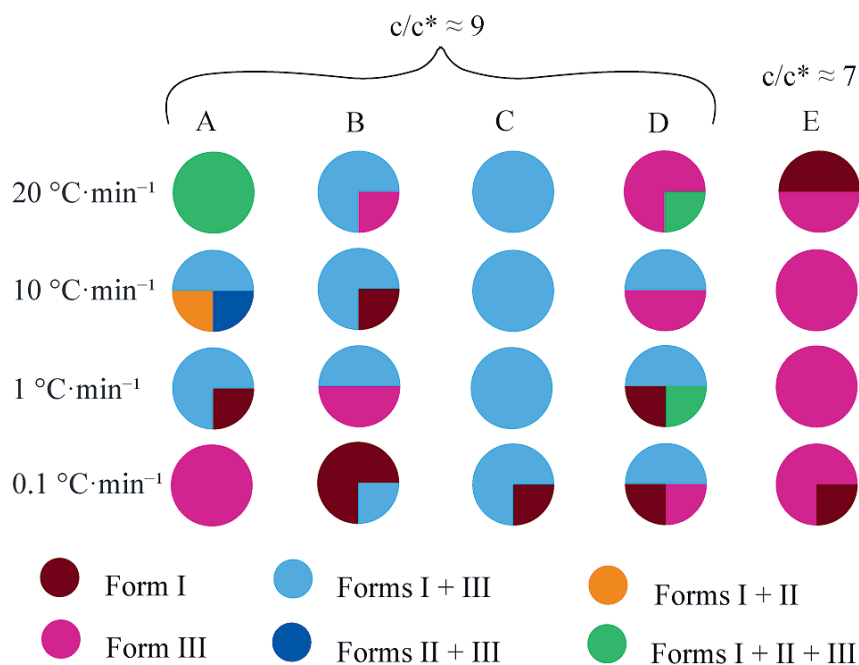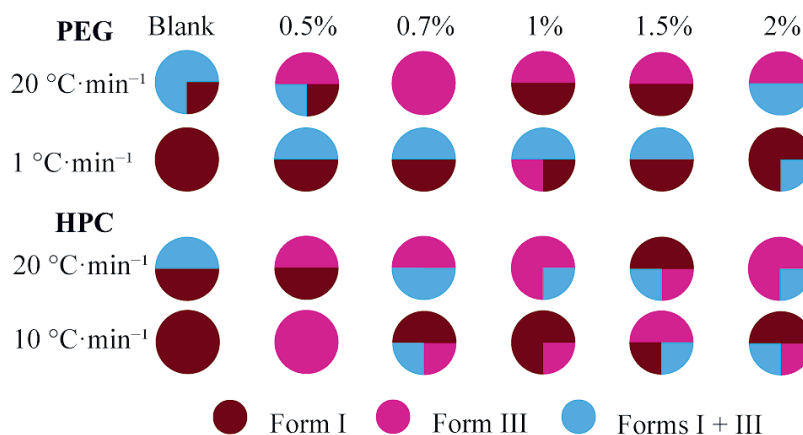

Figure 3.7. **Polymorphic outcome of the 2,6MeOBA crystallization experiments from water using different additives and cooling rates. Each ¼ of the pie chart represents one of the parallel experiments.**

In most of the crystallizations using both additives and the fastest cooling rate Form III was obtained (see Figure 3.8.). Again, the presence of additives did not provide selective crystallization of one of the polymorphs. Nevertheless, concomitant crystallization of both polymorphs was less frequent in the presence of HPC than in the presence of PEG. No clear correlation between the amount of additive selected and the crystallization outcome was observed.

Figure 3.8. **Polymorphic outcome of the 2,6MeOBA crystallization experiments from water in the presence of different quantities of additives. Each ¼ of the pie chart represents one of the parallel experiments.**

3.3.2. *Polymorphic outcome of crystallization of 2,6-dimethoxyphenylboronic acid*

In the cooling crystallization with the selected additives almost exclusively Form I was obtained (see Figure 3.9.). In contrast, Form II, Form III, or their mixture was obtained in evaporation crystallization in the presence of Span 20, Tween 20, and OGP. Moreover, the presence of Span 20 and OGP stabilized Form II, as in the presence of these two surfactants it was stable for up to one month. However, evaporation with stirring prevented crystallization of the metastable forms. Among the tested, the best conditions for obtaining the metastable forms were solvent evaporation at 50 °C without stirring. Under these conditions, the presence of Span 20 and OGP in the initial solution resulted in crystallization actually occurring from a MPBA solution in the surfactant after the evaporation of the initial solvent when the obtained mixture was cooled to room temperature. The crystals obtained in this procedure were very small, and pure polymorph III crystallized in the presence of Span 20 and OGP.
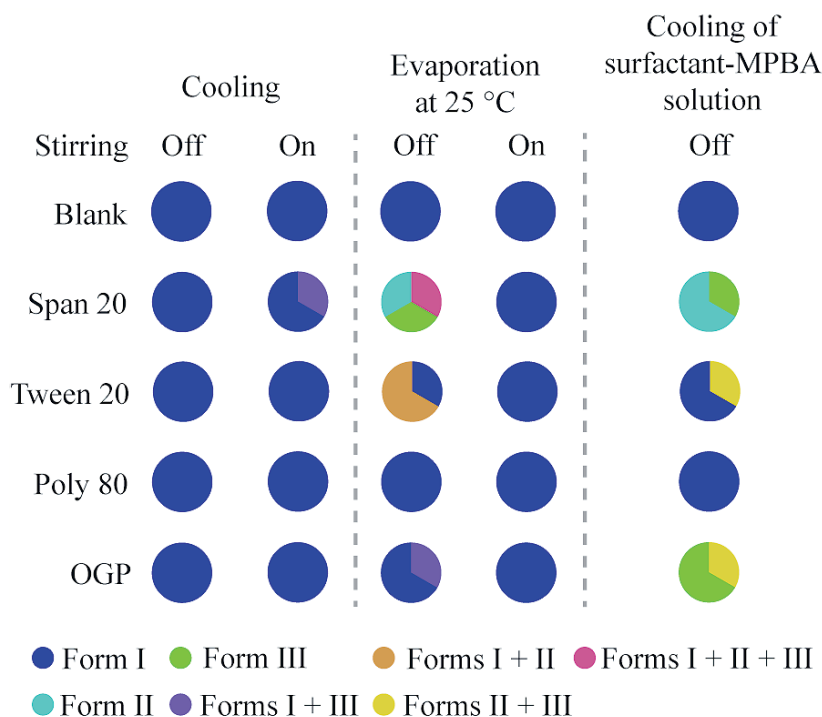
Figure 3.9. **Polymorphic outcome in MPBA crystallization from toluene in the presence of surfactants using different crystallization methods. Each ⅓ of the circle represents one of the parallel experiments.**

MPBA–Span 20 solution was also obtained using other solvents to determine whether the initial solvent has a role on the polymorph obtained if the crystallization is performed in this way. Pure Form II was obtained in all 15 experiments performed using acetone, IPA, THF, acetonitrile and toluene. Therefore, the formation of Form II under these conditions is purely determined by the Span 20.

3.3.3. *Polymorphic outcome of crystallization of isonicotinamide*

Almost all the selected additives facilitated the crystallization of Form III from IPA and 1,4-dioxane when the faster cooling rates were used (see Figure 3.10.). 2PA showed the highest ability to provide crystallization of Form III from IPA, as Form III was obtained even using the cooling rate of 1 °C min^{-1}, at which in presence of other additives mostly mixtures of Forms II, IV and VI were obtained. ND showed the best ability to maintain Form III even in slow cooling rates from 1,4-dioxane. 4CPBA facilitated the nucleation of Form I from this solvent. Note that in the crystallization from pure 1,4-dioxane only other polymorphs were obtained in this and previous studies.[78,85] The most selective additives were also tested in acetone and nitromethane, from which crystallization of Form III was not observed in the previous experiments. 2PA and 4CPBA provided crystallization control also in these solvents: 4CPBA facilitated the crystallization of Form III, but 2PA – Form I. In presence of 2PA at the fastest

cooling rate crystallization of Form III was facilitated, but at slower cooling rates pure Form I was mostly obtained. Overall, the results indicate that obtaining pure stable polymorph, Form I, in a direct crystallization is relatively challenging. In presence of all three tested additives formation of pure Form III was facilitated from nitromethane using the fastest cooling rates, whereas ND provided formation of pure Form III using all four cooling rates.
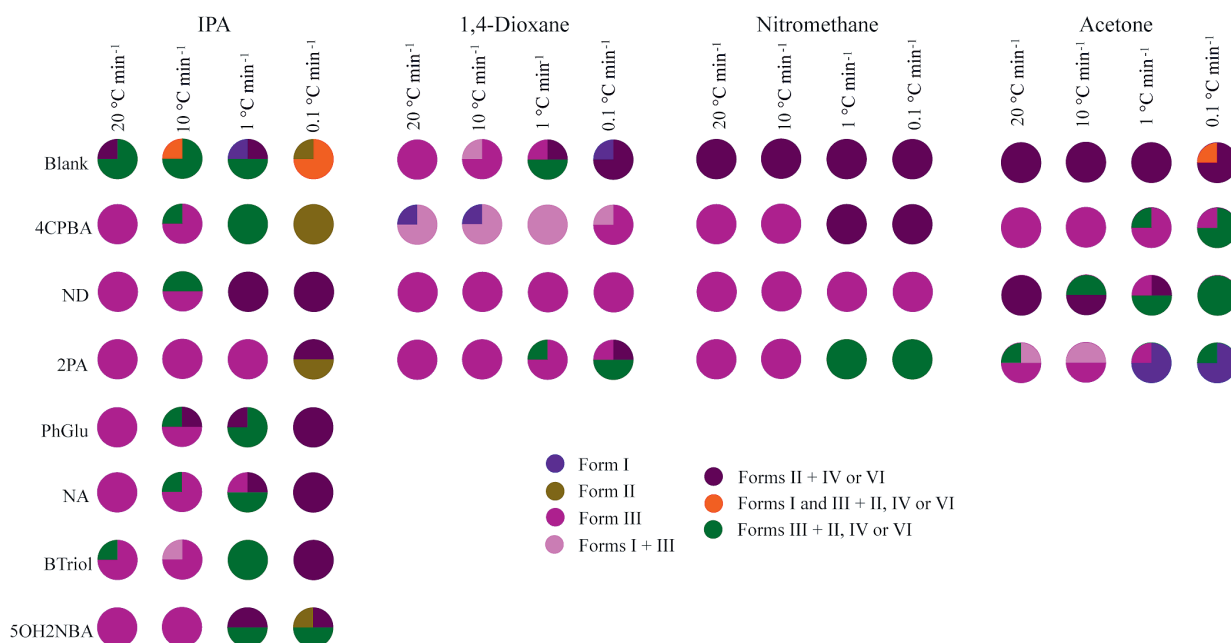
Figure 3.10. **Summary of INA polymorphs obtained in crystallization in presence of selected additives using different cooling rates. Each ¼ of the pie chart represents one of the parallel experiments.**

The effect of the stirring rate on the crystallization polymorphic outcome was also tested. It was observed that the use of fast cooling rate and slow stirring rate or even crystallization without stirring facilitated formation of Form I from IPA (see Figure 3.11.). The crystallization of Form III, however, was facilitated by the presence of the tested additives and use of faster cooling rate. The crystallization polymorphic outcome control by the tested additives was more feasible in 1,4-dioxane, particularly using stirring. The presence of any of the additives provided formation of the mixture of Forms I and III when fast cooling rate and no stirring was used. The most selective crystallization of Form III was achieved in presence of ND using the slow cooling rate, and stirring rate did not affect this. The experiments using slowest cooling rates, in which the suspension obtained after the crystallization was stirred for longer time until the set end temperature of 10 °C was reached, resulted in formation of more stable polymorphs (Forms II, IV or VI[85]) compared to Form III. Therefore, using the cooling rate of 1 °C min^{-1} almost none of the additives were able to provide crystallization of Form III or Form I.
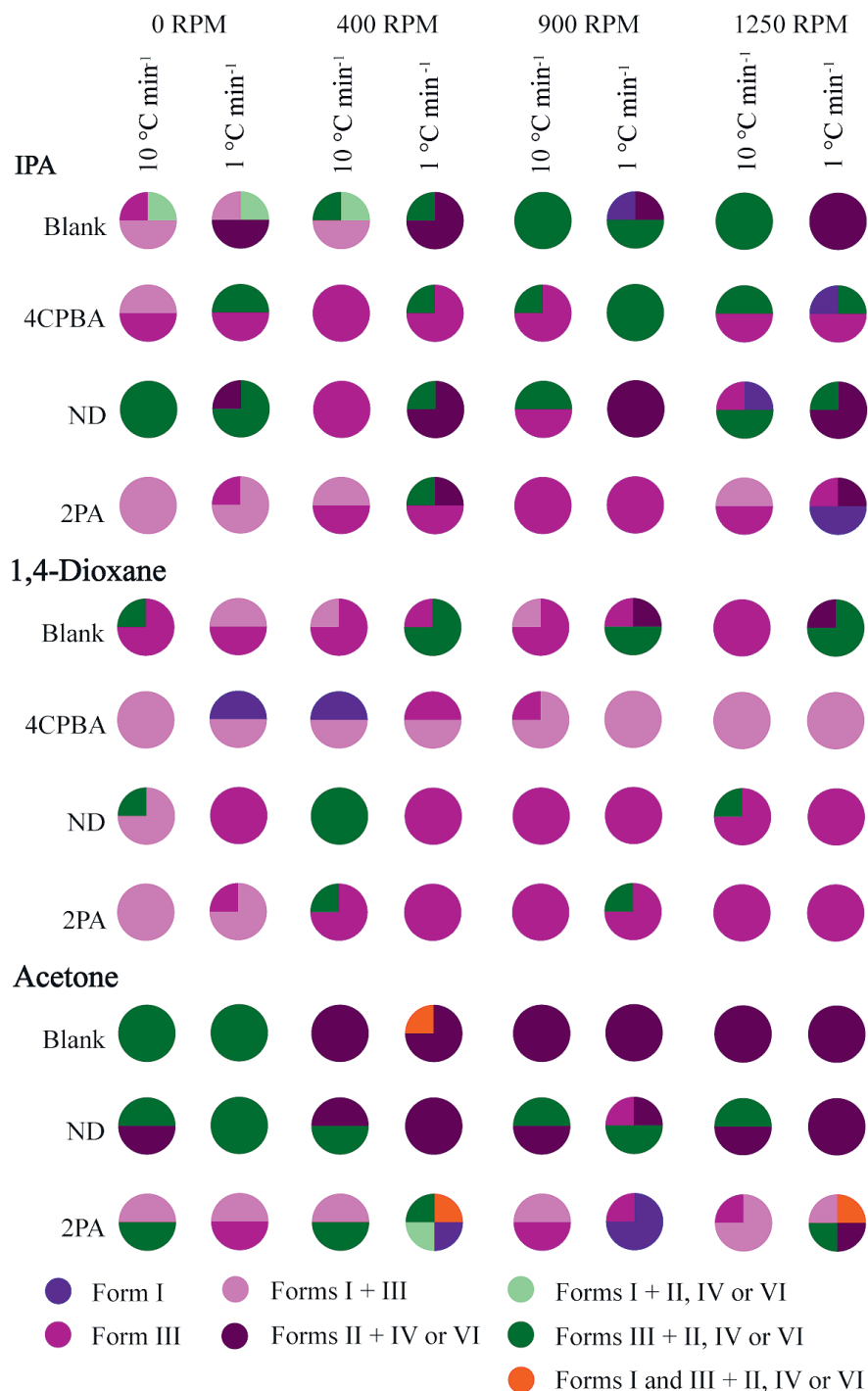
Figure 3.11. **Summary of INA polymorphs obtained in crystallization in presence of selected additives using two selected cooling rates and different stirring rates. Each ¼ of the pie chart represents one of the parallel experiments.**

3.4. Possible effects of crystallization additives on nucleation and crystal growth

The results presented in Section 3.3. clearly show that additives can facilitate crystallization of the metastable forms, but the exact mechanisms of how the additives provide the control of crystallization polymorphic outcome are unknown. In this study different approaches were used to gain an insight into the factors determining the polymorphic outcome

of all three model substances. These approaches included use of experimental data and theoretical calculations, such as:

- examination of the change of solubility (for 2,6MeOBA);
- examination of effect on the SMPT (for 2,6MeOBA, INA);
- comparison of crystal structure characteristics, such as lattice energy, Hirshfeld surfaces and their 2D fingerprint plots, FIMs and BFDH morphologies (for MPBA, INA).

The effect of additives on the solubility was investigated only for 2,6MeOBA, as for the other substances pure polymorphs could not be obtained in crystallization in the absence of additives. As calculations of lattice energy and analysis of Hirshfeld surfaces and their 2D fingerprint plots for 2,6MeOBA have already been published[74] they were not repeated as part of this study. Theoretical calculations were performed only for INA polymorphs obtained in the crystallization experiments, therefore, Form V was not analysed.

3.4.1. Solubility study

The most stable form has the lowest solubility, but additives in the solution can affect the solubility, therefore, increasing the likelihood of the crystallization of metastable form. For example, additives have been demonstrated to decrease the solubility but increase the crystal nucleation and growth rates of p-methylacetanilide.[88] The solubility of Form I is almost unaffected by the use of 1% PEG solution (see Figure 3.12.). At temperatures up to 30 °C, the solubility is almost identical to that in pure water, but at higher temperatures, the solubility slightly decreased. In contrast, the solubility of Form III in the presence of PEG increases slightly at temperatures up to 35 °C, but the solubility at higher temperatures is lower than in the pure solvent. The highly similar solubility of both forms can explain the nearly always observed concomitant crystallization in the presence of this additive, as observed in the crystallization experiments described in Section 3.3.1. The thermodynamic equilibrium point in 1% PEG solution was determined to be 8 °C lower than that in pure water (79 °C).
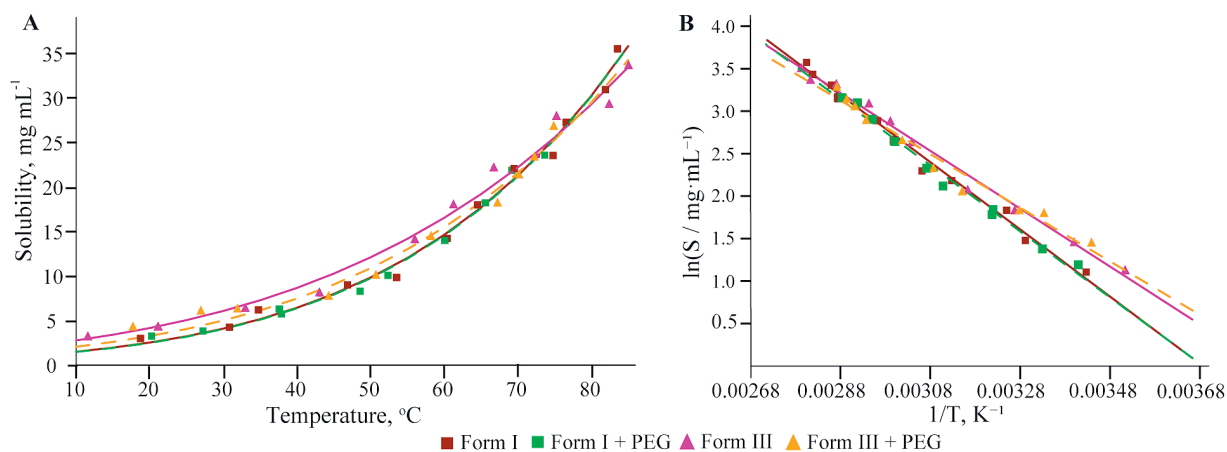
Figure 3.12. **The solubility curves of 2,6MeOBA polymorphs I and III in pure water and 1% PEG aqueous solution. A – exponential graph; B – linear graph. Brown solid line – Form I in pure water; Green dashed line – Form I in 1% PEG solution; Magenta solid line – Form III in pure water; Orange dashed line – Form III in a 1% PEG solution. Triangles and squares represent the experimental data.**

3.4.2. *Solvent mediated phase transition study*

Measurements of 2,6MeOBA SMPT kinetics show that the transformation rate in the slurry-bridging experiments is very fast (see Figure 3.13.). From a mixture of both polymorphs pure Form I was obtained in less than 15 min in the tested solvents and 1% PEG aqueous solution, but use of 0.1% HPC aqueous solution decelerated the SMPT to Form I. A complete transformation of pure Form III to pure Form I in water was slower. The time of SMPT from pure Form III in 1% PEG solution is longer than from the mixture of both polymorphs, but the use of 0.1% HPC solution inhibited the SMPT of pure Form III to Form I. SMPT was not detected even in a sample slurred for 24 h.
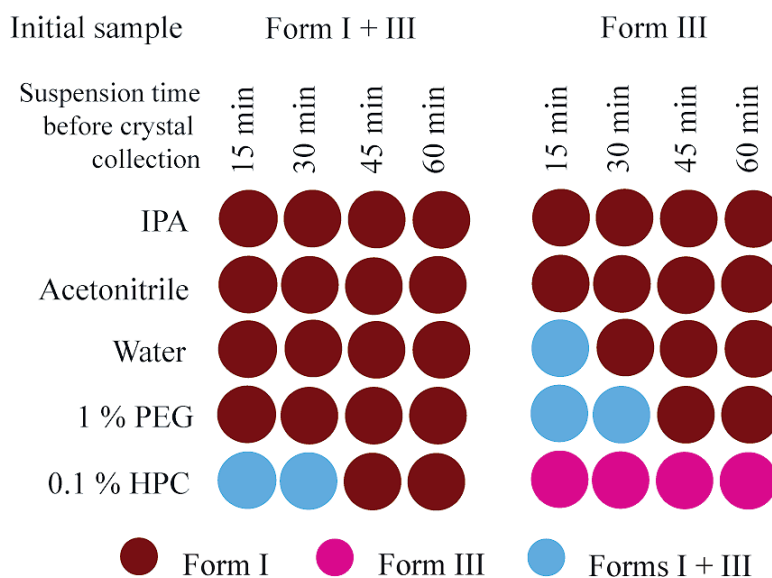
Figure 3.13. **Polymorphic composition of the solid phase after selected times during SMPT kinetic experiments at 25 °C.**

Crystallization outcome of INA in the presence of crystallization additives (see Section 3.3.3.) in general suggest a possibility that Form III nucleates first and then by stirring the suspension transforms into other more stable forms via SMPT. The results of SMPT experiments (see Figure 3.14.) showed that the crystal form obtained in presence of all the tested additives did not change notably within 30 minutes after the nucleation, which is in agreement with SMPT seeding experiment by Kulkarni et al.[89] Therefore, the various polymorphic outcome using different stirring rate is not because of an SMPT but instead because of the distinct ability of additives to affect the crystallization outcome. When higher cooling rates are used, the nucleation occurs at lower temperature and therefore at higher supersaturation, whereas, when slower cooling rates are used, the nucleation occurs at higher temperatures and therefore lower supersaturation. Additives decreased the nucleation temperature by increasing the supersaturation, and this, in fact, might be one of the potential effects of additives which could alter the obtained crystallization products.
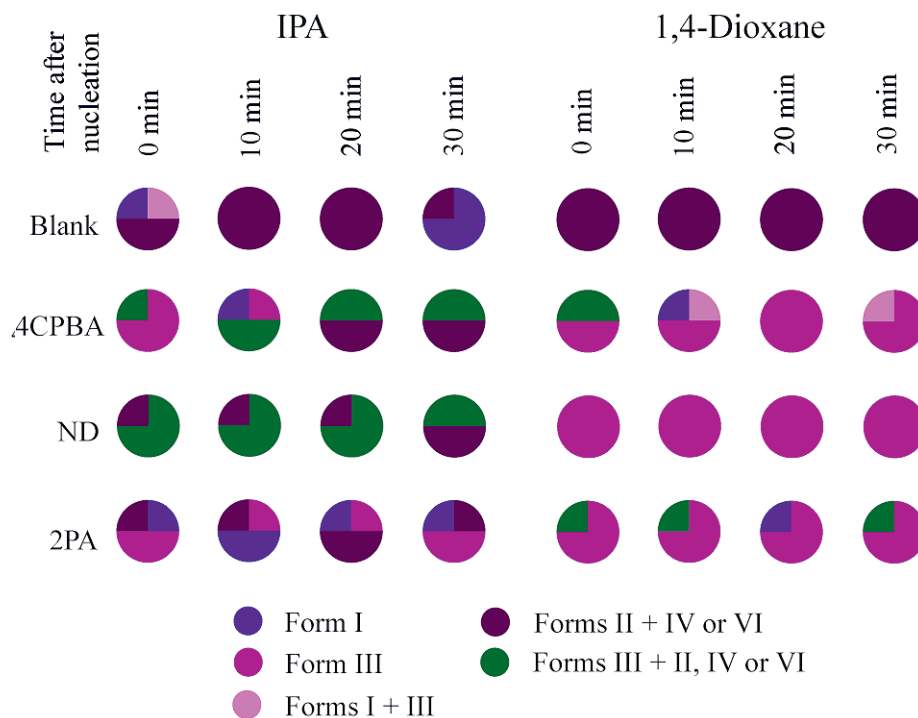
Figure 3.14. **Summary of INA polymorphs obtained in crystallization in presence of selected additives using 1 °C min⁻¹ cooling rate and different time when crystals were collected after the nucleation. Each ¼ of the pie chart represents one of the parallel experiments.**

3.4.3. *Crystallographic characterization*

The *anti* conformer of MPBA with two intramolecular hydrogen bonds between boronic acid hydroxyl groups and methoxy groups was found to be the global energy minimum conformation. Analysis of INA molecular conformation showed that in the most stable conformation the benzene ring and the amide group are twisted and the torsion angle between them is 21.9°.

For the calculation of intermolecular energy, the crystal structure of MPBA Form I in the monoclinic *Pc* space group without disorder in the dimers formed by the *syn-anti*-conformers was used. The lattice energy of both polymorphs is almost identical (see Table 3.5.). Although the calculated relative energy contradicts Form I being determined as the thermodynamically stable polymorph, the possibility for different hydrogen atom arrangement in dimers could provide an entropy increase, resulting in lowering of the free energy of Form I. For INA, the lowest lattice energy is calculated for Form I, with the lattice energy of the Form II being the second lowest of the lattice energy values. All the other polymorphs have almost identical lattice energy. The very close lattice energy values agree with the observed concomitant crystallization of the polymorphs. Calculated energy differences of polymorphs for both substances corresponds to the typical energy difference (<5 kJ·mol⁻¹) of organic polymorphs.[64,69]

Table 3.5.

Selected crystallographic and intramolecular, intermolecular and lattice energy data of MPBA and INA polymorphs.

Model substance	Polymorph	CSD Refcode	Z/Z'	E_{intra}, kJ mol^{-1}	E_{inter}, kJ mol^{-1}	$E_{lattice}$, kJ mol^{-1}
MPBA	Form I	UJACIT01 (original $P\bar{4}n2$ structure)	4/0.5 ($P\bar{4}n2$); 4/2 (Pc)	15.2	-144.4	-129.2
	Form II	UJACIT	12/1.5	6.0	-135.9	-129.8
INA	Form I	EHOWIH01	4 / 1	0.46	-124.7	-124.3
	Form II	EHOWIH02	8 / 2	0.05	-122.2	-122.2
	Form III	EHOWIH03	8 / 1	0.51	-120.6	-120.1
	Form IV	EHOWIH04	6 / 3	0.12	-119.8	-119.7
	Form VI	EHOWIH06	8 / 2	0.04	-121.4	-121.4

The pronounced differences in the hydrogen bonding in both MPBA polymorphs result in high differences in the lattice energy component contributions and energy frameworks of both forms. The electrostatic energy in Form I is the dominant component of the lattice energy, which can be associated with the extensive strong hydrogen bond network in this structure. In contrast, the electrostatic energy and dispersion energy in Form II have a very similar contribution in the lattice energy, because of a much smaller amount of intermolecular hydrogen bonds and higher importance of the aromatic interactions, including π-π stacking. To sum up, despite overall more efficient dispersion interactions in Form II, the notably stronger hydrogen bonds in Form I are the reason for the higher intermolecular energy of this form, which could also explain its higher stability. The ability of hydrogen bonding to provide stabilization of the crystal structure has been shown before, e.g., in studies of proteins[90,91] and ritonavir.[92] As expected, based on the highly similar intramolecular interactions and molecular packing, all INA polymorphs, except for Form I, have almost identical layout of energy frameworks. The main interactions stabilizing the crystal structure of all forms are dominated by electrostatic energy components, and the dispersion energy components are notably weaker than the electrostatic energy components. The most notable of electrostatic energy dominated interactions in Form I are interactions between molecules forming hydrogen bonded dimers. In contrast, the most notable interactions dominated by electrostatic energy in all the other INA polymorphs are among molecules forming hydrogen bonded INA molecule chains in two spatial directions and, therefore, forming hydrogen bonded INA molecule layers. The interactions having the most negative dispersion energy in Forms I and III are between the same molecules as those also have the most negative electrostatic energy. In contrast, in Form II, IV and VI these are aromatic and π-π interactions between oppositely oriented molecules from adjacent INA molecule layer and interactions with molecules hydrogen bonded to the mentioned molecules from adjacent layers.

Differences in the intermolecular interactions of both MPBA forms and similarity of INA Forms II, IV and VI can also clearly be seen on the Hirshfeld surfaces and in the analysis of their 2D fingerprint plots, but notable differences were observed in INA Forms I and III (see Figure 3.15.). In MPBA Form I the hydrogen bonds forming the boronic acid dimers and chains, and different H···C interactions are the main observable interactions. Both symmetrically independent molecules of MPBA Form II have only one sharp peak corresponding to being a donor (molecule A) or acceptor (molecule B) of the strong intermolecular hydrogen bond. Also, interactions associated with π-π stacking are present for MPBA Form II molecule B. In the Hirshfeld surface fingerprint plot of INA Form I there are two sharp peaks corresponding to interactions $CO\cdots H_2N$, whereas for all the other forms these peaks are wider and each corresponds to two interactions: $N_{pyr}\cdots H_2N$ or $CO\cdots H_2N$. In the fingerprint plots of Forms II, IV and VI there is a distinct peak in the middle of the plot corresponding to CH···HC interactions. Another difference between the fingerprint plots of these three forms and Forms I and III is present in the region corresponding to π-π interactions in the middle of the plot.
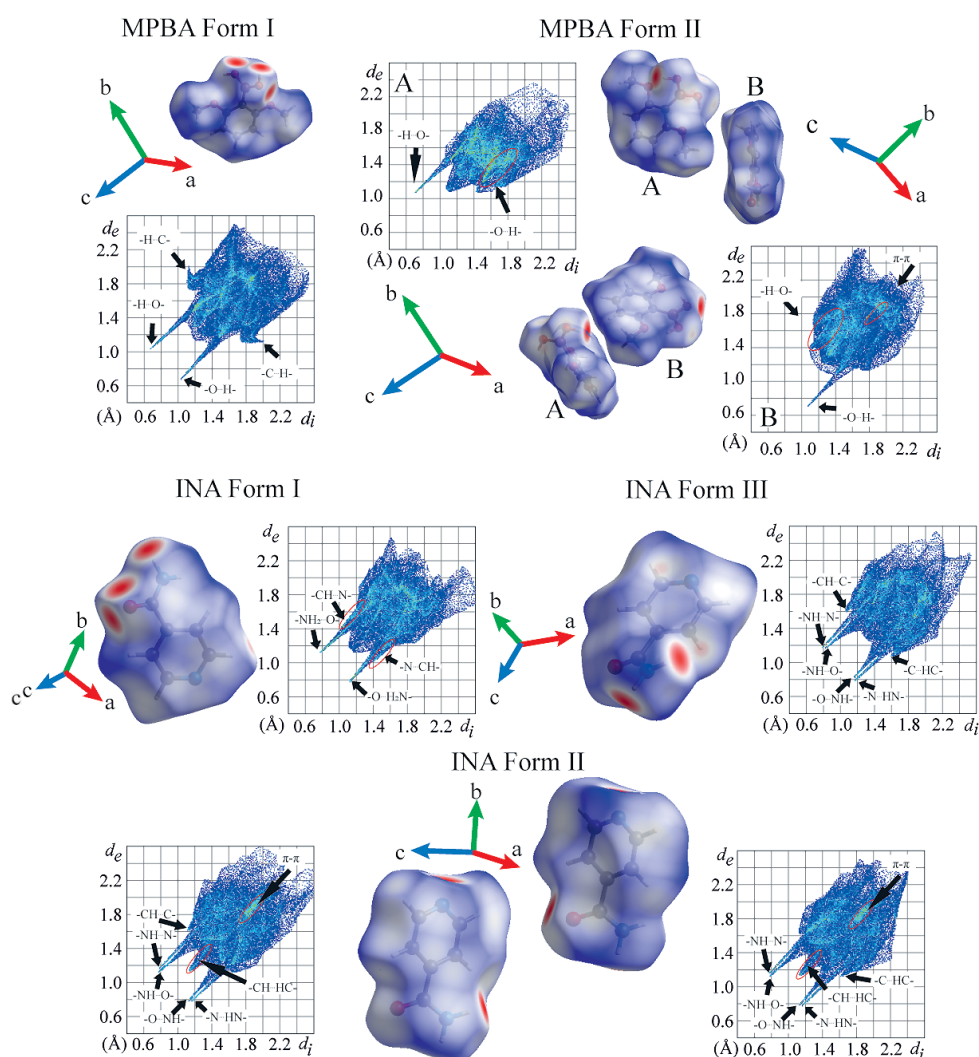

Figure 3.15. **Hirshfeld surfaces and their 2D fingerprinting plots of MPBA Forms I and II and INA Forms I – III by providing the most characteristic intermolecular interactions observed in the plots.**

3.4.4. FIM and BFDH analysis

In the MPBA Form I formed by homodimers, most of the interaction preferences are satisfied. In contrast, only half of the interaction preferences for hydrogen bonding are satisfied in Form II. Therefore, the hydrogen bonding in MPBA Form II does not match the interaction preferences as in the CSD, and the three unsatisfied hydrogen bond acceptors may be the reason for the low stability of Form II and formation of this polymorph only under specific conditions. FIM analysis for INA molecules were not performed, because in all polymorphs INA molecules adopt essentially identical conformation and all the interactions are satisfied.

There are large differences between both MPBA polymorphs when FIMs on crystal facets are compared (see Figure 3.16.). Form I crystals have a larger probability of being involved in hydrophobic interactions and interact with hydrogen bond acceptors when compared to Form II. The MPBA Form II crystal has a larger probability of interacting with hydrogen bond donors on the largest facets when compared to Form I. On these facets, the oxygen atoms of the boronic acid groups in *anti*-planar conformation are forming hydrogen bonds and the facets are growing by formation of trimers, so hydrogen bond acceptors are exposed and there is a great propensity to interact with hydrogen bond donors by these facets. Therefore, surfactants can interact as hydrogen bond donors with these facets more easily if compared to Form I, for which hydrogen bond acceptor groups cover a smaller area. Span 20 and OGP both have hydrogen bond donor groups that can interact with the boronic acid group of MPBA and stabilize Form II crystals. Additionally, the hydrophobic site of the surfactants can decelerate phase transition by forming micelles or hemispheres and therefore prevent the reorganization of molecules required for the transformation of Form II to Form I.
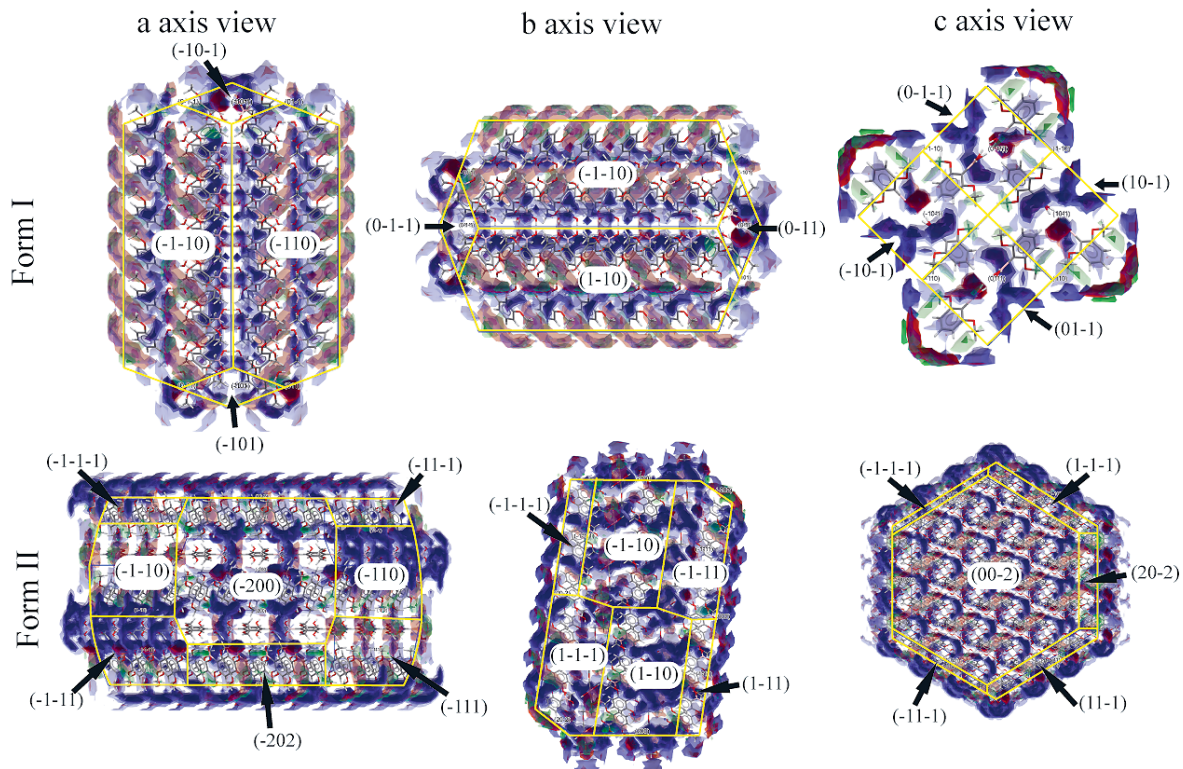
Figure 3.16. **FIMs combined on the BFDH morphology of MPBA Form I and II. Regions of hydrogen bond donor probability are shown in blue, hydrogen bond acceptors are shown in red, and hydrophobic interactions are shown in green.**

Because of the highly similar molecular packing also BFDH morphology and FIMs plotted on the crystal faces of INA Forms II, IV and VI are very similar (see Figure 3.17.). The largest crystal faces of these polymorphs are growing by attaching molecules linked by different π-π and CH···π interactions, whereas the smallest faster growing planes by attaching molecules linked by hydrogen bonds. In contrast, for INA Forms I and III also on the largest planes hydrogen bond acceptors and donors are exposed and therefore these are among the interactions forming by growth of these faces. Face group {100} of Form I is growing by formation of amide $R_2^2 8$ homodimers, but plane groups {111} and {002} of Form III are growing by continuation of CO···H_2N chains, therefore, hydrogen bond donors such as 2PA or 4CPBA can interact with this plane or facilitate growth of polymorph with such surface by activating the growth site and facilitating growth of these polymorphs.
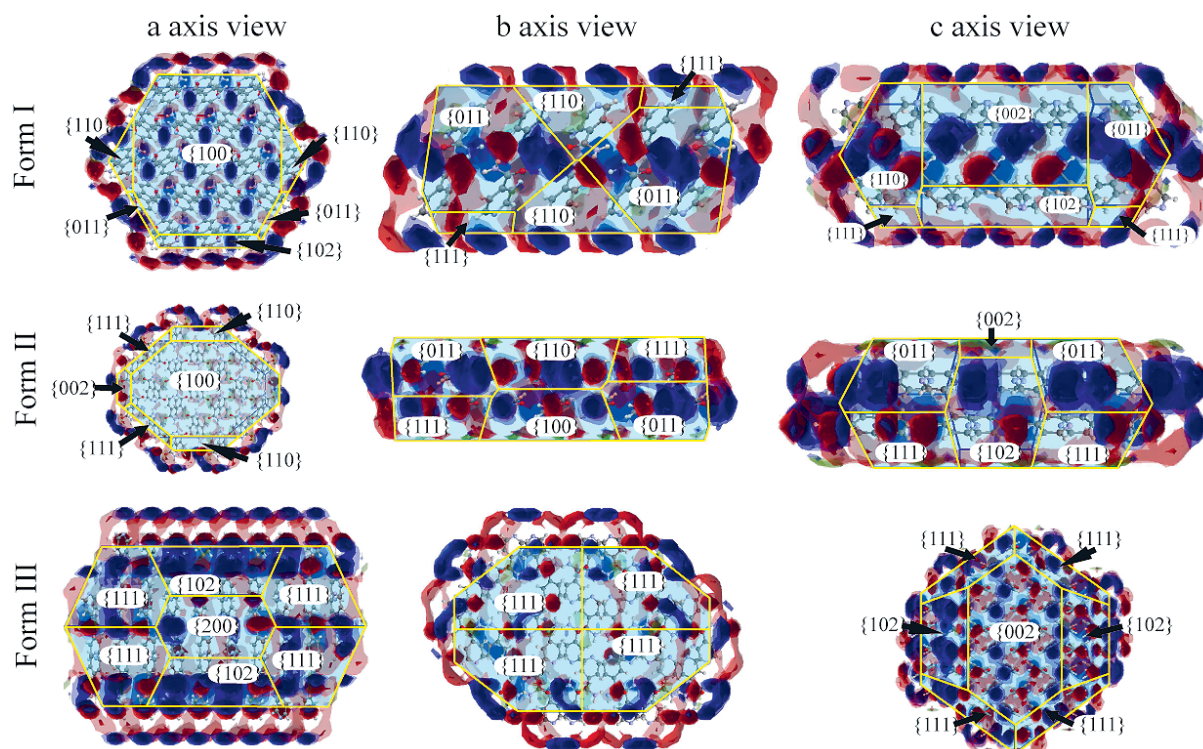
Figure 3.17. **FIMs combined on the BFDH morphology of INA Forms I-III. Regions of hydrogen bond donor probability are shown in blue, hydrogen bond acceptors are shown in red, and hydrophobic interactions are shown in green.**

CONCLUSIONS

1. In crystal structures of the four new (propionic acid, butyric acid mono- and disolvate, trifluoroethanol) and four already known (formic acid, acetic acid, formamide and propionic acid disolvate) isonicotinamide solvates similar hydrogen bond patterns are observed, and in general this allow prediction of intermolecular interactions and molecular packaging for new solvates/co-crystals with structurally similar solvents/co-formers.

2. Polyethylene glycol and hydroxypropyl cellulose facilitate the crystallization of 2,6-dimethoxybenzoic acid Form III, but the effect is not selective since it can also crystallise with impurity of Form I.

3. Hydroxypropyl cellulose inhibits the solvent mediated phase transformation of Form III of 2,6-dimethoxybenzoic acid, which enables this form to crystallize more frequently.

4. In the presence of sorbitan laurate (Span 20) and octyl β-D-glucopyranoside it is possible to crystallise 2,6-dimethoxyphenylboronic acid Form II. These crystallization additives improve the stability of 2,6-dimethoxyphenylboronic acid Form II by stabilising it for up to 1 month. It has been observed that in the presence of sorbitan laurate the solvent has no effect on the polymorph obtained in the crystallization of 2,6-dimethoxyphenylboronic acid.

5. Analysis of the morphology and full-interaction maps allowed to determine that the additives can adsorb on the surface of the crystal planes {002} and {110} of 2,6-dimethoxyphenylboronic acid Form II, which is likely to prevent the phase transition to Form I.

6. Crystallization of isonicotinamide in the presence of naphthalene-1,5-diol facilitated crystallization of Form III, while 2-picolinic acid facilitated crystallization of Form I. Most of the additives used reduced the content of other polymorphic forms in the crystallization products. By employing fast cooling rates (20 $^\circ$C min^{-1}) additives allowed crystallization of isonicotinamide Form III, but almost all the additives lost their ability to provide crystallization control at low cooling rates (0.1 $^\circ$C min^{-1}).

7. Isonicotinamide polymorphs crystallizing concomitantly (Forms II, IV and VI) exhibit similar lattice energy and intermolecular interactions. Therefore, it is possible that the energy barrier of the nucleation and crystal growth rate of these polymorphs are very similar, while the presence of additives, by altering the crystallization conditions, may lead to crystallization of structurally different forms.

8. Analysis of the morphology and full-interaction maps allowed to identificate that the additives can adsorb to the surface of the {100} crystal planes of isonicotinamide Form I and the {111} and {002} crystal planes of Form III, which could involve activation of these growth sites to crystallize Form I or III.

IZMANTOTĀ LITERATŪRA / REFERENCES

(1)   Brog, J.-P.; Chanez, C.-L.; Crochet, A.; Fromm, K. M. Polymorphism, What It Is and How to Identify It: A Systematic Review. *RSC Adv* **2013**, *3* (38), 16905.

(2)   Council of Europe. Substances for Pharmaceutical Use. In *European Pharmacopoeia*; Council of Europe: Strasbourg, 2023; Vol. 1, pp 949–951.

(3)   Tang, W.; Sima, A. D.; Gong, J.; Wang, J.; Li, T. Kinetic Difference between Concomitant Polymorphism and Solvent-Mediated Phase Transformation: A Case of Tolfenamic Acid. *Cryst Growth Des* **2020**, *20* (3), 1779–1788.

(4)   Pudipeddi, M.; Serajuddin, A. T. M. Trends in Solubility of Polymorphs. *J Pharm Sci* **2005**, *94* (5), 929–939.

(5)   Censi, R.; Martino, P. di. Polymorph Impact on the Bioavailability and Stability of Poorly Soluble Drugs. *Molecules* **2015**, *20*, 18759–18776.

(6)   Bernstein, J.; Davey, R. J.; Henck, J.-O. Concomitant Polymorphs. *Angewandte Chemie* **1999**, *38*, 3440–3461.

(7)   Ce Nicoud, L.; Licordari, F.; Myerson, A. S. Estimation of the Solubility of Metastable Polymorphs: A Critical Review. *Cryst Growth Des* **2018**, *18* (11), 7228–7237.

(8)   Tandon, R.; Tandon, N.; Thapar, R. K. Patenting of Polymorphs. *Pharm Pat Anal* **2018**, *7* (2), 59–63.

(9)   Hilfiker, R.; von Raumer, M. *Polymorphism: In the Pharmaceutical Industry*; Hilkifer, R., von Raumer, M., Eds.; Wiley-VCH Verlag GmbH & Co. KGaA: Weinheim, Germany, 2019.

(10)   Xu, S.; Cao, D.; Liu, Y.; Wang, Y. Role of Additives in Crystal Nucleation from Solutions: A Review. *Cryst Growth Des* **2021**, No. 3.

(11)   Yeh, K.-L.; Lee, H.-L.; Lee, T. Crystallization of Form II Paracetamol with the Assistance of Carboxylic Acids toward Batch and Continuous Processes. *Pharmaceutics* **2022**, *14* (5), 1099.

(12)   Kulkarni, S. A.; McGarrity, E. S.; Meekes, H.; ter Horst, J. H. Isonicotinamide Self-Association: The Link between Solvent and Polymorph Nucleation. *Chemical Communications* **2012**, *48* (41), 4983.

(13)   Bērziņš, A.; Semjonova, A.; Actiņš, A.; Salvalaglio, M. Speciation of Substituted Benzoic Acids in Solution: Evaluation of Spectroscopic and Computational Methods for the Identification of Associates and Their Role in Crystallization. *Cryst Growth Des* **2021**, *21* (9), 4823–4836.

(14)   Tulli, L. G.; Moridi, N.; Wang, W.; Helttunen, K.; Neuburger, M.; Vaknin, D.; Meier, W.; Shahgaldian, P. Polymorphism Control of an Active Pharmaceutical Ingredient

beneath Calixarene-Based Langmuir Monolayers. *Chemical Communications* **2014**, *50* (31), 3938–3940.

(15) Zhang, B.; Hou, X.; Dang, L.; Wei, H. Selective Polymorphic Crystal Growth on Self-Assembled Monolayer Using Molecular Modeling as an Assistant Method. *J Cryst Growth* **2019**, *518* (February), 81–88.

(16) Shi, P.; Xu, S.; Yang, H.; Wu, S.; Tang, W.; Wang, J.; Gong, J. Use of Additives to Regulate Solute Aggregation and Direct Conformational Polymorph Nucleation of Pimelic Acid. *IUCrJ* **2021**, *8*, 161–167.

(17) Council of Europe. Polymorphism. In *European Pharmacopoeia, Supplement 11.2*; Strasbourg, 2023; p 795.

(18) de Tros Ilarduya, M. C.; Martín, C.; Goñi, M. M.; Martínez-Uhárriz, M. C. Dissolution Rate of Polymorphs and Two New Pseudopolymorphs of Sulindac. *Drug Dev Ind Pharm* **1997**, *23* (11), 1095–1098.

(19) Gu, C. H.; Grant, D. J. W. Estimating the Relative Stability of Polymorphs and Hydrates from Heats of Solution and Solubility Data. *J Pharm Sci* **2001**, *90* (9), 1277–1287.

(20) Gupta, S.; Kesarla, R.; Omri, A. Formulation Strategies to Improve the Bioavailability of Poorly Absorbed Drugs with Special Emphasis on Self-Emulsifying Systems. *ISRN Pharm* **2013**, *2013*, 1–16.

(21) Nangia, A. K.; Desiraju, G. R. Crystal Engineering: An Outlook for the Future. *Angewandte Chemie International Edition* **2019**, *58* (13), 4100–4107.

(22) Venkata Narasayya, S.; Maruthapillai, A.; Sundaramurthy, D.; Arockia Selvi, J.; Mahapatra, S. Preparation, Pharmaceutical Properties and Stability of Lesinurad Co-Crystals and Solvate. *Mater Today Proc* **2019**, *14*, 532–544.

(23) Wang, K.; Sun, C. C. Direct Compression Tablet Formulation of Celecoxib Enabled with a Pharmaceutical Solvate. *Int J Pharm* **2021**, *596* (January), 120239.

(24) Dhondale, M. R.; Thakor, P.; Nambiar, A. G.; Singh, M.; Agrawal, A. K.; Shastri, N. R.; Kumar, D. Co-Crystallization Approach to Enhance the Stability of Moisture-Sensitive Drugs. *Pharmaceutics* **2023**, *15* (1), 189.

(25) Aitipamula, S.; Nangia, A. Polymorphism: Fundamentals and Applications. In *Supramolecular Chemistry*; John Wiley & Sons, Ltd: Chichester, UK, 2012.

(26) Pal, R.; Jelsch, C.; Malaspina, L. A.; Edwards, A. J.; Murshed, M. M.; Grabowsky, S. Syn and Anti Polymorphs of 2,6-Dimethoxy Benzoic Acid and Its Molecular and Ionic Cocrystals: Structural Analysis and Energetic Perspective. *J Mol Struct* **2020**, *1221*, 128721.

(27) Cruz-Cabeza, A. J.; Bernstein, J. Conformational Polymorphism. *Chem Rev* **2014**, *114* (4), 2170–2191.

(28) Bhogala, B. R.; Basavoju, S.; Nangia, A. Tape and Layer Structures in Cocrystals of Some Di- and Tricarboxylic Acids with 4,4′-Bipyridines and Isonicotinamide. From Binary to Ternary Cocrystals. *CrystEngComm* **2005**, *7*, 551–562.

(29) Lee, E. H. A Practical Guide to Pharmaceutical Polymorph Screening & Selection. *Asian J Pharm Sci* **2014**, *9* (4), 163–175.

(30) Lu, J.; Rohani, S. Polymorphism and Crystallization of Active Pharmaceutical Ingredients (APIs). *Curr Med Chem* **2009**, *16* (7), 884–905.

(31) Singhal, D.; Curatolo, W. Drug Polymorphism and Dosage Form Design: A Practical Perspective. *Adv Drug Deliv Rev* **2004**, *56* (3), 335–347.

(32) Du, W.; Yin, Q.; Bao, Y.; Xie, C.; Hou, B.; Hao, H.; Chen, W.; Wang, J.; Gong, J. Concomitant Polymorphism of Prasugrel Hydrochloride in Reactive Crystallization. *Ind Eng Chem Res* **2013**, *52* (46), 16182–16189.

(33) Jiang, S.; ter Horst, J. H.; Jansens, P. J. Concomitant Polymorphism of O-Aminobenzoic Acid in Antisolvent Crystallization. *Cryst Growth Des* **2008**, *8* (1), 37–43.

(34) Singh, A.; Lee, I. S.; Kim, K.; Myerson, A. S. Crystal Growth on Self-Assembled Monolayers. *CrystEngComm* **2011**, *13* (1), 24–32.

(35) Neumann, M. A.; van de Streek, J. How Many Ritonavir Cases Are There Still out There? *Faraday Discuss* **2018**, *211*, 441–458.

(36) European Medicines Agency. *Public statement: Suply of Norvir Hard Capsules.* The European Agency for the Evaluation of Medicinal Products Human Medicines Evaluation Unit. https://www.ema.europa.eu/en/documents/public-statement/public-statement-supply-norvir-hard-capsules_en.pdf (accessed 2022-01-30).

(37) Thorat, A. A.; Dalvi, S. v. Ultrasound-Assisted Modulation of Concomitant Polymorphism of Curcumin during Liquid Antisolvent Precipitation. *Ultrason Sonochem* **2016**, *30*, 35–43.

(38) Sugiyama, T.; Wang, S.-F. Manipulation of Nucleation and Polymorphism by Laser Irradiation. *Journal of Photochemistry and Photobiology C: Photochemistry Reviews* **2022**, *52*, 100530.

(39) Song, S.; Wang, L.; Yao, C.; Wang, Z.; Xie, G.; Tao, X. Crystallization of Sulfathiazole in Gel: Polymorph Selectivity and Cross-Nucleation. *Cryst Growth Des* **2020**, *20* (1), 9–16.

(40) Bora, P.; Saikia, B.; Sarma, B. Oriented Crystallization on Organic Monolayers to Control Concomitant Polymorphism. *Chemistry – A European Journal* **2020**, *26* (3), 699–710.

(41) Song, R. Q.; Cölfen, H. Additive Controlled Crystallization. *CrystEngComm* **2011**, *13* (5), 1249–1276.

(42) Hernández Espinell, J. R.; López-Mejías, V.; Stelzer, T. Revealing Polymorphic Phase Transformations in Polymer-Based Hot Melt Extrusion Processes. *Cryst Growth Des* **2018**, *18* (4), 1995–2002.

(43) Caridi, A.; Kulkarni, S. A.; Di Profio, G.; Curcio, E.; Ter Horst, J. H. Template-Induced Nucleation of Isonicotinamide Polymorphs. *Cryst Growth Des* **2014**, *14*, 1135–1141.

(44) Simone, E.; Cenzato, M. v.; Nagy, Z. K. A Study on the Effect of the Polymeric Additive HPMC on Morphology and Polymorphism of Ortho-Aminobenzoic Acid Crystals. *J Cryst Growth* **2016**, *446*, 50–59.

(45) Watson, S.; Nie, M.; Wang, L.; Stokes, K. Challenges and Developments of Self-Assembled Monolayers and Polymer Brushes as a Green Lubrication Solution for Tribological Applications. *RSC Adv* **2015**, *5* (109), 89698–89730.

(46) Simone, E.; Steele, G.; Nagy, Z. K. Tailoring Crystal Shape and Polymorphism Using Combinations of Solvents and a Structurally Related Additive. *CrystEngComm* **2015**, *17* (48), 9370–9379.

(47) Black, J. F. B.; Cruz-Cabeza, A. J.; Davey, R. J.; Willacy, R. D.; Yeoh, A. The Kinetic Story of Tailor-Made Additives in Polymorphic Systems: New Data and Molecular Insights for p-Aminobenzoic Acid. *Cryst Growth Des* **2018**, *18* (12), 7518–7525.

(48) Kras, W.; Carletta, A.; Montis, R.; Sullivan, R. A.; Cruz-Cabeza, A. J. Switching Polymorph Stabilities with Impurities Provides a Thermodynamic Route to Benzamide Form III. *Commun Chem* **2021**, *4* (1), 38.

(49) Abdin, A. Y.; Yeboah, P.; Jacob, C. Chemical Impurities: An Epistemological Riddle with Serious Side Effects. *Int J Environ Res Public Health* **2020**, *17* (3), 1030.

(50) Sinko, P. J. Pharmaceutical Polymers. In *Martin's Physical Pharmacy and Pharmaceutical Sciences*; Troy, D. B., Ed.; Wolters Kluwer, Lippincott Williams & Wilkins, 2016; pp 508–514.

(51) Telford, R.; Seaton, C. C.; Clout, A.; Buanz, A.; Gaisford, S.; Williams, G. R.; Prior, T. J.; Okoye, C. H.; Munshi, T.; Scowen, I. J. Stabilisation of Metastable Polymorphs: The Case of Paracetamol Form III. *Chemical Communications* **2016**, *52* (81), 12028–12031.

(52) Bērziņš, A.; Trimdale-Deksne, A.; Belyakov, S.; ter Horst, J. H. Switching Nitrofurantoin Polymorphic Outcome in Solvent-Mediated Phase Transformation and Crystallization Using Solvent and Additives. *Cryst Growth Des* **2023**, *23* (8), 5469–5476.

(53) Poon, G. G.; Seritan, S.; Peters, B. A Design Equation for Low Dosage Additives That Accelerate Nucleation. *Faraday Discuss* **2015**, *179*, 329–341.

(54) Urwin, S. J.; Yerdelen, S.; Houson, I.; ter Horst, J. H. Impact of Impurities on Crystallization and Product Quality: A Case Study with Paracetamol. *Crystals (Basel)* **2021**, *11* (11), 1344.

(55) Parambil, J. v.; Poornachary, S. K.; Heng, J. Y. Y.; Tan, R. B. H. Template-Induced Nucleation for Controlling Crystal Polymorphism: From Molecular Mechanisms to Applications in Pharmaceutical Processing. *CrystEngComm* **2019**, *21* (28), 4122–4135.

(56) Maranas, C. D.; Floudas, C. A. Global Minimum Potential Energy Conformations of Small Molecules. *Journal of Global Optimization* **1994**, *4* (2), 135–170.

(57) Giannozzi, P.; Baroni, S.; Bonini, N.; Calandra, M.; Car, R.; Cavazzoni, C.; Ceresoli, D.; Chiarotti, G. L.; Cococcioni, M.; Dabo, I.; Dal Corso, A.; de Gironcoli, S.; Fabris, S.; Fratesi, G.; Gebauer, R.; Gerstmann, U.; Gougoussis, C.; Kokalj, A.; Lazzeri, M.; Martin-Samos, L.; Marzari, N.; Mauri, F.; Mazzarello, R.; Paolini, S.; Pasquarello, A.; Paulatto, L.; Sbraccia, C.; Scandolo, S.; Sclauzero, G.; Seitsonen, A. P.; Smogunov, A.; Umari, P.; Wentzcovitch, R. M. QUANTUM ESPRESSO: A Modular and Open-Source Software Project for Quantum Simulations of Materials. *Journal of Physics: Condensed Matter* **2009**, *21* (39), 395502.

(58) Giannozzi, P.; Andreussi, O.; Brumme, T.; Bunau, O.; Buongiorno Nardelli, M.; Calandra, M.; Car, R.; Cavazzoni, C.; Ceresoli, D.; Cococcioni, M.; Colonna, N.; Carnimeo, I.; Dal Corso, A.; De Gironcoli, S.; Delugas, P.; Distasio, R. A.; Ferretti, A.; Floris, A.; Fratesi, G.; Fugallo, G.; Gebauer, R.; Gerstmann, U.; Giustino, F.; Gorni, T.; Jia, J.; Kawamura, M.; Ko, H. Y.; Kokalj, A.; Kücükbenli, E.; Lazzeri, M.; Marsili, M.; Marzari, N.; Mauri, F.; Nguyen, N. L.; Nguyen, H. V.; Otero-De-La-Roza, A.; Paulatto, L.; Poncé, S.; Rocca, D.; Sabatini, R.; Santra, B.; Schlipf, M.; Seitsonen, A. P.; Smogunov, A.; Timrov, I.; Thonhauser, T.; Umari, P.; Vast, N.; Wu, X.; Baroni, S. Advanced Capabilities for Materials Modelling with Quantum ESPRESSO. *Journal of Physics Condensed Matter* **2017**, *29* (46).

(59) Lund, A. M.; Orendt, A. M.; Pagola, G. I.; Ferraro, M. B.; Facelli, J. C. Optimization of Crystal Structures of Archetypical Pharmaceutical Compounds: A Plane-Wave DFT-D Study Using Quantum Espresso. *Cryst Growth Des* **2013**, *13* (5), 2181–2189.

(60) Gavezzotti, A. Efficient Computer Modeling of Organic Materials. The Atom–Atom, Coulomb–London–Pauli (AA-CLP) Model for Intermolecular Electrostatic-Polarization, Dispersion and Repulsion Energies. *New Journal of Chemistry* **2011**, *35* (7), 1360.

(61) Thomas, S. P.; Spackman, P. R.; Jayatilaka, D.; Spackman, M. A. Accurate Lattice Energies for Molecular Crystals from Experimental Crystal Structures. *J Chem Theory Comput* **2018**, *14* (3), 1614–1623.

(62) Gavezzotti, A. Calculation of Lattice Energies of Organic Crystals: The PIXEL Integration Method in Comparison with More Traditional Methods. *Z Kristallogr Cryst Mater* **2005**, *220* (5–6), 499–510.

(63) Cutini, M.; Civalleri, B.; Corno, M.; Orlando, R.; Brandenburg, J. G.; Maschio, L.; Ugliengo, P. Assessment of Different Quantum Mechanical Methods for the Prediction of Structure and Cohesive Energy of Molecular Crystals. *J Chem Theory Comput* **2016**, *12* (7), 3340–3352.

(64) Nyman, J.; Day, G. M. Static and Lattice Vibrational Energy Differences between Polymorphs. *CrystEngComm* **2015**, *17* (28), 5154–5165.

(65) Turner, M. J.; Thomas, S. P.; Shi, M. W.; Jayatilaka, D.; Spackman, M. A. Energy Frameworks: Insights into Interaction Anisotropy and the Mechanical Properties of Molecular Crystals. *Chemical Communications* **2015**, *51* (18), 3735–3738.

(66) Spackman, M. A.; Byrom, P. G. A Novel Definition of a Molecule in a Crystal. *Chem Phys Lett* **1997**, *267* (3–4), 215–220.

(67) Spackman, P. R.; Turner, M. J.; McKinnon, J. J.; Wolff, S. K.; Grimwood, D. J.; Jayatilaka, D.; Spackman, M. A. CrystalExplorer : A Program for Hirshfeld Surface Analysis, Visualization and Quantitative Analysis of Molecular Crystals. *J Appl Crystallogr* **2021**, *54* (3), 1006–1011.

(68) Wood, P. A.; Olsson, T. S. G.; Cole, J. C.; Cottrell, S. J.; Feeder, N.; Galek, P. T. A.; Groom, C. R.; Pidcock, E. Evaluation of Molecular Crystal Structures Using Full Interaction Maps. *CrystEngComm* **2013**, *15* (1), 65–72.

(69) Cruz-Cabeza, A. J.; Reutzel-Edens, S. M.; Bernstein, J. Facts and Fictions about Polymorphism. *Chem Soc Rev* **2015**, *44* (23), 8619–8635.

(70) Taylor, R.; Wood, P. A. A Million Crystal Structures: The Whole Is Greater than the Sum of Its Parts. *Chem Rev* **2019**, *119* (16), 9427–9477.

(71) Chadwick, K.; Chen, J.; Santiso, E. E.; Trout, B. L. Molecular Modeling Applications in Crystallization. In *Handbook of Industrial Crystallization*; Cambridge University Press, 2019; pp 136–171.

(72) Bryan, R. F.; White, D. H. 2,6-Dimethoxybenzoic Acid. *Acta Crystallogr B* **1982**, *38* (3), 1014–1016.

(73) Portalone, G. A New Polymorph of 2,6-Dimethoxybenzoic Acid. *Acta Crystallogr Sect E Struct Rep Online* **2011**, *67* (12).

(74) Portalone, G. Crystal Structure and Hirshfeld Surface Analysis of a Third Polymorph of 2,6-Dimethoxybenzoic Acid. *Acta Crystallogr E Crystallogr Commun* **2020**, *76* (12), 1823–1826.

(75) Portalone, G. Redetermination of 2,6-Dimethoxy-Benzoic Acid. *Acta Crystallogr Sect E Struct Rep Online* **2009**, *65* (2).

(76) Cyrański, M. K.; Klimentowska, P.; Rydzewska, A.; Serwatowski, J.; Sporzyński, A.; Stępień, D. K. Towards a Monomeric Structure of Phenylboronic Acid: The Influence of Ortho-Alkoxy Substituents on the Crystal Structure. *CrystEngComm* **2012**, *14* (19), 6282–6294.

(77) Li, J.; Bourne, S. A.; Caira, M. R. New Polymorphs of Isonicotinamide and Nicotinamide. *Chem. Commun.* **2011**, *47* (5), 1530–1532.

(78) Aakeröy, C. B.; Beatty, A. M.; Helfrich, B. A.; Nieuwenhuyzen, M. Do Polymorphic Compounds Make Good Cocrystallizing Agents? A Structural Case Study That Demonstrates the Importance of Synthon Flexibility. *Cryst Growth Des* **2003**, *3* (2), 159–165.

(79) Eccles, K. S.; Deasy, R. E.; Fábián, L.; Braun, D. E.; Maguire, A. R.; Lawrence, S. E. Expanding the Crystal Landscape of Isonicotinamide: Concomitant Polymorphism and Co-Crystallisation. *CrystEngComm* **2011**, *13* (23), 6923–6925.

(80) Vicatos, A. I.; Caira, M. R. A New Polymorph of the Common Coformer Isonicotinamide. *CrystEngComm* **2019**, *21* (5), 843–849.

(81) Báthori, N. B.; Lemmerer, A.; Venter, G. A.; Bourne, S. A.; Caira, M. R. Pharmaceutical Co-Crystals with Isonicotinamide-Vitamin B3, Clofibric Acid, and Diclofenac-and Two Isonicotinamide Hydrates. *Cryst Growth Des* **2011**, *11* (1), 75–87.

(82) Oswald, I. D. H. Rationalisation and Design of Hydrogen Bonding Patterns in Co-Crystals and Polymorphs, University of Edinburgh, 2004. http://hdl.handle.net/1842/15564.

(83) Oswald, I. D. H.; Motherwell, W. D. S.; Parsons, S. A 1:2 Co-Crystal of Isonicotinamide and Propionic Acid. *Acta Crystallogr Sect E Struct Rep Online* **2004**, *60* (12), o2380–o2383.

(84) Oswald, I. D. H.; Motherwell, W. D. S.; Parsons, S. Isonicotinamide – Formamide (1/1). *Acta Crystallogr Sect E Struct Rep Online* **2005**, *61* (10), 3161–3163.

(85) Fellah, N.; Zhang, C. J.; Chen, C.; Hu, C. T.; Kahr, B.; Ward, M. D.; Shtukenberg, A. G. Highly Polymorphous Nicotinamide and Isonicotinamide: Solution versus Melt Crystallization. *Cryst Growth Des* **2021**, *21* (8), 4713–4724.

(86) Ostwald, W. Studien Über Die Bildung Und Umwandlung Fester Körper. *Zeitschrift für Physikalische Chemie* **1897**, *22U* (1), 289–330.

(87) Lin, J.; Shi, P.; Wang, Y.; Wang, L.; Ma, Y.; Liu, F.; Wu, S.; Gong, J. Template Design Based on Molecular and Crystal Structure Similarity to Regulate Conformational Polymorphism Nucleation: The Case of α,ω-Alkanedicarboxylic Acids. *IUCrJ* **2021**, *8* (5), 814–822.

(88) Wu, H.; Wang, J.; Liu, Q.; Zong, S.; Tian, B.; Huang, X.; Wang, T.; Yin, Q.; Hao, H. Influences and the Mechanism of Additives on Intensifying Nucleation and Growth of P-Methylacetanilide. *Cryst Growth Des* **2020**, *20* (2), 973–983.

(89) Kulkarni, S. A.; Meekes, H.; ter Horst, J. H. Polymorphism Control through a Single Nucleation Event. *Cryst Growth Des* **2014**, *14*, 1493–1499.

(90) Takahashi, T.; Endo, S.; Nagayama, K. Stabilization of Protein Crystals by Electrostatic Interactions as Revealed by a Numerical Approach. *J Mol Biol* **1993**, *234* (2), 421–432.

(91) Takahashi, T. Significant Role of Electrostatic Interactions for Stabilization of Protein Assemblies. *Adv Biophys* **1997**, *34* (5), 41–54.

(92) Wang, C.; Rosbottom, I.; Turner, T. D.; Laing, S.; Maloney, A. G. P.; Sheikh, A. Y.; Docherty, R.; Yin, Q.; Roberts, K. J. Molecular, Solid-State and Surface Structures of the Conformational Polymorphic Forms of Ritonavir in Relation to Their Physicochemical Properties. *Pharm Res* **2021**, *38* (6), 971–990.

Promocijas darbs "Organisku vielu polimorfisma kontrole, izmantojot kristalizācijas piedevas" izstrādāts Latvijas Universitātes Ķīmijas fakultātē.

Ar savu parakstu apliecinu, ka pētījums veikts patstāvīgi, izmantoti tikai tajā norādītie informācijas avoti un iesniegtā darba elektroniskā kopija atbilst izdrukai.

Autore: A. Semjonova _____ _____

                                (personiskais paraksts)   (datums)

Rekomendēju darbu aizstāvēšanai

Vadītājs: Dr. chem. Agris Bērziņš _____ _____

                                (personiskais paraksts)   (datums)

Darbs iesniegts Latvijas Universitātes Ķīmijas zinātņu nozares promocijas padomē

_____

     (datums)

Padomes sekretāre: _____ V. Rudoviča

                              (personiskais paraksts)

PUBLIKĀCIJAS / PUBLICATIONS

I

Semjonova, A., Bērziņš, A.

CONTROLLING THE POLYMORPHIC OUTCOME OF 2,6-DIMETHOXYBENZOIC ACID CRYSTALLIZATION USING ADDITIVES

Controlling the Polymorphic Outcome of 2,6-Dimethoxybenzoic Acid Crystallization Using Additives

Aina Semjonova * and Agris Bērziņš [ORCID]

Faculty of Chemistry, University of Latvia, Jelgavas iela 1, LV-1004 Rīga, Latvia
* Correspondence: aina.semjonova@lu.lv

Abstract: In this study, 2,6-dimethoxybenzoic acid (2,6MeOBA) was used as a model substance to investigate the use of additives to control the polymorphic outcome of crystallization. 2,6MeOBA exists as three polymorphs. Two of the 2,6MeOBA polymorphs, I and III, obtained in most of the crystallization experiments, were characterized by thermal analysis, and their relative thermodynamic stability was determined. Forms I and III are enantiotropically related, where form III is the high-temperature form. Pure form II was very difficult to obtain. Crystallization of 2,6MeOBA was explored under different conditions by performing evaporation and cooling crystallization from different solvents. Surfactants, polymers, and different molecular compounds with diverse possibilities for the formation of intermolecular interactions were tested as additives. The additives facilitating the crystallization of the metastable forms were additionally studied under different crystallization conditions. The effect of additives polyethylene glycol (PEG) and hydroxypropyl cellulose (HPC) on the thermodynamic stability and solvent-mediated phase transition (SMPT) kinetics was evaluated. HPC and PEG showed the potential to favor the formation of form III in crystallization from water.

Keywords: 2,6-dimethoxybenzoic acid; polymorphism; crystallization; crystallization additives; solvent-mediated phase transition

1. Introduction

Polymorphism is the ability of compounds to crystallize in different solid crystal structures [1,2]. It is often one of the most challenging steps in the development of pharmaceutical drugs [3–5]. Polymorphism and its control possibilities are not completely predictable, despite extensive research in this field. As polymorphs are also considered intellectual property, pharmaceutical companies often patent-protect the discovered crystalline forms [6,7]. A general understanding of the mechanism of polymorph formation can reduce the research and development time for the invention of new active substances or generic drugs [8]. For a better understanding of the phenomenon of polymorphism and factors affecting their appearance and crystallization, well-explored or specifically selected model substances are often used for research.

Solids with different crystal structures have different physical properties, for example, solubility [9], dissolution rate [10], stability [11], and bioavailability [12,13]. It is important to characterize all crystalline forms of API before developing the dosage form of the drug [14,15] because the selection of the dosage form, required excipients, and dose of the API depends on these physical properties [16]. In pharmaceutical manufacturing, it is safer to use the most stable polymorph with the lowest energy, but many APIs have low solubility in water. Crystallization of metastable forms improves solubility and bioavailability [17]. Unfortunately, the crystallization of such polymorphs is often complicated, with concomitant crystallization along with the stable form being one of the potential complications [18–20].

Concomitant crystallization occurs when at least two different polymorphs crystallize in the same sample [20]. This can occur due to competitive nucleation and growth rates of

more than one polymorph [21]. The appearance of concomitant crystallization is caused by different kinetic and thermodynamic factors [22,23]. Frequently, a mixture of forms is exposed to a solvent-mediated phase transition (SMPT), and only the stable form is present in the collected product [18,21,24,25]. Modification of the crystallization process can prevent concomitant crystallization. One such modification is the use of crystallization additives, which can stabilize metastable forms [26–28], promote their nucleation [29], or prevent nucleation of the stable form.

Crystallization with the presence of additives or templates is one of the empirical methods for controlling polymorphic outcomes. There are many approaches to additive crystallization [30]—heterogeneous nucleation with insoluble additives or templates (for example, Langmuir monolayers [31,32], self-assembled monolayers (SAM) [23,33–35], polymers [24,36,37], or other insoluble additives [38]) or homogeneous nucleation with soluble additives [29,37]. Additives typically lower the activation energy of nucleation and control crystal morphology, polymorphism, and crystal size [23]. Langmuir monolayers and SAMs are efficient templates for crystallization control but are selective for each polymorph, it is necessary to regenerate the monolayers after crystallization, or it is difficult to collect the obtained crystals without impurities from the layers [39]. Homogeneous additives can be easier to separate from the crystals but sometimes integrate into the crystal structure [29]. Therefore, excipients from drug dosage forms can be used as additives for the crystallization of API [37,40], as there would be no need to separate these additives after crystallization. There are many possible mechanisms by which additives can control the outcomes of crystallization. For example, additives can selectively adsorb to some of the crystal surface faces by inhibiting their growth and, therefore, the growth of this polymorph. Additives can also help to align crystallizable substance molecules to obtain the desired polymorph [28,30,32,37,41]. However, the exact mechanism for the control mechanism by additives in most cases is still unknown.

Here, we report a study of polymorphs and crystallization of 2,6-dimethoxybenzoic acid (2,6MeOBA). 2,6MeOBA has been reported to crystallize in three polymorphic forms [42–46]. Form I is the stable polymorphic form [45,46]. Metastable polymorphs II and III, in previous studies, were described as disappearing polymorphs [45,46]. In this study, we explore the relative stability of 2,6MeOBA polymorphs and the ability of additives to alter the polymorphic outcome of its crystallization. 2,6MeOBA was selected for this study because of two factors. First, the two distinct hydrogen bonding patterns present in the stable and metastable polymorphs could more easily allow the additives to alter the polymorphic outcome of crystallization. Second, we selected this compound to try to find an approach for additive crystallization that would allow a reliable preparation procedure for the disappearing polymorphs. Our previous study [47] has already confirmed that polymorphs II and III can be obtained by varying the crystallization conditions. In this study, we additionally characterized forms I and III, performed screening of additives allowing control of the polymorphic outcome in the crystallization, explored the most promising additives for the crystallization control, and explored the effect of additives on phase transitions.

2. Materials and Methods

2,6-dimethoxybenzoic acid (2,6MeOBA) (purity 99%, polymorph I), polyethylene glycol (PEG, MW = 6000), and hydroxypropyl cellulose (HPC, MW = 100,000) were purchased from Alfa Aesar. 2,6-dimethoxybenzoic boronic acid (2,6MeOPheBorA) (purity 97%) was purchased from Fluorochem. The molecular structures of 2,6MeOBA and selected additives are shown in Figure 1. The water was deionized in the laboratory. Other additives (see Supplementary Materials, Table S1) and analytical grade organic solvents were purchased from commercial sources.
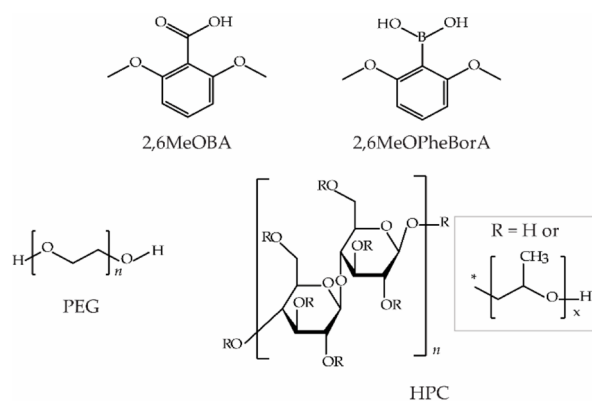
Figure 1. Molecular structure of 2,6MeOBA, 2,6MeOPheBorA, PEG, and HPC.

2.1. Crystallization Experiments

Several widely used solvents from different solvent classes were selected for the polymorph screening of 2,6MeOBA. For evaporation crystallization, 30–50 mg of 2,6MeOBA were dissolved in 2 to 3 mL of solvent and evaporated at 5, 25, and 50 °C. For cooling crystallization, 2,6MeOBA was dissolved in a selected solvent at 40 to 80 °C, depending on the boiling point of the solvent. The solutions obtained were filtered and cooled to 5 °C. The obtained products were collected by filtration, air-dried, and characterized with PXRD. Tetrahydrofuran (THF), acetonitrile (MeCN), and water were selected for the screening of additives, allowing control of crystallization polymorphic outcome.

Crystallization in the presence of additives in THF and MeCN was performed as a complete solvent evaporation. In 2 to 3 mL of solvent, 20 to 30 mg of additive and 30 to 50 mg of 2,6MeOBA were dissolved, and the solution was filtered and evaporated at room temperature. Crystallization in the presence of additives in water was performed as cooling crystallization. In 3–4 mL of water at 80 °C, 10–15 mg of additive and 20–25 mg of 2,6MeOBA were dissolved, filtered, and cooled to 5 °C. Three parallel crystallization experiments were performed for each additive. The products obtained were collected by filtration, air-dried, and characterized with PXRD.

Further cooling crystallization experiments were performed using Crystal16 (*Technobis*). Of all additives tested, three additives (2,6MeOPheBorA, PEG, HPC) were selected for these additional studies. Highly concentrated solutions (having supersaturation $c/c^* \approx 9$ at 25 °C) of 2,6MeOBA were made. A concentrated solution of 2,6MeOBA was prepared in the 50 mL flask of water equipped with an air reflux condenser. The solution was prepared by boiling and stirring for 2 to 3 h. The identical preparation process was used for solutions with additives using ~0.1 wt % HPC, 1 wt % PEG, or 0.5 wt % 2,6MeOPheBorA (the concentration given with respect to the water added). After boiling, the solution was stored at 90 °C and filtered. Then, 1 mL of the sample was transferred to preheated HPLC vial, which was placed in *Crystal16* preheated to 90 °C and then cooled to 10 °C with different cooling rates—20, 10, 1, and 0.1 °C·min^{-1} by using the stirring rate of 900 rpm. Another series of experiments with HPC suspension was prepared in situ in *Crystal16.* HPC has a low critical dissolution temperature of 45 °C [48], which means that at temperatures above 45 °C, it is insoluble in water. The suspension was prepared by using 23–25 mg of 2,6MeOBA ($c/c^* \approx 7$ at 25 °C) and 0.5 wt % of HPC added to 1 mL of water in an HPLC vial, heated to 90 °C using *Crystal16*, thermostated for 30 min to completely dissolve 2,6MeOBA, and cooled with the same cooling rates by additional stirring. Four parallel crystallization experiments were performed in all cases. The obtained products were collected by filtration, air dried, and characterized with PXRD.

To determine the effect of the amount of additive on the crystallization results, 2,6MeOBA solutions were prepared in situ in *Crystal16*. The additive weight fractions tested were 0.5; 0.7; 1; 1.5, and 2 wt %. HPC solutions were prepared as described above for

the 0.5 wt % solutions. The cooling rate was chosen based on the previous experiments—20 and 10 °C·min^{-1}. The solutions containing PEG were prepared by first making aqueous PEG solutions. Subsequently, 33 to 35 mg of 2,6MeOBA (c/c* $\approx$ 10 at 25 °C) and 1 mL of different concentration PEG solutions were added to the HPLC vial, heated to 90 °C for 30 min in *Crystal16*, and cooled with a cooling rate of 20 and 1 °C·min^{-1} by stirring. For each of the different crystallization conditions, blank crystallization experiments without any additive were performed. Each experiment was carried out as four parallel crystallizations. The obtained products were collected by filtration, air dried, and characterized with PXRD.

2.2. Solubility Measurements and Solvent-MediatedPhase Transition (SMPT) Studies

For these experiments, the 2,6MeOBA form I from the commercial sample was used as received, the form III was prepared in a phase transition that occurred by heating the form I at 160 °C in the air thermostat for 1 h. The phase purity of both forms was verified with PXRD (Bruker AXS, Karlsruhe, Germany).

Solubility measurements were performed using *Crystal16* (Technobis Crystallization Systems, Alkmaar, Netherlands). From 4 to 34 mg of each 2,6MeOBA polymorph was weighted in an HPLC vial, 1 mL of water or 1 wt % of the aqueous solution of PEG was added, and the mixtures were heated at a heating rate of 0.1 °C·min^{-1} from 10 to 90 °C. The stirring rate was 900 rpm. The temperature of dissolution was determined by recording the temperature at which the solution became transparent using turbidity measurements [49]. The experimental dependence of the temperature of solubility was fitted with linear regression and the van't Hoff equation by the least-squares approach using the Microsoft Excel Linest add-in.

To determine the thermodynamic stability of 2,6MeOBA polymorphs at different temperatures, slurry-bridging experiments were performed. Forms I and III with a 1:1 mass ratio were suspended in 1 mL of water, toluene, and aqueous solutions of 0.1 wt % HPC and 1 wt % PEG for 24 h at 25, 50, 70, and 80 °C with a stirring rate of 900 rpm.

The solvent-mediated phase transition kinetics in 2,6MeOBA suspensions in water, isopropanol (IPA), MeCN, and ~0.1 wt % of HPC, and 1 wt % of PEG aqueous solutions were determined at 25 °C. Four experiments in each of the solvents were prepared using a 1:1 ratio (*w/w*) of both polymorphs as well as pure polymorph III. The samples were collected after 15, 30, 45, and 60 min of stirring by filtration, air dried, and characterized with PXRD. Form III in 0.1 wt % HPC solution was suspended for 24 h because no SMPT was observed for 60 min.

2.3. Solid Phase Characterization

The PXRD patterns were measured at ambient temperature on a Bruker D8 Advance diffractometer using copper radiation (Cu K$_\alpha$; λ = 1.54180Å), equipped with a LynxEye position-sensitive detector. The tube voltage and current were set to 40 kV and 40 mA, respectively. The divergence slit was set at 0.6 mm. The anti-scatter slit was set at 8.0 mm. The PXRD patterns were recorded from 3° to 35° on the 2 θ scale. A scan speed of 0.2 s/0.02° was used.

Differential scanning calorimetry/thermogravimetry (DSC/TG) analysis was performed using the Mettler Toledo TGA/DSC 2 (Mettler Toledo, Greifensee, Switzerland). Closed aluminum pans were used. The heating of the samples from 25 to 250 °C was carried out at a heating rate of 10 °C·min^{-1}. Samples of 5 to 8 mg mass were used. The nitrogen flow rate was 30 mL·min^{-1}.

2.4. Rietveld Refinement for Form Quantification

The Rietveld refinement for the quantification of the polymorphs was performed with Profex 4.3.6 (Dobelin, N., Kleeberg, R., Solothurn, Switzerland) [50]. For this analysis, crystal structures of 2,6MeOBA polymorphs were acquired from the CSD with Ref. codes DMOXBA01 (form I), DMOXBA03 (form II), and DMOXBA07 (form III).

3. Results and Discussion

3.1. Characterization of 2,6MeOBA Polymorph

2,6MeOBA polymorphs are both conformational polymorphs and synthon polymorphs [44–46]. According to previous investigations, the most stable polymorph is form I, which crystallizes in the orthorhombic space group $P2_12_12_1$ [42,43] and contains 2,6MeOBA molecules in the *anti*-planar conformation linked by hydrogen-bonded chains that form the catemer synthon (see Figure 2). Both metastable polymorphs form II and form III contain 2,6MeOBA molecules in a *syn*-planar conformation that forms carboxylic acid homodimers [42,43]. Form II crystallizes in the tetragonal space group $P4_12_12$ [44]. After various screenings and additive experiments performed as part of this study, pure form II was never obtained, suggesting that it is the least stable 2,6MeOBA polymorph. Form III crystallizes in the monoclinic centrosymmetric space group $P2_1/c$ [45,46].
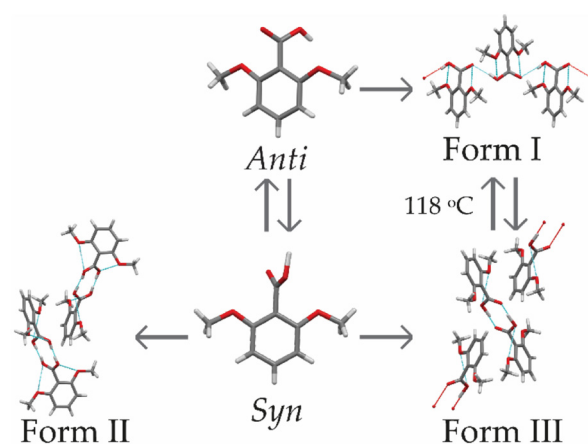
Figure 2. Relationships between 2,6MeOBA conformations and polymorphs. The connection between forms I and III is elucidated in this study.

3.1.1. Thermal Characterization and Solubility

In the DSC, traces of form I two endothermic events can be observed (see Figure 3). The peak onset at 118 °C corresponds to a phase transition of form I to form III, as confirmed by the PXRD analysis, while the second is the melting of form III. Form I and form III are enantiotropically related by the heat-of-transition rule [51], as the phase transition is endothermic. The melting point onset of form III is 190 °C. There is no change in the TG curves for any of these forms, except for the decomposition that occurs above 200 °C.
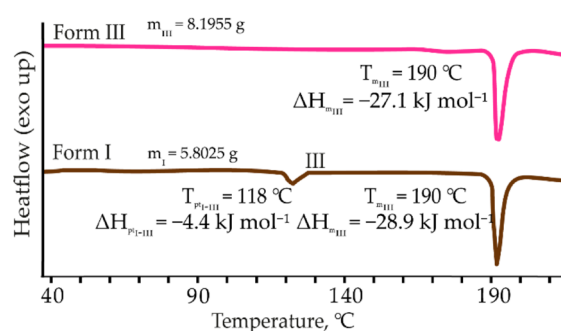
Figure 3. DSC curves of 2,6MeOBA polymorphs I and III (heating rate 10 °C·min^{-1}). The onset temperatures were used to describe each process observed in the DSC traces.

The solubility of forms I and III in water shows that form I is the stable polymorph (as determined from the lower solubility) at temperatures up to 79 °C (see Figure 4). At ambient temperature, the solubility of form III is 1.3 times higher than that of form I. Form III becomes the most stable polymorph above 79 °C. The theoretical solubility temperature dependence lines for each polymorph were obtained by fitting the natural logarithm of obtained solubility (ln$S$, where S in mg mL^{-1}) and the inverse of temperature ($1/T$, where T in K) to the van't Hoff Equation (1):

$$\ln S = \frac{a}{T} + b \tag{1}$$

Table 1. Coefficients of the van't Hoff equation for solubility curves of 2,6MeOBA polymorphs in pure water.

Polymorph	a	b	R^2	SE for lnS$_{calc}$
I	−3960 ± 130	15 ± 0.4	0.9894	0.09
III	−3400 ± 110	13 ± 0.3	0.9909	0.08
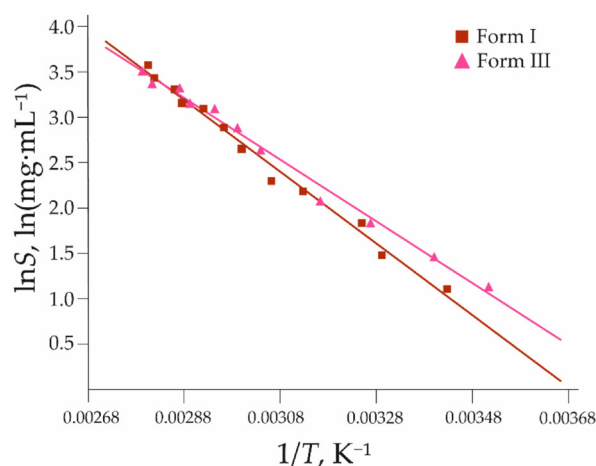
Figure 4. The solubility of 2,6MeOBA polymorphs I and III. Squares and triangles represent experimental data (see Supplementary Materials Tables S2 and S3), while lines are calculated using Equation (1) with coefficients a and b found in the fitting using the least-squares approach, given in Table 1.

3.1.2. Solvent-Mediated Phase Transition (SMPT)

The thermodynamic stability determined using slurry-bridging experiments at different temperatures agrees with the results obtained in the DSC/TG analysis and from the solubility curves. After 24 h, pure form I was obtained in water and toluene by suspending a mixture of both forms at 25, 50, and 70 °C. However, form III was obtained in both solvents at a temperature of 80 °C. These results confirm that the solubility curves of both forms cross between 70 and 80 °C.

Measurements of solvent-mediated phase transition kinetics show that the transformation rate in the slurry-bridging experiments is very fast (see Figure 5). Pure form I was obtained in less than 15 min at 25 °C in the mixture of both forms in the three solvents tested. The complete transformation of pure form III to pure form I in IPA and MeCN occurred as fast as from the polymorph mixture, but in water, it is slower and requires between 15 and 30 min. This can be explained by the lower solubility of 2,6MeOBA in water or the better possibilities of hydrogen bonding with water for 2,6MeOBA in *syn* conformation.
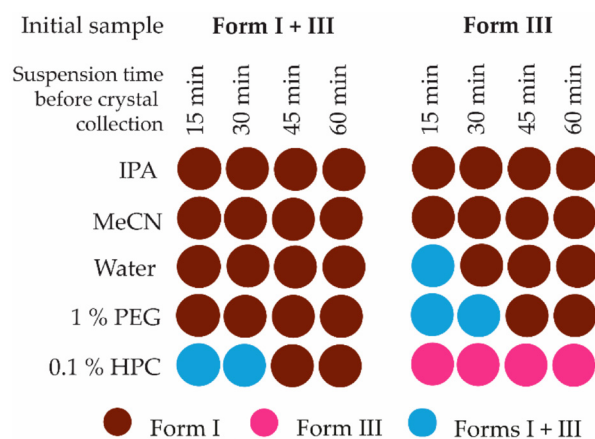
Figure 5. Polymorphic composition of the solid phase after selected times during SMPT kinetic experiments at 25 °C.

3.2. Crystallization from Pure Solvents

In most cases of the cooling crystallization, form I was obtained, although impurity of form III was sometimes present. The polymorph obtained correlated with the temperature in the evaporation crystallization experiments: at lower temperatures (5 °C) in most of the experiments, form I was obtained, frequently with some impurities of form III. However, at higher temperatures (50 °C), the polymorphic outcome is the opposite. The thermodynamic equilibrium point is rather close to 50 °C; therefore, form III is more likely to be obtained compared to evaporation at 5 °C. 1,4-dioxane, MeCN, and ketones can be used as solvents to obtain form III by evaporation, but these are not selective solvents. Water was the only solvent from which form I was obtained in almost all crystallizations. Using these preliminary crystallization experiments, three solvents were selected for crystallization experiments in the presence of additives: MeCN, THF, and water. The results of the crystallization experiments from pure solvents with phase composition of samples containing polymorph mixtures obtained using the Rietveld analysis are given in the supporting information, Table S4 and Figure S2.

3.3. Crystallization with Additives

The additives selected for the crystallization were polymers and surfactants that have the ability to form different intermolecular interactions. The polymorphic outcome of the crystallization in the presence of the selected additives was the same in most cases as that in crystallization from a pure solvent. From THF, some of the additives resulted in the crystallization of form III, whereas tween 20 promoted the formation of form I in all three parallel samples (see Figure 6, detailed results can be seen in Table S5). This additive was not further studied because the study aimed to find an approach for crystallization of the metastable form. Additives facilitated the concomitant crystallization of forms I and III from MeCN. Despite the very low solubility, polyvinyl chloride promoted the crystallization of form I. Overall, it can be concluded that the outcome of the evaporation crystallization from these solvents is difficult to control, even in the presence of the selected additives.

Repeated crystallizations from pure water with immediate filtration and analysis of the obtained crystals confirmed that a mixture of forms I and III crystallizes, followed by a solvent-mediated phase transition in the case that the crystals remain in suspension (see Figure 6). Therefore, only form I was observed in the preliminary crystallization experiments. Phenylboronic acid and several of its derivatives were tested as additives in crystallization from water because it was used as an additive to crystallize form II in one of the previous studies [44]. Concomitant crystallization of forms I and III or the stable form I was observed using several of the tested additives, including phenylboronic acid,

4-iodphenylboronic acid, and 4-carboxyphenylboronic acid. Some of the additives (e.g., BIS-TRIS, PEG) facilitated the formation of form II in a mixture with other polymorphs. All three crystallizations in the presence of HPC occurred very fast and produced form III. Almost the same crystallization rate was observed in the presence of 2,6MeOPheBorA, but the crystallization product was form III with minor impurities of form I. Crystallization in the presence of PEG was slower than in the presence of HPC and 2,6MeOPheBorA, but also, in this case, in two of the crystallizations, pure form III was obtained, although in the third crystallization, a mixture of all three polymorphs was formed. Additionally, form III was obtained in crystallization from THF in the presence of PEG in two of three experiments. Based on the results obtained, HPC, 2,6MeOPheBorA, and PEG were chosen for more detailed studies.
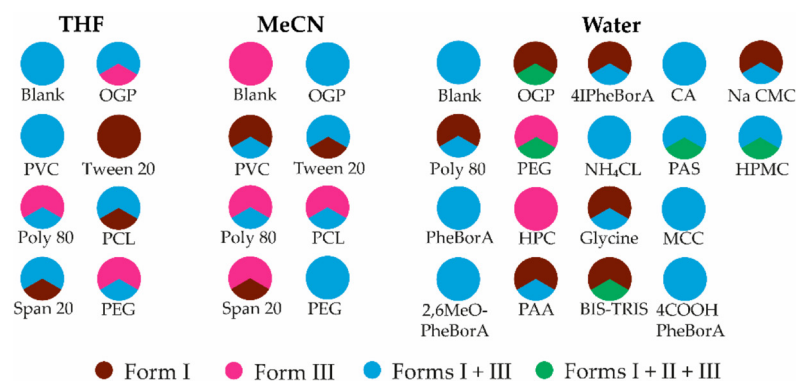
Figure 6. Polymorphic outcome of crystallization experiments in the presence of additives from THF, MeCN, and water. Each 1/3 of the pie chart represents one of the parallel experiments.

3.3.1. Crystallization from Highly Concentrated Water Solution

Highly concentrated 2,6MeOBA water solutions were used for these experiments to understand the additive effect on the crystallization of concentrated solutions. Mixtures of three polymorphs were obtained in crystallization from a highly concentrated pure water solution with the fastest cooling rate of 20 °C·min^{-1} (see Figure 7, column A). This result agrees with Ostwald's rule of stages [52]: instead of the nucleation of the most stable form, the polymorph corresponding to the nearest minimum energy nucleates. Two different polymorph mixtures were obtained at a cooling rate of 10 °C·min^{-1}. A medium cooling rate resulted in the formation of a mixture of forms I and III. The cooling rate needs to be fast to obtain form II, but such an approach cannot prevent concomitant crystallization with other forms. Additionally, form II very rapidly transforms into more stable forms. Supersaturation can also play an important role in obtaining unstable polymorphs [53,54]. A higher concentration of 2,6MeOBA was used for samples cooled with a specific cooling rate compared to the preliminary crystallization experiments from pure solvents. Nevertheless, the effect of supersaturation on the polymorphic outcome was not examined. The four samples with the lowest cooling rate (0.1 °C·min^{-1}) produced form III; however, at a slower cooling rate, the formation of the thermodynamically stable form I was expected. In these experiments, the crystals appeared at approximately 60 °C, which is rather closer to the thermodynamical equilibrium point of forms I and III. The crystals appeared at lower temperatures (40–50 °C) in crystallizations using faster cooling rates. The phase transition to form I was prevented as the crystals formed near the water surface and formed large agglomerates. In contrast, the crystals in the SMPT kinetics experiments and in the case of using faster cooling rates were smaller and evenly suspended in the solution. Using PEG (see Figure 7, column B, detailed results can be seen in Table S6) and 2,6MeOPheBorA (see Figure 7, column C) as additives and 2,6MeOBA solution with a concentration corresponding to c/c* ≈ 9 at 25 °C, a mixture of forms I and III was obtained in most of the crystallizations. In contrast, using HPC as an additive (see Figure 7, columns D and E) at

both additive concentrations, pure form III was the most frequent crystallization product. The formation of form III was facilitated by the fastest cooling rates (20 and 10 °C·min^{-1}). On the contrary, under the same conditions as those of pure water, concomitant crystallization of 2,6MeOBA polymorphs always occurred. Interestingly, at the slowest cooling rate (0.1 °C·min^{-1}), additives promoted crystallization of form I. Using 0.5% HPC suspension and 2,6MeOBA solution with lower concentration (corresponding to c/c* ≈ 7 at 25 °C), crystallization of form III is promoted more clearly if compared to crystallization from 0.1% HPC solution and a higher concentration of 2,6MeOBA (corresponding to c/c* ≈ 9 at 25 °C). It is possible that more HPC molecules can interact with 2,6MeOBA in heterogeneous crystallization and stabilize the *syn* conformation during nucleation, similar to the research by Lin et al. studying the crystallization of α,ω-alkanedicarboxylic acids [55]. Lin et al. [55] developed a method to control the crystallization outcome for conformation polymorphs having similar structures. The desired polymorph was crystallized on the template lattice, where dimer formation was possible. An additional explanation for why the crystallization control in homogeneous 0.1% HPC solution is not so effective can be the higher supersaturation; there are more 2,6MeOBA molecules but fewer HPC molecules, which apparently provide formation of form III. PEG also has the potential to control the crystallization outcome in the case of a moderately slow cooling rate (1 °C·min^{-1}) from a highly concentrated solution. It is possible that the additives slow down the phase transition to form I, which can initiate right after the nucleation, but not enough to obtain pure form III, as stirring is still employed after the nucleation. The phase transition time can, in fact, be reduced as the crystal sizes obtained in additive crystallization are smaller than those obtained in crystallization from pure water. In general, the tested additives do not provide fully selective crystallization control. Nevertheless, PEG and HPC under multiple conditions distinctly favor the formation of form III, whereas, under the tested conditions, 2,6MeOPheBorA still provided a mixture of 2,6MeOBA polymorphs. Crystallizations in the presence of PEG with a cooling rate of 20 and 1 °C·min^{-1} and in the presence of HPC with 20 and 10 °C·min^{-1} were selected for further study to test the effect of the amount of additive on the crystallization result.
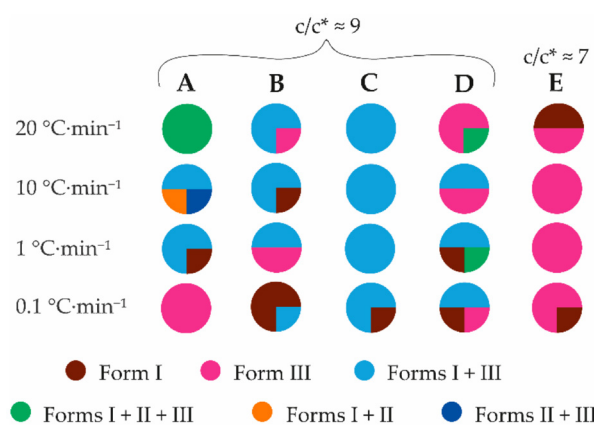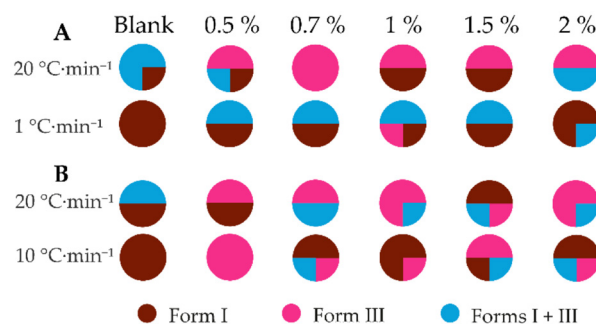

Figure 7. Polymorphic outcome of the crystallization experiments from water using different additives and cooling rates. A—pure water; B—1% PEG; C—0.5% 2,6MeOPheBorA; D—0.1% HPC; E—heterogeneous crystallization using 0.5% HPC.

3.3.2. The Effect of the Additive Quantity on the Crystallization Outcome

From pure water using the slowest cooling rate in most of the crystallizations, form I was obtained, but a mixture of forms I and III or the stable form I was obtained using the fastest cooling rate (see Figure 8, detailed results can be seen in Table S7). Form III was obtained in most of the crystallizations using both additives and the fastest cooling rate. Again, the presence of additives did not provide selective crystallization of either of

the polymorphs. Concomitant crystallization of both polymorphs was less frequent in the presence of HPC than in the presence of PEG. No clear correlation was observed between the amount of additive selected and the crystallization outcome. It is likely that additives decrease the interfacial energy and, therefore, lower the nucleation Gibbs energy, facilitating the crystallization of form III from this solution compared to the pure water solution.

Figure 8. Polymorphic outcome of the crystallization experiments from water in the presence of different quantities of (**A**) PEG and (**B**) HPC.

3.4. Effect of Additives on Polymorph Solubility and Solvent-Mediated Phase Transitions

The solubility of form I is almost unaffected by the addition of 1% PEG (see Figure 9). At temperatures up to 30 °C, the solubility is almost identical to that in pure water, but at higher temperatures, the solubility slightly decreased. In contrast, the solubility of form III in the presence of PEG increases slightly at temperatures up to 35 °C, but the solubility at higher temperatures is lower than in the pure solvent. As the PEG solution separated into two phases above 75 °C, the solubility in this solution cannot be determined above this temperature. Additives have been shown to affect the solubility and crystal growth of organic compounds in the literature. For example, additives have been demonstrated to decrease the solubility but increase the crystal nucleation and growth rates of *p*-methylacetanilide [56]. The highly similar solubility of both forms can explain the nearly always observed concomitant crystallization in the presence of this additive, as observed in the crystallization experiments described in Section 3.3.1. The thermodynamic equilibrium point determined is 8 °C lower than that in pure water.

Table 2. Coefficients of the van't Hoff equation for solubility curves of 2,6MeOBA polymorphs in 1% aqueous solution of PEG.

Polymorph	a	b	R^2	SE for lnS_{calc}
I + PEG	-3910 ± 150	14 ± 0.5	0.9885	0.08
III + PEG	-3180 ± 200	12 ± 0.6	0.9698	0.12

Slurry-bridging experiments in the presence of PEG and HPC additives led to the same conclusions as those performed in pure water and toluene (see Section 3.1.2); after 24 h, the pure form I was obtained at 25, 50, and 70 °C, while at 80 °C, pure form III was obtained.

Using both additives, the results of the SMPT kinetic experiments were almost identical to those of the pure solvents (see Figure 6). In the presence of 1% PEG, the SMPT time of the 1:1 mixture of both polymorphs is the same as in pure solvents (less than 15 min), but 0.1% HPC decelerates the SMPT to form I at 25 °C, as the SMPT time in the presence of HPC is between 30 and 45 min. The time of SMPT from pure form III in the presence of 1% PEG is longer (between 30 and 45 min) than from the mixture of both polymorphs, but the addition of 0.1% HPC inhibited the SMPT of pure form III to form I. SMPT was not detected by sample slurrying for 24 h. It is likely that PEG and HPC interact with the carboxyl group of 2,6MeOBA and stabilize the *syn* configuration in nucleation and inhibit the nucleation of form I.
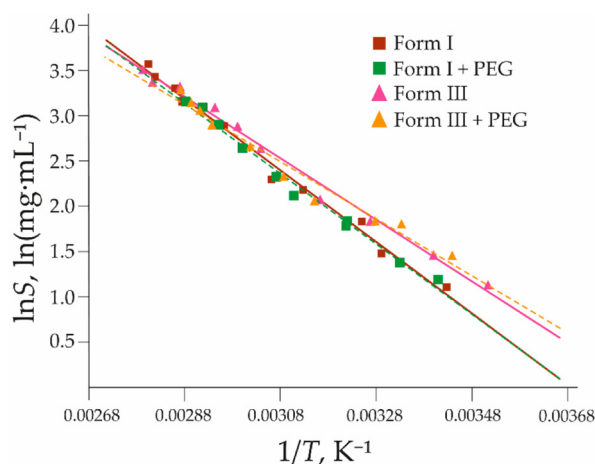
Figure 9. The solubility curves of 2,6MeOBA polymorphs I and III in pure water and 1% aqueous solution of PEG. Brown solid line—form I in pure water; Green dashed line—form I in 1% PEG solution; Magenta solid line—form III in pure water; Orange dashed line—form III in a 1% PEG solution. Triangles and squares represent the experimental data (see Supplementary Materials Tables S8 and S9); lines are calculated using Equation (1) with coefficients a and b found in the fitting using the least-squares approach, given in Table 2.

4. Conclusions

The three previously reported polymorphs of 2,6MeOBA can be crystallized using different crystallization methods. Thermodynamic stability determined based on solvent-mediated phase transformations and solubility data shows that form III is stable at temperatures above 79 °C, whereas form I is thermodynamically stable at lower temperatures. The solvent-mediated phase transition from metastable to thermodynamically stable 2,6MeOBA polymorphs is very fast (less than 15 min at 25 °C and high stirring rates), which could explain why the preparation of metastable 2,6MeOBA polymorphs II and III is challenging.

The cooling rate and supersaturation are among the main variables that change the possibility of obtaining metastable polymorphs of 2,6MeOBA. Form III can be crystallized from water using a slow cooling rate and a fast stirring rate. Crystallization additives were shown to be able to improve the control of the crystallization polymorphic outcome, allowing nucleation for the pure metastable polymorph and decelerating the solvent-mediated phase transition rate by inhibiting the nucleation of the thermodynamically stable form. HPC can be used to slow the phase transition of form III to form I, although it cannot selectively provide the nucleation of only pure form III. PEG can be used to increase the probability of crystallization of metastable polymorphs of 2,6MeOBA.

for form I in 1% PEG water solution and coefficients a and b from Equation (1) found in the fitting using the least-squares approach; Table S9: Experimental solubility data for form III in 1% PEG water solution and coefficients a and b from Equation (1) found in the fitting using the least-squares approach.

Author Contributions: Investigation, writing—original draft preparation and visualization, A.S.; Conceptualization, methodology, and writing—review and editing, A.S. and A.B.; Supervision, A.B. All authors have read and agreed to the published version of the manuscript.

Institutional Review Board Statement: Not applicable.

Informed Consent Statement: Not applicable.

Data Availability Statement: No new data were created or analyzed in this study. Data sharing is not applicable to this article.

Conflicts of Interest: The authors declare that they have no conflict of interest.

Abbreviations

PVC—polyvinyl chloride; Poly 80—polysorbate 80; OGP—octyl β-D-glucopyranoside; PCL—polycaprolactone; PEG—polyethylene glycol; PheBorA—phenylboronic acid; 2,6MeOPheBorA— 2,6-dimethoxyphenylboronic acid; HPC—hydroxypropyl cellulose; PAA—poly(acrylic amide); 4IPheBorA—4-iodphenylboronic acid; BIS-TRIS—bis(2-hydroxyethyl)amino-tris-(hydroxymethyl) methane; CA—cellulose acetate; PAS—poly-(acrylic acid); MCC—microcrystalline cellulose; 4COOHPheBorA—4-carboxyphenylboronic acid; Na CMC—sodium carboxymethyl cellulose; HPMC—hydroxypropylmethyl cellulose.

References

1. Aitipamula, S.; Nangia, A. Polymorphism: Fundamentals and Applications. In *Supramolecular Chemistry*; John Wiley & Sons, Ltd.: Chichester, UK, 2012; ISBN 9780470661345.
2. Hilfiker, R. *Polymorphism: In the Pharmaceutical Industry*; Hilkifer, R., Ed.; Wiley-VCH Verlag GmbH & Co. KGaA: Weinheim, Germany, 2006; ISBN 9783527311460.
3. Fabbiani, F.P.A.; Allan, D.R.; Parsons, S.; Pulham, C.R. An Exploration of the Polymorphism of Piracetam Using High Pressure. *CrystEngComm* **2005**, *7*, 179–186. [CrossRef]
4. Karpinski, P.H. Polymorphism of Active Pharmaceutical Ingredients. *Chem. Eng. Technol.* **2006**, *29*, 233–237. [CrossRef]
5. Lu, J.; Rohani, S. Polymorphism and Crystallization of Active Pharmaceutical Ingredients (APIs). *Curr. Med. Chem.* **2009**, *16*, 884–905. [CrossRef]
6. Tandon, R.; Tandon, N.; Thapar, R.K. Patenting of Polymorphs. *Pharm. Pat. Anal.* **2018**, *7*, 59–63. [CrossRef] [PubMed]
7. Rakoczy, W.A.; Mazzochi, D.M. The Case of the Disappearing Polymorph: "Inherent Anticipation" and the Impact of SmithKline Beecham Corp. v Apotex Corp. (Paxil®) on Patent Validity and Infringement by Inevitable Conversion. *J. Generic Med.* **2006**, *3*, 131–139. [CrossRef]
8. Snider, D.A.; Addicks, W.; Owens, W. Polymorphism in Generic Drug Product Development. *Adv. Drug Deliv. Rev.* **2004**, *56*, 391–395. [CrossRef]
9. Pudipeddi, M.; Serajuddin, A.T.M. Trends in Solubility of Polymorphs. *J. Pharm. Sci.* **2005**, *94*, 929–939. [CrossRef] [PubMed]
10. De Tros Ilarduya, M.C.; Martín, C.; Goñi, M.M.; Martínez-Uhárriz, M.C. Dissolution Rate of Polymorphs and Two New Pseudopolymorphs of Sulindac. *Drug Dev. Ind. Pharm.* **1997**, *23*, 1095–1098. [CrossRef]
11. Gu, C.H.; Grant, D.J.W. Estimating the Relative Stability of Polymorphs and Hydrates from Heats of Solution and Solubility Data. *J. Pharm. Sci.* **2001**, *90*, 1277–1287. [CrossRef] [PubMed]
12. Vippagunta, S.R.; Brittain, H.G.; Grant, D.J.W. Crystalline Solids. *Adv. Drug Deliv. Rev.* **2001**, *48*, 3–26. [CrossRef]
13. Gupta, S.; Kesarla, R.; Omri, A. Formulation Strategies to Improve the Bioavailability of Poorly Absorbed Drugs with Special Emphasis on Self-Emulsifying Systems. *ISRN Pharm.* **2013**, *2013*, 848043. [CrossRef] [PubMed]
14. Bauer, J.; Spanton, S.; Henry, R.; Quick, J.; Dziki, W.; Porter, W.; Morris, J. Ritonavir: An Extraordinary Example of Conformational Polymorphism. *Pharm. Res.* **2001**, *18*, 859–866. [CrossRef] [PubMed]
15. Aguiar, A.J.; Krc, J.; Kinkel, A.W.; Samyn, J.C. Effect of Polymorphism on the Absorption of Chloramphenicol from Chloramphenicol Palmitate. *J. Pharm. Sci.* **1967**, *56*, 847–853. [CrossRef] [PubMed]

16. Singhal, D.; Curatolo, W. Drug Polymorphism and Dosage Form Design: A Practical Perspective. *Adv. Drug Deliv. Rev.* **2004**, *56*, 335–347. [CrossRef] [PubMed]

17. Censi, R.; Martino, P. di Polymorph Impact on the Bioavailability and Stability of Poorly Soluble Drugs. *Molecules* **2015**, *20*, 18759–18776. [CrossRef] [PubMed]

18. Tang, W.; Sima, A.D.; Gong, J.; Wang, J.; Li, T. Kinetic Difference between Concomitant Polymorphism and Solvent-Mediated Phase Transformation: A Case of Tolfenamic Acid. *Cryst. Growth Des.* **2020**, *20*, 1779–1788. [CrossRef]

19. Su, Y.; Xu, J.; Shi, Q.; Yu, L.; Cai, T. Polymorphism of Griseofulvin: Concomitant Crystallization from the Melt and a Single Crystal Structure of a Metastable Polymorph with Anomalously Large Thermal Expansion. *Chem. Commun.* **2018**, *54*, 358–361. [CrossRef]

20. Du, W.; Yin, Q.; Bao, Y.; Xie, C.; Hou, B.; Hao, H.; Chen, W.; Wang, J.; Gong, J. Concomitant Polymorphism of Prasugrel Hydrochloride in Reactive Crystallization. *Ind. Eng. Chem. Res.* **2013**, *52*, 16182–16189. [CrossRef]

21. Jiang, S.; ter Horst, J.H.; Jansens, P.J. Concomitant Polymorphism of O-Aminobenzoic Acid in Antisolvent Crystallization. *Cryst. Growth Des.* **2008**, *8*, 37–43. [CrossRef]

22. Munshi, P.; Venugopala, K.N.; Jayashree, B.S.; Guru Row, T.N. Concomitant Polymorphism in 3-Acetylcoumarin: Role of Weak C-H · · · O and C-H · · · π Interactions. *Cryst. Growth Des.* **2004**, *4*, 1105–1107. [CrossRef]

23. Singh, A.; Lee, I.S.; Kim, K.; Myerson, A.S. Crystal Growth on Self-Assembled Monolayers. *CrystEngComm* **2011**, *13*, 24–32. [CrossRef]

24. Hernández Espinell, J.R.; López-Mejías, V.; Stelzer, T. Revealing Polymorphic Phase Transformations in Polymer-Based Hot Melt Extrusion Processes. *Cryst. Growth Des.* **2018**, *18*, 1995–2002. [CrossRef] [PubMed]

25. Svard, M.; Rasmuson, Å.C. M-Hydroxybenzoic Acid: Quantifying Thermodynamic Stability and Influence of Solvent on the Nucleation of a Polymorphic System. *Cryst. Growth Des.* **2013**, *13*, 1140–1152. [CrossRef]

26. Telford, R.; Seaton, C.C.; Clout, A.; Buanz, A.; Gaisford, S.; Williams, G.R.; Prior, T.J.; Okoye, C.H.; Munshi, T.; Scowen, I.J. Stabilisation of Metastable Polymorphs: The Case of Paracetamol Form III. *Chem. Commun.* **2016**, *52*, 12028–12031. [CrossRef] [PubMed]

27. Lee, E.H.; Byrn, S.R. Stabilization of Metastable Flufenamic Acid by Inclusion of Mefenamic Acid: Solid Solution or Epilayer? *J. Pharm. Sci.* **2010**, *99*, 4013–4022. [CrossRef] [PubMed]

28. Moshe, H.; Levi, G.; Mastai, Y. Polymorphism Stabilization by Crystal Adsorption on a Self-Assembled Monolayer. *CrystEngComm* **2013**, *15*, 9203–9209. [CrossRef]

29. Simone, E.; Steele, G.; Nagy, Z.K. Tailoring Crystal Shape and Polymorphism Using Combinations of Solvents and a Structurally Related Additive. *CrystEngComm* **2015**, *17*, 9370–9379. [CrossRef]

30. Song, R.Q.; Cölfen, H. Additive Controlled Crystallization. *CrystEngComm* **2011**, *13*, 1249–1276. [CrossRef]

31. Tulli, L.G.; Moridi, N.; Wang, W.; Helttunen, K.; Neuburger, M.; Vaknin, D.; Meier, W.; Shahgaldian, P. Polymorphism Control of an Active Pharmaceutical Ingredient beneath Calixarene-Based Langmuir Monolayers. *Chem. Commun.* **2014**, *50*, 3938–3940. [CrossRef] [PubMed]

32. Moridi, N.; Danylyuk, O.; Suwinska, K.; Shahgaldian, P. Monolayers of an Amphiphilic Para-Carboxy-Calix[4]Arene Act as Templates for the Crystallization of Acetaminophen. *J. Colloid Interface Sci.* **2012**, *377*, 450–455. [CrossRef] [PubMed]

33. Hiremath, R.; Basile, J.A.; Varney, S.W.; Swift, J.A. Controlling Molecular Crystal Polymorphism with Self-Assembled Monolayer Templates. *J. Am. Chem. Soc.* **2005**, *127*, 18321–18327. [CrossRef]

34. Hiremath, R.; Varney, S.W.; Swift, J.A. Selective Growth of a Less Stable Polymorph of 2-Iodo-4-Nitroaniline on a Self-Assembled Monolayer Template. *Chem. Commun.* **2004**, *23*, 2676–2677. [CrossRef] [PubMed]

35. Zhang, B.; Hou, X.; Dang, L.; Wei, H. Selective Polymorphic Crystal Growth on Self-Assembled Monolayer Using Molecular Modeling as an Assistant Method. *J. Cryst. Growth* **2019**, *518*, 81–88. [CrossRef]

36. López-Mejías, V.; Kampf, J.W.; Matzger, A.J. Nonamorphism in Flufenamic Acid and a New Record for a Polymorphic Compound with Solved Structures. *J. Am. Chem. Soc.* **2012**, *134*, 9872–9875. [CrossRef]

37. Simone, E.; Cenzato, M.V.; Nagy, Z.K. A Study on the Effect of the Polymeric Additive HPMC on Morphology and Polymorphism of Ortho-Aminobenzoic Acid Crystals. *J. Cryst. Growth* **2016**, *446*, 50–59. [CrossRef]

38. Caridi, A.; Kulkarni, S.A.; di Profio, G.; Curcio, E.; ter Horst, J.H. Template-Induced Nucleation of Isonicotinamide Polymorphs. *Cryst. Growth Des.* **2014**, *14*, 1135–1141. [CrossRef]

39. Watson, S.; Nie, M.; Wang, L.; Stokes, K. Challenges and Developments of Self-Assembled Monolayers and Polymer Brushes as a Green Lubrication Solution for Tribological Applications. *RSC Adv.* **2015**, *5*, 89698–89730. [CrossRef]

40. Rossi, A.; Savioli, A.; Bini, M.; Capsoni, D.; Massarotti, V.; Bettini, R.; Gazzaniga, A.; Sangalli, M.E.; Giordano, F. Solid-State Characterization of Paracetamol Metastable Polymorphs Formed in Binary Mixtures with Hydroxypropylmethylcellulose. *Thermochim. Acta* **2003**, *406*, 55–67. [CrossRef]

41. Parambil, J.V.; Poornachary, S.K.; Heng, J.Y.Y.; Tan, R.B.H. Template-Induced Nucleation for Controlling Crystal Polymorphism: From Molecular Mechanisms to Applications in Pharmaceutical Processing. *CrystEngComm* **2019**, *21*, 4122–4135. [CrossRef]

42. Bryan, R.F.; White, D.H. 2,6-Dimethoxybenzoic Acid. *Acta Crystallogr. Sect. B Struct. Crystallogr. Cryst. Chem.* **1982**, *38*, 1014–1016. [CrossRef]

43. Portalone, G. Redetermination of 2,6-Dimethoxy-Benzoic Acid. *Acta Crystallogr. Sect. E Struct. Rep. Online* **2009**, *65*, o327–o328. [CrossRef] [PubMed]

44. Portalone, G. A New Polymorph of 2,6-Dimethoxybenzoic Acid. *Acta Crystallogr. Sect. E Struct. Rep. Online* **2011**, *67*, o3394–o3395. [CrossRef] [PubMed]

45. Portalone, G. Crystal Structure and Hirshfeld Surface Analysis of a Third Polymorph of 2,6-Dimethoxybenzoic Acid. *Acta Crystallogr. Sect. E Crystallogr. Commun.* **2020**, *76*, 1823–1826. [CrossRef] [PubMed]

46. Pal, R.; Jelsch, C.; Malaspina, L.A.; Edwards, A.J.; Murshed, M.M.; Grabowsky, S. Syn and Anti Polymorphs of 2,6-Dimethoxy Benzoic Acid and Its Molecular and Ionic Cocrystals: Structural Analysis and Energetic Perspective. *J. Mol. Struct.* **2020**, *1221*, 128721. [CrossRef]

47. Bērziņš, A.; Semjonova, A.; Actiņš, A.; Salvalaglio, M. Speciation of Substituted Benzoic Acids in Solution: Evaluation of Spectroscopic and Computational Methods for the Identification of Associates and Their Role in Crystallization. *Cryst. Growth Des.* **2021**, *21*, 4823–4836. [CrossRef]

48. Brady, J.; Drig, T.; Lee, P.I.; Li, J.X. Polymer Properties and Characterization. In *Developing Solid Oral Dosage Forms: Pharmaceutical Theory and Practice*, 2nd ed.; Qiu, Y., Chen, Y., Zhang, G., Yu, L., Mantri, R.V., Eds.; Elsevier: Amsterdam, The Netherlands, 2017; pp. 181–223. ISBN 9780128024478.

49. Reus, M.A.; van der Heijden, A.E.D.M.; ter Horst, J.H. Solubility Determination from Clear Points upon Solvent Addition. *Org. Process Res. Dev.* **2015**, *19*, 1004–1011. [CrossRef]

50. Doebelin, N.; Kleeberg, R. Profex: A Graphical User Interface for the Rietveld Refinement Program BGMN. *J. Appl. Crystallogr.* **2015**, *48*, 1573–1580. [CrossRef]

51. Burger, A.; Ramberger, R. On the Polymorphism of Pharmaceuticals and Other Molecular Crystals. I. *Mikrochim. Acta* **1979**, *72*, 259–271. [CrossRef]

52. Ostwald, W. Studien Über Die Bildung Und Umwandlung Fester Körper. *Z. Phys. Chem.* **1897**, *22U*, 289–330. [CrossRef]

53. Datta, S.; Grant, D.J.W. Effect of Supersaturation on the Crystallization of Phenylbutazone Polymorphs. *Cryst. Res. Technol.* **2005**, *40*, 233–242. [CrossRef]

54. Liu, Y.; van den Berg, M.H.; Alexander, A.J. Supersaturation Dependence of Glycine Polymorphism Using Laser-Induced Nucleation, Sonocrystallization and Nucleation by Mechanical Shock. *Phys. Chem. Chem. Phys.* **2017**, *19*, 19386–19392. [CrossRef] [PubMed]

55. Lin, J.; Shi, P.; Wang, Y.; Wang, L.; Ma, Y.; Liu, F.; Wu, S.; Gong, J. Template Design Based on Molecular and Crystal Structure Similarity to Regulate Conformational Polymorphism Nucleation: The Case of α,ω-Alkanedicarboxylic Acids. *IUCrJ* **2021**, *8*, 814–822. [CrossRef] [PubMed]

56. Wu, H.; Wang, J.; Liu, Q.; Zong, S.; Tian, B.; Huang, X.; Wang, T.; Yin, Q.; Hao, H. Influences and the Mechanism of Additives on Intensifying Nucleation and Growth of P-Methylacetanilide. *Cryst. Growth Des.* **2020**, *20*, 973–983. [CrossRef]

II

Semjonova, A., Bērziņš, A.

SURFACTANT PROVIDED CONTROL OF CRYSTALLIZATION POLYMORPHIC OUTCOME AND STABILIZATION OF METASTABLE POLYMORPHS OF 2,6-DIMETHOXYPHENYLBORONIC ACID

Crystals, **2022,** *12*, 1738

Article

Surfactant Provided Control of Crystallization Polymorphic Outcome and Stabilization of Metastable Polymorphs of 2,6-Dimethoxyphenylboronic Acid

Aina Semjonova * ![ORCID] **and Agris Bērziņš** ![ORCID]

Faculty of Chemistry, University of Latvia, Jelgavas iela 1, LV-1004 Rīga, Latvia
* Correspondence: aina.semjonova@lu.lv

Abstract: 2,6-Dimethoxyphenylboronic acid was used as a model substance to investigate the additive crystallization approach for polymorph control in phenylboronic acids. It was crystallized under different conditions by performing evaporation and cooling crystallization from different solvents. Most of the crystallizations from pure solvents produced the thermodynamically stable Form I, but in evaporation crystallization from alcohols, Form II or even a new polymorph, Form III, could be obtained. Structurally related substances, polymers, and surfactants with diverse intermolecular interaction possibilities were tested as additives. Surfactants were found to facilitate the crystallization of the metastable forms and therefore were investigated more extensively. The surfactants Span 20 and *n*–octyl-β-D-glucopyranoside provided crystallization of the metastable forms in the evaporation crystallization and notably stabilized Form II. The lattice energy, energy frameworks, Hirshfeld surface analysis, full interaction maps, and morphology prediction were used to identify the structural differences between Forms I and II and rationalize the ability of the additives to provide formation of Form II in the crystallization and to stabilize it.

1. Introduction

Most of the drug dosage forms of active pharmaceutical ingredients (APIs) are in solid form. These drug dosage forms include not only tablets and capsules, but also powders for parenteral applications and powder inhalers [1]. Approximately half of APIs show the ability to crystallize in different polymorphs [1,2]. Polymorphs have the same chemical composition but different molecule packing and/or conformation in the crystal lattice [3,4]. They have different physical properties—for example, solubility [5,6], bioavailability [7] or sometimes colour [8]. It is important to perform polymorph screening and identify the stable polymorph before drug manufacturing [1,4]. In addition, it is required to check the stability of the selected polymorph in long-term storage. There have been several cases [9] where a new and more stable polymorph appeared many years after drug development. Such late appearance of a more stable polymorph can cause problems for patients, from low drug efficacy to eventually disrupting the supply of medicines [10]. Metastable polymorphs, although having better solubility and dissolution rates [4], can transform to the stable form [6]. Therefore, there is a need to improve the stability of metastable forms. One way to achieve this is to inhibit the transformation rate by using additives in the crystallization process or in the drug dosage form. Additives usually improve the kinetic stability of the metastable form [11] but can also change the relative stability of polymorphs [12,13]. The effect of additives on nucleation has been extensively studied [14], but there is still too little evidence for understanding the mechanism of additive provided crystallization polymorphic outcome control. Additives can affect the kinetics of nucleation and related parameters [14–18], the thermodynamic aspects of crystallization, or both of these aspects

simultaneously [11]. Additive crystallization is widely used in natural and industrial processes, from biomineralization to material synthesis [19].

It is known that crystals containing similar hydrogen bond synthons can epitaxially grow on structurally related additives [20]. Structurally similar additives can inhibit [21] or promote [15,22–25] nucleation of a specific polymorph. Nucleation inhibition can occur by blocking the movement of surface steps, kinks, or terraces, therefore inhibiting crystal growth [18]. On the contrary, small, structurally similar molecular compounds can also be integrated into the lattice and operate as a pre-nucleation precursor [11,18] but will lead to this additive being an impurity of the obtained crystals. According to the European Pharmacopoeia, it is important to identify impurities to ensure the safety of pharmaceutical products [26], and structurally related additives can have a pharmacological or toxic effect [27–30]. Therefore, not all structurally related additives can be used to stabilize the polymorphic form in pharmaceutical formulations.

In contrast, many surfactants and polymers can be used in drug dosage forms [31,32]. Polymers are often used as tablet binders, for film formation, as taste-maskers, drug-release controllers, thickeners, etc. [31], but surfactants can be used in suspensions, emulsions, gels, or drug delivery systems as drug protectors (e.g., nanoparticles or liposomes in drug dosage forms) [32]. This is an advantage of these additives compared to the structurally related additives. Some polymers, such as polyethylene glycol, polystyrene, and poly-methylmethacrylate, can decrease surface tension and act as a surfactant [33]. As surface tension and nucleation rates are inversely related, surfactants decrease surface tension and can promote nucleation of the metastable form [11]. Surfactants can decelerate phase transitions [19,34] by increasing the activation barrier for nucleation of the stable form [19]. Surfactants can also increase the solubility and dissolution rate of API by incorporating it into their micelles or hemispheres [11,35]. The hydrophilic part of the surfactant can be strongly attached to the crystal surface, but the hydrophobic chain can cover the crystal surface and prevent other interactions [17]. Larger additives can adsorb on a non-specific crystal surface and therefore inhibit crystal growth by hindering the deposition of growth units [34]. Polymer additives can act as nucleation sites by absorbing into pre-nucleated clusters and therefore reducing interfacial free energy and changing the interactions between the solute molecules [11].

In this study we investigated additive assisted crystallization by focusing on the preparation of a metastable polymorph to obtain a better understanding of the mechanism of additive provided polymorphic outcome control. 2,6-Dimethoxyphenylboronic acid (MPBA), existing as two polymorphs [36], was used as a model compound. Overall, some arylboronic acids are important in the pharmaceutical industry due to their biological activity and the possibility of pharmacological effects [37–42]. MPBA was selected due to the different hydrogen bonding motifs present in both of its polymorphs, including a trimeric motif uncharacteristic of phenylboronic acids. We explored structurally related molecules, polymers, and surfactants with diverse possibilities for intermolecular interaction as additives. To explore additive assisted crystallization of MPBA, we performed polymorph screening, tested which additives allow crystallization of the metastable form, and explored the most promising additives for crystallization of the metastable polymorph by varying the crystallization conditions. To access the mechanism of additive provided crystallization and stabilization of the metastable form, we used crystallographic analysis and theoretical calculations.

2. Materials and Methods

2,6-Dimethoxyphenylboronic acid (MPBA, purity 97%, polymorph I) and *n*-octyl-β-D-glucopyranoside (OGP, purity > 99 %) was purchased from Fluorochem. Span 20 (sorbitan monolaurate) with ≤1.0 % water was purchased from Merck. Molecular structures of MPBA and the most extensively studied additives are shown in Figure 1. The water was deionized in the laboratory. Other additives (see Supplementary Materials, Table S1) and organic solvents of analytical grade were purchased from different commercial sources.
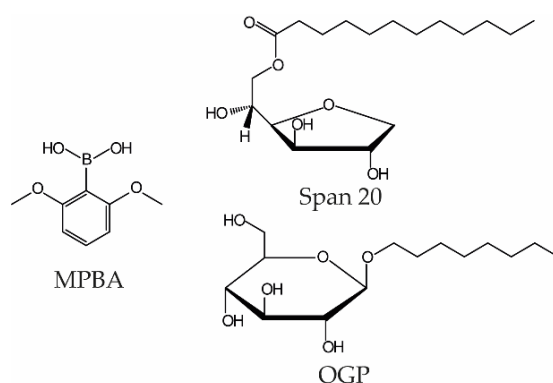
Figure 1. Molecular structure of MPBA, Span 20, and OGP.

2.1. Solubility Measurements

The approximate solubility of MPBA in selected solvents was determined gravimetrically. Saturated solutions of MPBA in water, acetonitrile, toluene, tetrahydrofuran, nitromethane, and isopropanol were prepared at ambient temperature. Solutions (1 or 5 mL) were evaporated at 80 °C, and the mass of residual solid was used for calculation of the solubility. Approximate solubilities of MPBA Form I are listed in Table S2.

2.2. Crystallization Experiments

Commonly used solvents from different solvent classes were selected for the crystallization of MPBA. For evaporation crystallization, 30 to 50 mg of MPBA were dissolved in 2 to 3 mL of solvent and evaporated at 25 or 50 °C. For cooling crystallization, MPBA was dissolved at 40 to 80 °C, depending on the boiling points of the solvent. The obtained solutions were filtered and cooled to 5 °C. The obtained solid products were collected by filtration, air dried, and characterized with powder X-ray diffraction (PXRD).

Cooling crystallizations were also performed using Crystal16 (Technobis Crystallization Systems, Alkmaar, Netherlands). Solutions of different supersaturation ($S = c/c^*$, where c is the initial concentration and c^* is the solubility at 25 °C, for toluene $c/c^* = 2$–11; for water $c/c^* = 5$–10) were prepared in situ (the required mass of MPBA and 1.00 mL of solvent were transferred into the HPLC vial, and dissolution was achieved by heating in Crystal16) and cooled with a cooling rate of 10 °C·min^{-1} by stirring at a rate of 900 rpm. Toluene solutions with $c/c^* = 10$ were cooled with different cooling rates—20, 10, 1, and 0.1 °C·min^{-1}—to determine the effect of the cooling rate on the polymorphic outcome. Water solutions with high supersaturation, obtained using higher temperatures for dissolution or a long cooling time, oiled out and were not used for phase analysis. Four parallel crystallization experiments were performed in all cases. The obtained solid products were collected by filtration, air-dried, and characterized with PXRD.

Crystallization from toluene and water in the presence of additives was performed using cooling. Soluble additives were selected for the crystallization. In 2 mL of water at 70 °C, 20–25 mg of additive and 40–45 mg of MPBA were dissolved, and the solution was filtered and cooled to 5 °C. In 2 mL of toluene at 90 °C, 20–25 mg of additive and 100–110 mg of MPBA were dissolved, then the solution was filtered and cooled to 5 °C. Crystallization from toluene in the presence of surfactants was carried out also using different crystallization methods: complete solvent evaporation at 5, 25, and 50 °C and evaporation crystallization with stirring at 25 °C. For evaporation at 5 and 25 °C, solutions were prepared by dissolving 40–50 mg of MPBA and 100–110 mg of a liquid surfactant or 20–25 mg of a solid surfactant in 3 mL of toluene at 70 °C. The solutions were filtered and kept at the specified temperature for evaporation (no crystal nuclei formed at cooling). For evaporation crystallization at 50 °C solutions were prepared by dissolving 100–110 mg of

MPBA and 230–250 mg of a liquid surfactant or 100–110 mg of a solid surfactant in 2 mL of toluene at 70 °C. The solutions were filtered and kept at 50 °C for evaporation. For cooling crystallization with stirring at 25 °C, solutions were prepared by dissolving 140–150 mg of MPBA and 100–110 mg of a liquid surfactant or 40–50 mg of a solid surfactant in 2 mL of toluene at 70 °C; the solution was then filtered and cooled to 25 °C by stirring the solution at 700 rpm.

Crystallization in the presence of other viscous additives was performed using several crystallization methods—complete solvent evaporation at 25 and 50 °C and cooling crystallization at 5 °C. 100–110 mg of additive and 100–110 mg of MPBA were dissolved in 2 mL of toluene at 90 °C, and the solution was filtered and kept under the specified conditions for crystallization. Crystallization from other solvents in the presence of Span 20 was performed by evaporation crystallization. 100–110 mg of Span 20 and 100–110 mg of MPBA were dissolved in 2 mL of solvent at 40 to 90 °C depending on the boiling point of the solvent. The solution was filtered and placed at 50 °C for evaporation. For each additive, three parallel crystallization experiments were performed. The obtained products were collected by filtration or by scraping from the crystallization container, air-dried, and characterized with PXRD.

2.3. Solid Phase Characterization

The PXRD patterns were measured at ambient temperature on a Bruker D8 Advance (Bruker AXS, Karlsruhe, Germany) diffractometer equipped with a LynxEye position sensitive detector using copper radiation (Cu K$_\alpha$; $\lambda = 1.54180$ Å). Tube voltage and current were set to 40 kV and 40 mA, respectively. The divergence slit was set at 0.6 mm. The anti-scatter slit was set at 8.0 mm. The PXRD patterns were recorded from 3° to 35° on the 2 θ scale. The scan speed of 0.2 s/0.02° was used.

DSC analysis of MPBA polymorphs was performed using a TA DSC 25 (TA Instruments, New Castle, DE, USA) calorimeter. Closed aluminium pans were used. The heating of the samples from 25 to 200 °C was carried out at a heating rate of 10 °C·min^{-1} or 2 °C·min^{-1} for Form II. Samples of 1 mg mass were used. The nitrogen flow rate was 50 mL·min^{-1}. TG analysis was performed using the Mettler Toledo TGA/DSC 2 (Mettler Toledo, Greifensee, Switzerland). Closed aluminium pans were used. The heating of the samples from 25 to 200 °C was carried out at a heating rate of 10 °C·min^{-1}. Samples of 5 to 8 mg mass were used. The nitrogen flow rate was 30 mL·min^{-1}.

2.4. Phenylboronic Acid Derivative CSD Structure Analysis and Theoretical Calculations

Cambridge Structural Database (CSD) version 5.43 [43] was searched to analyse the intermolecular interactions present in phenylboronic acid derivative structures using ConQuest 2022.2.0 [44]. A total of 510 structures with phenylboronic acid fragments were found. Structures containing more than one component, compounds with metal coordinative bonds, and organoboronic compounds not classified as boronic acid were excluded from the analysis. Hydrogen bond interactions were analysed in Mercury 2020.3.0 [45].

Geometry optimization of the crystal structures of both polymorphs was performed in Quantum ESPRESSO 6.4.1 [46] by relaxing the positions of all atoms. The initial geometry of the crystal structures was taken from the CSD database (Form I—UJACIT01; Form II—UJACIT). The crystal structure of Form I was modified to remove the disorder in the boronic acid group appearing because of the symmetry. This was done by reducing the symmetry of the structure to the *P*1 space group and, in several different ways, by removing the redundant hydrogen atoms from the boronic acid groups by obtaining ordered dimers formed by MPBA in *syn-anti*-conformation. Then, among the obtained structures, a monoclinic *Pc* structure with Z′ = 2 was identified as the structure with the highest possible symmetry with the ISOCIF tool (version 3.1.0) [47]. All calculations were performed using the PBE functional with ultrasoft pseudopotentials from the original pseudopotential library and a 90 Ry plane-wave cutoff energy with vdW interactions treated according to the D3 method of Grimme [48] using a 2 × 2 × 2 k-point

grid. Geometry optimized structures were used for further analysis performed using Crystal Explorer 21 [49].

Intramolecular energy was calculated by performing full geometry optimization of the MPBA molecule and geometry optimization with dihedral angle of the boronic acid group constrained to the value as present in the crystal structures of Form I and Form II in the gas phase. Calculations were performed in Gaussian 09 Revision D.01 [50] with the density functional theory M06-2X and 6-31++G(d,p) basis set. Intramolecular energy was calculated as the difference between the energy of the conformer as in the crystal structure and the global minimum energy.

Calculations of pairwise intermolecular interaction energy in crystal structures were performed in CrystalExplorer 21 at the B3LYP-D2/6-31G(d,p) level. The sum of all pairwise interaction energies with molecules for which the atoms are within 15 Å of the central molecule was used to estimate the intermolecular energy. The lattice energy was calculated by summing the intermolecular energy calculated in CrystalExplorer, and intramolecular energy was calculated using Gaussian09 [51].

Hirshfeld surfaces, their 2D fingerprint plots summarizing the information about intermolecular interactions and generation of energy frameworks from the calculated pairwise interaction energies, and their electrostatic and dispersion components were calculated with CrystalExplorer 21.

Generation of Full Interaction Maps (FIM) providing molecule interaction preferences and analysis of Bravais–Friedel–Donnay–Harker (BFDH) morphology [52] were performed with Mercury 2020.3.0. FIMs of individual molecules as well as crystal structures with crystal facets of BFDH morphologies were generated for each polymorph.
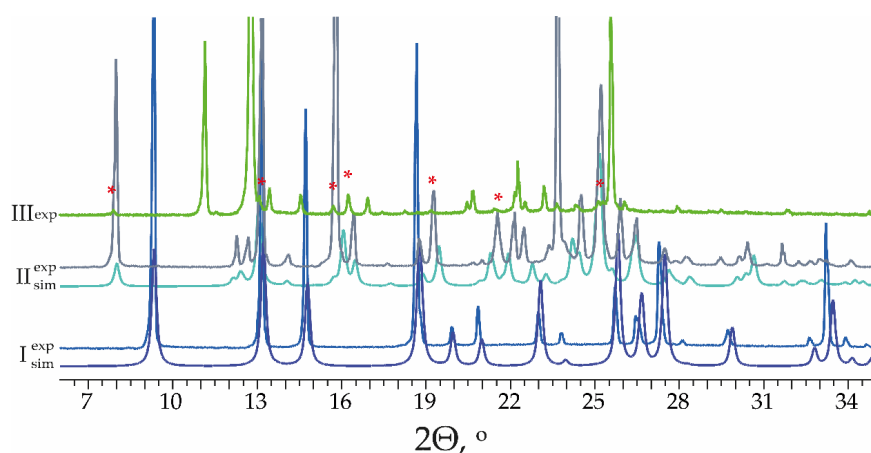
3. Results and Discussion

3.1. Crystallization from Pure Solvents

We crystallized MPBA from popular solvents from different solvent classes. In almost all crystallizations, particularly from aprotic solvents, pure Form I was obtained (see Table 1). However, from polar protic solvent (isopropanol, methanol, and isobutanol) it was possible to obtain the metastable MPBA Form II. Besides the already known polymorphs, we also obtained a new MPBA polymorph, designated as Form III (see Figure 2). Form III crystallized together with Form II in evaporation crystallization from isopropanol, isobutanol, and heptanol. For further crystallization studies aimed at identifying which additives would allow crystallization of the metastable forms, we selected water and toluene because of their better suited MPBA solubility (see Supplementary Materials, Table S2), higher boiling point, and crystallization of the stable polymorph I from these solvents (see below).

Table 1. Polymorphic outcome of crystallization from pure solvents.

Solvent	Cooling	Evaporation	
		25 °C	**50 °C**
Acetone; acetonitrile; ethyl acetate; toluene; nitromethane; *o*–xylene; chloroform; 1,4-dioxane; methyl tert-butyl ether; dichloromethane; diethyl carbonate; tetrahydrofuran; methyl isobutyl ketone; cyclohexanol	I	I	I
2,2,2-Trifluorethanol; water	I	I	I + II
Heptanol	I	II + III	I
Isopentanol	I	I + II	I
Isobutanol	I	I + II	II
Isopropanol	I	II/II + III	I + II
Methanol	II	II	I

Figure 2. Simulated and experimental PXRD patterns of MPBA polymorphs. The possible Form II impurity in the Form III sample is marked with red asterisks.

For more thorough characterization of the crystallization of MPBA from water and toluene, we investigated the effect of supersaturation, as it can have a great impact on the polymorphic outcome. Usually, higher supersaturation results in the formation of metastable forms [53–55]. Water solutions with supersaturation ($S = c/c^*$) from 5 to 10 (11–22 mg·mL^{-1}) were crystallized with a cooling rate of 10 °C·min^{-1} and a stirring rate of 900 rpm. Higher supersaturation, heating the solution above 70 °C, or long stirring at an elevated temperature resulted in the solution oiling out. Furthermore, before the nucleation at cooling the solution always oiled out and only then did nucleation occur. Toluene solutions with supersaturation between 2 and 11 (24–132 mg·mL^{-1}) were crystallized under the same conditions, except that solutions with $c/c^* = 10$ were also cooled at different cooling rates, from very fast (20 °C·min^{-1}) to very slow (0.1 °C·min^{-1}). The toluene solutions did not oil out, but in all solutions, solid particles (a few small crystals in the solution) were observed before extensive nucleation, when numerous MPBA crystals appeared and began to grow by forming a suspension. For solutions with lower supersaturation, the solid particle formation point was near 20–30 °C, but more crystals were obtained only when the mixture reached 10 °C and was stirred for 5 to 10 min. When supersaturation was increased, the solid particle formation and nucleation occurred at a higher temperature (for $c/c^* = 10$ it was at ~80 °C and 32–20 °C, respectively). Nevertheless, neither in water nor in toluene did the supersaturation and cooling rate (tested for toluene) affect the polymorphic outcome, as Form I was always obtained in the crystallization. Therefore, we have demonstrated that metastable forms do not crystallize in cooling crystallization from toluene and water under the investigated conditions.

3.2. Characterization of MPBA Polymorphs

3.2.1. Structure Analysis of MPBA Polymorphs and Analysis of Phenylboronic Acid Moiety Interaction Preferences in CSD Structures

MPBA has two known polymorphic forms characterized by Cyrański et al. [36]. Form I crystallizes in the tetragonal crystal system $P\bar{4}n2$ with Z′ = 0.5 and contains typical hydrogen bonded homodimers of boronic acid that adopts *syn-anti*-conformation. Form II crystallizes in the monoclinic crystal system $C2/c$ with Z′ = 1.5 and contains an unusual hydrogen-bonded boronic acid synthon formed by three molecules (see Figure 3). The trimer synthon consists of two symmetry independent molecules in the *anti* conformation—the middle molecule (A) forms hydrogen bonds with terminal molecules (B), which act as hydrogen bond acceptors. Additionally, in the terminal molecules (B), there are two intramolecular hydrogen bonds between the hydroxyl and methoxy groups. As we demonstrate below,

the hydrogen bonding as in Form II is unusual for arylboronic acids. Unfortunately, our attempts to determine the crystal structure of Form III were unsuccessful, as suitable crystals for SCXRD analysis were not obtained and the bulk sample contained an impurity of Form II (see Figure 2).

Form I (UJACIT01)   Form II (UJACIT)
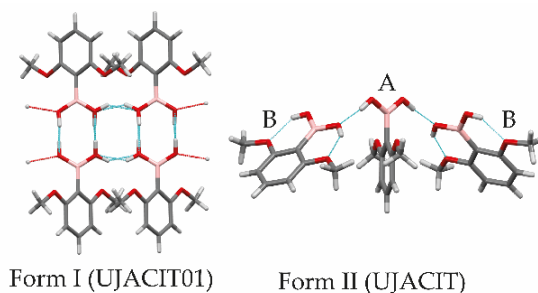
**Figure 3.** Hydrogen bonding in the crystal structures of MPBA polymorphs and labelling of molecules in Form II.

In CSD, 209 crystal structures of single component phenylboronic acid phases (see Supplementary Materials, Figure S1) were found, resulting in analysis of 192 unique crystal structures. The analysis showed that polymorphism in phenylboronic acid is rarely reported in CSD: only 7 of 185 (3.8%) unique compounds have structures of two polymorphs. For five of the phenylboronic acid derivatives, polymorphs have different intermolecular interactions, including dimers, chains, and intramolecular and specific intermolecular hydrogen bonds (see Supplementary Materials, Table S3). Boronic acid homodimers are present in most of the phenylboronic acid structures (82.8%), while only 14.6% of structures have chain-like hydrogen bonding. In two structures (1.0%) there are dimers and chains (see Figure S4), but in three structures (1.6%), only intramolecular hydrogen bonds. The dimers can be divided into six different types (see Supplementary Materials Figure S2 and Table S4) according to the hydrogen bonding in the crystal structure. MPBA Form I contains A1 type dimers (formed by $R_2^2(8)$ dimers connected by 2 mutual C(4) chains), which is common for phenylboronic acids (28.3% of all the dimeric structures). The most abundant phenylboronic acid dimer synthon is type B1 (35.8% of all the dimers), an isolated dimer with additional intramolecular hydrogen bonds.

Other types of hydrogen bond synthons formed by phenylboronic acid moieties are quite different but can be divided into eight types (see Supplementary Materials, Figure S3 and Table S5). The most abundant among these are hydrogen bonds with other atoms in the molecule (35.5% of all non-dimers) (Figure S3, type H). Boronic acid trimers as in Form II (Figure S3, type K) are unique and not observed in any other structure, although there are structures in which there are only intramolecular hydrogen bonds as present in molecule B (9.7%), and two structures (type J) in which there are either different isolated hydrogen bonds with molecules in *anti* conformation or chains C(2) formed by such hydrogen bonds.

Therefore, the performed CSD analysis confirms that dimers are the main hydrogen bond type for phenylboronic acids as suggested before [37,38,56–60] and that MPBA Form II is a unique trimer containing structure. Overall, there is a relatively low possibility for formation of a phenylboronic acid derivative structure not containing dimers, particularly if there are no other functional groups which could lead to disruption of hydrogen bonds formed by only boronic acid moiety. Nevertheless, we believe that the polymorphism of phenylboronic acid derivatives is not thoroughly studied, as suggested by the notably low number of polymorphic molecules. For example, a study by Cruz-Cabeza et al. shows that polymorphism occurrence in single component crystals is at least 37% and more polymorphic structures are reported for more thoroughly studied substances with pharmacology effect [61].

3.2.2. Thermal Characterization of MPBA Polymorphs

Thermal analysis showed that the melting point of Form I is 108 °C (see Figure 4). In DSC analysis of Form II at 2 °C·min^{-1} an exothermic peak corresponding to phase transition to Form I was detected at 74 °C (confirmed by PXRD). This indicates the monotropic relationship between Form I and Form II [62]. The phase transition of Form II to Form I at 80 °C was confirmed by heating in a thermostat for an hour. The newly obtained Form III has a melting peak at 52 °C. As Form III has a lower melting enthalpy and melting point than Form I, these polymorphs are also monotropically related by the heat of fusion rule [62]. When the Form III sample was stored at a 60 °C thermostat, transformation to Form I occurred before the melting. Such a high melting point difference of more than 50 °C between Form I (108 °C) and Form III (52 °C) is rarely observed [63] and indicates low thermodynamic stability of Form III. The absence of mass change in the TG curves (see Supplementary Materials, Figures S5–S7) confirmed that all the obtained phases are polymorphs. We note that Form II and Form III are not stable in ambient conditions: Form II transforms into Form I in <24 h, whereas Form III transforms into Form II in <1 h. In contrast, Form II is stable notably longer at lower temperatures in the freezer.
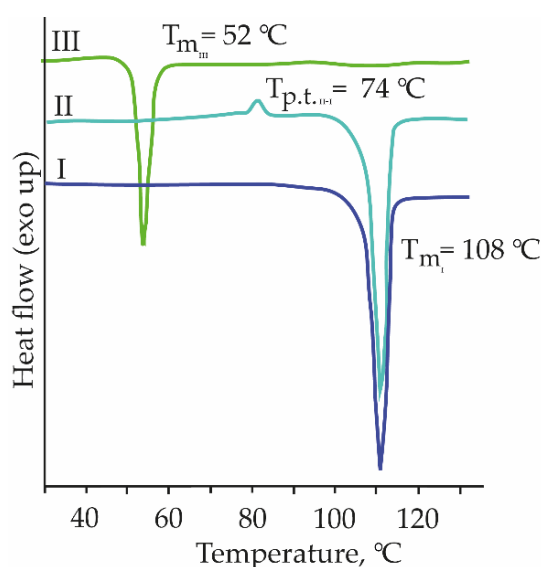
Figure 4. DSC curves of MPBA polymorphs (heating rate 10 °C·min^{-1} for Forms I and III, 2 °C·min^{-1} for Form II). The onset temperatures were used to characterize the thermal process occurring in the DSC traces.
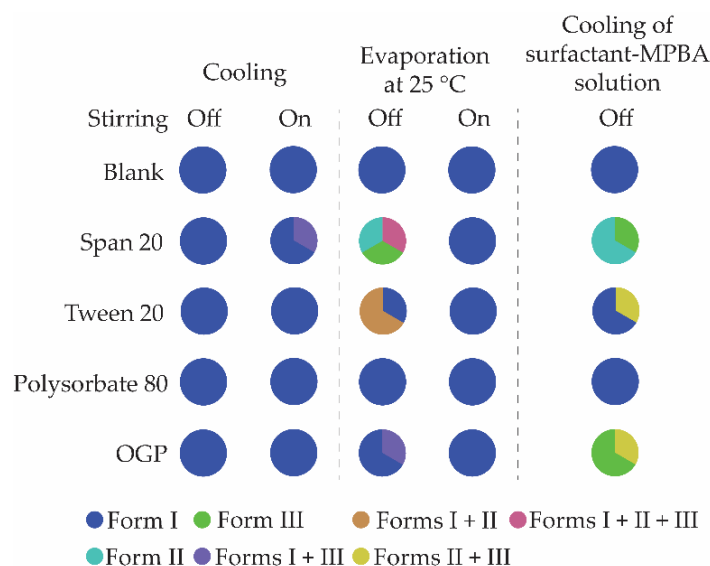
3.3. Crystallization in the Presence of Additives

When crystallizing from water, the hot sample at the beginning of the cooling always oiled out first and crystallized only later. However, the nucleation was very slow, as a solid was obtained after only a few hours or even a few days, and only Form I was obtained by cooling a water solution in the presence of additives.

Overall, polymorph I was obtained in most of the cooling crystallizations of toluene solutions in the presence of additives, in agreement with this polymorph obtained in cooling crystallization of pure solvent (see Supplementary Materials, Figure S8). However, in the presence of octyl β-D-glucopyranoside (OGP) and 2,6-dimethoxybenzoic acid (2,6MeOBA), a mixture of Forms I and II can be obtained. We note that MPBA as an additive promotes the formation of the metastable form of 2,6MeOBA [64]. As the polymorphs of both substances differ by *syn-* and *anti* conformers in the structure, it is possible that the 2,6MeOBA *syn*

conformation stabilizes the MPBA *anti* conformation by forming hydrogen bonds, therefore allowing easier nucleation of Form II.

Serendipitously, we discovered that evaporation of the filtrate obtained in crystallization from toluene in the presence of all the surfactants (OGP, Polysorbate 80, Span 20 and Tween 20) resulted in formation of Form II crystals. Therefore, surfactants were selected for further additive crystallization experiments. Crystallization was performed using two different approaches: cooling and evaporation crystallization. In the cooling crystallization with these additives, almost exclusively Form I was obtained (see Figure 5), whereas the metastable Form II was obtained in only one of the experiments. In contrast, Form II, Form III, or their mixture was obtained in evaporation crystallization in the presence of Span 20, Tween 20, and OGP. We observed that the presence of Span 20 and OGP stabilizes Form II but not Form III, because it very rapidly transformed into Form II as observed by the PXRD analysis. However, Form II was stable for up to one month in the presence of these two surfactants. We also observed that evaporation with stirring prevented crystallization of the metastable forms. Among the tested conditions, the best for obtaining metastable forms was solvent evaporation at 50 °C without stirring. Under these conditions, the presence of Span 20 and OGP in the initial solution resulted in crystallization actually occurring from a MPBA solution in the surfactant after the evaporation of the initial solvent when the obtained mixture was cooled to room temperature. The crystals obtained in this procedure were very small, and pure polymorph III crystallized in the presence of Span 20 and OGP. Nevertheless, single crystals were not obtained, and the presence of the wide peaks of Span 20 and OGP also prevented structure determination from the PXRD data.
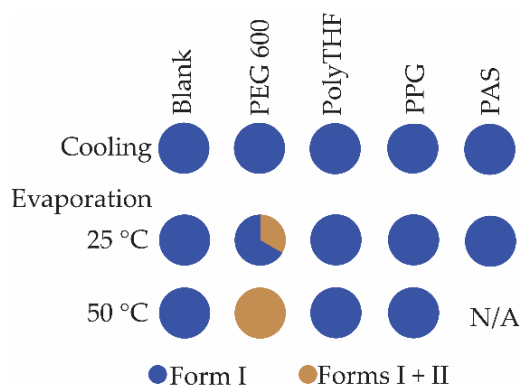

Figure 5. Polymorphic outcome in crystallization from toluene in the presence of surfactants using different crystallization methods. Each third of the circle represents one of the parallel experiments.

MPBA–Span 20 solution was also obtained using other solvents to determine whether the initial solvent has a role if the crystallization is performed in this way. Five solvents were selected: four solvents from which only Form I was previously obtained and isopropanol from which Form II was obtained. A clear MPBA solution in Span 20 later crystallizing at room temperature was obtained after the evaporation of all these solvents. Pure Form II was obtained in all 15 experiments. Therefore, the formation of Form II under these conditions is purely determined by Span 20.

Span 20 and OGP at 50 °C are viscous liquid substances. Therefore, other viscous liquid substances were also examined. Crystallization was performed using cooling crystallization and evaporation crystallization without stirring, as the stirring did not allow for formation of the metastable forms. The results showed that the formation of metastable forms is not provided by any viscous liquid, as among the tested, only PEG 600 showed the potential for crystallization of Form II in evaporation crystallization (see Figure 6). Therefore, the main reason for polymorph control apparently is the intermolecular interactions between the surfactant molecules and the MPBA.

Figure 6. Polymorphic outcome in crystallization from toluene in the presence of viscous liquids as additives using different crystallization methods. Each third of the circle represents one of the parallel experiments. Abbreviations: PEG—polyethylene glycol; PolyTHF—poly tetrahydrofuran; PPG—polypropylene glycol; PAS—poly(acrylic acid).

3.4. Theoretical Analysis of MPBA Crystal Structures

To find the intramolecular energy of MPBA in its crystal structures, two conformers—*syn-anti* and *anti*—were considered. The *anti* conformer with two intramolecular hydrogen bonds between boronic acid hydroxyl groups and methoxy groups (as in B molecule of Form II) was found to be the global energy minimum. The *syn-anti* conformer (similar to conformation in Form I but with the boronic acid group almost in plane with the benzene ring and therefore having one intramolecular hydrogen bond) was found to be less efficient by 12 kJ·mol^{-1} (see Supplementary Materials, Table S6). Not surprisingly, the intramolecular hydrogen bonds in MPBA result in differing energy of conformers compared to those reported in studies of phenylboronic acid in aprotic solvents and in vacuo, where generally the *syn-anti*-conformers are energetically more stable than the *anti* by ~5 kJ·mol^{-1} [65]. The geometry optimizations with constrained torsion angle between the benzene ring and boronic acid group were used to calculate the intramolecular energy of MPBA. These calculations showed that in Form II, the B molecule almost fully corresponds to the global energy minimum, the twisted *anti* conformation of A molecule in Form II has intramolecular energy of 18 kJ·mol^{-1}, and the twisted *syn-anti* conformation of Form I has intramolecular energy of 15 kJ·mol^{-1}. Therefore, the intramolecular energy of Form II is lower by 9 kJ·mol^{-1}.

For the calculation of intermolecular energy, the crystal structure of Form I in the monoclinic *Pc* space group without disorder in the dimers formed by the *syn-anti*-conformers was used. Therefore, the lattice energy calculations are somewhat approximate and can have some deviations because of the lower symmetry used. Based on the obtained results, Form I has 8.5 kJ·mol^{-1} lower intermolecular energy than Form II (see Table 2). Therefore, the lattice energy of both polymorphs is almost identical, with that of Form II being calculated as 0.7 kJ·mol^{-1} lower, corresponding to the typical energy difference (<5 kJ·mol^{-1}) of organic polymorphs [61,66]. Although the calculated relative energy contradicts Form I being determined as the thermodynamically stable polymorph, the possibility for different

hydrogen atom arrangement in dimers could provide an entropy increase, resulting in lowering of the free energy of Form I.

Table 2. Selected crystallographic data and the calculated intramolecular, intermolecular, and lattice energies of MPBA polymorphs.

| Polymorph	Form I	Form II
CSD Ref. code	UJACIT01 (original $P\bar{4}n2$ structure)	UJACIT
Z/Z′	4/0.5 (for $P\bar{4}n2$ structure) 4/2 (for Pc structure)	12/1.5
E_{intra}, kJ·mol^{-1}	15.2	6.0
E_{inter}, kJ·mol^{-1}	−144.4	−135.9
$(E_{ele} + E_{pol})/E_{disp}$	1.3	1.0
$E_{lattice}$, kJ·mol^{-1}	−129.2	−129.8

The pronounced differences in the hydrogen bonding in both polymorphs, as described above, result in high differences in the lattice energy component contributions and energy frameworks of both forms. As shown in Table 2, the electrostatic energy in Form I is the dominant component of the lattice energy, which can be associated with the extensive strong hydrogen bond network in this structure. Interestingly, despite the presence of hydrogen bonded chains in the structure of Form I, the electrostatic (Coulomb) energy (see Figure 7) is dominated by the interactions between the molecules that form the homodimers in the bc plane, while the interactions between the adjacent dimers in adjacent layers are notably less efficient. The strongest dispersion energy is observed between two molecules forming a $CH_3 \cdots \pi$ interaction along the a-axis. In contrast, the electrostatic energy and dispersion energy in Form II have a very similar contribution in the lattice energy, because of a much smaller amount of intermolecular hydrogen bonds and higher importance of the aromatic interactions, including $\pi \cdots \pi$ stacking. This is also observed in the electrostatic energy framework of Form II, as the strongest interactions observed between the molecules in the trimer are still notably less efficient than those in Form I. However, in this structure there are several molecule pairs with efficient dispersion energy in a different spatial arrangement, with the strongest dispersion interactions observed between the adjacent B molecules connected in a shifted $\pi \cdots \pi$ stacking manner and forming the hydrogen bonded trimers in a perpendicular direction. To sum up, despite overall more efficient dispersion interactions in Form II, the notably stronger hydrogen bonds in Form I are the reason for the higher intermolecular energy of this form, which could also explain its higher stability. The ability of hydrogen bonding to provide stabilization of the crystal structure has been shown before, e.g., in studies of proteins [67,68] and ritonavir [69].

Differences in the intermolecular interactions of both forms can also clearly be seen on the Hirshfeld surfaces and in the analysis of their 2D fingerprint plots (see Figure 8). As could be expected from the artificially decreased symmetry, both *symmetry independent* molecules of the structure in the Pc space group have identical 2D fingerprint plots with hydrogen bonds forming the boronic acid dimers and chains, and different -H $\cdots$ C- and -C $\cdots$ H- interactions (particularly from $CH_3 \cdots \pi$ interactions) being the main observable interactions. Logically, both molecules (A and B) of Form II had different Hirshfeld surfaces and their 2D fingerprint plots. Both molecules A and B have only one sharp peak corresponding to being a donor (A) or acceptor (B) of the strong intermolecular hydrogen bond, as can be seen in the fingerprint plots. Also, interactions associated with $\pi \cdots \pi$ stacking are present for molecule B, as also demonstrated by the energy framework diagrams of this polymorph.

3.5. Use of Full Interaction Maps to Understand Polymorph Stability and Effect of Crystallization Additives

The Full Interaction Map (FIM) visualizes regions around the molecule where, based on pre-extracted *IsoStar* interaction data from the CSD [52], intermolecular interactions are expected, allowing to evaluate whether interaction preferences within the lattice are satisfied.

FIM analysis has been shown to allow prediction of the stability of polymorphs [61,70,71]. Moreover, we speculate that if in a structure there are regions of the molecule in which the crystal lattice interactions are not satisfied, the additional interactions provided by the additives may stabilize the respective polymorph.
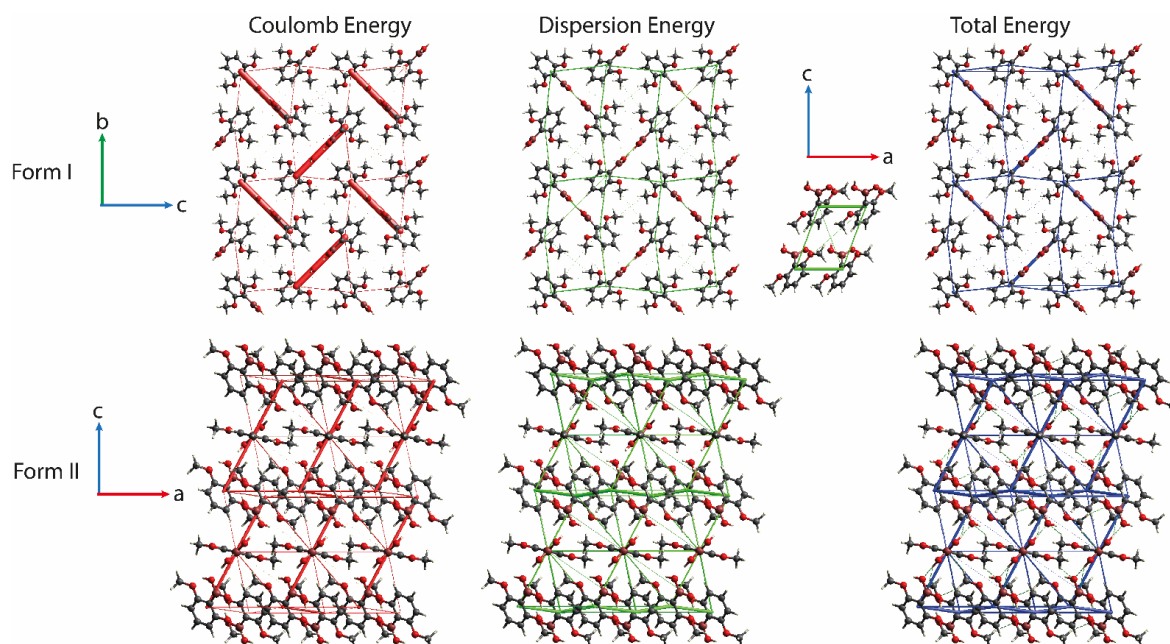

Figure 7. Energy-framework diagrams for E_{Coul}, E_{dis} and E_{tot} for MPBA Forms I and II. All images have the same tube size.
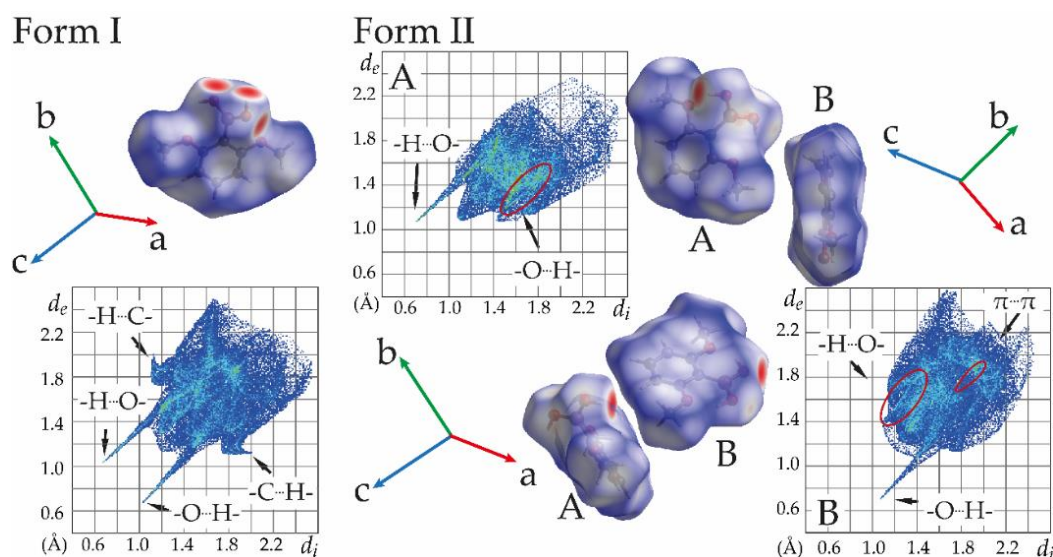
Figure 8. Hirshfeld surfaces and their 2D fingerprinting plots of MPBA Forms I and II. In the labels, the atom on the left is inside the Hirshfeld surface.

FIM analysis was performed for the original disordered Form I structure in the $P\bar{4}n2$ space group and for this polymorph with removed disorder in the Pc space group. Nearly identical FIMs were obtained for both symmetry independent molecules of the Pc structure, and they were highly similar to FIMs of this polymorph in the $P\bar{4}n2$ space group (except that the hydrogen bond donor and acceptor sites in dimer were discriminated) (see Figure 9). The MPBA molecule has two hydroxyl groups able to act as both hydrogen bond acceptors and donors. In the homodimers as in Form I, most of the interaction preferences are satisfied. Both hydrogen bond donors and acceptor sites in the boronic acid group are involved in dimer formation and hydrogen bonding between the dimers. Apart from this, both methoxy groups are potential hydrogen bond acceptors, and there is a preference for the involvement of aromatic C-H in weak hydrogen bonds or aromatic interactions and also a preference for aromatic π electrons to be involved in some interactions. These preferences are partly fulfilled by formation of weak hydrogen bonds, $CH_3 \cdots \pi$ interactions, and other aromatic interactions. In contrast, only half of the interaction preferences for hydrogen bonding are satisfied in Form II (see Figure 9). According to the FIM, the boronic acid group of molecule A prefers to be involved as the hydrogen bond acceptor with two donors, but instead only weak hydrogen bonds with the benzene C–H and methoxy groups (with $C \cdots O$ distance of 3.55 Å and 3.58 Å, respectively) are formed. There is an identical preference also for molecule B, and it is fulfilled for one of the oxygen atoms by the hydrogen bond O_A-$H \cdots O_B$, but the second oxygen atom forms a weak hydrogen bond with a methoxy group ($C \cdots O$ distance 3.32 Å). Therefore, the hydrogen bonding in Form II does not match the interaction preferences as in the CSD, and the three unsatisfied hydrogen bond acceptors may be the reason for the low stability of Form II and formation of this polymorph only under specific conditions. All the hydrogen bond donor capabilities in Form II, however, are satisfied by two O_A-$H \cdots O_B$ bonds for molecule A and the intramolecular hydrogen bonds for molecule B.
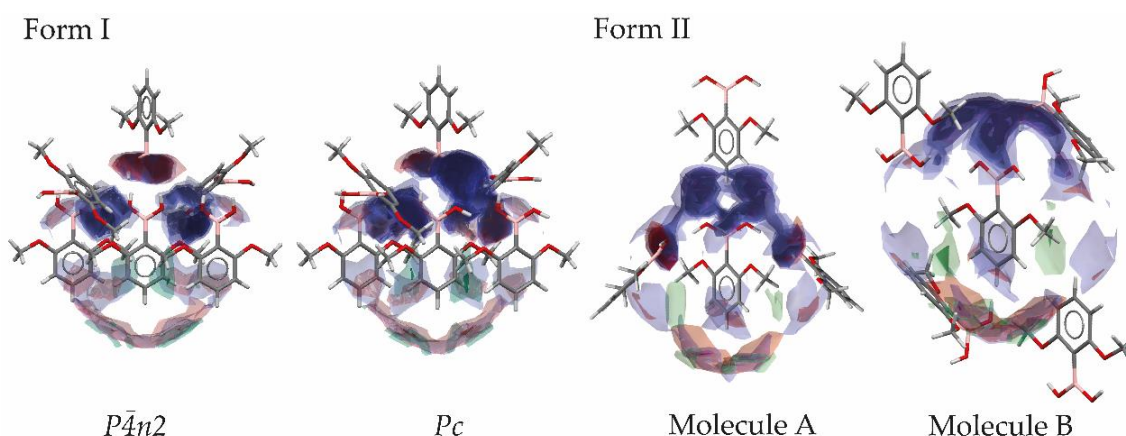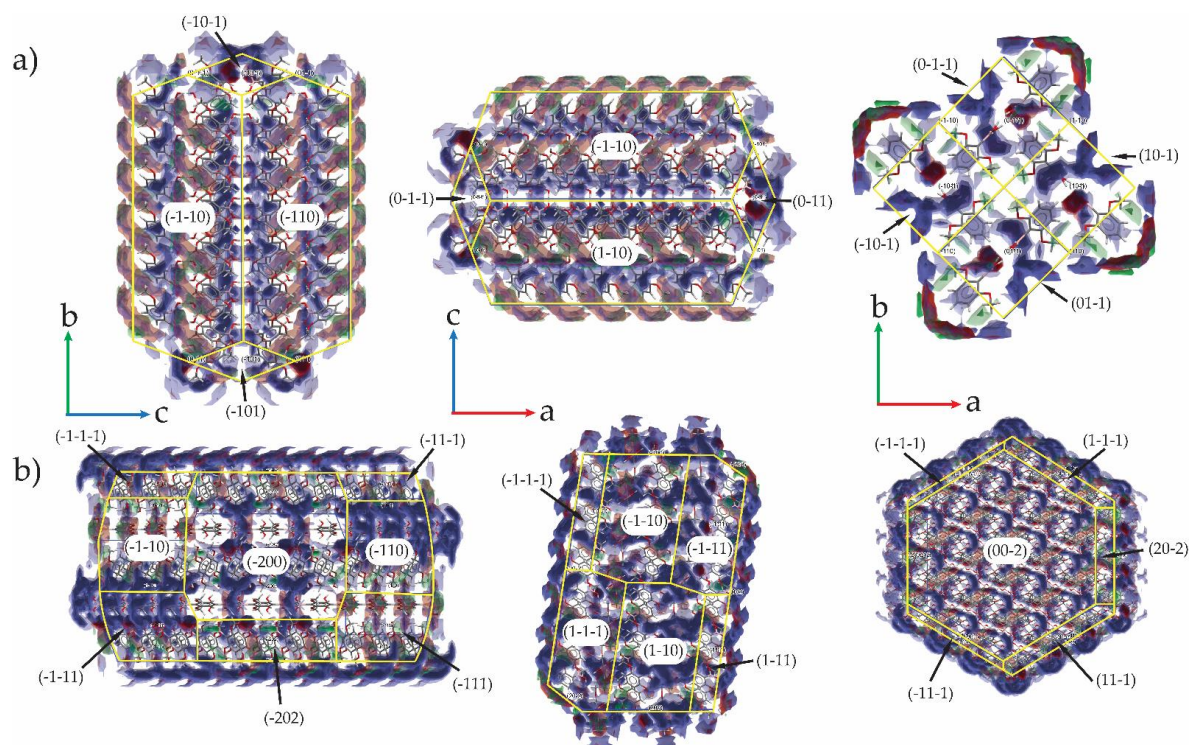

Figure 9. FIMs for MPBA polymorphs. Regions of hydrogen bond donor probability are shown in blue, hydrogen bond acceptors are shown in red, and hydrophobic interactions are shown in green.

If the morphology generated from the Form I structure in the $P\bar{4}n2$ and Pc space groups are compared, the effects of disorder in the $P\bar{4}n2$ structure and the lower symmetry of the Pc structure are visible. Because of the symmetry generated redundant hydrogen atoms in the disordered structure, FIMs on the $P\bar{4}n2$ Form I crystal have a larger hydrogen bond donor probability than on the Pc Form I crystal facets, which have a larger hydrogen bond acceptor probability (see Figure S9). Nevertheless, we analyse FIMs on $P\bar{4}n2$ morphology due to the loss of crystal symmetry in the Pc space group.

Overall, there are large differences between both polymorphs when FIMs on crystal facets are compared (see Figure 10). Form I crystals have a larger probability of being

involved in hydrophobic interactions (green) and interact with hydrogen bond acceptors (red) when compared to Form II. The largest facets {110} of Form I (space group $P\bar{4}n2$) have exposed benzene rings and grow through interactions with the benzene ring. The benzene rings on these facets can act as weak hydrogen bond acceptors (blue colour). This facet also grows by formation of dimers and requires attachment of a hydrogen bond acceptor such as oxygen (red colour). Smaller facets {101} and {10$\bar{1}$} of Form I are growing by formation of dimer chains; therefore, the probability of interacting with hydrogen bond donors (blue colour) is higher for these facets.

Figure 10. FIMs combined on the BFDH morphology of MPBA Form I (**a**) and Form II (**b**). Regions of hydrogen bond donor probability are shown in blue, hydrogen bond acceptors are shown in red, and hydrophobic interactions are shown in green.

The Form II crystal has a larger probability of interacting with hydrogen bond donors on the largest facets when compared to Form I (see the increase in blue coloured regions in Figure 10). On the largest edges {002} and {110} of Form II, in contrast to Form I, many hydrogen bond acceptor groups are exposed. On these facets, the oxygen atoms of the boronic acid groups in *anti*-planar conformation are forming hydrogen bonds and are growing by formation of trimers, so hydrogen bond acceptors are exposed and there is a great propensity to interact with hydrogen bond donors by these facets. Therefore, surfactants can interact as hydrogen bond donors with these facets more easily if compared to Form I, for which hydrogen bond acceptor groups cover a smaller area. The interactions between the crystals and additives could be similar to those Kim et al. [17] demonstrated between the crystals of hexahydro-1,3,5-trinitro-1,3,5-triazine (RDX) and amphiphilic additives using molecular simulations. Span 20 and OGP both have hydrogen bond donors (three and four, respectively) that can interact with the boronic acid group of MPBA and stabilize Form II crystals. Additionally, the hydrophobic site of the surfactants can decelerate phase transition by forming micelles or hemispheres and therefore prevent the reorganization

of molecules required for the transformation of Form II to Form I. This can also explain the small crystal size of Form II obtained in the experiments using these surfactants. It is possible that the hydrophobic part of the surfactants in surfactant micelles or hemispheres could inhibit crystal growth by steric effects preventing attachment of new growth units to the crystal facets.

4. Conclusions

Our studies of MPBA demonstrated that Form I is obtained in evaporation crystallization from most solvents and cooling crystallization from almost all the tested solvents. However, evaporation crystallization from alcohols produced Form II, and evaporation of an isopropanol solution produced the new polymorph Form III. Thermal characterization showed that Form I is the most stable polymorph and that both Form II and Form III are monotropically related to Form I. We observed that Form II and Form III are unstable—Form II transformed to Form I in <24 h, whereas Form III transformed to Form II in <1 h.

The MPBA molecule in planar *anti* conformation is the most stable conformer as shown in the ab initio calculations. Therefore, Form II has lower intramolecular energy. However, Form I has lower intermolecular energy, and its structure is mostly stabilized by the electrostatic energy of strong hydrogen bonds, whereas in Form II the electrostatic and dispersion energy contributions are almost equal, partly because of the less efficient hydrogen bonding. Nevertheless, the lattice energy obtained as sum of the intra- and intermolecular energy of Form II is slightly lower.

More extensive exploration of the crystallization from toluene and water showed that the cooling rate and supersaturation do not affect the crystallization polymorphic outcome. By performing crystallizations in the presence of additives, we found that Span 20 and OGP provide crystallization of the metastable forms in evaporation crystallization at 50 °C. We also showed that the solvent does not play any role in regulating the crystallization outcome in the presence of Span 20 under these conditions, as crystallization is actually occurring from a MPBA solution in liquid Span 20. Moreover, OGP and Span 20 stabilize Form II for up to 1 month at ambient temperature. Although Span 20 also allowed for the crystallization of Form III, this form was not stabilized by Span 20. We showed that not every viscous liquid allows crystallization of the metastable forms because, among several other viscous additives tested, only PEG 600 facilitated crystallization of Form II.

We propose that Span 20 and OGP provide crystallization and stabilization of Form II by intermolecular interactions. On the crystal edges of Form I, mostly atoms keen to form hydrophobic interactions and hydrogen bond donors (boronic acid groups and benzene rings) are exposed, whereas the edges of Form II can interact with hydrogen bond donors because of the many exposed hydrogen bond acceptor groups (boronic acid oxygen atoms). Furthermore, for Form II, the FIM regions where interactions with hydrogen bond donors are likely to occur are larger and more sterically available than for Form I. Although many of the tested additives are hydrogen bond donors, only Span 20 and OGP efficiently interacted with MPBA and provided crystallization of Form II. It is possible that the hydrogen bond donor groups interact with Form II crystal edges, but hydrophobic parts of these additives decelerate the phase transition and provide the stabilization of this polymorph.

Supplementary Materials: The following supporting information can be downloaded at: https://www.mdpi.com/article/10.3390/cryst12121738/s1, Table S1: List of additives used in the study; Table S2: Approximate solubility of MPBA Form I in different solvents; Figure S1: CSD search results for phenylboronic acid derivatives; Figure S2: Types of dimeric hydrogen bond motifs observed in the crystal structures of phenylboronic acid derivatives in CSD; Figure S3: Types of non-dimeric hydrogen bond motifs observed in the crystal structures of phenylboronic acid derivatives in CSD; Table S3: Polymorphism observed in phenylboronic acid derivatives; Table S4: Types of dimeric structures from CSD search results for phenylboronic acid derivatives; Table S5: Types of non-dimeric structures from the CSD search results for phenylboronic acid derivatives; Figure S4: Hydrogen bonding phenylboronic acid derivative structures containing chains and dimers; Figure S5: DSC/TG curves of MPBA Form I; Figure S6: DSC/TG curves of MPBA Form II; Figure S7: DSC/TG curves of

MPBA Form III; Figure S8: Results of the crystallization in the presence of additives from toluene and water; Table S6: Intramolecular energies and torsion angle data of MPBA polymorphs; Figure S9: FIMs combined on the BFDH morphology of MPBA polymorph I using different crystal structure models.

Author Contributions: Investigation, writing—original draft preparation and visualization, A.S.; Conceptualization, methodology, and writing—review and editing, A.S. and A.B.; Supervision, A.B. All authors have read and agreed to the published version of the manuscript.

Data Availability Statement: No new data were created or analyzed in this study. Data sharing is not applicable to this article.

Conflicts of Interest: The authors declare that they have no conflict of interest.

References

1. Hilfiker, R. (Ed.) *Polymorphism: In the Pharmaceutical Industry*; Wiley-VCH Verlag GmbH & Co. KGaA: Weinheim, Germany, 2006; ISBN 9783527311460.
2. Aitipamula, S.; Nangia, A. Polymorphism: Fundamentals and Applications. In *Supramolecular Chemistry*; John Wiley & Sons, Ltd.: Chichester, UK, 2012; ISBN 9780470661345.
3. Lu, J.; Rohani, S. Polymorphism and Crystallization of Active Pharmaceutical Ingredients (APIs). *Curr. Med. Chem.* **2009**, *16*, 884–905. [CrossRef] [PubMed]
4. Lee, E.H. A Practical Guide to Pharmaceutical Polymorph Screening & Selection. *Asian J. Pharm. Sci.* **2014**, *9*, 163–175. [CrossRef]
5. Pudipeddi, M.; Serajuddin, A.T.M. Trends in Solubility of Polymorphs. *J. Pharm. Sci.* **2005**, *94*, 929–939. [CrossRef] [PubMed]
6. Nicoud, L.; Licordari, F.; Myerson, A.S. Estimation of the Solubility of Metastable Polymorphs: A Critical Review. *Cryst. Growth Des.* **2018**, *18*, 7228–7237. [CrossRef]
7. Censi, R.; di Martino, P. Polymorph Impact on the Bioavailability and Stability of Poorly Soluble Drugs. *Molecules* **2015**, *20*, 18759–18776. [CrossRef]
8. Nogueira, B.A.; Castiglioni, C.; Fausto, R. Color Polymorphism in Organic Crystals. *Commun. Chem.* **2020**, *3*, 34. [CrossRef]
9. Neumann, M.A.; van de Streek, J. How Many Ritonavir Cases Are There Still out There? *Faraday Discuss.* **2018**, *211*, 441–458. [CrossRef]
10. European Medicines Agency Public Statement: Suply of Norvir Hard Capsules. Available online: https://www.ema.europa.eu/en/documents/public-statement/public-statement-supply-norvir-hard-capsules_en.pdf (accessed on 30 January 2022).
11. Xu, S.; Cao, D.; Liu, Y.; Wang, Y. Role of Additives in Crystal Nucleation from Solutions: A Review. *Cryst. Growth Des.* **2021**, *22*, 2001–2022. [CrossRef]
12. Kras, W.; Carletta, A.; Montis, R.; Sullivan, R.A.; Cruz-Cabeza, A.J. Switching Polymorph Stabilities with Impurities Provides a Thermodynamic Route to Benzamide Form III. *Commun. Chem.* **2021**, *4*, 38. [CrossRef]
13. Bērziņš, A.; Trimdale-Deksne, A.; Belyakov, S.; ter Horst, J.H. Reversing the Polymorphic Outcome of Crystallization and the Apparent Relative Stability of Nitrofurantoin Polymorphs Using Additives, University of Latvia, Faculty of Chemistry, Riga, Latvia. 2022, *manuscript in preparation; to be submitted*.
14. Poornachary, S.K.; Han, G.; Kwek, J.W.; Chow, P.S.; Tan, R.B.H. Crystallizing Micronized Particles of a Poorly Water-Soluble Active Pharmaceutical Ingredient: Nucleation Enhancement by Polymeric Additives. *Cryst. Growth Des.* **2016**, *16*, 749–758. [CrossRef]
15. Wu, H.; Wang, J.; Liu, Q.; Zong, S.; Tian, B.; Huang, X.; Wang, T.; Yin, Q.; Hao, H. Influences and the Mechanism of Additives on Intensifying Nucleation and Growth of P-Methylacetanilide. *Cryst. Growth Des.* **2020**, *20*, 973–983. [CrossRef]
16. Quan, Y.; Yang, Y.; Xu, S.; Zhu, P.; Liu, S.; Jia, L.; Gong, J. Insight into the Role of Piperazine in the Thermodynamics and Nucleation Kinetics of the Triethylenediamine-Methyl Tertiary Butyl Ether System. *CrystEngComm* **2019**, *21*, 948–956. [CrossRef]
17. Kim, J.W.; Park, J.H.; Shim, H.M.; Koo, K.K. Effect of Amphiphilic Additives on Nucleation of Hexahydro-1,3,5-Trinitro-1,3,5-Triazine. *Cryst. Growth Des.* **2013**, *13*, 4688–4694. [CrossRef]
18. Pino-García, O.; Rasmuson, Å.C. Influence of Additives on Nucleation of Vanillin: Experiments and Introductory Molecular Simulations. *Cryst. Growth Des.* **2004**, *4*, 1025–1037. [CrossRef]
19. Poon, G.G.; Seritan, S.; Peters, B. A Design Equation for Low Dosage Additives That Accelerate Nucleation. *Faraday Discuss.* **2015**, *179*, 329–341. [CrossRef]
20. Lin, J.; Shi, P.; Wang, Y.; Wang, L.; Ma, Y.; Liu, F.; Wu, S.; Gong, J. Template Design Based on Molecular and Crystal Structure Similarity to Regulate Conformational Polymorphism Nucleation: The Case of α,ω-Alkanedicarboxylic Acids. *IUCrJ* **2021**, *8*, 814–822. [CrossRef]
21. Singh, M.K. Controlling the Aqueous Growth of Urea Crystals with Different Growth Inhibitors: A Molecular-Scale Study. *RSC Adv.* **2021**, *11*, 12938–12950. [CrossRef]

22. Simone, E.; Steele, G.; Nagy, Z.K. Tailoring Crystal Shape and Polymorphism Using Combinations of Solvents and a Structurally Related Additive. *CrystEngComm* **2015**, *17*, 9370–9379. [CrossRef]

23. Urwin, S.J.; Yerdelen, S.; Houson, I.; ter Horst, J.H. Impact of Impurities on Crystallization and Product Quality: A Case Study with Paracetamol. *Crystals* **2021**, *11*, 1344. [CrossRef]

24. Agnew, L.R.; Cruickshank, D.L.; McGlone, T.; Wilson, C.C. Controlled Production of the Elusive Metastable Form II of Acetaminophen (Paracetamol): A Fully Scalable Templating Approach in a Cooling Environment. *ChemComm* **2016**, *52*, 7368–7371. [CrossRef]

25. Shi, P.; Xu, S.; Yang, H.; Wu, S.; Tang, W.; Wang, J.; Gong, J. Use of Additives to Regulate Solute Aggregation and Direct Conformational Polymorph Nucleation of Pimelic Acid. *IUCrJ* **2021**, *8*, 161–167. [CrossRef] [PubMed]

26. European Medicines Agency. Council of Europe Control of Impurities in Substances for Pharmaceutical Use. In *European Pharmacopoeia, Supplement 10.8*; European Medicines Agency: Strasbourg, France, 2022; pp. 763–765.

27. Giordani, C.F.A.; Campanharo, S.; Wingert, N.R.; Bueno, L.M.; Manoel, J.W.; Costa, B.; Cattani, S.; Arbo, M.D.; Garcia, S.C.; Garcia, C.V.; et al. In Vitro Toxic Evaluation of Two Gliptins and Their Main Impurities of Synthesis. *BMC Pharmacol. Toxicol.* **2019**, *20*, 1–9. [CrossRef] [PubMed]

28. Prajapati, P.; Agrawal, Y.K. Analysis and Impurity Identification in Pharmaceuticals. *Rev. Anal. Chem.* **2014**, *33*, 123–133. [CrossRef]

29. Abdin, A.Y.; Yeboah, P.; Jacob, C. Chemical Impurities: An Epistemological Riddle with Serious Side Effects. *Int. J. Environ. Res. Public Health* **2020**, *17*, 1030. [CrossRef]

30. Smith, S.W. Chiral Toxicology: It's the Same Thing . . . Only Different. *Toxicol. Sci.* **2009**, *110*, 4–30. [CrossRef]

31. Sinko, P.J. Pharmaceutical Polymers. In *Martin's Physical Pharmacy and Pharmaceutical Sciences*; Troy, D.B., Ed.; Wolters Kluwer, Lippincott Williams & Wilkins: Philadelphia, PA, USA, 2016; pp. 508–514, ISBN 9781451191455.

32. Tadros, T.F. Surfactants in Pharmaceutical Formulations. In *Applied Surfactants: Principles and Applications*; Wiley-VCH: Weinheim, Germany, 2005; pp. 433–501. ISBN 9783527306299.

33. Tadros, T.F. Surfactants, Industrial Applications. In *Encyclopedia of Physical Science Technology*, 3rd ed.; Meyers, R.A., Ed.; Academic Press: Cambridge, MA, USA, 2003; Volume 16, pp. 423–438, ISBN 9780122274107. [CrossRef]

34. Garti, N.; Zour, H. The Effect of Surfactants on the Crystallization and Polymorphic Transformation of Glutamic Acid. *J. Cryst. Growth* **1997**, *172*, 486–498. [CrossRef]

35. Feng, Y.; Meng, Y.; Tan, F.; Lv, L.; Li, Z.; Wang, Y.; Yang, Y.; Gong, W.; Yang, M. Effect of Surfactants and Polymers on the Dissolution Behavior of Supersaturable Tecovirimat-4-Hydroxybenzoic Acid Cocrystals. *Pharmaceutics* **2021**, *13*, 1772. [CrossRef]

36. Cyrański, M.K.; Klimentowska, P.; Rydzewska, A.; Serwatowski, J.; Sporzyński, A.; Stępień, D.K. Towards a Monomeric Structure of Phenylboronic Acid: The Influence of Ortho-Alkoxy Substituents on the Crystal Structure. *CrystEngComm* **2012**, *14*, 6282–6294. [CrossRef]

37. Adamczyk-Woźniak, A.; Gozdalik, J.T.; Kaczorowska, E.; Durka, K.; Wieczorek, D.; Zarzeczańska, D.; Sporzyński, A. (Trifluoromethoxy)Phenylboronic Acids: Structures, Properties, and Antibacterial Activity. *Molecules* **2021**, *26*, 2007. [CrossRef]

38. Adamczyk-Woźniak, A.; Gozdalik, J.T.; Wieczorek, D.; Madura, I.D.; Kaczorowska, E.; Brzezińska, E.; Sporzyński, A.; Lipok, J. Synthesis, Properties and Antimicrobial Activity of 5-Trifluoromethyl-2-Formylphenylboronic Acid. *Molecules* **2020**, *25*, 799. [CrossRef] [PubMed]

39. Borys, K.M.; Wieczorek, D.; Pecura, K.; Lipok, J.; Adamczyk-Woźniak, A. Antifungal Activity and Tautomeric Cyclization Equilibria of Formylphenylboronic Acids. *Bioorg. Chem.* **2019**, *91*, 103081. [CrossRef] [PubMed]

40. Hiller, N.D.J.; do Amaral e Silva, N.A.; Tavares, T.A.; Faria, R.X.; Eberlin, M.N.; de Luna Martins, D. Arylboronic Acids and Their Myriad of Applications Beyond Organic Synthesis. *Eur. J. Org. Chem.* **2020**, *2020*, 4841–4877. [CrossRef]

41. Cruz, C.D.; Wrigstedt, P.; Moslova, K.; Iashin, V.; Mäkkylä, H.; Ghemtio, L.; Heikkinen, S.; Tammela, P.; Perea-Buceta, J.E. Installation of an Aryl Boronic Acid Function into the External Section of -Aryl-Oxazolidinones: Synthesis and Antimicrobial Evaluation. *Eur. J. Med. Chem.* **2021**, *211*, 113002. [CrossRef]

42. Silva, M.P.; Saraiva, L.; Pinto, M.; Sousa, M.E. Boronic Acids and Their Derivatives in Medicinal Chemistry: Synthesis and Biological Applications. *Molecules* **2020**, *25*, 4323. [CrossRef]

43. Groom, C.R.; Bruno, I.J.; Lightfoot, M.P.; Ward, S.C. The Cambridge Structural Database. *Acta Crystallogr. B Struct. Sci. Cryst. Eng. Mater.* **2016**, *72*, 171–179. [CrossRef] [PubMed]

44. Bruno, I.J.; Cole, J.C.; Edgington, P.R.; Kessler, M.; Macrae, C.F.; McCabe, P.; Pearson, J.; Taylor, R. New Software for Searching the Cambridge Structural Database and Visualizing Crystal Structures. *Acta Crystallogr. B* **2002**, *58*, 389–397. [CrossRef] [PubMed]

45. Macrae, C.F.; Sovago, I.; Cottrell, S.J.; Galek, P.T.A.; McCabe, P.; Pidcock, E.; Platings, M.; Shields, G.P.; Stevens, J.S.; Towler, M.; et al. Mercury 4.0: From Visualization to Analysis, Design and Prediction. *J. Appl. Crystallogr.* **2020**, *53*, 226–235. [CrossRef]

46. Giannozzi, P.; Baroni, S.; Bonini, N.; Calandra, M.; Car, R.; Cavazzoni, C.; Ceresoli, D.; Chiarotti, G.L.; Cococcioni, M.; Dabo, I.; et al. QUANTUM ESPRESSO: A Modular and Open-Source Software Project for Quantum Simulations of Materials. *J. Phys. Condens. Matter* **2009**, *21*, 395502. [CrossRef]

47. Stokes, H.T.; Hatch, D.M.; Campbell, B.J. ISOCIF, ISOTROPY Software Suite, Department of Physics and Astronomy, Brigham Young University, Provo, Utah, 84602, USA. 2022. Available online: iso.byu.edu/iso/isocif.php (accessed on 21 June 2022).

48. Grimme, S.; Antony, J.; Ehrlich, S.; Krieg, H. A Consistent and Accurate Ab Initio Parametrization of Density Functional Dispersion Correction (DFT-D) for the 94 Elements H-Pu. *J. Chem. Phys.* **2010**, *132*, 154104. [CrossRef]

49. Spackman, P.R.; Turner, M.J.; McKinnon, J.J.; Wolff, S.K.; Grimwood, D.J.; Jayatilaka, D.; Spackman, M.A. CrystalExplorer: A Program for Hirshfeld Surface Analysis, Visualization and Quantitative Analysis of Molecular Crystals. *J. Appl. Crystallogr.* **2021**, *54*, 1006–1011. [CrossRef]

50. Frisch, J.; Trucks, G.W.; Schlegel, H.B.; Scuseria, G.E.; Robb, M.A.; Cheeseman, J.R.; Scalmani, G.; Barone, V.; Petersson, G.A.; Nakatsuji, H.; et al. *Gaussian 09W, Revision D.01*; Gaussian, Inc.: Wallingford, CT, USA, 2016.

51. Karamertzanis, P.G.; Day, G.M.; Welch, G.W.A.; Kendrick, J.; Leusen, F.J.J.; Neumann, M.A.; Price, S.L. Modeling the Interplay of Inter- and Intramolecular Hydrogen Bonding in Conformational Polymorphs. *J. Chem. Phys.* **2008**, *128*, 244708. [CrossRef] [PubMed]

52. Wood, P.A.; Olsson, T.S.G.; Cole, J.C.; Cottrell, S.J.; Feeder, N.; Galek, P.T.A.; Groom, C.R.; Pidcock, E. Evaluation of Molecular Crystal Structures Using Full Interaction Maps. *CrystEngComm* **2013**, *15*, 65–72. [CrossRef]

53. Ouyang, J.; Xing, X.; Chen, J.; Zhou, L.; Liu, Z.; Heng, J.Y.Y. Effects of Solvent, Supersaturation Ratio and Silica Template on Morphology and Polymorph Evolution of Vanillin during Swift Cooling Crystallization. *Particuology* **2022**, *65*, 93–104. [CrossRef]

54. Ouyang, J.; Chen, J.; Rosbottom, I.; Chen, W.; Guo, M.; Heng, J.Y.Y. Supersaturation and Solvent Dependent Nucleation of Carbamazepine Polymorphs during Rapid Cooling Crystallization. *CrystEngComm* **2021**, *23*, 813–823. [CrossRef]

55. Datta, S.; Grant, D.J.W. Effect of Supersaturation on the Crystallization of Phenylbutazone Polymorphs. *Cryst. Res. Technol.* **2005**, *40*, 233–242. [CrossRef]

56. Bemisderfer, K.; Nazarenko, A.Y. Two Forms of (Naphthalen-1-Yl)Boronic Acid. *Acta Crystallogr. E Crystallogr. Commun.* **2016**, *72*, 1285–1289. [CrossRef] [PubMed]

57. Dąbrowski, M.; Durka, K.; Luliński, S.; Serwatowski, J. (2,4-Dipropoxyphenyl)Boronic Acid. *Acta Crystallogr. Sect. E Struct. Rep. Online* **2011**, *67*, o3455. [CrossRef]

58. Bai, S.Z.; Lou, X.H.; Li, H.M.; Yang, W.C.; Shi, H. Refinement of Crystal Structure of 2-Biphenylboronic Acid, $C_{12}H_{11}BO_2$. *Z. Krist.-New Cryst. Struct.* **2010**, *225*, 295–296. [CrossRef]

59. Durka, K.; Kliś, T.; Serwatowski, J. Crystal Structure of (2-Benzyloxypyrimidin-5-Yl)Boronic Acid. *Acta Crystallogr. Sect. E Struct. Rep. Online* **2014**, *70*, o1259–o1260. [CrossRef]

60. Cárdenas-Valenzuela, A.J.; González-García, G.; Zárraga-Nuñez, R.; Höpfl, H.; Campos-Gaxiola, J.J.; Cruz-Enríquez, A. Crystal Structure and Hirshfeld Surface Analysis of 3-Cyanophenylboronic Acid. *Acta Crystallogr. E Crystallogr. Commun.* **2018**, *74*, 441–444. [CrossRef]

61. Cruz-Cabeza, A.J.; Reutzel-Edens, S.M.; Bernstein, J. Facts and Fictions about Polymorphism. *Chem. Soc. Rev.* **2015**, *44*, 8619–8635. [CrossRef]

62. Burger, A.; Ramberger, R. On the Polymorphism of Pharmaceuticals and Other Molecular Crystals. I. *Mikrochim. Acta* **1979**, *72*, 259–271. [CrossRef]

63. Rietveld, I.B.; Barrio, M.; Lloveras, P.; Céolin, R.; Tamarit, J.-L. Polymorphism of Spironolactone: An Unprecedented Case of Monotropy Turning to Enantiotropy with a Huge Difference in the Melting Temperatures. *Int. J. Pharm.* **2018**, *552*, 193–205. [CrossRef] [PubMed]

64. Semjonova, A.; Bērziņš, A. Controlling the Polymorphic Outcome of 2,6-Dimethoxybenzoic Acid Crystallization Using Additives. *Crystals* **2022**, *12*, 1161. [CrossRef]

65. Larkin, J.D.; Bhat, K.L.; Markham, G.D.; Brooks, B.R.; Schaefer, H.F.; Bock, C.W. Structure of the Boronic Acid Dimer and the Relative Stabilities of Its Conformers. *J. Phys. Chem. A* **2006**, *110*, 10633–10642. [CrossRef] [PubMed]

66. Nyman, J.; Day, G.M. Static and Lattice Vibrational Energy Differences between Polymorphs. *CrystEngComm* **2015**, *17*, 5154–5165. [CrossRef]

67. Takahashi, T.; Endo, S.; Nagayama, K. Stabilization of Protein Crystals by Electrostatic Interactions as Revealed by a Numerical Approach. *J. Mol. Biol.* **1993**, *234*, 421–432. [CrossRef]

68. Takahashi, T. Significant Role of Electrostatic Interactions for Stabilization of Protein Assemblies. *Adv. Biophys.* **1997**, *34*, 41–54. [CrossRef]

69. Wang, C.; Rosbottom, I.; Turner, T.D.; Laing, S.; Maloney, A.G.P.; Sheikh, A.Y.; Docherty, R.; Yin, Q.; Roberts, K.J. Molecular, Solid-State and Surface Structures of the Conformational Polymorphic Forms of Ritonavir in Relation to Their Physicochemical Properties. *Pharm. Res.* **2021**, *38*, 971–990. [CrossRef]

70. Taylor, R.; Wood, P.A. A Million Crystal Structures: The Whole Is Greater than the Sum of Its Parts. *Chem. Rev.* **2019**, *119*, 9427–9477. [CrossRef]

71. Feeder, N.; Pidcock, E.; Reilly, A.M.; Sadiq, G.; Doherty, C.L.; Back, K.R.; Meenan, P.; Docherty, R. The Integration of Solid-Form Informatics into Solid-Form Selection. *J. Pharm. Pharmacol.* **2015**, *67*, 857–868. [CrossRef] [PubMed]

III

Semjonova, A., Bērziņš, A.

CRYSTALLIZATION OF METASTABLE ISONICOTINAMIDE POLYMORPHS AND PREVENTING CONCOMITANT CRYSTALLIZATION BY ADDITIVES

Crystal Growth & Design, **2023**, 23 (12), 8584-8596

Article

Crystallization of Metastable Isonicotinamide Polymorphs and Prevention of Concomitant Crystallization by Additives

Aina Semjonova* and Agris Bērziņš

Cite This: *Cryst. Growth Des.* 2023, 23, 8584−8596

Read Online

ACCESS | Metrics & More | Article Recommendations | Supporting Information

ABSTRACT: Concomitant crystallization of polymorphs is a major problem for the pharmaceutical industry, and in general, a better understanding of this phenomenon is necessary to ensure the crystallization of just one desired polymorph. Isonicotinamide (INA) forms six polymorphs which often crystallize concomitantly. Here, we studied whether the use of crystallization additives can facilitate the formation of INA metastable forms and prevent concomitant crystallization. Crystallization of INA was explored under different conditions by performing cooling and evaporative crystallization from different pure solvents and in the presence of crystallization additives. Some additives, such as naphthalene-1,5-diol, 4-carboxybenzeneboronic acid, and 2-picolinic acid, provided achieving crystallization control. Theoretical calculations allowed us to gain partial insight into the factors responsible for the polymorphic outcome of INA crystallization. The crystal structures of INA polymorphs II, IV, and VI, which often crystallize concomitantly, are almost identical. Therefore, it is possible that the energy barriers of nucleation and crystal growth rates for these polymorphs are highly similar, whereas, in the presence of additives, the crystallization of structurally more different Forms III or I could be achieved by altering these energy barriers.
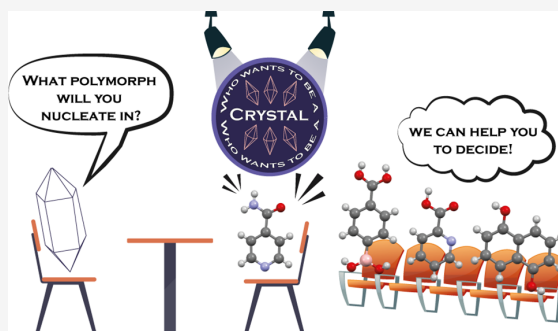
■ INTRODUCTION

Polymorphism is the ability of a substance to crystallize in different crystal lattices.[1,2] The polymorph control is crucial in many industrial processes, e.g., in the production of pharmaceuticals,[3−5] dyes,[6,7] explosives,[8] etc. Even though most of the substances are polymorphic,[2] highly polymorphous systems are rare, as only ∼2% of polymorphic compounds have more than four polymorphs.[9] The formation of different polymorphs is determined by crystallization kinetics and thermodynamics. The main step responsible for the polymorphic outcome is nucleation.[10] A metastable polymorph can nucleate due to kinetic aspects, but it can then transform to the thermodynamically stable form in solvent-mediated phase transformation (SMPT).[10−12] Concomitant nucleation of two or even more polymorphs later competing in growth is also possible.[13] Concomitant nucleation is reported to be commonly observed if the lattice energy differences between polymorphs are lower than a few kJ mol^{-1}.[2,9]

Therefore, common crystallization approaches often cannot provide crystallization of a pure polymorph. In such cases, other crystallization methods or approaches are introduced: antisolvent crystallization,[14] ultrasound-assisted crystallization,[15] laser-induced nucleation,[16] crystallization in gels,[17,18] and in the presence of additives (including tailor-made or structurally related additives,[19,20] polymers[21,22] and surfactants[23]) and templates (self-assembled monolayer[24−26] or other templates[27]). Structurally related additives have been used to obtain metastable forms of paracetamol,[28−32] *para*-aminobenzoic acid,[33] benzamide,[34] etc. It has been demonstrated that metacetamol allowed the formation of paracetamol Form II[29,31,32] by blocking the growth of Form I via strong adsorption on the main crystal faces.[32] Similarly, structurally related benzoic acids provided the selective formation of the metastable and difficult-to-obtain *para*-aminobenzoic acid *β* form by inhibiting crystallization of the stable *α* form.[33] Additionally, the relative stability of benzamide polymorphs I and III has been reversed using nicotinamide as an additive because of the formation of a solid solution.[34] The apparent relative stability and crystallization polymorphic outcome can be reversed also by structurally unrelated additives, as demonstrated for nitrofurantoin.[35] Although these few examples show the potential of crystallization additives to control the polymorphic outcome, there is still no general understanding of how to select an appropriate additive and

predict which polymorph would be facilitated in the presence of this additive.

In this study, we explored the use of crystallization in the presence of additives for minimizing concomitant crystallization that is often observed for pharmaceuticals[36−38] by studying isonicotinamide (INA) as the model substance. INA is widely used as a common conformer for the cocrystallization of pharmaceuticals[39−41] and has the potential for pharmacological effects.[42,43] INA is reported to crystallize in six polymorphs[44−47] (corresponding to Cambridge Structural Database (CSD) entries EHOWIH01-06), two monohydrates,[40] and few solvates.[48−50] INA Form I contains amide homodimers arranged in isolated corrugated sheets.[45] In contrast, all the other INA polymorphs contain hydrogen bond chains formed by amide functionals and by amide and pyridine moieties.[42−45] In a detailed comparison of the differences in the INA crystal structures, Fellah et al.[39] have shown that crystal structures of Forms II, IV, and VI are very similar and these polymorphs tend to crystallize concomitantly.[39] We note that different authors have used different INA polymorph designation schemes. Here, we use the scheme in which the dimer structure (EHOWIH01) is designated as Form I and the hydrogen bond chain structure (EHOWIH02) as Form II.[39,45,51]

Although Form I has been shown to be the stable polymorph in ambient conditions,[39,44,46] it is not the polymorph usually obtained in the crystallization.[39,47] Crystallization of INA in the presence of additives and templates has been studied previously,[46,47,52] but selective and repeatable crystallization of any of the polymorphs was not achieved. The presence of allopurinol facilitated the crystallization of Form VI, but this form still crystallized concomitantly with other polymorphs.[47] TiO$_2$ facilitated the crystallization of Form III, but it still crystallized concomitantly with Form II.[52] Form V has been obtained only in the presence of 3-arylbutanoic acid, but Form V crystallized together with Form IV.[46] Therefore, in this study, we investigated the crystallization of INA in the presence of numerous additives and showed that there are many additives repeatably providing crystallization of pure Form III or Form I from different solvents. We also used crystal structure analysis and theoretical calculations to provide a possible explanation for the polymorphic outcome control in the presence of these crystallization additives.

■ EXPERIMENTAL SECTION

Materials. INA (purity 99%, polymorphs I and II with a small impurity of hydrate I) was purchased from Alfa Aesar and ThermoScientific. Before the experiments, INA was kept at 120 °C to prepare pure Form II. Naphthalene-1,5-diol (ND, 95%), 4-carboxybenzeneboronic acid (4CPBA, 98%, quarter-hydrate), 2-picolinic acid (2PA, 98%), benzene-1,2,3-triol (BTriol, 95%), phloroglucinol (PhGlu, 99%, anhydrous), and nicotinic acid (NA, 95%) were purchased from Fluorochem. 5-Hydroxy-2-nitrobenzoic acid (5OH2NBA, 98%) was purchased from Carbosynth Ltd. Molecular structures of INA and selected additives are shown in Figure 1. Water was deionized in the laboratory. Other additives (see Table S1, Supporting Information) and organic solvents of analytical grade were purchased from commercial sources.

Powder X-ray Diffraction (PXRD). PXRD patterns were measured at ambient temperature on a Bruker D8 Advance diffractometer using copper radiation (Cu K$_\alpha$; λ = 1.54180 Å) and a LynxEye position-sensitive detector. The voltage and current of the tube were set to 40 kV and 40 mA, respectively. The divergence slit was set at 0.6 mm. The anti-scatter slit was set at 8.0 mm. The PXRD
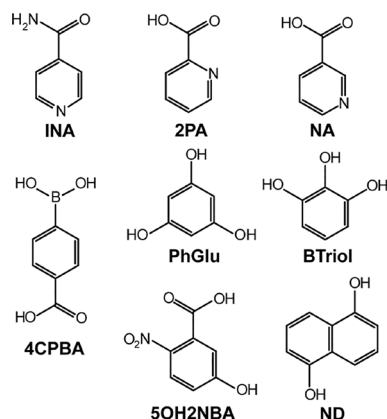

Figure 1. Molecular structure of INA and selected additives.

patterns were recorded from 3° to 35° on the 2θ scale using a scan speed of 0.2 s/0.02°.

Crystallization from Pure Solvents. Common solvents (see Table S2) from different solvent classes were selected for the crystallization of INA. For evaporation crystallization, 30−50 mg of INA were dissolved in 2−3 mL of solvent and the obtained solutions were evaporated at 25 and 50 °C. For cooling crystallization, INA was dissolved at 40−80 °C, depending on the boiling points of the solvent, and the obtained solutions were filtered and cooled to 5 °C. The obtained products were collected by filtration, air-dried, and characterized with PXRD.

Cooling crystallizations were performed using Crystal16 (Technobis). Solutions of different supersaturation (isopropanol (IPA) c/c^* = 1.5−4; 1,4-dioxane; c/c^* = 2−9; nitromethane c/c^* = 7−16; acetone c/c^* = 2, where c/c^* is a supersaturation ratio, c is the initial concentration and c^* is the solubility at 25 °C) were prepared in situ. The required amount of INA was weighted in an HPLC vial, 1 mL of solvent was added, and the vial was placed in Crystal16, where it was heated to achieve dissolution and then cooled with a cooling rate of 10 °C min^{-1} and a stirring rate of 900 rpm. Selected solutions (IPA and 1,4-dioxane with c/c^* = 3; nitromethane with c/c^* = 12; and acetone with c/c^* = 2) were cooled with different cooling rates −20, 10, 1, and 0,1 °C min^{-1} to determine the effect of the cooling rate on the polymorphic outcome. Four parallel crystallization experiments were performed in all cases. The obtained products were collected by filtration after the set end temperature of 10 °C was reached, air-dried, and characterized with PXRD. The supersaturation ratio was calculated using solubility reported in the literature: I PA 44 mg mL^{-1},[53] 1,4-dioxane 18 mg mL^{-1},[53] nitromethane 3 mg mL^{-1},[53] and acetone 25 mg mL^{-1}.[51]

Crystallization in the Presence of Additives. The effect of soluble additives on the crystallization polymorphic outcome was tested in IPA and 1,4-dioxane using cooling crystallization. In 2 mL of IPA, 20−25 mg of a solid additive or 2−3 drops (60−80 mg) of a liquid additive and 260−270 mg of INA ($c/c^* \approx$ 3) were dissolved at 70 °C, the solution was filtered and cooled to 5 °C. In 2 mL of 1,4-dioxane, 20−25 mg of a solid additive or 2−3 drops (60−80 mg) of a liquid additive and 110−120 mg of INA ($c/c^* \approx$ 3) were dissolved at 70 °C, and the solution was filtered and cooled to 5 °C. Three parallel crystallization experiments were performed for each additive. The obtained products were collected by filtration, air-dried, and characterized with PXRD.

The additives allowing the control of crystallization polymorphic outcome were chosen for further cooling crystallization using Crystal16. These were PhGlu, NA, 4CPBA, BTriol, 5OH2NBA, ND, and 2PA for crystallization from IPA and 2PA, 4CPBA, and ND for crystallization from 1,4-dioxane, acetone, and nitromethane. Solutions with c/c^* = 3 and additive concentration of 10 mg mL^{-1} were prepared in situ (similar as described above) for all the additives, except for the ND and 4CPBA. The solutions were heated to 70 °C

(IPA) or 95 °C (1,4-dioxane) and then cooled using a cooling rate of 20, 10, 1, or 0.1 °C min^{-1} and a stirring rate of 900 rpm. ND and 4CPBA solutions, except for 4CPBA solutions in IPA, were prepared differently, as ND solubility in these solvents is less than 10 mg mL^{-1}, and 4CPBA significantly decreased the solubility of INA in 1,4-dioxane, acetone, and nitromethane and has a solubility <10 mg mL^{-1} in nitromethane. These solutions were prepared by adding the required amount of INA, 0.3 g of additive, and 30 mL of solvent to the flask boiling under reflux, and stirring for 2 h. After boiling, the solution was kept at 50 °C (acetone), 70 °C (IPA), or 90 °C (1,4-dioxane and nitromethane) in a thermostat and filtered. One milliliter of the solution was transferred to preheated HPLC vials which were placed in Crystal16 at the same temperature as used in the thermostat and cooled identically to the solutions prepared in situ. Four parallel crystallization experiments were performed in all cases. The obtained products were collected by filtration after the set end temperature of 10 °C was reached, air-dried, and characterized with PXRD.

Three additives were chosen for crystallization using different stirring rates: 2PA, 4CPBA, and ND in IPA and 1,4-dioxane, and 2PA and ND in acetone. The crystallization experiments were set up as described above, but the cooling rates were 10 and 1 °C min^{-1} and the stirring rates were 0, 400, and 1250 rpm. The obtained products were collected by filtration after the set end temperature of 10 °C was reached, air-dried, and characterized with PXRD.

The same additives as in the experiments evaluating the effect of stirring rate were chosen for SMPT studies with a cooling rate of 1 °C min^{-1} and a stirring rate of 900 rpm. The obtained products were collected by filtration immediately after nucleation and 10, 20, or 30 min after the nucleation.

Theoretical Calculations. Molecular packaging of INA polymorphs was compared with CrystalCMP[54,55] using crystal structures from the CSD database (Form I − EHOWIH01;[45] Form II − EHOWIH02;[45] Form III − EHOWIH03;[44] Form IV − EHO-WIH04;[46] Form V − EHOWIH05;[46] and Form VI − EHO-WIH06[47]).

The geometry of five INA polymorph crystal structures (forms I−IV and VI) was optimized in Quantum ESPRESSO 6.4.1.[56] by relaxing the positions of all atoms. The initial structure models were taken from the CSD database. All calculations were performed using the PBE functional with ultrasoft pseudopotentials from the original pseudopotential library and a 90 Ry plane-wave cutoff energy with vdW interactions treated according to the D3 method of Grimme[57] using a 2 × 2 × 2 k-point grid. The geometry-optimized structures were used for further analysis performed using Crystal Explorer 21.[58] To calculate the lattice energy including the conformational penalty,[59] full geometry optimization of INA molecules and geometry optimization of INA molecules with torsion angle between the benzene ring and the amide group constrained to the value as observed in the crystal structures were performed. These geometry optimizations were carried out in Gaussian 09[60] with the density functional theory M06-2X and 6-31++G(d,p) basis set in the gas phase. Intramolecular energy was calculated as the difference between the energy of the conformer as in the crystal structure and the global minimum energy. The calculations of the pairwise intermolecular interaction energy in crystal structures were performed at the B3LYP-D2/6-31G(d,p) level in Crystal Explorer 21. The sum of all the pairwise interaction energies with molecules for which there are atoms within 15 Å of the central molecule was used to calculate the intermolecular energy. The lattice energy was calculated by summing the calculated intermolecular energy and the intramolecular energy. Crystal Explorer 21 was also used to calculate the Hirshfeld surfaces, their 2D fingerprint plots summarizing the information about intermolecular interactions, and generate the energy frameworks from the calculated pairwise interaction energies and their electrostatic and dispersion components. Form V was not analyzed because this form was not obtained in any of the performed crystallization experiments.

Generation of Full Interaction Maps (FIM) providing molecule interaction preferences and analysis of Bravais−Friedel−Donnay−Harker (BFDH) morphology[61] were performed with Mercury 2020.3.0.[62] FIMs of crystal structures with crystal faces of BFDH morphology and structure slicing along the crystallographic planes corresponding to faces present on the crystal morphology were generated for each polymorph.

■ RESULTS AND DISCUSSION

Summary of the Published Studies of INA Crystallization. Crystal structures of the first two INA polymorphs Form I (EHOWIH01) and Form II (EHOWIH02) were described in 2003.[45] Form I was crystallized from nitromethane and Form II from tetrahydrofuran and 1,4-dioxane. In 2010, a new Form III (EHOWIH03) was crystallized from chloroform.[44] In 2011, two additional forms, Form IV (EHOWIH04) and Form V (EHOWIH05), were unexpectedly crystallized as impurities during cocrystallization experiments in acetone.[46] It was noted that Forms II and IV often crystallize together.[46]

Kulkarni et al.[53] studied the link between the self-association of INA in different solvents and the polymorph obtained from this solvent. They noted that in strong hydrogen bond acceptor solvents, INA form chainlike associates and crystallize in chainlike structures (Form II), whereas in weak hydrogen bond acceptor solvents, INA form dimers and crystallize in structures containing dimers (Form I). They also report[53] that from chloroform, in which dimers or chains were not observed, a new structurally uncharacterized polymorph Form VI is obtained. In 2018, Vicatos et al.[47] obtained and structurally characterized Form VI (EHOWIH06) in cocrystallization experiments.

Caridi et al.[52] observed that in the crystallization of INA from ethanol at low supersaturation only Form I could be obtained, whereas at higher supersaturation, in the presence of anatase, a mixture of Forms II and III formed. Kulkarni et al.,[63] however, observed crystallization of Form I from ethanol, whereas Forms II and IV were obtained from ethanol-nitromethane and ethanol-nitrobenzene, respectively, although in part of the experiments these polymorphs crystallized concomitantly with Form I.

Hansen et al.[51] investigated INA crystallization from various solvents and found that Form I is obtained using low supersaturation levels, whereas Form II is favored at higher supersaturation.

Recently Fellah et al.[39] conducted an extensive study of INA crystallization from both melt and solution. Only Form II could be crystallized from the melt, whereas from solutions, mixtures of different polymorphs could be obtained.[39] The results show that higher supersaturation is required to obtain Form III due to its higher solubility and free energy, although Form IV should be obtained more easily if compared to Form III. Similar to the study of Vicatos et al.,[47] in the experiments performed in this study, Form V could not be obtained.
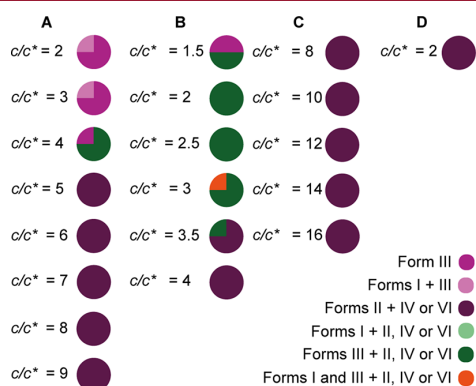
A summary of INA polymorph obtained in different crystallization experiments as presented in various articles, including the current study, is provided in Table S2.

Crystallization from Pure Solvents. INA was crystallized from pure solvents under three different conditions: using cooling crystallization and evaporation at 25 and 50 °C. In most of the conditions, several INA polymorphs were present in the obtained crystallization products (see Table S2) which agrees with the results from other studies.[39,47] Usually, Forms II and VI or Forms II and IV crystallized together, but from some solvents, a mixture of all these three forms was obtained. In cooling crystallization from acetone Form I was favored, in

agreement with the study of Kulkarni et al.[53] Form I with impurities of other forms was obtained by evaporation from acetonitrile in agreement with the study of Fellah et al.[39] In cooling crystallization from 1,4-dioxane Form III was favored, but in the evaporation, more stable forms were favored. In addition, Form III with impurities of other forms was obtained from tetrahydrofuran and IPA. Nitromethane was the only solvent from which under all three crystallization conditions a mixture of the same polymorphs, Forms II and IV, was obtained. In contrast, Aakeröy et al.[45] and Fellah et al.[39] report obtaining Form I in some of the experiments from this solvent. In general, however, the polymorphic outcome of the crystallization does not correlate with the evaporation temperature or the solvent used. Overall, the polymorph obtained does not correlate with observations of Kulkarni et al.[53] about the solvent type. For example, weak hydrogen bond acceptors (acetone, 1,4-dioxane) in this study did not provide a dimer structure (Form I), and this form was also not obtained from strong hydrogen bond donors such as IPA and methanol. In fact, despite Form I being determined to be the stable polymorph,[39,44,46] it was rarely obtained in the crystallization, whereas Form II, the high-temperature polymorph, was the most common crystallization outcome. IPA, acetone, and 1,4-dioxane in which different polymorphs were obtained under different conditions as well as nitromethane from which a mixture of Forms II and IV was always obtained were chosen for further crystallization experiments. Additionally, the solubility of INA in these solvents was suitable for the selected approach of performing the crystallization experiments.

Cooling crystallizations from the selected solvents with different supersaturations were performed using Crystal16. The crystallization products of IPA and 1,4-dioxane had different compositions containing different forms (see Figures 2 and S1–S2; INA forms obtained in each experiment are
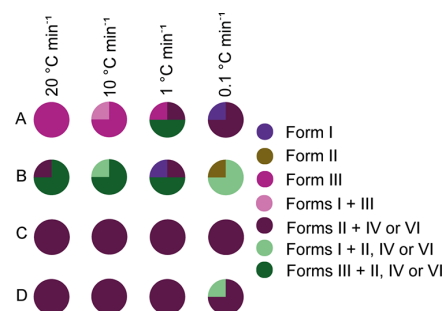

Figure 2. Summary of INA polymorphs obtained in crystallization from 1,4-dioxane (A), IPA (B), nitromethane (C), and acetone (D) with different supersaturation ratios (c/c^*) using a cooling rate of 10 °C min^{-1} and a stirring rate of 900 rpm. Each 1/4 of the pie chart represents one of the parallel experiments.

given in Table S3). At the lowest supersaturations from both solvents, pure Form III or its mixture with other forms was obtained. The increase of the supersaturation ratio reduced the possibility of the formation of Form III but increased the possibility to obtain a mixture of Forms II, IV, and VI. Using all five tested supersaturation ratios in nitromethane a mixture of Forms II, IV, and VI, all containing similar intermolecular

interactions, was obtained (see Figure S3). Only one supersaturation ratio could be prepared for acetone, and in this crystallization experiment a mixture of Forms II and VI was obtained. IPA and 1,4-dioxane solutions with supersaturation $c/c^* = 3$ allowing the formation of Form III in a mixture with other forms was selected for further experiments. For the other two solvents solutions with experimentally more convenient supersaturation of $c/c^* = 12$ (nitromethane) or $c/c^* = 2$ (acetone) were selected.

The solutions with the selected supersaturation ratios were cooled with four different cooling rates to determine the effect of the cooling rate on the crystallization polymorphic outcome. Pure Form III was obtained from 1,4-dioxane using the fastest cooling rate of 20 °C min^{-1} (see Figure 3 and Table S4), but
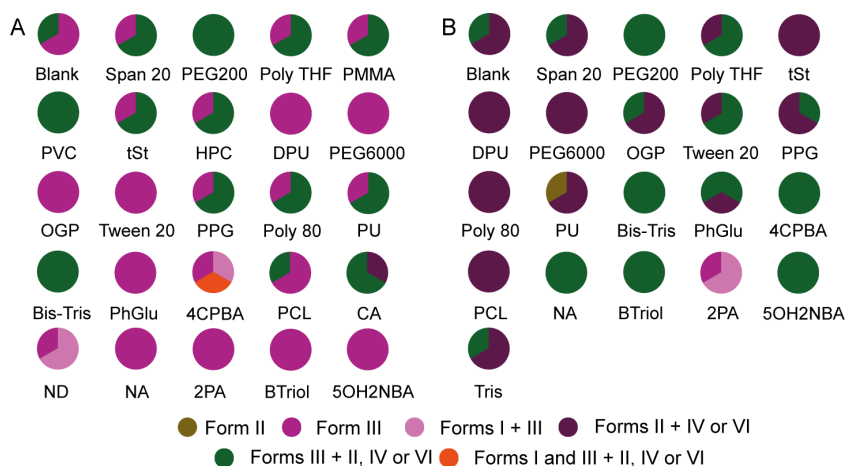

Figure 3. Summary of INA polymorphs obtained from 1,4-dioxane (A), IPA (B), nitromethane (C), and acetone (D) solutions with the selected supersaturations using different cooling rates and a stirring rate of 900 rpm. Each 1/4 of the pie chart represents one of the parallel experiments.

the decrease of the cooling rate facilitated the formation of the more stable Forms II and VI, as determined by the lattice energy calculations before.[39] Different polymorph mixtures containing Form III were obtained from IPA using the fastest cooling rates of 20 and 10 °C min^{-1}, but in longer experiments (using a slower cooling rate), more stable forms were obtained. In contrast, Form III did not form from nitromethane or acetone. The slowest cooling and therefore the longest stirring in nitromethane and 1,4-dioxane decreased the Form IV content in the crystallization product which likely did not nucleate as often as using a faster cooling rate or transformed to more stable forms. The concomitant formation and similar stability of Forms II and VI could be explained by their nearly identical conformation (see section Theoretical calculation below), with these forms only differing in the packing arrangement.[47]

Crystallization in the Presence of Additives. The polymorphic outcome of crystallization in the presence of additives is affected by complex and not fully characterized interactions between the compound being crystallized, the solvent, and the additives as well as by the crystallization conditions (e.g., cooling and stirring rate). The polymorphic outcome can be altered by changes in any of these aspects. In this study, we are investigating crystallization in the presence of additives by changing the crystallization conditions to better understand the role of the additive on the crystallization outcome.

Preliminary crystallizations in the presence of additives were performed from 1,4-dioxane (Figures S4 and S5) and IPA. Some of the tested additives facilitated the crystallization of

Figure 4. Summary of INA polymorphs obtained in crystallization in the presence of selected soluble additives from 1,4-dioxane (A) and IPA (B). Each 1/3 of the pie chart represents one of the parallel experiments.

pure Form III (see Figure 4A, and Table S5), and a few additives such as 4CPBA and ND facilitated the crystallization of Form I from 1,4-dioxane. In contrast to 1,4-dioxane, in crystallization from IPA, the tested additives did not prevent the formation of INA polymorph mixtures. Moreover, the additives even facilitated the formation of polymorph mixtures by facilitating the crystallization of Form III (see the increase in the green-colored slices in Figure 4B and Table S6). The presence of 2PA, however, facilitated the formation of Form I, which previously from IPA was obtained only in a few of the crystallization experiments as an impurity. ND, 4CPBA, and 2PA were selected for further crystallization experiments from 1,4-dioxane, as the first two facilitated the crystallization of Form I and 2PA favored the crystallization of Form III also from IPA. A larger number of additives (4CPBA, 2PA, BTriol, PhGlu, NA, and 5OH2NBA) were selected for further crystallization experiments from IPA, as many of the tested additives facilitated the formation of Form III. We note that these additives also facilitated the crystallization of Form III from 1,4-dioxane. In none of the performed crystallizations, in the presence of 2PA, we observed the formation of INA-2PA cocrystal reported in the literature.[64]

We note that the seven selected additives can provide different types of intermolecular interactions with INA (see Figure 5). For example, 2PA and NA are highly similar to the INA molecule and can bond intermolecularly by forming carboxyl acid—amide dimers and bonds with the pyridine nitrogen atom. PhGlu and BTriol are isomers providing various hydrogen bonding possibilities acting as donors and acceptors. Similar hydrogen bonding is possible also with ND, but the hydroxy groups are on different sides of the molecule; therefore, simultaneously only one strong hydrogen bond with INA can be formed. 5OH2NBA can form carboxylic acid—amide dimers and employ the hydroxy group as a hydrogen bond donor or acceptor or the nitro group as a hydrogen bond acceptor. 4CPBA can form hydrogen bonds using both of its acid groups: boronic acid and carboxyl group. Moreover, all the additives can interact with INA via aromatic interactions.

The effect of additives on the polymorphic outcome of crystallization was tested at selected INA supersaturation with different cooling rates to understand the ability of additives to control the outcome of crystallization under different
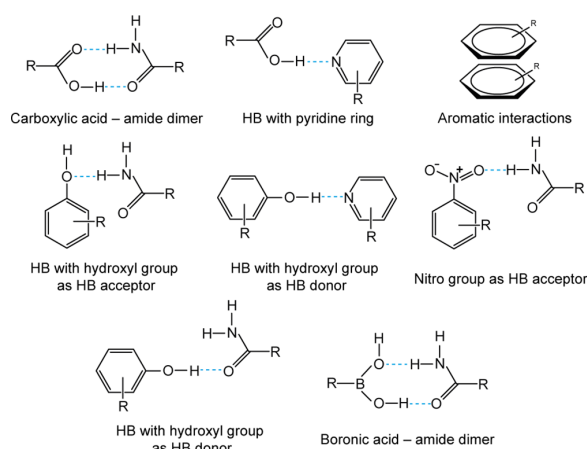

Figure 5. Schematic illustration of possible intermolecular interactions between INA and the tested additives. HB: hydrogen bond.

conditions. Almost all the additives in IPA and 1,4-dioxane facilitated the crystallization of Form III when the faster cooling rates were used (see the increase in the magenta-colored slices in Figures 6 and S6—S11), but this control effect was not observed using slower cooling, where a mixture of different polymorphs formed. We note that 2PA showed the highest ability to provide crystallization of Form III from IPA (see the first column group in Figure 6 and Table S7), as Form III was obtained even using the cooling rate of 1 °C min^{-1}, where, in the presence of other additives, mostly mixtures of Forms II, IV, and VI were obtained. Using the slowest cooling rate (0.1 °C min^{-1}) in crystallization from IPA, none of the tested additives was able to provide nucleation of Form III from the solution, and Forms II or VI dominated in the crystallization products.

As demonstrated by the crystallizations from pure solvents (see Figure 3), IPA and 1,4-dioxane have different effects on the polymorphic outcome. This is also reflected in the crystallization in the presence of additives, as Form III is the main polymorph obtained in the crystallization from 1,4-dioxane (see the second column group in Figure 6 and Table S8), and additives ND and 2PA provided the most reliable
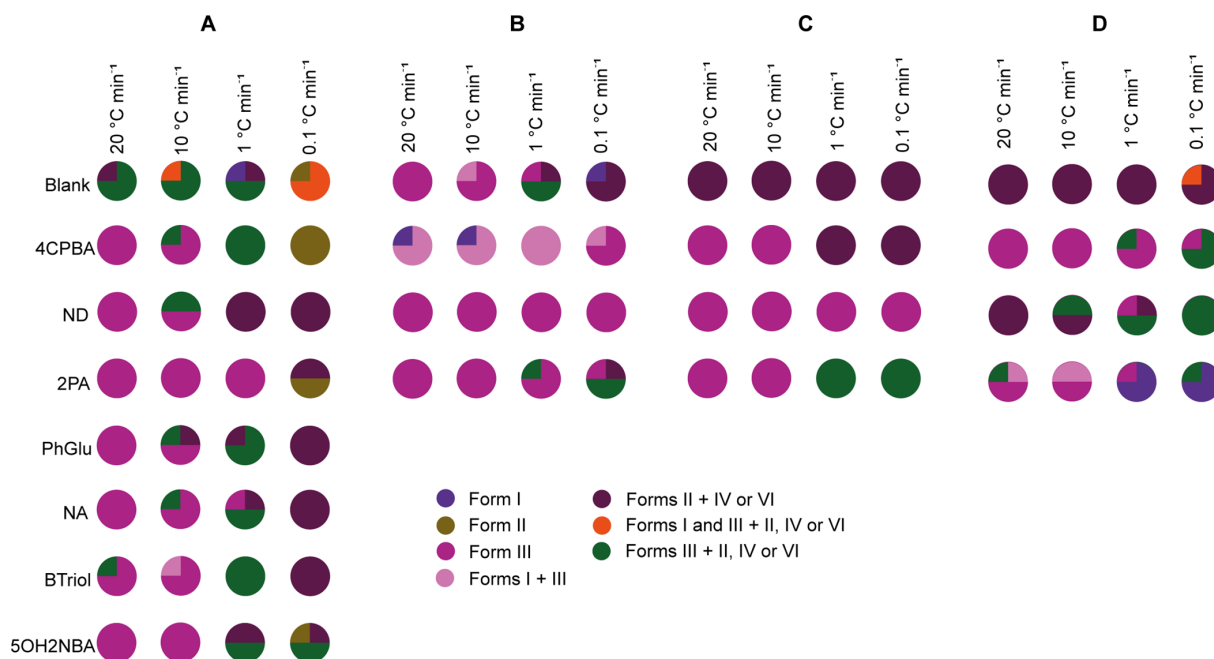
Figure 6. Summary of INA polymorphs obtained in crystallization in the presence of selected additives from IPA (A), 1,4-dioxane (B), nitromethane (C), and acetone (D) using different cooling rates. Each 1/4 of the pie chart represents one of the parallel experiments.

crystallization of pure Form III (see Figure S12). The effect of 2PA in this solvent was maintained only at fast cooling rates in contrast to crystallization from IPA, whereas ND showed the best ability to maintain Form III even in slow cooling rates, where the obtained crystals were kept in a suspension until the set end temperature of 10 °C was reached. Interestingly, in contrast to the other two additives which facilitated the nucleation of Form III from 1,4-dioxane, 4CPBA facilitated the nucleation of Form I from this solvent (see Figure S13). We note that the crystal structures of this additive[65] contain synthons similar to those present in INA Form I. Furthermore, this additive can form two different dimers with INA: carboxylic acid-amide heterodimers and boronic acid-amide heterodimers (see Figure 5). In fact, the formation of Form I in the presence of 4CPBA agrees with the observation of Kulkarni et al.[53] that INA forms dimers in 1,4-dioxane solution and subsequently forms pure Form I in crystallization, although from pure 1,4-dioxane other polymorphs were obtained in the current study and other studies[39,45] (see Table S2). This observation implies that the formation of associates in solution does not provide a fully selective crystallization outcome; however, the introduction of a crystallization additive can provide the formation of the dimeric structure by maintaining the associate throughout the processes of nucleation.

The most selective additives were also tested in acetone and nitromethane, from which crystallization of Form III was not observed in the previous experiments (see Figure 3). The tested additives had different effects on the crystallization outcome from acetone. In the presence of ND, different polymorph mixtures were mostly obtained. In contrast, 2PA and 4CPBA provided crystallization control, although facilitating the formation of different polymorphs than from IPA and 1,4-dioxane: 4CPBA facilitated the crystallization of Form III, but 2PA − Form I (see the third column group in Figure 6 and Table S9). In the presence of 2PA at the fastest cooling rate

crystallization of Form III was facilitated, but at slower cooling rates pure Form I was mostly obtained. We note that Form I was obtained from acetone also in our previous experiments and in other studies,[39,46] although in our experiments, Form I was obtained mostly in a mixture with other polymorphs, and overall, our results indicate that obtaining pure stable polymorph, Form I, through direct crystallization is relatively challenging. However, the addition of 2PA to the acetone solution and crystallization with a slow cooling rate facilitate the formation of the thermodynamically stable form.

In the presence of all three tested additives, the formation of pure Form III was facilitated from nitromethane using the fastest cooling rates, whereas ND provided the formation of pure Form III using all four cooling rates (see the fourth column group in Figure 6 and Table S10). In contrast to the other solvents, Form I was never among the crystallization products from nitromethane, which, however, does not agree with part of the previous studies.[39,45]

In further experiments, we tested the effect of the stirring (agitation) rate on the crystallization polymorphic outcome. In previous studies, it has been shown that the agitation rate can decrease the possibility of a dimer-containing form of *m*-hydroxybenzoic acid, and it has been suggested that the agitation rate affects the associates in the solution and therefore inhibits the formation of the dimer form.[66] In the above-described experiments, in which the effect of cooling rate on the INA polymorphic outcome was tested, a rather high stirring rate of 900 rpm was used. In these experiments, Forms I and III nucleated concomitantly from 1,4-dioxane in the presence of 4CPBA and from acetone in the presence of 2PA. For the experiments testing the stirring rate, two cooling rates were selected: 10 °C min^{-1} as a fast-cooling rate and 1 °C min^{-1} as a slow-cooling rate. Nitromethane as a solvent and 4CPBA as an additive in acetone were not tested due to

the low amount of solid obtained in such crystallization experiments.

We observed that the use of fast cooling rate and slow stirring rate or even crystallization without stirring facilitated the formation of Form I from IPA (see Figure 7A and Table
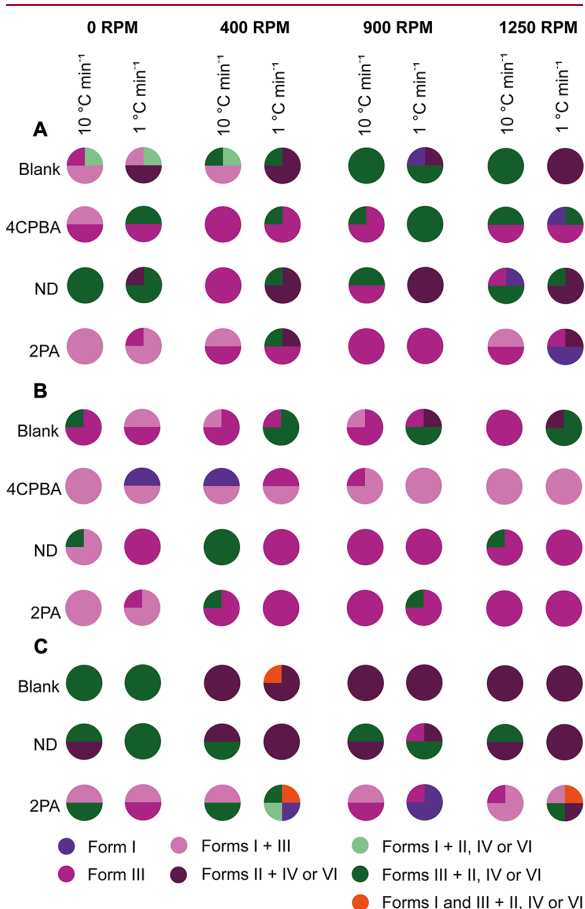
Figure 7. Summary of INA polymorphs obtained in crystallization in the presence of selected additives from IPA (A), 1,4-dioxane (B), and acetone (C) using two cooling rates and different stirring rates. Each 1/4 of the pie chart represents one of the parallel experiments.

S11). The crystallization of Form III, however, was facilitated by the presence of the tested additives and the use of a faster cooling rate. In the presence of 4CPBA pure Form III crystallized more often than from pure solvents, but in some experiments, impurities of other polymorphs were also present. In the presence of 2PA without stirring, a mixture of Forms I and III was obtained, and the application of stirring facilitated the nucleation of pure Form III, whereas the fastest stirring rate again favored the nucleation of pure Form I.

In 1,4-dioxane, the crystallization polymorphic outcome control by the tested additives was more reliable, particularly using stirring (see Figure 7B and Table S12). From pure solvent, Form III was mostly obtained but often contained impurities of other polymorphs. The presence of any of the additives provided the formation of the mixture of Forms I and III when a fast cooling rate and no stirring were used. In fact, Forms I and III crystallized concomitantly using any stirring regime in the presence of 4CPBA, with some exceptions when

pure forms were obtained. The most selective crystallization of Form III was achieved in the presence of ND using the slow cooling rate, and the stirring rate did not affect this. In the presence of 2PA, however, Form III was obtained in crystallization with stirring, whereas in crystallization without stirring a mixture of Forms I and III was obtained.

The presence of 2PA facilitated crystallization of Form III or I from acetone (see Figure 7C, Table S13 and Figure S14), but, in contrast to 1,4-dioxane and IPA, in most of the cases, still different polymorph mixtures were obtained. In these experiments, ND did not provide control of the crystallization outcome as observed in other experiments. We note that in these experiments, we did not consider 4CPBA, the additive providing the most reliable crystallization control from acetone in the previously described experiments.

Overall, in the crystallization experiments, using the fastest cooling rates, Form III was obtained, but in the experiments using the slowest cooling rates, in which the suspension obtained after the crystallization was stirred for a longer time until the set end temperature of 10 °C was reached, more stable polymorphs (Forms II, IV or VI[39]) compared to Form III were obtained. This resulted in almost all the additives not being able to provide crystallization of Form III or Form I with the cooling rate of 1 °C min^{-1}. Such results in general suggest a possibility that Form III nucleates first and then by stirring the suspension transforms into other more stable forms in SMPT. For example, using the cooling rate of 1 °C min^{-1} resulted in stirring the obtained crystallization product up to 30 min. Therefore, we investigated whether using the cooling rate of 1 °C min^{-1} the more stable INA polymorphs form in SMPT or are obtained right after the nucleation (see Figure 8 and Tables
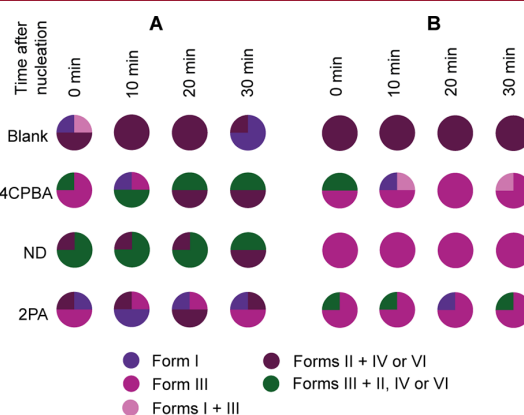
Figure 8. Summary of INA polymorphs obtained in crystallization in the presence of selected additives from IPA (A) and 1,4-dioxane (B) using 1 °C min^{-1} cooling rate and different time when crystals were collected after the nucleation. Each 1/4 of the pie chart represents one of the parallel experiments.

S14, S15). The results showed that the crystal form obtained in the presence of all the tested additives did not change notably within 30 min after the nucleation, which is in agreement with the SMPT seeding experiment by Kulkarni et al.[63] in which phase transition in ethanol solution took more than 7 h. Therefore, the various polymorphic outcome using different stirring rate is not because of an SMPT but instead because of the distinct ability of additives to affect the crystallization outcome. Most likely, this is because, when higher cooling
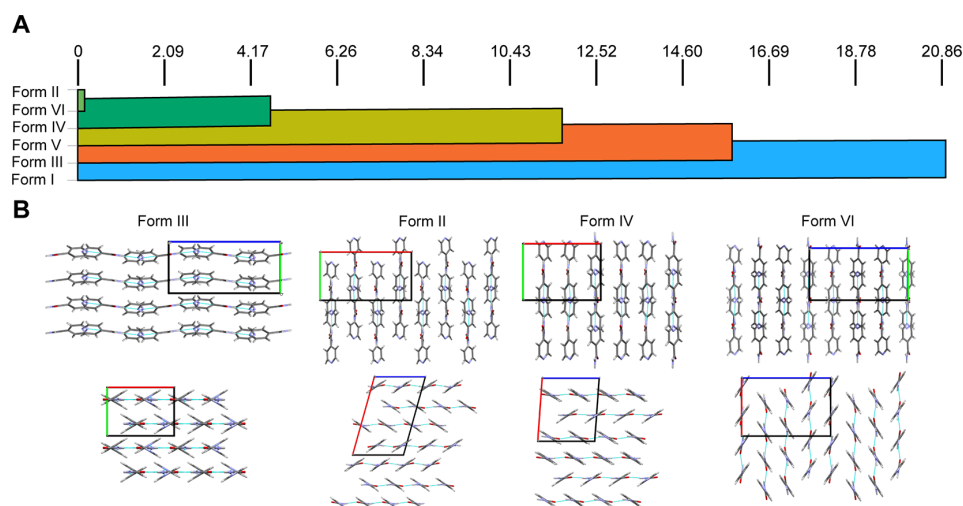
Figure 9. Packing similarity dendrogram (A) and molecular packing (B) of INA polymorphs.

Table 1. Selected Crystallographic and Intramolecular, Intermolecular, and Lattice Energy Data of INA Polymorphs

| polymorph	CSD Refcode	Z/Z'	E_{intra}, kJ mol^{-1}	E_{inter}, kJ mol^{-1}	$(E_{ele} + E_{pol})/E_{disp}$	$E_{lattice}$, kJ mol^{-1}
Form I	EHOWIH01	4/1	0.46	−124.7	1.53	−124.3
Form II	EHOWIH02	8/2	0.05	−122.2	1.70	−122.2
Form III	EHOWIH03	8/1	0.51	−120.6	1.56	−120.1
Form IV	EHOWIH04	6/3	0.12	−119.8	1.58	−119.7
Form VI	EHOWIH06	8/2	0.04	−121.4	1.70	−121.4

rates are used, the nucleation occurs at lower temperatures and therefore at higher supersaturation, whereas, when slower cooling rates are used, the nucleation occurs at higher temperatures and therefore lower supersaturation. For example, in crystallization from IPA at a cooling rate of 1 °C min^{-1}, INA nucleated at 41−42 °C, whereas at a cooling rate of 20 °C min^{-1} only at 13−17 °C. In the presence of 2PA as an additive, the nucleation temperature decreases to 38−40 and ∼10 °C, respectively. Also, other additives decreased the nucleation temperature by increasing the supersaturation, and this in fact might be one of the potential effects of additives that could alter the obtained crystallization products.

Theoretical Calculations. A comparison of molecular packaging of INA polymorphs using CrystalCMP confirmed that Forms II and VI are almost identical as previously described by Vicatos et al.[47] (see Figure 9A and Table S16). Moreover, Form IV is highly similar to Forms II and VI, having packing similarity PS$_{ab}$ of only 4−5. A comparison of molecular packing also showed that Form I is structurally the most diverse polymorph (PS$_{ab}$ above 19), apparently because the hydrogen-bonded dimers in this structure result in notably different molecule arrangements. Moreover, the next most diverse polymorph is Form III (PS$_{ab}$ with Forms II, IV, V, and VI above 11), likely due to different arrangements of INA molecules forming N$_{pyr}$···H$_2$N hydrogen bond (see Figure 9B). In Forms II, IV, and VI all molecules forming the N$_{pyr}$···H$_2$N hydrogen bond and lying in the same *bc*-plane are arranged in identical directions, whereas in Form III INA molecules from adjacent rows in similar planes (in this case in the *ac* direction) are oriented perpendicularly.

Analysis of INA molecular conformation showed that in the most stable conformation, the benzene ring and the amide group are twisted and the torsion angle between them is 21.88°

(see Table S17). Overall, in all the polymorphs, the INA molecule adopts an almost identical conformation, with differences being characteristic for conformation adjustments because of different molecule packing. In one of the symmetry-independent molecules of Form VI, the torsion angle value corresponds to the global minimum value and results in Form VI having the lowest intramolecular energy (see Table 1). In Forms III and I, the amide group has a somewhat larger deviation from the plane of the benzene ring (29°) than in other polymorphs, resulting in these forms having higher intramolecular energy, although the difference between all the forms is very small, consistent with the minor conformation differences. The five considered polymorphs also have highly similar intermolecular interaction energy and therefore lattice energies. The lowest lattice energy is calculated for Form I (−124.3 kJ mol^{-1}), but the lattice energy of Form II is 2 kJ mol^{-1} higher and is the second lowest of the lattice energy values. All the other polymorphs have almost identical lattice energy (−120 to −121 kJ mol^{-1}), which supports the concomitant crystallization of the polymorphs as observed experimentally. Moreover, the energy difference between Forms II and VI as well as Forms III and IV, often crystallizing concomitantly, is less than 1 kJ mol^{-1}. Evaluation of the different contributions in interaction energy shows that electrostatic interactions are the most important energy component in all INA polymorphs.

As expected, based on the highly similar intramolecular interactions and molecular packing, all INA polymorphs, except for Form I, have almost identical layouts of energy frameworks (see Figures 10 and S15). The main interactions stabilizing the crystal structure of all forms are dominated by electrostatic energy components, and the dispersion energy components are notably weaker than the electrostatic energy
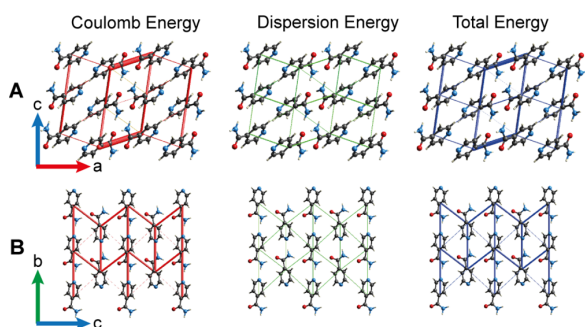
Figure 10. Energy framework diagrams for electrostatic, dispersion, and total energy for a cluster of molecules in INA Forms I (A) and II (B). Other frameworks are given in Figure S15. All images use the same tube size for energy.

components. The most notable of electrostatic energy-dominated interactions in Form I are interactions between molecules forming hydrogen-bonded dimers. Each such dimer additionally interacts by weak hydrogen bonds with INA molecules from the layers above and below. In contrast, the most notable interactions dominated by electrostatic energy in all the other INA polymorphs are among molecules forming hydrogen-bonded INA molecule chains in two spatial directions and therefore forming hydrogen-bonded INA molecule layers. The interactions having the most negative dispersion energy in Forms I and III are between the same molecules as those that also have the most negative electrostatic energy. In contrast, in Forms II, IV, and VI, these are aromatic and $\pi-\pi$ interactions between oppositely oriented molecules from adjacent INA molecule layers and interactions with molecules hydrogen bonded to the mentioned molecules from adjacent layers. Because of the identical hydrogen bonding between INA molecules forming the layer, the energy framework within the layer is identical for Forms II, III, IV, and VI. There are, however, some differences in the stacking of such INA layers between Forms II−VI (see Figure S15) as the INA layers are not stacked face to face, but

with different orientations and relative displacements. Similarly, Forms III and II also have a highly similar energy framework with the difference being in the framework representing the stacking of INA layers.

The 2D fingerprint plots of INA Forms II, IV, and VI were highly similar, but notable differences were observed in those of Forms I and III (see Figure 11). In the Hirshfeld surface fingerprint plot of Form I, there are two sharp peaks corresponding to interactions CO···H$_2$N, whereas for all the other forms, these peaks are wider and each corresponds to two interactions: N$_{pyr}$···H$_2$N or CO···H$_2$N. In the fingerprint plots of Forms II, IV (except for one of the symmetry-independent molecules shown in the middle in Figure S16), and VI, there is a distinct peak in the middle of the plot corresponding to −CH···HC− interactions. Another difference between the fingerprint plots of these three forms and Forms I and III is present in the region corresponding to $\pi-\pi$ interactions in the middle of the plot. Moreover, in the fingerprint plots of Forms IV and VI, there is a larger peak corresponding to π···HC interactions.

Because of the highly similar molecular packing, the BFDH morphology and FIMs plotted on the crystal faces of Forms II, IV, and VI are very similar (see Figure 12, Table S18, and Figure S17). The largest crystal faces of these polymorphs grow by attaching molecules linked by different $\pi-\pi$ and CH···π interactions, whereas the smallest faster-growing planes by attaching molecules linked by hydrogen bonds. In contrast, for INA Forms I and III also on the largest planes hydrogen bond acceptors and donors are exposed and therefore these are among the interactions formed by the growth of these faces. Face group {100} of Form I grows by the formation of amide $R_2^2(8)$ homodimers, therefore hydrogen bond donors such as 2PA or 4CPBA can interact with this plane or facilitate the growth of polymorphs with such surfaces by activating the growth site. Plane groups {111} and {002} of Form III grow by the continuation of CO···H$_2$N chains. Moreover, based on the analysis of FIMs, the relative area of the exposed hydrogen bond donors and acceptors on these faces are notably higher if compared to that on {100} of Form II, {100} of Form IV, and
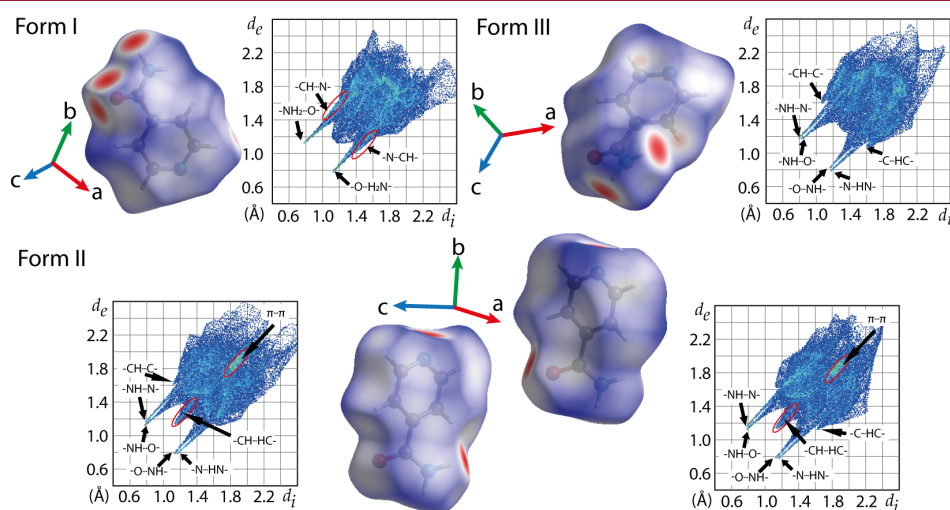
Figure 11. Hirshfeld surfaces and the corresponding 2D fingerprint plots of INA Forms I−III by providing the most characteristic intermolecular interactions observed in the plots. Other forms are depicted in Figure S16.

148
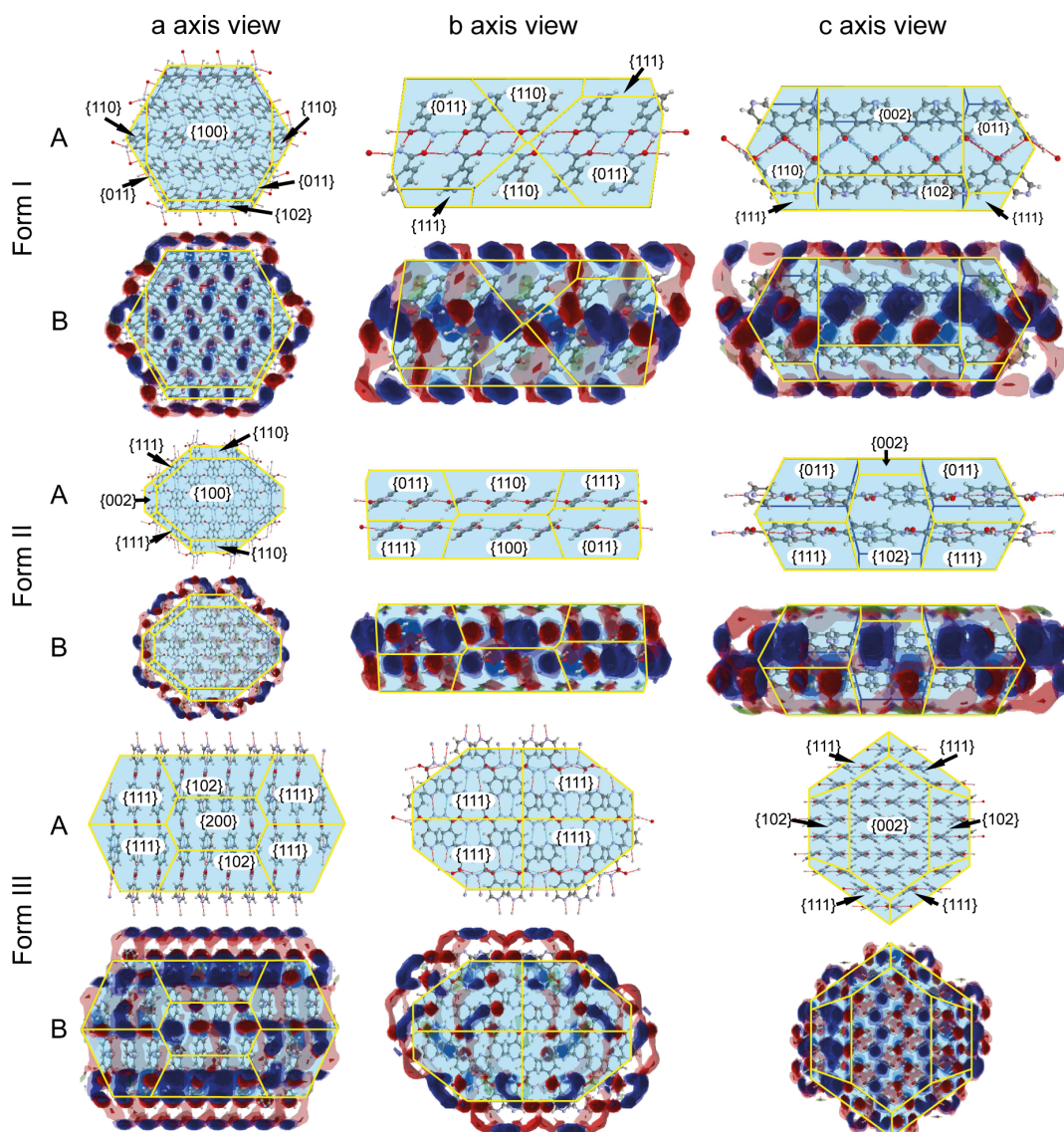
Figure 12. FIMs combined on the BFDH morphology of INA Forms I−III. Regions of hydrogen bond donor probability are shown in blue, hydrogen bond acceptors are shown in red, and hydrophobic interactions are shown in green. (A) Simulated BFDH morphology; (B) FIMs combined on the BFDH morphology.

{002} of Form VI. Therefore, it is possible that the additives are adsorbed on the largest faces of Forms I and III, therefore facilitating the growth of these polymorphs.

■ CONCLUSIONS

In summary, in crystallization from pure solvents, mostly several INA polymorphs crystallized concomitantly. From nitromethane and acetone, mostly polymorph mixtures not containing Forms I or III were obtained, whereas pure Form III or its mixture with other polymorphs formed in crystallization from lower supersaturation IPA and 1,4-dioxane solutions. The decrease of supersaturation at the moment of nucleation resulted in acquiring more stable INA polymorphs as crystallization products.

Crystallization in the presence of additives facilitated the acquisition of Form III by reducing the content of other polymorphs in the crystallization products or by fully inhibiting the nucleation of other forms. Some of the additives (2PA, 4CPBA, ND) also facilitated the crystallization of Form I, which was rarely obtained in crystallization from pure solvents. Additives allowed the crystallization of pure Form III using fast cooling rates, but almost all the additives lost their ability to provide Form III as the final crystallization product using lower cooling rates. The additives allowed better control of the crystallization polymorphic outcome in solvents where the respective INA form was already the primary crystallization product. Interestingly, 4CPBA in 1,4-dioxane and 2PA in acetone facilitated the crystallization of Form I, even though in other solvents, these additives facilitated the crystallization of

Form III. Crystallization of Form I was also facilitated by the absence of stirring, but under such conditions, it crystallized with impurities of other INA polymorphs. SMPT of the obtained polymorphs to more stable forms was not observed by stirring the obtained suspensions for up to 30 min as used in the experiments with the lowest cooling rate.

Theoretical calculations provided some insight into the polymorphic outcome of INA crystallization. The calculations and analysis showed that molecular packing and therefore lattice energy, energy frameworks, and Hirshfeld surface fingerprint plots of the INA polymorphs often crystallizing concomitantly (Forms II, IV, and VI) are almost identical. Therefore, it is possible that the energy barriers of nucleation and crystal growth rates for these polymorphs are highly similar, whereas in the presence of the additives, the crystallization of structurally more different Forms III or I can be achieved by altering these factors.

■ ASSOCIATED CONTENT

Ⓢ Supporting Information

The Supporting Information is available free of charge at https://pubs.acs.org/doi/10.1021/acs.cgd.3c00687.

> Full list of additives used in the study; more detailed results of crystallization polymorphic outcome and examples of PXRD patterns, packaging similarity, and geometry optimization; additional energy framework diagrams; Hirshfeld surfaces, corresponding 2D fingerprint plots, as well as intermolecular interactions on different crystal faces; and FIMs combined on the BFDH morphology (PDF)

■ AUTHOR INFORMATION

Corresponding Author

Aina Semjonova − *Faculty of Chemistry, University of Latvia, LV-1004 Riga, Latvia;* ⓞ orcid.org/0000-0002-7781-7380; Phone: +(371)-67033907; Email: aina.semjonova@lu.lv

Author

Agris Bērziņš − *Faculty of Chemistry, University of Latvia, LV-1004 Riga, Latvia;* ⓞ orcid.org/0000-0002-4149-8971

Complete contact information is available at:
https://pubs.acs.org/10.1021/acs.cgd.3c00687

Author Contributions

The manuscript was written through contributions of all authors. All authors have given approval to the final version of the manuscript.

Notes

The authors declare no competing financial interest.

■ ABBREVIATIONS

PEG	polyethylene glycol
Poly THF	poly(tetrahydrofuran)
PMMA	poly(methyl methacrylate)
PVC	polyvinyl chloride
tSt	*trans*-stilbene
HPC	hydroxypropyl cellulose
DPU	1,3-diphenylurea
OGP	octyl β-D-glucopyranoside
PPG	polypropylene glycol
Poly 80	polysorbate 80
PU	polyurethane
Bis-Tris	bis(2-hydroxyethyl)amino-tris(hydroxymethyl)-methane
PhGlu	phloroglucinol
4CPBA	4-carboxyphenylboronic acid
PCL	polycaprolactone
CA	cellulose acetate
ND	naphthalene-1,5-diol
NA	nicotinic acid
2PA	2-picolinic acid
BTriol	benzene-1,2,3-triol
5OH2NBA	5-hydroxy-2-nitrobenzoic acid
Tris	2-amino-2-(hydroxymethyl)propane-1,3-diol

■ REFERENCES

(1) Brog, J.-P.; Chanez, C.-L.; Crochet, A.; Fromm, K. M. Polymorphism, What It Is and How to Identify It: A Systematic Review. *RSC Adv.* **2013**, 3 (38), 16905.

(2) Cruz-Cabeza, A. J.; Reutzel-Edens, S. M.; Bernstein, J. Facts and Fictions about Polymorphism. *Chem. Soc. Rev.* **2015**, 44 (23), 8619−8635.

(3) Karpinski, P. H. Polymorphism of Active Pharmaceutical Ingredients. *Chem. Eng. Technol.* **2006**, 29 (2), 233−237.

(4) Lu, J.; Rohani, S. Polymorphism and Crystallization of Active Pharmaceutical Ingredients (APIs). *Curr. Med. Chem.* **2009**, 16 (7), 884−905.

(5) Dezena, R. M. B. Ritonavir Polymorphism: Analytical Chemistry Approach to Problem Solving in the Pharmaceutical Industry. *Braz. J. Anal. Chem.* **2020**, 7 (26), 12−17.

(6) Shen, C. A.; Bialas, D.; Hecht, M.; Stepanenko, V.; Sugiyasu, K.; Würthner, F. Polymorphism in Squaraine Dye Aggregates by Self-Assembly Pathway Differentiation: Panchromatic Tubular Dye Nanorods versus J-Aggregate Nanosheets. *Angew. Chem., Int. Ed.* **2021**, 60 (21), 11949−11958.

(7) Bernstein, J. Polymorphism of Pigments and Dyes. In *Polymorphism in Molecular Crystals*; Bernstein, J., Ed.; Oxford University Press, 2020; pp 376−397.

(8) Bernstein, J. Polymorphism of High Energy Materials. In *Polymorphism in Molecular Crystals*; Bernstein, J., Ed.; Oxford University Press, 2020; pp 398−428.

(9) Cruz-Cabeza, A. J.; Bernstein, J. Conformational Polymorphism. *Chem. Rev.* **2014**, 114 (4), 2170−2191.

(10) Davey, R. J.; Allen, K.; Blagden, N.; Cross, W. I.; Lieberman, H. F.; Quayle, M. J.; Righini, S.; Seton, L.; Tiddy, G. J. T. Crystal Engineering − Nucleation, the Key Step. *CrystEngComm* **2002**, 4 (47), 257−264.

(11) Ostwald, W. Studien Über Die Bildung Und Umwandlung Fester Körper. *Z. Phys. Chem.* **1897**, 22U (1), 289−330.

(12) Tang, W.; Sima, A. D.; Gong, J.; Wang, J.; Li, T. Kinetic Difference between Concomitant Polymorphism and Solvent-Mediated Phase Transformation: A Case of Tolfenamic Acid. *Cryst. Growth Des.* **2020**, 20 (3), 1779−1788.

(13) Bernstein, J.; Davey, R. J.; Henck, J.-O. Concomitant Polymorphs. *Angew. Chem. Int. Ed. Engl.* **1999**, 38, 3440−3461.

(14) Suresh, M.; Srinivasan, K. Concomitant Polymorphism and Nucleation Control of DL-Methionine Through Antisolvent Crystallization. *Chem. Eng. Technol.* **2021**, 44 (4), 614−621.

(15) Thorat, A. A.; Dalvi, S.; v. Ultrasound-Assisted Modulation of Concomitant Polymorphism of Curcumin during Liquid Antisolvent Precipitation. *Ultrason. Sonochem.* **2016**, 30, 35−43.

(16) Sugiyama, T.; Wang, S.-F. Manipulation of Nucleation and Polymorphism by Laser Irradiation. *J. Photochem. Photobiol., C* **2022**, *52*, No. 100530.

(17) Song, S.; Wang, L.; Yao, C.; Wang, Z.; Xie, G.; Tao, X. Crystallization of Sulfathiazole in Gel: Polymorph Selectivity and Cross-Nucleation. *Cryst. Growth Des.* **2020**, *20* (1), 9−16.

(18) Diao, Y.; Whaley, K. E.; Helgeson, M. E.; Woldeyes, M. A.; Doyle, P. S.; Myerson, A. S.; Hatton, T. A.; Trout, B. L. Gel-Induced Selective Crystallization of Polymorphs. *J. Am. Chem. Soc.* **2012**, *134* (1), 673−684.

(19) Simone, E.; Steele, G.; Nagy, Z. K. Tailoring Crystal Shape and Polymorphism Using Combinations of Solvents and a Structurally Related Additive. *CrystEngComm* **2015**, *17* (48), 9370−9379.

(20) Shi, P.; Xu, S.; Yang, H.; Wu, S.; Tang, W.; Wang, J.; Gong, J. Use of Additives to Regulate Solute Aggregation and Direct Conformational Polymorph Nucleation of Pimelic Acid. *IUCrJ.* **2021**, *8*, 161−167.

(21) v.; Nagy, Z. K. Simone, E.; Cenzato, M. A Study on the Effect of the Polymeric Additive HPMC on Morphology and Polymorphism of Ortho-Aminobenzoic Acid Crystals. *J. Cryst. Growth* **2016**, *446*, 50−59.

(22) Semjonova, A.; Bērziņš, A. Controlling the Polymorphic Outcome of 2,6-Dimethoxybenzoic Acid Crystallization Using Additives. *Crystals* **2022**, *12* (8), 1161.

(23) Semjonova, A.; Bērziņš, A. Surfactant Provided Control of Crystallization Polymorphic Outcome and Stabilization of Metastable Polymorphs of 2,6-Dimethoxyphenylboronic Acid. *Crystals* **2022**, *12* (12), 1738.

(24) Singh, A.; Lee, I. S.; Kim, K.; Myerson, A. S. Crystal Growth on Self-Assembled Monolayers. *CrystEngComm* **2011**, *13* (1), 24−32.

(25) Zhang, B.; Hou, X.; Dang, L.; Wei, H. Selective Polymorphic Crystal Growth on Self-Assembled Monolayer Using Molecular Modeling as an Assistant Method. *J. Cryst. Growth* **2019**, *518*, 81−88.

(26) Bora, P.; Saikia, B.; Sarma, B. Oriented Crystallization on Organic Monolayers to Control Concomitant Polymorphism. *Chem.—Eur. J.* **2020**, *26* (3), 699−710.

(27) Tulli, L. G.; Moridi, N.; Wang, W.; Helttunen, K.; Neuburger, M.; Vaknin, D.; Meier, W.; Shahgaldian, P. Polymorphism Control of an Active Pharmaceutical Ingredient beneath Calixarene-Based Langmuir Monolayers. *Chem. Commun.* **2014**, *50* (30), 3938.

(28) Yeh, K.-L.; Lee, H.-L.; Lee, T. Crystallization of Form II Paracetamol with the Assistance of Carboxylic Acids toward Batch and Continuous Processes. *Pharmaceutics* **2022**, *14* (5), 1099.

(29) Urwin, S. J.; Yerdelen, S.; Houson, I.; ter Horst, J. H. Impact of Impurities on Crystallization and Product Quality: A Case Study with Paracetamol. *Crystals* **2021**, *11* (11), 1344.

(30) Telford, R.; Seaton, C. C.; Clout, A.; Buanz, A.; Gaisford, S.; Williams, G. R.; Prior, T. J.; Okoye, C. H.; Munshi, T.; Scowen, I. J. Stabilisation of Metastable Polymorphs: The Case of Paracetamol Form III. *Chem. Commun.* **2016**, *52* (81), 12028−12031.

(31) Agnew, L. R.; Cruickshank, D. L.; McGlone, T.; Wilson, C. C. Controlled Production of the Elusive Metastable Form II of Acetaminophen (Paracetamol): A Fully Scalable Templating Approach in a Cooling Environment. *Chem. Commun.* **2016**, *52* (46), 7368−7371.

(32) Liu, Y.; Gabriele, B.; Davey, R. J.; Cruz-Cabeza, A. J. Concerning Elusive Crystal Forms: The Case of Paracetamol. *J. Am. Chem. Soc.* **2020**, *142* (14), 6682−6689.

(33) Black, J. F. B.; Cruz-Cabeza, A. J.; Davey, R. J.; Willacy, R. D.; Yeoh, A. The Kinetic Story of Tailor-Made Additives in Polymorphic Systems: New Data and Molecular Insights for p-Aminobenzoic Acid. *Cryst. Growth Des.* **2018**, *18* (12), 7518−7525.

(34) Kras, W.; Carletta, A.; Montis, R.; Sullivan, R. A.; Cruz-Cabeza, A. J. Switching Polymorph Stabilities with Impurities Provides a Thermodynamic Route to Benzamide Form III. *Commun. Chem.* **2021**, *4* (1), 38.

(35) Bērziņš, A.; Trimdale-Deksne, A.; Belyakov, S.; Ter Horst, J. H. Switching Nitrofurantoin Polymorphic Outcome in Solvent-Mediated

Phase Transformation and Crystallization Using Solvent and Additives. *Cryst. Growth Des.* **2023**, *23* (8), 5469−5476.

(36) Gong, N.; Hu, K.; Jin, G.; Du, G.; Lu, Y. Concomitant Polymorphs of Methoxyflavone (5-Methyl-7-Methoxyflavone). *RSC Adv.* **2016**, *6* (45), 38709−38715.

(37) Abbas, N.; Oswald, I. D. H.; Pulham, C. R. Accessing Mefenamic Acid Form II through High-Pressure Recrystallisation. *Pharmaceutics* **2017**, *9* (2), 16.

(38) Abu Bakar, M. R.; Nagy, Z. K.; Rielly, C. D.; Dann, S. E. Investigation of the Riddle of Sulfathiazole Polymorphism. *Int. J. Pharm.* **2011**, *414* (1−2), 86−103.

(39) Fellah, N.; Zhang, C. J.; Chen, C.; Hu, C. T.; Kahr, B.; Ward, M. D.; Shtukenberg, A. G. Highly Polymorphous Nicotinamide and Isonicotinamide: Solution versus Melt Crystallization. *Cryst. Growth Des.* **2021**, *21* (8), 4713−4724.

(40) Báthori, N. B.; Lemmerer, A.; Venter, G. A.; Bourne, S. A.; Caira, M. R. Pharmaceutical Co-Crystals with Isonicotinamide-Vitamin B3, Clofibric Acid, and Diclofenac-and Two Isonicotinamide Hydrates. *Cryst. Growth Des.* **2011**, *11* (1), 75−87.

(41) Guo, M.; Sun, X.; Chen, J.; Cai, T. Pharmaceutical Cocrystals: A Review of Preparations, Physicochemical Properties and Applications. *Acta Pharm. Sin. B* **2021**, *11* (8), 2537−2564.

(42) Godin, A. M.; Ferreira, W. C.; Rocha, L. T. S.; Seniuk, J. G. T.; Paiva, A. L. L.; Merlo, L. A.; Nascimento, E. B.; Bastos, L. F. S.; Coelho, M. M. Antinociceptive and Anti-Inflammatory Activities of Nicotinamide and Its Isomers in Different Experimental Models. *Pharmacol., Biochem. Behav.* **2011**, *99* (4), 782−788.

(43) Alba Sorolla, M.; Nierga, C.; José Rodríguez-Colman, M.; Reverter-Branchat, G.; Arenas, A.; Tamarit, J.; Ros, J.; Cabiscol, E. Sir2 Is Induced by Oxidative Stress in a Yeast Model of Huntington Disease and Its Activation Reduces Protein Aggregation. *Arch. Biochem. Biophys.* **2011**, *510* (1), 27−34.

(44) Li, J.; Bourne, S. A.; Caira, M. R. New Polymorphs of Isonicotinamide and Nicotinamide. *Chem. Commun.* **2011**, *47* (5), 1530−1532.

(45) Aakeröy, C. B.; Beatty, A. M.; Helfrich, B. A.; Nieuwenhuyzen, M. Do Polymorphic Compounds Make Good Cocrystallizing Agents? A Structural Case Study That Demonstrates the Importance of Synthon Flexibility. *Cryst. Growth Des.* **2003**, *3* (2), 159−165.

(46) Eccles, K. S.; Deasy, R. E.; Fábián, L.; Braun, D. E.; Maguire, A. R.; Lawrence, S. E. Expanding the Crystal Landscape of Isonicotinamide: Concomitant Polymorphism and Co-Crystallisation. *CrystEngComm* **2011**, *13* (23), 6923−6925.

(47) Vicatos, A. I.; Caira, M. R. A New Polymorph of the Common Coformer Isonicotinamide. *CrystEngComm* **2019**, *21* (5), 843−849.

(48) Bhogala, B. R.; Basavoju, S.; Nangia, A. Tape and Layer Structures in Cocrystals of Some Di- and Tricarboxylic Acids with 4,4′-Bipyridines and Isonicotinamide. From Binary to Ternary Cocrystals. *CrystEngComm* **2005**, *7*, 551−562.

(49) Oswald, I. D. H.; Motherwell, W. D. S.; Parsons, S. Isonicotinamide - Formamide (1/1). *Acta Crystallogr., Sect. E: Struct. Rep. Online* **2005**, *61* (10), 3161−3163.

(50) Oswald, I. D. H.; Motherwell, W. D. S.; Parsons, S. A 1:2 Co-Crystal of Isonicotinamide and Propionic Acid. *Acta Crystallogr., Sect. E: Struct. Rep. Online* **2004**, *60* (12), o2380−o2383.

(51) Hansen, T. B.; Taris, A.; Rong, B. G.; Grosso, M.; Qu, H. Polymorphic Behavior of Isonicotinamide in Cooling Crystallization from Various Solvents. *J. Cryst. Growth* **2016**, *450*, 81−90.

(52) Caridi, A.; Kulkarni, S. A.; Di Profio, G.; Curcio, E.; Ter Horst, J. H. Template-Induced Nucleation of Isonicotinamide Polymorphs. *Cryst. Growth Des.* **2014**, *14*, 1135−1141.

(53) Kulkarni, S. A.; McGarrity, E. S.; Meekes, H.; ter Horst, J. H. Isonicotinamide Self-Association: The Link between Solvent and Polymorph Nucleation. *Chem. Commun.* **2012**, *48* (41), 4983.

(54) Rohlíček, J.; Skořepová, E.; Babor, M.; Čejka, J. CrystalCM-P:An Easy-to-Use Tool for Fast Comparison of Molecular Packing. *J. Appl. Crystallogr.* **2016**, *49* (6), 2172−2183.

(55) Rohlíček, J.; Skořepová, E. CrystalCMP:Automatic Comparison of Molecular Structures. *J. Appl. Crystallogr.* **2020**, *53* (3), 841−847.

151

(56) Giannozzi, P.; Baroni, S.; Bonini, N.; Calandra, M.; Car, R.; Cavazzoni, C.; Ceresoli, D.; Chiarotti, G. L.; Cococcioni, M.; Dabo, I.; Dal Corso, A.; de Gironcoli, S.; Fabris, S.; Fratesi, G.; Gebauer, R.; Gerstmann, U.; Gougoussis, C.; Kokalj, A.; Lazzeri, M.; Martin-Samos, L.; Marzari, N.; Mauri, F.; Mazzarello, R.; Paolini, S.; Pasquarello, A.; Paulatto, L.; Sbraccia, C.; Scandolo, S.; Sclauzero, G.; Seitsonen, A. P.; Smogunov, A.; Umari, P.; Wentzcovitch, R. M. QUANTUM ESPRESSO: A Modular and Open-Source Software Project for Quantum Simulations of Materials. *J. Phys.: Condens. Matter* **2009**, *21* (39), No. 395502.

(57) Grimme, S.; Antony, J.; Ehrlich, S.; Krieg, H. A Consistent and Accurate Ab Initio Parametrization of Density Functional Dispersion Correction (DFT-D) for the 94 Elements H-Pu. *J. Chem. Phys.* **2010**, *132* (15), 154104.

(58) Spackman, P. R.; Turner, M. J.; McKinnon, J. J.; Wolff, S. K.; Grimwood, D. J.; Jayatilaka, D.; Spackman, M. A. CrystalExplorer:A Program for Hirshfeld Surface Analysis, Visualization and Quantitative Analysis of Molecular Crystals. *J. Appl. Crystallogr.* **2021**, *54* (3), 1006−1011.

(59) Karamertzanis, P. G.; Day, G. M.; Welch, G. W. A.; Kendrick, J.; Leusen, F. J. J.; Neumann, M. A.; Price, S. L. Modeling the Interplay of Inter- and Intramolecular Hydrogen Bonding in Conformational Polymorphs. *J. Chem. Phys.* **2008**, *128* (24), 244708.

(60) Frisch, J.; Trucks, G. W.; Schlegel, H. B.; Scuseria, G. E.; Robb, M. A.; Cheeseman, J. R.; Scalmani, G.; Barone, V.; Petersson, G. A.; Nakatsuji, H.; Li, X.; Caricato, M.; Marenich, A.; Blobino, J.; Janesko, B. G.; Gomperts, R.; Mennucci, B.; Hratchian, H. P.; Ortiz, J. V.; Izmaylov, A. F.; Sonnenberg, J. L.; Williams-Young, D.; Ding, F.; Lipparini, F.; Egidi, F.; Goings, J.; Peng, B.; Petrone, A.; Henderson, T.; Ranasinghe, D.; Zakrzewski, V. G.; Gao, J.; Rega, N.; Zheng, G.; Liang, W.; Hada, M.; Ehara, M.; Toyota, K.; Fukuda, R.; Hasegawa, J.; Ishida, M.; Nakajima, T.; Honda, Y.; Kitao, O.; Nakai, H.; Vreven, T.; Throssell, K.; Montgomery, J. A., Jr.; Peralta, J. E.; Ogliaro, F.; Bearpark, M.; Heyd, J. J.; Brothers, E.; Kudin, K. N.; Staroverov, V. N.; Keith, T.; Kobayashi, R.; Normand, J.; Raghavachari, K.; Rendell, A.; Burant, J. C.; Iyengar, S. S.; Tomasi, J.; Cossi, M.; Millam, J. M.; Klene, M.; Adamo, C.; Cammi, R.; Ochterski, J. W.; Martin, R. L.; Morokuma, K.; Farkas, O.; Foresman, J. B.; Fox, D. J. *Gaussian 09W, Revision D.01*; Gaussian, Inc.: Wallingford CT, USA, 2016.

(61) Wood, P. A.; Olsson, T. S. G.; Cole, J. C.; Cottrell, S. J.; Feeder, N.; Galek, P. T. A.; Groom, C. R.; Pidcock, E. Evaluation of Molecular Crystal Structures Using Full Interaction Maps. *CrystEngComm* **2013**, *15* (1), 65−72.

(62) Macrae, C. F.; Sovago, I.; Cottrell, S. J.; Galek, P. T. A.; McCabe, P.; Pidcock, E.; Platings, M.; Shields, G. P.; Stevens, J. S.; Towler, M.; Wood, P. A. Mercury 4.0:From Visualization to Analysis, Design and Prediction. *J. Appl. Crystallogr.* **2020**, *53* (1), 226−235.

(63) Kulkarni, S. A.; Meekes, H.; ter Horst, J. H. Polymorphism Control through a Single Nucleation Event. *Cryst. Growth Des.* **2014**, *14*, 1493−1499.

(64) Ganduri, R.; Cherukuvada, S.; Sarkar, S.; Guru Row, T. N. Manifestation of Cocrystals and Eutectics among Structurally Related Molecules: Towards Understanding the Factors That Control Their Formation. *CrystEngComm* **2017**, *19* (7), 1123−1132.

(65) Seethalekshmi, N.; Pedireddi, V. R. Solid-State Structures of 4-Carboxyphenylboronic Acid and Its Hydrates. *Cryst. Growth Des.* **2007**, *7* (5), 944−949.

(66) Liu, J.; Svärd, M.; Rasmuson, Å. C. Influence of Agitation and Fluid Shear on Nucleation of M-Hydroxybenzoic Acid Polymorphs. *Cryst. Growth Des.* **2014**, *14* (11), 5521−5531.

152

IV

Semjonova, A., Kons, A., Belyakov, S., Mishnev, A., Bērziņš, A.

DIVERSITY AND SIMILARITY IN ISONICOTINAMIDE TWO-COMPONENT PHASES WITH ALKYL CARBOXYLIC ACIDS: FOCUS ON SOLVATES

Crystal Growth & Design, **2024**, *24* (5), 2082-2093.

Reprinted with permission from American Chemical Society (ACS).

Diversity and Similarity in Isonicotinamide Two-Component Phases with Alkyl Carboxylic Acids: Focus on Solvates

Aina Semjonova,* Artis Kons, Sergey Belyakov, Anatoly Mishnev, and Agris Bērziņš*

Read Online

ACCESS | Metrics & More | Article Recommendations | SI Supporting Information

ABSTRACT: We present an investigation of solvate formation of isonicotinamide (INA) with linear monocarboxylic acids and several other solvents and characterization of the obtained solvates, their structure, and structural similarity with INA polymorphs and multicomponent phases. We report the crystal structures of four new INA solvates and present the results of crystallographic analysis of a total of eight solvates. All eight solvates crystallize in a monoclinic or triclinic crystal system and have similar hydrogen-bonding patterns. To characterize and better understand the formation of INA linear monocarboxylic acid solvates, these phases were characterized by using thermal analysis and their crystal structures by using theoretical calculations, energy frameworks, and Hirshfeld surface fingerprint plots.
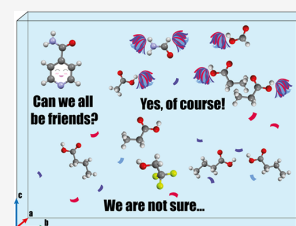
INTRODUCTION

Active pharmaceutical ingredients (APIs) can form different crystalline solid forms.[1] These include single-component solid forms (polymorphs) and different types of two- and multi-component systems such as solvates, cocrystals, and so forth. The European Pharmacopoeia and Food and Drug Administration describe solvates as crystal forms, which contain stoichiometric or variable amounts of a solvent,[2,3] but cocrystals as materials composed of two or more different nonionized molecules in the same crystal structure in a stoichiometric ratio.[4,5] The main difference of solvates and cocrystals is the state of matter of at least one of the pure components.[6]

Solvates and cocrystals usually have physicochemical properties different from those of the pure API. These properties have an impact on the drug dosage form and the manufacturing route.[7] Therefore, crystal engineering opens new opportunities to obtain APIs with better physicochemical properties.[6,8] Solvates and cocrystals often have better solubility and dissolution rate than phases formed by pure API and, therefore, increase bioavailability and drug efficacy,[6,9−13] synergistic effect, and lower the necessary drug dose,[8] or just have more optimal properties for the manufacturing processes.[14] Changes in the crystal form can also enhance the chemical stability of API.[15]

Isonicotinamide (INA) is widely used as a coformer in cocrystals, with application in pharmaceutical and other industries.[11,16−20] Cocrystals with INA have been used to improve drug solubility[11] and efficacy.[21] INA is reported to crystallize in six polymorphs,[18,22−24] and often several polymorphs crystallize concomitantly.[25,26] INA does not form solvates with most of the commonly used solvents such as methanol, ethanol, 1,4-dioxane, tetrahydrofuran, and so forth,[25,26] but it is reported to form two hydrates,[16] acetic acid (AA),[19] formic acid (FA),[27] propionic acid (PA),[28] and formamide (FAM)[29] solvates. INA is reported to form cocrystals with alkyl carboxylic diacids, and they have been extensively studied by Vishweshwar et al.[30] and Thompson et al.[31] In this study, however, we investigate the solvate formation of INA with linear saturated monocarboxylic acids and selected noncommon solvents. Part of the linear saturated monocarboxylic acids (formic and acetic acid) is classified as class 3 solvents with low toxicity (accepted dose ≤50 mg/day), but acids with C ≥ 3 even are not classified in the ICH residual solvent guideline[32] or European Pharmacopeia[33] as residual solvents. The obtained solvates were characterized, and their structural relationship with INA polymorphs and cocrystals was studied. To compare the newly obtained solvates with those already known, we additionally characterize all the INA solvates (except for the hydrates) using thermal analysis and theoretical calculations.

EXPERIMENTAL SECTION

Materials. INA (purity 99%, a mixture of forms I and II with a small hydrate I impurity) was purchased from ThermoScientific. Before use in crystallization, INA was heated to remove the hydrate impurity. Organic solvents of analytical grade were purchased from commercial sources and used without further purification.

Crystallization. Common organic solvents (see Table S1) chosen from different solvent classes were selected for the crystallization of INA. Additionally, alkyl carboxylic acids were selected for screening because INA is described to form acetic acid solvate[19] (S_AA) and propionic acid disolvate[28] (S_dPA). Solid form screening was performed

using cooling crystallization. 100–150 mg of INA was dissolved in 2–3 mL of the selected solvent at 50–90 °C, depending on the boiling point of the solvent. The solutions obtained were filtered and cooled to 5 or −10 °C depending on the solvent melting point. Solid products formed within minutes after the solutions were cooled; they were collected by filtration, air-dried (if needed), and characterized with powder X-ray diffraction (PXRD). PXRD patterns not matching with the known INA solid forms were obtained from 2,2,2-trifluoroethanol (TFE), butyric acid (BA), FA and PA. A repeated crystallization was performed to prepare single crystals suitable for crystal structure determination by single-crystal X-ray diffraction (SCXRD). If crystals suitable for SCXRD could not be obtained, crystal structures were determined using PXRD data. Butyric acid monosolvate (S_{mBA}) was obtained by heating the butyric acid disolvate (S_{dBA}) at 50 °C for 1 h, whereas the propionic acid monosolvate (S_{mPA}) was obtained by crystallization at 5 °C. In contrast, the propionic acid disolvate (S_{dPA}) was obtained in cooling crystallization at −10 °C.

Powder X-ray Diffraction (PXRD) and Crystal Structure Determination. The PXRD patterns for phase identification were measured at ambient temperature on a Bruker D8 Advance diffractometer using copper radiation (Cu K_α; λ = 1.54180 Å) equipped with a LynxEye position sensitive detector. The voltage and current of the tube were set to 40 kV and 40 mA. The divergence slit was set at 0.6 mm and the antiscatter slit at 8.0 mm. The patterns were recorded from 3 to 35° on the 2θ scale using the scan speed of 0.2 s/0.02°. To prevent desolvation, during the analysis, the samples were covered with a 10 μm polyethylene film.

The PXRD patterns for crystal structure determination were measured on a Bruker D8 Discover diffractometer using copper radiation (Cu K_α; λ = 1.54180 Å), equipped with a LynxEye position sensitive detector in transmission mode. Samples were sealed in rotating (60 rpm) borosilicate glass capillaries of 0.5 mm outer diameter (Hilgenberg glass No. 10), and a capillary sample stage with upper and lower knife edges was used. The diffractometer incident beam path was equipped with Göbel Mirror, Soller slits, and a 0.6 mm divergence slit, while the diffracted beam path was equipped only with Soller slits. The diffraction patterns were collected using 36 s/0.01° scanning speed from 3 to 70° on the 2θ scale.

Indexing, space group determination, and structure solution from PXRD data were performed using EXPO2014[34] for formic acid solvate (S_{FA}), S_{mPA}, and S_{mBA}. The unit cell dimensions were determined by applying the N-TREOR09[35] and Dicvol06[36] indexing procedures with a set of 20–25 reflections found in 4.5–30° 2θ range. Space group determination was carried out using a statistical assessment of systematic absences, and Z' was determined on the basis of density considerations. The cell and diffraction pattern profile parameters were refined according to the Le Bail algorithm.[37,38] The background was modeled by a 20th order polynomial function of the Chebyshev type; peak profiles were described by the Pearson VII function. The initial geometry of INA was taken from the crystal structure of Form I,[23] but those of solvents were taken from INA propionic acid disolvate,[28] butyric acid disolvate (determined from the SCXRD data), and R-encenicline formic acid disolvate.[39] Simulating annealing algorithm was used to optimize the INA and solvent models against the experimental powder diffraction pattern set in direct space by adjusting the conformation, position, and orientation of the trial model in the unit cell. The best structure solution was then used for Rietveld refinement using TOPAS5.[40] The background was modeled with Chebyshev polynomials,[41] and the modified Thompson–Cox–Hastings pseudo-Voigt function[42] was used for peak shape fitting. The geometry of each molecule was defined as a rigid body. Rotation and translation parameters were refined simultaneously with the dihedrals of each independent molecule in the asymmetric unit. A global isotropic atomic displacement parameter (B_{iso}) was refined for nonhydrogen atoms, and for hydrogen atoms, it was set to $1.2B_{iso}$.

Single-Crystal X-ray Diffraction (SCXRD) and Crystal Structure Determination. Single crystals of INA S_{dBA} and 2,2,2-trifluoroethanol solvate (S_{TFE}) were investigated on a Rigaku XtaLAB Synergy-S dualflex diffractometer equipped with a HyPix6000 detector and a microfocus-sealed X-ray tube with copper radiation (Cu K_α; λ = 1.54180 Å). Single crystals were fixed with oil in a nylon loop of a magnetic CryoCap and set on a goniometer head. The samples were kept at 150 K during data collection, and ω scans were performed with a step size of 0.5°. The structures were solved with the ShelXT[43] program using intrinsic phasing and refined with the full-matrix least-squares method using SHELXL.[43] For S_{dBA}, positions of amide H atoms were found from the difference Fourier synthesis and refined isotropically. For S_{TFE}, positions of amide H atoms were generated using AFIX 93 and refined in the riding mode, and for the OH group, AFIX 147 was applied to choose the torsion angle which maximizes the electron density. All the other H atoms were added geometrically and refined with the riding model.

Differential Scanning Calorimetry/Thermogravimetry (DSC/TG). DSC/TG analysis was performed using Mettler Toledo TGA/DSC2. Samples of 5–11 mg mass were used. The nitrogen flow rate was 100 mL min^{-1}. Open 100 μm aluminum pans were used. The heating of the samples from 25 to 200 °C was carried out at a heating rate of 10 °C min^{-1}.

Crystal Structure Analysis and Theoretical Calculations. The search for crystal structures of INA cocrystals with different alkyl carboxylic acids was performed using ConQuest 2022.2.0[44] in Cambridge Structural Database (CSD) version 5.43.[45] A total of 652 structures containing the INA fragment were found. From these, a set of structures with different alkyl carboxylic acids and their derivatives was selected for the analysis.

Hydrogen bonds were identified and displayed in Mercury 2020.3.0[46] using the default settings. Hydrogen-bond lengths and distances between molecules were calculated from experimental structures.

Geometry optimization of crystal structures of all INA solvates (except for the hydrates) was performed in Quantum ESPRESSO[47,48] by relaxing the positions of all atoms. The initial geometry was taken from the CSD (refcodes JAWWAG for S_{AA}, HANBOO for S_{dPA} and GAVHER for S_{FAM}) or from the structures determined in this study. All the calculations were performed using the PBE functional with ultrasoft pseudopotentials from the original pseudopotential library and a 90 Ry plane-wave cutoff energy with vdW interactions treated according to the D3 method of Grimme[49] using a 2 × 2 × 2 k-point grid. As during the geometry optimization because of a proton transfer the formic acid solvate transformed into a structure of a salt, for the geometry optimization of S_{FA} the coordinates of the hydroxyl group of formic acid were constrained.

The geometry-optimized structures were further analyzed using CrystalExplorer 21.[50] Calculation of the pairwise intermolecular interaction energy in crystal structures was performed at the B3LYP-D2/6-31G(d,p) level. The sum of all pairwise interaction energies with molecules for which the atoms are within 15 Å of the central molecule was used to estimate the total intermolecular energy, which is equal to the lattice energy, as in all the structures INA adopt an essentially identical conformation, and conformations of both components correspond to the global energy minimum. CrystalExplorer 21 was also used to generate the Hirshfeld surfaces, their 2D fingerprint plots summarizing the information about intermolecular interactions, and for the generation of energy frameworks from the calculated pairwise interaction energies and their electrostatic and dispersion energy components.

■ RESULTS AND DISCUSSION

Crystallization Outcome and Characterization of the Obtained Solvates. In crystallization from selected common solvents (see Table S1), only INA polymorphs were always obtained, with crystallization usually resulting in obtaining a mixture of polymorphs. In contrast, crystallization products with distinct and differing PXRD patterns from the known INA polymorphs or solvates (see Figure 1) were obtained in cooling crystallization from FA, PA, BA, and TFE. In crystallization from AA and FAM, the already known INA solvates[19,29] were
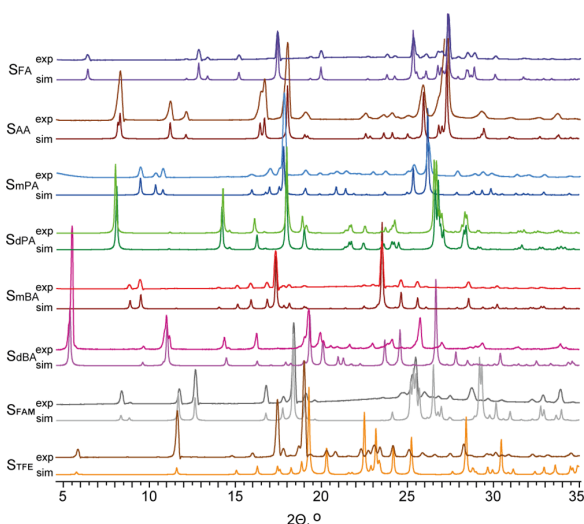
Figure 1. Experimental and simulated PXRD patterns (obtained from crystal structures) of INA solvates.

obtained. Molecular structures of INA and the solvents forming solvates can be seen in Figure 2.
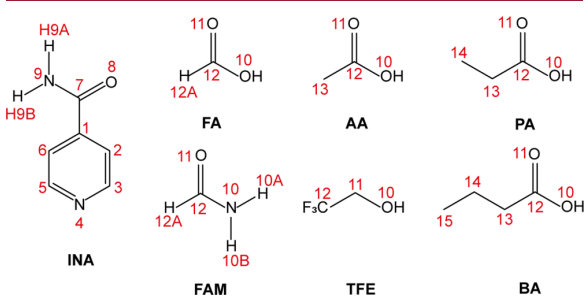
Figure 2. Molecular structure and atom numbering scheme of INA and the solvents forming solvates.

The DSC/TG analysis (see the section Thermal Characterization below) indicated that the obtained phases are solvates, which was additionally confirmed by crystal structure determination using the SCXRD or PXRD data. Moreover, in the cooling crystallization from BA, a disolvate S_{dBA} was obtained, and heating of S_{dBA} at 50 °C for 1 h resulted in the formation of a monosolvate S_{mBA}. In contrast, monosolvate S_{mPA} was the primary outcome of the cooling crystallization from PA in 5 °C temperature, whereas the already known disolvate S_{dPA} was obtained in a cooling crystallization at −10 °C. This confirms that disolvates are more stable at lower temperatures, whereas monosolvates at higher temperatures. Upon storage at ambient temperature, all solvates desolvated by forming a mixture of INA forms II, IV, and VI, but the rate of desolvation differed. Transformation of S_{dPA} to S_{mPA} was very fast (<15 min) and was followed by the desolvation of S_{mPA}, with complete transformation occurring in less than an hour. The desolvation of S_{FA}, S_{AA}, S_{mBA}, and S_{TFE} occurred within a few days, but S_{dBA} and S_{FAM} were the most stable of the obtained solvates and desolvated in about a week.

Thermal Characterization. The desolvation process of the solvates was also studied by DSC/TG analysis. The reported

weight loss was measured for the most distinct weight loss stage in the TG curve, and for S_{FA} and S_{mPA} additionally using the end of the desolvation peak in the DSC curve. For S_{FA} and S_{mPA}, the theoretical weight loss is notably higher than the observed weight loss, as evaporation of the respective high-boiling solvents still continued after the desolvation event characterized by the steepest weight loss. As the weight loss for S_{FAM} and S_{mBA} was not associated with the desolvation event in the DSC curve and occurred at a notably high temperature, the experimental weight loss is not reported for these solvates. It was observed that S_{FA} has a desolvation temperature close to the boiling point of the solvent (see Figure 3), whereas other solvates start to desolvate below the boiling point of the respective solvent. Both disolvates are characterized by two distinct endothermic desolvation peaks, followed by a wide endothermic peak corresponding to the evaporation of the solvent. Using PXRD, it was confirmed that the first peak is the decomposition of the disolvate by forming the respective monosolvate, and the second peak is the decomposition of the monosolvate, after which a moist sample containing INA polymorphs is obtained. In contrast to the other solvates, upon heating, melting of S_{FAM} occurs, and the melting point is very low if compared to the high boiling point of FAM. In the DSC traces of most of the characterized solvates, the INA melting peak at ~156 °C is present, as also observed in previous studies.[18,22,24,26] Moreover, in the DSC/TG traces of S_{mBA}, different INA polymorph phase transformations are observed, as in the desolvation a mixture of forms II, IV, and VI is obtained.

Comparison of the Solvate Structures. The crystal structures of solvates S_{mPA}, S_{mBA}, S_{dBA}, and S_{TFE} are reported here for the first time, and their crystallographic data are given in Table 1 along with the crystallographic data of S_{FA}. The crystal structures of S_{AA}, S_{FAM}, and S_{dPA}, however, are available in the CSD (JAWWAG, GAVHER, and HANBOO, respectively) and described by Oswald et al.[28,29] and Bhogala et al.[19] The crystal structure of S_{FA}, although not deposited in the CSD, is described by Oswald,[27] and it is reported that S_{FA} at low temperatures (below 240 K) transforms into a salt, with hydrogen being disordered between the sites linked to N4 of INA and O10 of FA.

It can be seen that all the INA solvates crystallize either in the monoclinic or triclinic crystal system. Almost all the monoclinic solvates crystallize in the $P2_1/c$ space group except for S_{mBA} ($C2/c$), and all the triclinic solvates crystallize in the $P\bar{1}$ space group. In all the structures, INA adopts an essentially identical conformation, with the amide group being close to planar to the pyridine ring; see Table 1.

In INA solvates, two distinct types of hydrogen-bonding motifs can be observed, which can further be divided into five subtypes based on additional hydrogen bonding and relative arrangement of the hydrogen-bonded units. The first hydrogen-bonding motif contains typical INA $R_2^2(8)$ homodimers (see Figure 4) formed by N9—H9A···O8 interactions, and the linkage between INA and the solvent is provided by O10—H···N4, therefore, resulting in hydrogen-bonded tetramers solvent···INA dimer···solvent. Isolated hydrogen-bonded tetramers, as observed in S_{mPA}, are classified here as hydrogen-bonding type A1. In other structures, however, the hydrogen-bonded tetramers solvent···INA dimer···solvent are additionally linked to other tetramers by hydrogen bonds N9—H9B···O11. The resulting hydrogen bonding is classified as type A2 if the linked tetramers lay in the same plane, as observed in S_{FA}
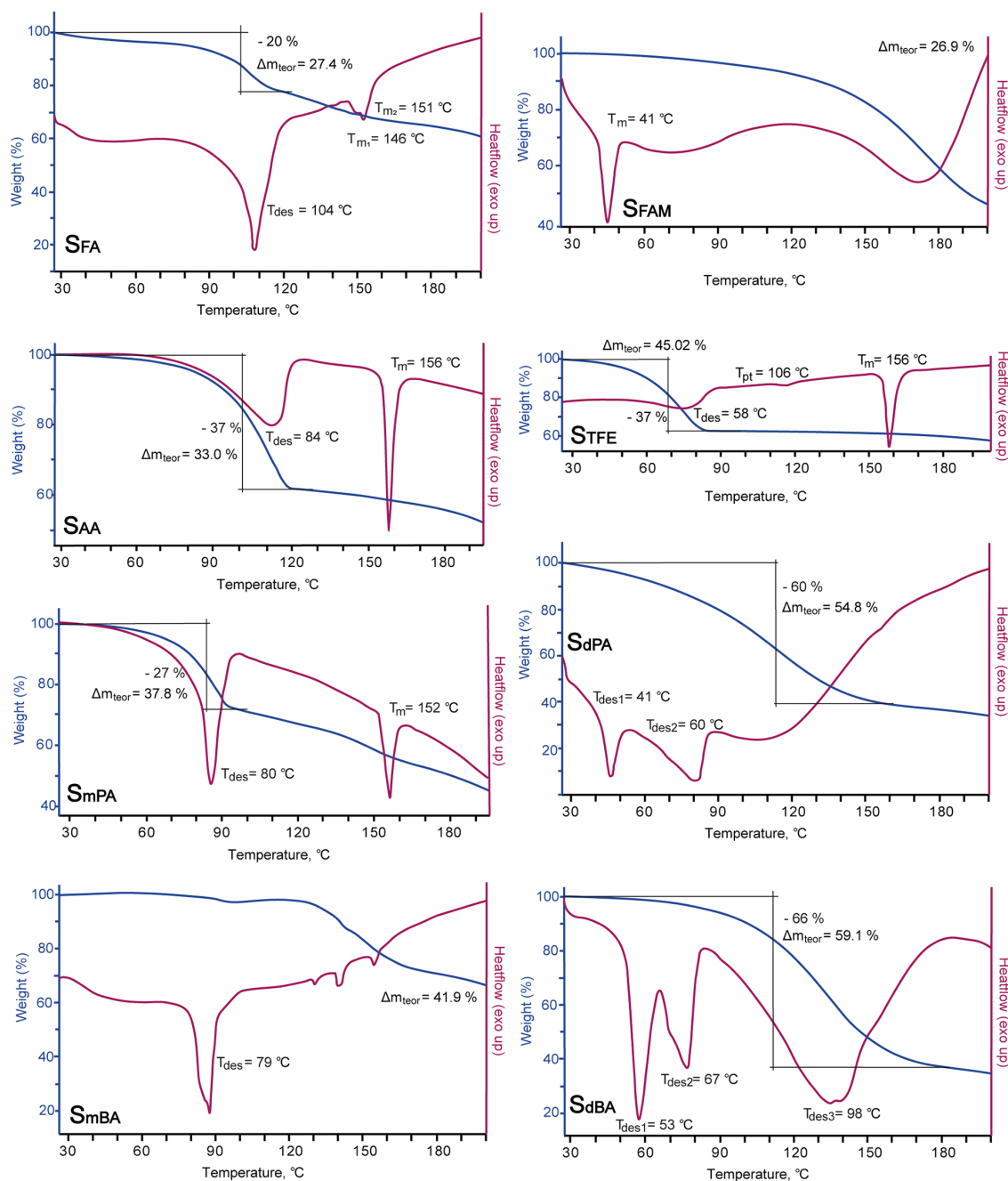
Figure 3. DSC/TG traces of INA solvates (heating rate of 10 °C min⁻¹). The onset temperatures are used to describe each process observed in the DSC traces.

and S_{AA}, or as type A3 if the linked tetramers are lying perpendicularly to each other by creating packaging with the adjacent molecule planes arranged perpendicular to each other, as observed in S_{mBA} and also S_{TFE} (in which, however, the adjacent tetramers are linked by N9−H9B···O10 due to the different molecular structure of the solvent).

The second motif type B is substantially different, as INA homodimers are not employed. In both subtypes of B, INA forms $R_2^2(8)$ heterodimers with the carboxylic acid (see Figure

4), employing hydrogen bonds N9−H9A···O11 and O10−H···O8, and this dimer is linked to another carboxylic acid by a hydrogen bond O10−H···N4, resulting in a trimer solvent···INA:solvent (where "···" represents a hydrogen bond and ":" a hydrogen bond pair; see Figure 4). In hydrogen-bonding type B1, adjacent trimers lying in the same plane are linked by N9−H9B···O11, as observed in S_{dBA}. In type B2, however, trimers are hydrogen-bonded by N9−H9B···O11 to two other perpendicularly aligned trimers, as observed in S_{dPA}, thereby

Table 1. Crystallographic Data of INA Solvates Determined in This Study[a]

	S_{FA}	S_{mPA}	S_{mBA}	S_{dBA}	S_{TFE}
CSD identifier	2236716	2236717	2236718	2302845	2237737
formula	$C_6H_6N_2O \cdot CH_2O_2$	$C_6H_6N_2O \cdot C_3H_6O_2$	$C_6H_6N_2O \cdot C_4H_8O_2$	$C_6H_6N_2O \cdot 2C_4H_8O_2$	$C_6H_6N_2O \cdot C_2H_3F_3O$
M, g mol^{-1}	168.15	196.20	210.23	298.33	222.17
method of structure solution	powder	powder	powder	single crystal	single crystal
crystal	N/A	N/A	N/A	colorless needle	colorless needle
crystal system	monoclinic	triclinic	monoclinic	triclinic	monoclinic
space group	$P2_1/c$	$P\bar{1}$	$C2/c$	$P\bar{1}$	$P2_1/c$
a, Å	3.8177(16)	5.88988	21.806(15)	5.24839(10)	15.2031(9)
b, Å	27.480(11)	9.685489	10.505(7)	9.28144(13)	5.3244(12)
c, Å	7.565(3)	10.19433	11.190(8)	16.3015(3)	11.7225(7)
α, °	90	112.4861	90	89.7515(12)	90
β, °	95.1158(12)	93.0070	114.2902(17)	89.8978(14)	91.303(6)
γ, °	90	105.726	90	80.7138(14)	90
Z, Z'	4, 1	2, 1	8, 1	2, 1	4, 1
volume, Å^3	790.486	509.192	2336.4	783.67(2)	948.7(2)
T, K	298	298	298	150.0(1)	150(2)
radiation	Cu K$_\alpha$	Cu K$_\alpha$	Cu K$_\alpha$	Cu K$_\alpha$	Cu K$_\alpha$
λ, Å	1.54184	1.54184	1.54184	1.54184	1.54184
R ($F^2 > 2\sigma F^2$)				0.036	0.063
$wR(F^2)$				0.103	0.177
S				1.09	1.09
R_{wp} (R_p)	0.0514 (0.0349)	0.0627 (0.0422)	0.0579 (0.0395)	-	-
GoF	4.2	5.6	4.4	1.1	1.1
dihedral angle O8−C7−C1−C2/°	12.03	5.43	−7.34	4.71	−1.68

[a]Rietveld fit and structure overlays for the structures determined from PXRD data are depicted in Figures S1−S6.
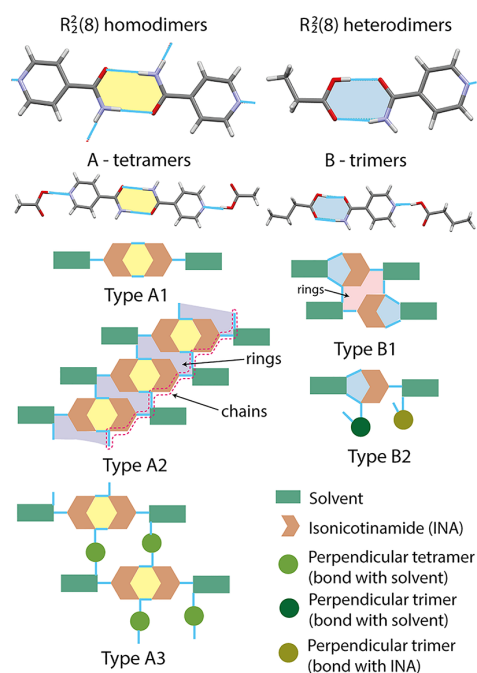

Figure 4. Schematic representation of the characteristic hydrogen-bonding motifs in INA solvates.

resulting in similar packing to that observed in the structures containing the type A3 motif.

The hydrogen bonding in S_{FAM} is different from that in other solvates and therefore does not correspond to the described hydrogen-bonding types. In this structure, two different $R_2^2(8)$ homodimers are formed by INA (linked by N9−H9A···O8) and FAM (linked by N10−H10A···O11), and these homodimers are linked to each other by hydrogen bonds N10−H10B···N4 and N9−H9B···O11 (see Figure 5). This results in a packing where FAM homodimers connect the layer of the INA molecules, with the INA molecules from adjacent layers being $\pi-\pi$-stacked (distance between centroids, 3.75 Å), and in a perpendicular direction, solvent molecules form structure channels.

Solvates Containing Tetramers: Type A Solvates. As described above, type A solvates are divided into three subtypes based on the bonding and relative arrangement of the hydrogen-bonded tetramers consisting of INA homodimers linked to two solvent molecules by two hydrogen bonds O10−H···N4. In the first subtype (A1), there is no hydrogen bonding between the tetramers. S_{mPA} belonging to type A1 crystallizes in the $P\bar{1}$ space group (see Table 1), with one molecule of each component in the asymmetric unit. The molecule arrangement and hydrogen bonding in S_{mPA} are illustrated in Figure 6 by showing the isolated PA···INA dimer···PA fragments. Interestingly, adjacent tetramers in fact form a weak interaction N9−H9B···O11, with the distance O···N being 3.15 Å. In the crystal packing, INA and solvent molecules form channels (see Figure 7).

In the second subtype (A2), each tetramer is linked to two adjacent tetramers with hydrogen bonds N9−H9B···O11. These tetramers are essentially parallel to each other and form tetramer layers (Figure 6). S_{FA} and S_{AA} belonging to type A2 contain one molecule of each component in the asymmetric unit but crystallize in different space groups ($P2_1/c$ and $P\bar{1}$, respectively). Moreover, because of different relative arrangements of INA molecules and acid molecules in the tetramers (carboxyl groups aligned in the same direction in S_{FA} and in opposite directions in S_{AA}), FA···INA dimer···FA fragments are
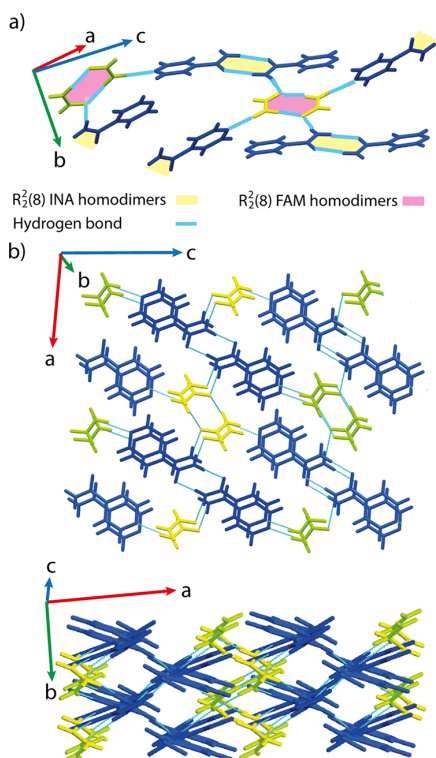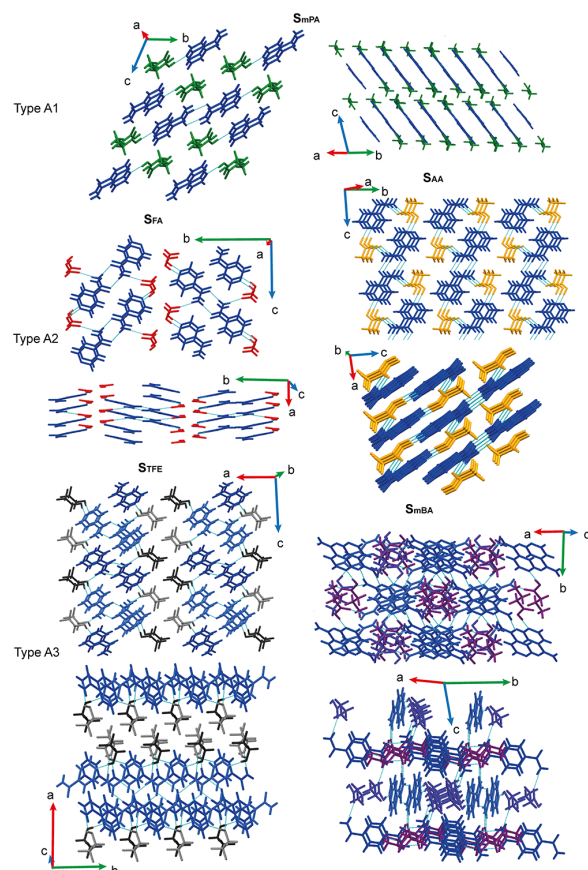
Figure 5. Hydrogen bonding (a) and molecular packaging (b) in S_{FAM}.
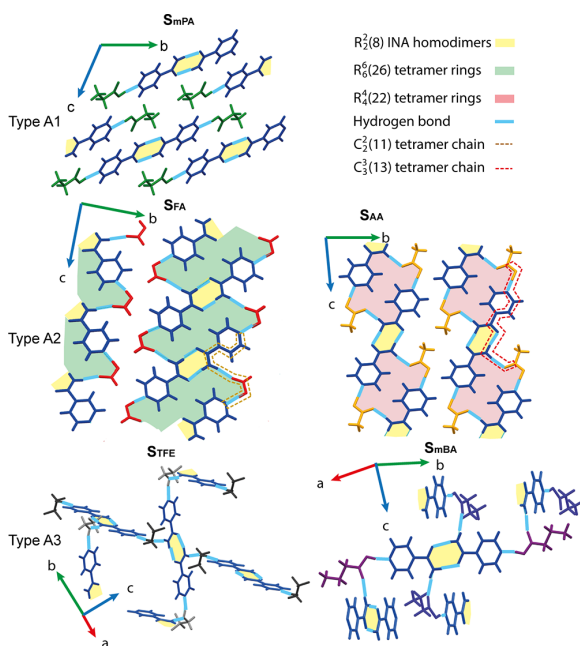
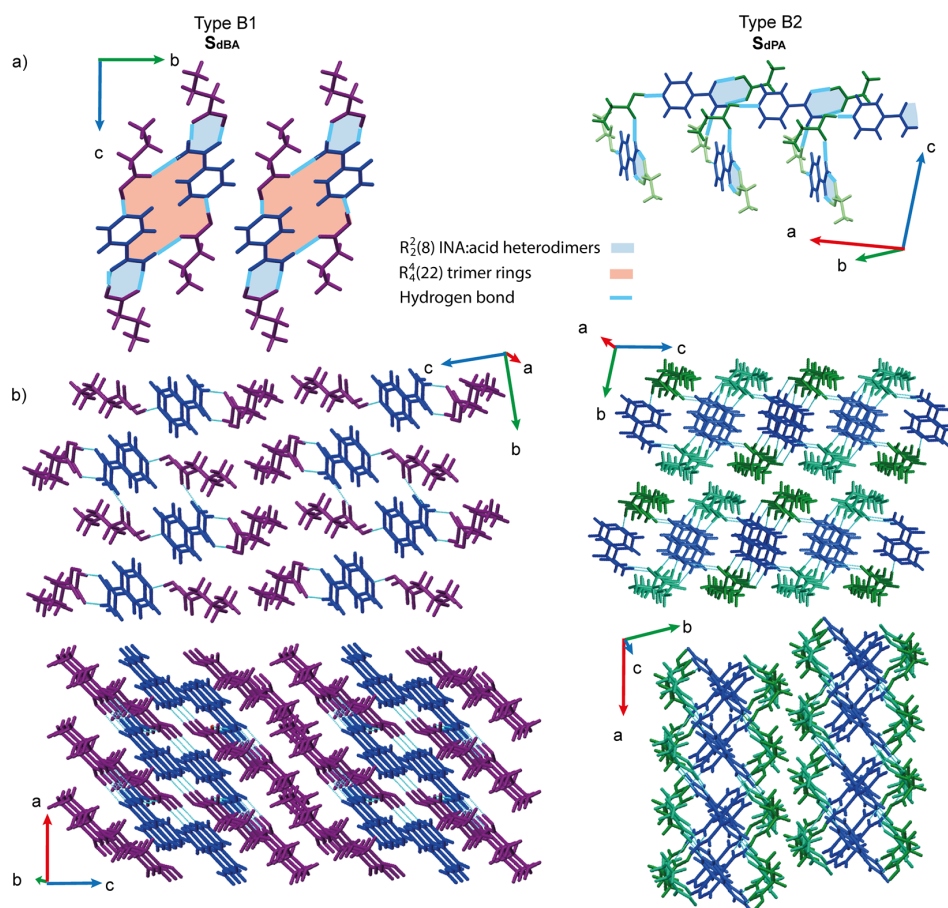**Figure 6.** Hydrogen bonding in type A solvates.

Figure 7. Molecular packaging in the crystal structures of type A solvates.

respectively). INA and solvent molecules in the S_{FA} crystal structure form layers, whereas solvent molecules in the S_{AA} crystal structure form channels (see Figure 7). In fact, the molecular arrangement in the parallel layer formed from the tetramers in S_{mPA} is very similar to that in S_{AA}. Apparently, the difference in the solvent size results in differences in the ability to form hydrogen bonds between the tetramers within a layer and different arrangements of such layers.

In contrast to the other two subtypes, in the third subtype (A3) in one of the directions, the adjacent tetramers are arranged perpendicularly to each other, therefore resulting in the final structure not consisting from the parallel molecule layers. In S_{TFE} and S_{mBA} belonging to type A3, each tetramer is bonded by N9−H9B⋯O10 (in S_{TFE}) or N9−H9B⋯O11 (in S_{mBA}) to almost perpendicularly arranged adjacent tetramers (see Figure 6). Such different packing could be caused by the BA molecule being larger than the other solvents, whereas TFE having only one O atom, therefore resulting in the hydroxyl group being both hydrogen-bond donor and acceptor, apparently leading to the tetramers not being able to arrange in an efficient parallel packaging as in the above-described solvates. Both solvates contain one molecule of each component in the asymmetric unit but crystallize in different space groups ($P2_1/c$ and $C2/c$, respectively). INA and solvent molecules in the S_{TFE} crystal structure form layers, whereas

linked by $C_2^2(11)$ chains and form $R_6^6(26)$ rings, whereas AA⋯ INA dimer⋯AA fragments by $C_3^3(13)$ chains and form $R_4^4(22)$ rings. INA molecules in both solvates are $\pi−\pi$-stacked (the distance between INA molecules is 3.82 and 3.92 Å,

159

**Figure 8.** Hydrogen bonding (a) and molecular packaging (b) in the crystal structures of type B solvates.

solvent molecules in the S_{mBA} crystal structure form channels (see Figure 7).

Solvates Containing Trimer Structures: Type B Solvates. Both disolvates belong to type B solvates, which are further divided into two subtypes. In the first subtype (B1), the solvent···INA:solvent trimer is linked with N9−H9B···O11 hydrogen bonds to an adjacent trimer related by the symmetry center (see Figure 8) and forms $R_4^4(22)$ rings, as observed in S_{dBA} which crystallizes in the $P\bar{1}$ space group (see Table 1) with one INA and two BA molecules in the asymmetric unit. In the molecular packing in S_{dBA}, INA molecules are situated in a structure channel (see Figure 8), in contrast to other solvates in which channels were formed by solvent molecules. As adjacent layers of parallel molecules are shifted with respect to each other, INA molecules are not $\pi-\pi$-stacked (distance between centroids >5 Å).

Considering the packing, the second subtype (B2) is similar to type A3 as the solvent···INA:solvent trimers in one of the directions are arranged perpendicularly to each other by resulting in a structure not consisting of parallel molecule layers, as observed in S_{dPA}. This solvate crystallizes in the $P\bar{1}$ space group, with two INA and four PA molecules in the asymmetric unit. In this structure, each trimer forms two N9−H9B···O11 hydrogen bonds with two adjacent almost perpendicularly arranged trimers (see Figure 8). In the structure, solvent molecules and INA molecules are arranged

in distinct layers. Although parallelly arranged trimers are shifted with respect to each other, the amide moieties provide $\pi-\pi$ stacking of INA molecules (distance between centroids, 4.20 and 4.18 Å).

Crystal Structures of INA Cocrystals with Other Alkyl Carboxylic Acids. Considering the extensive studies of two component phases formed by INA and the fact that only a small number of alkyl carboxylic acids are liquids, we complement the crystallographic analysis with the available crystal structures of INA and alkyl carboxylic acid cocrystals. A total of 31 different crystal structures formed in 22 nonionized two-component systems containing INA and different alkyl carboxylic acids on some occasions in different stoichiometries were found in the CSD. In three of these systems (with citric, oxalic, and adipic acid), there was more than one polymorph (see Table S2). As two of the found structures (S_{AA} and S_{dPA}) correspond to solvates and are described above, they are not analyzed here. INA:alkyl carboxylic acid cocrystals usually crystallize in triclinic (52%) or monoclinic (45%) crystal systems, except for the INA:succinamic acid cocrystal which belongs to the orthorhombic system. Furthermore, the INA and alkyl carboxylic acid ratio in these structures is either 1:1 (62%) or 2:1 (38%), with the ratio 2:1 observed only for the acids containing multiple carboxyl groups. Although the ratio 1:2 as discovered in S_{dPA} and S_{dBA} is not observed in any of the analyzed cocrystals, considering the proportion of INA:car-
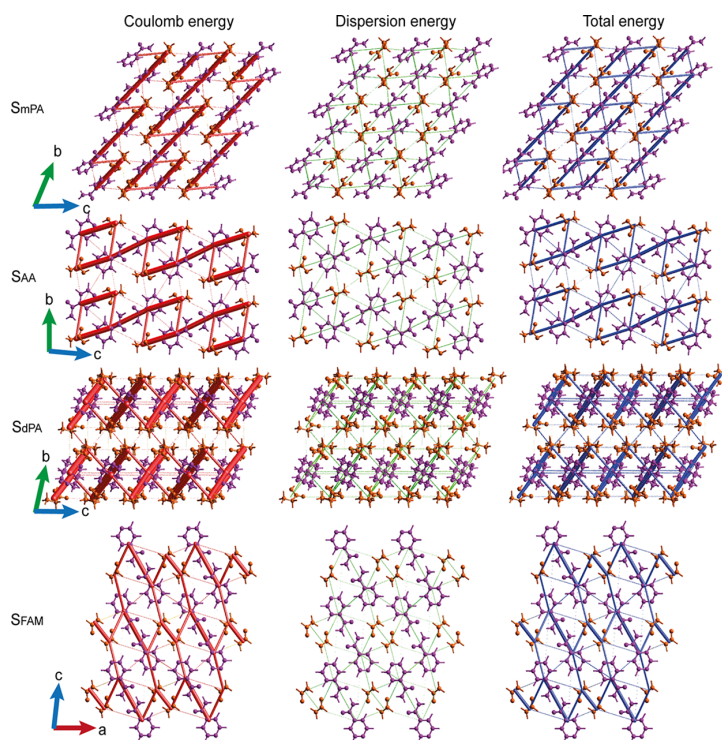
Figure 9. Energy framework diagrams for Coulomb, dispersion, and total energy of INA solvates representing different hydrogen-bonding types. All images have the same tube size. The frameworks of other solvates are provided in Figure S7.

boxyl group, the ratio 1:2 in fact is rather common. In INA cocrystals with monochloroacetic acid and malonic acid, there is a proton disorder similar to that reported for the FA solvate by Oswald.[27]

There is a high possibility that the structure will contain INA homodimers, as 76% of the analyzed structures contain such a motif, whereas 21% contain INA heterodimers with alkyl carboxylic acid, as observed in the crystal structures of both disolvates. Only one of the structures (INA:pimelic acid 2:1 cocrystal, HOFYOT[51]) contains a different synthon formed from hydrogen-bonded INA chains (N9–H9A···O8), with pimelic acid hydrogen-bonded to N4 atom.

In contrast, in single-component phases, INA is not very keen to form structures containing homodimers,[25,26] as INA homodimers are present in only one of the six INA polymorphs, and formation of this polymorph is not favored in the crystallization if compared to other INA polymorphs containing hydrogen-bond chains.[25] Therefore, it can be concluded that INA prefers to crystallize in structures containing homodimers in the case where a second component containing additional hydrogen-bond donors is introduced.

In the solvates described above, there is an almost equal probability to observe solvent layers and channels, whereas in the analyzed cocrystals, coformer layers are present in only ∼1/3 of the structures, whereas in the majority of structures, the coformers are situated in channels. It can be concluded that longer alkyl groups increase the possibility of formation of layers in case the INA and acid are in equimolar stoichiometry, which can be a result of efficient hydrophobic interactions between the alkyl groups, whereas the ratio 2:1 mostly leads to coformer channels. Isolated acid···INA dimer···acid tetramers

as in S_{mPA} (type A1 in Figure 4) are also rarely observed among the cocrystals (present in one of the structures). Most of the cocrystals, however, contain hydrogen-bonded tetramers linked by additional hydrogen bonds, i.e., type A2 (38% of the cocrystal structures, similar motif in additional 7%) or A3 (10% of the cocrystal structures) motifs (see Table S2).

Theoretical Calculations. Intermolecular interactions in INA solvates were characterized by calculating lattice energy using pairwise intermolecular interaction energies calculated in CrystalExplorer. The FA solvate has the least negative lattice energy of all the considered solvates, related to it containing the smallest of the solvents; see Table S3. Lattice energy of other carboxylic acid monosolvates S_{AA}, S_{mPA}, and S_{mBA} is almost identical (difference below 2 kJ mol^{-1}), meaning that the increase of the size of alkyl group has almost no effect on the total interaction energy. Logically, increase of the solvent:INA stoichiometry from 1:1 to 2:1 lowers the lattice energy (expressed per mole of INA) by ∼80 to 100 kJ mol^{-1}. In all the solvates of alkyl carboxylic acids, the electrostatic energy has a higher contribution than the dispersion energy, with the electrostatic-to-dispersion energy ratio 2−2.3 for almost all the solvates except for S_{dBA}, for which it is 1.8. Overall, the lattice energy of S_{TFE} and S_{FAM} is similar to that of the carboxylic acid monosolvates. The contribution of the electrostatic energy, however, is slightly smaller than that for the carboxylic acid monosolvates, apparently because of the different hydrogen bonding present in these structures.

Each solvate structure is characterized by a distinct energy framework (see Figures 9 and S7), but the same trend as observed for the hydrogen-bonding motifs can be identified: in general, the strongest interactions for monosolvates are formed
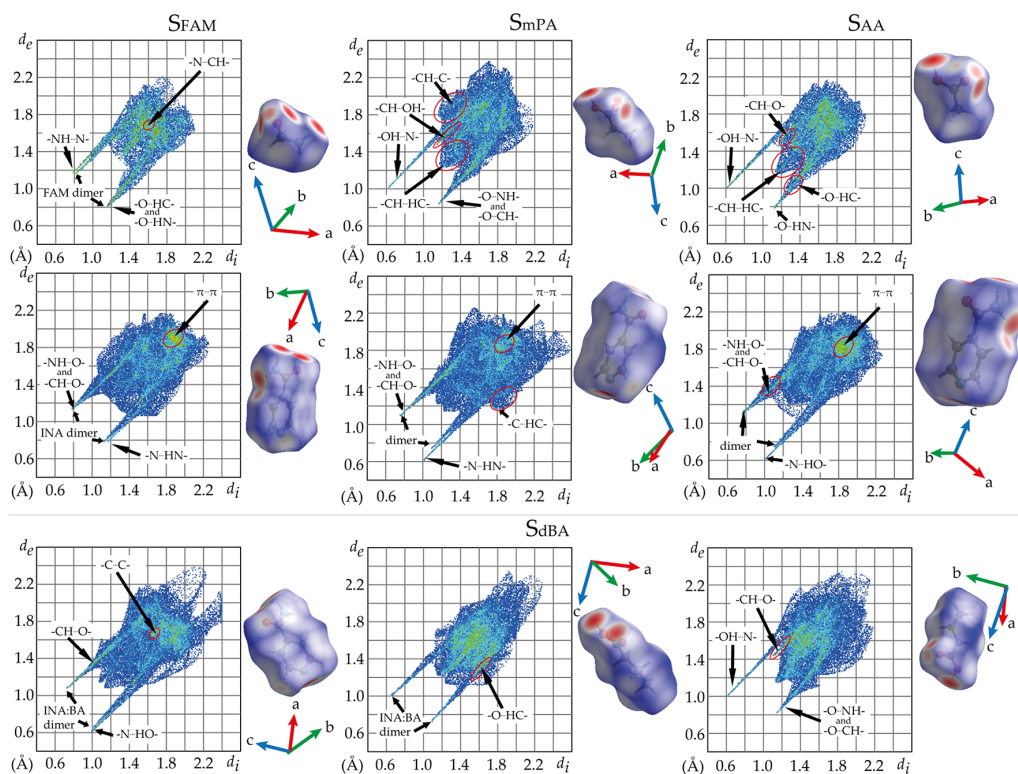
Figure 10. Hirshfeld surfaces and their 2D fingerprint plots with the indicated location of the most characteristic intermolecular interactions for INA solvates with different hydrogen-bonding types. Hirshfeld surfaces and their fingerprint plot for other solvates are provided in Figure S8.

in solvent···INA dimer···solvent tetramers and for disolvates in solvent···INA:solvent trimers. In most of the carboxylic acid solvates in which INA molecules form homodimers, the interaction with the strongest electrostatic energy is between the molecules linked by the hydrogen bond O10—H···N4 (S_{AA}, S_{mPA}, S_{dPA}), but the interaction between the INA molecules forming homodimers is slightly weaker. In contrast, the opposite is true for S_{FA} and S_{TFE}, where the strongest interaction is between INA molecules forming homodimers. In both disolvates, the strongest interaction is between INA and acid forming the heterodimer. The electrostatic energy between molecules linking such tetramers or trimers (thus linked by hydrogen bond N9—H9B···O11 or N9—H9B···O10 in S_{TFE}) is almost 2−3 times weaker than that between the molecules linked by hydrogen bonds forming a tetramer or trimer. S_{FAM} has a notably different energy framework due to a completely distinct hydrogen bonding in this structure, with equally strong electrostatic (Coulomb) energy observed between molecules forming INA homodimers and FAM homodimers and the energy between the molecules providing hydrogen-bond linkage between these dimers being almost 2 times lower. The dispersion energy between any molecule pairs in all INA solvates is rather weak if compared to the electrostatic energy, which in a summarized version is illustrated in Table S3 as a notably lower total dispersion energy. The main source of dispersion energy in these structures is the π−π stacking of INA molecules (in S_{FA}, S_{AA}, S_{FAM}, S_{mPA}, S_{dPA}, and S_{dBA}) or weak −CH···HC− interactions (in S_{mBA}, S_{TFE}), with π−π stacking in general resulting in 2

times more efficient dispersion energy compared to the weak −CH···HC− interactions.

For each molecule in the asymmetric unit of INA solvates, we additionally calculated the Hirshfeld surfaces and constructed their 2D fingerprint plots (see Figures 10 and S8). Logically, distinct fingerprint plots were obtained for each different solvent molecule, whereas for INA molecules, the plots were similar. In all the plots, the peak representing INA being a hydrogen-bond donor is rather wide and correspond to several different intermolecular interactions, including the hydrogen bonds in INA homodimers N9—H9A···O8 or dimers with carboxylic acid N9—H9A···O11 as well as hydrogen bond with the solvent N9—H9B···O11. Moreover, at the larger distance regions of this peak, also weak hydrogen bonds C2/C5−H···O10/O11 (C···O distance 3−4 Å) contribute. Interactions in which INA is a hydrogen-bond acceptor, however, appear as two very sharp and in some structures fully overlapping peaks. One of these peaks correspond to the hydrogen bonds in INA homodimers O8···H9A−N9 or dimers with carboxylic acid O8···H−O10 and the second peak to the hydrogen bond between INA and the solvent O10−H···N4. The relative length of these peaks indicates that based on the similarity of hydrogen-bond geometry the solvates can be divided in two groups, first consisting of Type A solvates S_{FA}, S_{AA}, S_{TFE}, S_{mPA}, and S_{mBA} and the second of S_{FAM} and both Type B solvates. For part of the solvates, π−π stacking of INA or C···C interactions between INA and solvent molecules can also be observed in the plots. In the plot of S_{mBA}, there is a wide wing on the right side formed by C···H interactions between the INA pyridine ring carbon atoms and BA alkyl

chains. In S_{TFE}, a strong interaction between INA and the fluorine atom of TFE C5/6—H⋯F can be observed.

In the Hirshfeld surfaces and their 2D fingerprint plots of carboxylic acids apart from the interactions with INA molecules, acid⋯acid interactions can also be observed. In the fingerprint plot of FA, a weak hydrogen bond C5—H⋯O10 can be observed. An increase in the size of the alkyl group leads to an increase in CH⋯HC interactions, appearing as a wide peak in the middle of the plot. The fingerprint plots of PA and BA in the monosolvate and disolvate are different. The fingerprint plots of the solvent in S_{mPA} and S_{mBA} contain a wide wing on the left side arising from H⋯C interactions between the hydrogen atoms of PA/BA alkyl chains and the carbon atoms of the INA pyridine ring. Additionally, in S_{mPA}, there is a sharp and short peak arising from the weak hydrogen bond C14—H⋯O10 (with a C⋯O distance of 3.636 Å) between the solvent molecules. Despite a similar interaction also being observed in the Hirshfeld surface of S_{mBA}, no separate peak could be detected in the fingerprint plot. For S_{dPA} and S_{dBA}, the fingerprint plots of solvent molecules forming the INA:acid dimer are similar, all containing sharp peaks from the interactions N9—H9A⋯O11 and O8⋯H—O10. Additionally, the weak hydrogen bonds formed between solvent molecules C13—H⋯O11 (with a C⋯O distance of 3.541 Å) in S_{dPA} and C15—H⋯O10 (with a C⋯O distance of 3.862 Å) in S_{dBA} as well as the hydrogen bond with the INA molecule C13—H⋯O8 (with a C⋯O distance of 4.057 Å) in S_{dBA} contribute to these peaks. The plots of the other solvent molecules are different, but all contain identical peaks from the weak hydrogen bond C13/15—H⋯O10/11 between the solvent molecules. The fingerprint plot of FAM resembles that of INA but contains four sharp peaks. The two central peaks arise from the interaction N10—H10A⋯O11 forming FAM dimers, but the outer peaks from the hydrogen bonds O11⋯H10B—N10 and N10—H10B⋯N4 formed with INA molecules. Additionally, the interaction N10⋯C12 from the parallelly stacked FAM molecules can also be seen. The fingerprint plot of TFE is notably different from the plots of other solvents (see Figure S8). It contains a sharp peak corresponding to the hydrogen bond O10—H⋯N4, a wider peak corresponding to the hydrogen bond O10⋯H9B—N9, as well as smaller sharp peaks from weak hydrogen bonds C11—H⋯F between solvent molecules. In the middle of the plot, an area corresponding to F⋯F interactions can also be observed.

■ CONCLUSIONS

Crystal structures of four new INA solvates are reported, and structures of in total eight solvates are described and characterized in this study. In all of these solvates, similar hydrogen-bond patterns can be observed. All the monosolvates contain INA $R_2^2(8)$ homodimers, whereas disolvates contain INA:solvent $R_2^2(8)$ heterodimers. Based on the hydrogen-bond motif present, almost all solvates can be divided in two distinct types: type A (containing solvent⋯INA dimer⋯solvent tetramer) and type B (solvent:INA dimer⋯solvent trimer), except for S_{FAM} containing INA dimers and FAM $R_2^2(8)$ homodimers. Based on the additional interactions and packaging, type A solvates are divided in three subtypes: type A1 solvates (S_{mPA}) in which tetramers are isolated, type A2 solvates (S_{AA} and S_{FA}) in which hydrogen-bonded tetramers form layers, and type A3 solvates (S_{TFE} and S_{mBA}) in which hydrogen-bonded tetramers are arranged perpendicular to each other. Also, type B solvates can be divided into

subtypes: in type B1 solvate (S_{dBA}), hydrogen-bonded trimers form rings, but B2 solvate (S_{dPA}) is similar to type A3. Hydrogen-bonding pattern as in type A is the most common pattern also among the INA alkyl carboxylic acid cocrystals.

The lattice energies of most of the monosolvates are almost identical, except for the formic acid and formamide solvates, whereas those of the disolvates, as expected, are lower. The similar hydrogen bonding in INA solvates results in high similarity of their energy frameworks and Hirshfeld surfaces and their 2D fingerprint plots, with the most notable differences being observed in the fingerprint plots of solvent molecules. Extension of the set of analyzed structures by including also INA cocrystals allowed to conclude that almost all INA alkyl carboxylic acid solvates and cocrystals crystallize in structures with highly similar hydrogen-bond patterns, which in general could allow the prediction of intermolecular interactions and molecular packaging for new solvates/cocrystals with structurally similar solvents/coformers.

■ ASSOCIATED CONTENT

ⓢ Supporting Information

The Supporting Information is available free of charge at https://pubs.acs.org/doi/10.1021/acs.cgd.3c01411.

> INA phase obtained in crystallization from all the tested solvents; Rietveld fit and structure overlays for the structures determined from PXRD data; selected crystallographic information on INA alkyl carboxylic acid cocrystals; lattice energy results; and additional energy framework diagrams, Hirshfeld surfaces, and the corresponding 2D fingerprint plots (PDF)

Accession Codes

CCDC 2236716−2236718, 2237737, and 2302845 contain the supplementary crystallographic data for this paper. These data can be obtained free of charge via www.ccdc.cam.ac.uk/data_request/cif, or by emailing data_request@ccdc.cam.ac.uk, or by contacting The Cambridge Crystallographic Data Centre, 12 Union Road, Cambridge CB2 1EZ, UK; fax: +44 1223 336033.

■ AUTHOR INFORMATION

Corresponding Authors

Aina Semjonova − *Faculty of Chemistry, University of Latvia, Riga LV-1004, Latvia;* ⓞ orcid.org/0000-0002-7781-7380; Phone: +(371)-67033907; Email: aina.semjonova@lu.lv

Agris Bērziņš − *Faculty of Chemistry, University of Latvia, Riga LV-1004, Latvia;* ⓞ orcid.org/0000-0002-4149-8971; Phone: +(371)-67033903; Email: agris.berzins@lu.lv

Authors

Artis Kons − *Faculty of Chemistry, University of Latvia, Riga LV-1004, Latvia;* ⓞ orcid.org/0000-0002-4055-8442

Sergey Belyakov − *Latvian Institute of Organic Synthesis, Riga LV-1006, Latvia*

Anatoly Mishnev − *Latvian Institute of Organic Synthesis, Riga LV-1006, Latvia*

Complete contact information is available at:
https://pubs.acs.org/10.1021/acs.cgd.3c01411

Author Contributions

The manuscript was written through contributions of all authors. All authors have given approval to the final version of the manuscript.

Notes

The authors declare no competing financial interest.

■ REFERENCES

(1) Hilfiker, R.; von Raumer, M. *Polymorphism: In the Pharmaceutical Industry*; Hilkifer, R.; von Raumer, M., Eds.; Wiley-VCH Verlag GmbH & Co. KGaA: Weinheim, Germany, 2019.

(2) Council of Europe. Polymorphism. In *European Pharmacopoeia*, Supplement 11.2; Council of Europe: Strasbourg, 2023; p. 795.

(3) U.S. Department of Health and Human Services; Food and Drug Administration; Center for Drug Evaluation and Research. *ANDAs: Pharmaceutical Solid Polymorphism*; Rockville, MD, U.S., 2007. https://www.fda.gov/media/71375/download.

(4) U.S. Department of Health and Human Services; Food and Drug Administration; Center for Drug Evaluation and Research. *Regulatory Classification of Pharmaceutical Co-Crystals*; Silver Spring, MD, U.S., 2018. https://www.fda.gov/files/drugs/published/Regulatory-Classification-of-Pharmaceutical-Co-Crystals.pdf.

(5) European Medicines Agency. *Reflection paper on the use of cocrystals of active substances in medicinal products.* https://www.ema.europa.eu/en/documents/scientific-guideline/reflection-paper-use-cocrystals-active-substances-medicinal-products_en.pdf.

(6) Aitipamula, S.; Banerjee, R.; Bansal, A. K.; Biradha, K.; Cheney, M. L.; Choudhury, A. R.; Desiraju, G. R.; Dikundwar, A. G.; Dubey, R.; Duggirala, N.; Ghogale, P. P.; Ghosh, S.; Goswami, P. K.; Goud, N. R.; Jetti, R. K. R.; Karpinski, P.; Kaushik, P.; Kumar, D.; Kumar, V.; Moulton, B.; Mukherjee, A.; Mukherjee, G.; Myerson, A. S.; Puri, V.; Ramanan, A.; Rajamannar, T.; Reddy, C. M.; Rodriguez-Hornedo, N.; Rogers, R. D.; Row, T. N. G.; Sanphui, P.; Shan, N.; Shete, G.; Singh, A.; Sun, C. C.; Swift, J. A.; Thaimattam, R.; Thakur, T. S.; Kumar Thaper, R.; Thomas, S. P.; Tothadi, S.; Vangala, V. R.; Variankaval, N.; Vishweshwar, P.; Weyna, D. R.; Zaworotko, M. J. Polymorphs, Salts, and Cocrystals: What's in a Name? *Cryst. Growth Des* **2012**, *12* (5), 2147–2152.

(7) Healy, A. M.; Worku, Z. A.; Kumar, D.; Madi, A. M. Pharmaceutical Solvates, Hydrates and Amorphous Forms: A Special Emphasis on Cocrystals. *Adv. Drug Deliv Rev.* **2017**, *117*, 25–46.

(8) Nangia, A. K.; Desiraju, G. R. Crystal Engineering: An Outlook for the Future. *Angew. Chem., Int. Ed.* **2019**, *58* (13), 4100–4107.

(9) Chadha, R.; Kuhad, A.; Arora, P.; Kishor, S. Characterisation and Evaluation of Pharmaceutical Solvates of Atorvastatin Calcium by Thermoanalytical and Spectroscopic Studies. *Chem. Cent J.* **2012**, *6* (1), 114.

(10) Zhang, C.; Kersten, K. M.; Kampf, J. W.; Matzger, A. J. Solid-State Insight Into the Action of a Pharmaceutical Solvate: Structural, Thermal, and Dissolution Analysis of Indinavir Sulfate Ethanolate. *J. Pharm. Sci.* **2018**, *107* (10), 2731–2734.

(11) Kerr, H. E.; Softley, L. K.; Suresh, K.; Nangia, A.; Hodgkinson, P.; Evans, I. R. A Furosemide–Isonicotinamide Cocrystal: An Investigation of Properties and Extensive Structural Disorder. *CrystEngComm* **2015**, *17* (35), 6707–6715.

(12) Venkata Narasayya, S.; Maruthapillai, A.; Sundaramurthy, D.; Arockia Selvi, J.; Mahapatra, S. Preparation, Pharmaceutical Properties and Stability of Lesinurad Co-Crystals and Solvate. *Mater. Today Proc.* **2019**, *14*, 532–544.

(13) Hisada, N.; Takano, R.; Takata, N.; Shiraki, K.; Ueto, T.; Tanida, S.; Kataoka, M.; Yamashita, S. Characterizing the Dissolution Profiles of Supersaturable Salts, Cocrystals, and Solvates to Enhance in Vivo Oral Absorption. *Eur. J. Pharm. Biopharm.* **2016**, *103*, 192–199.

(14) Wang, K.; Sun, C. C. Direct Compression Tablet Formulation of Celecoxib Enabled with a Pharmaceutical Solvate. *Int. J. Pharm.* **2021**, *596*, No. 120239.

(15) Dhondale, M. R.; Thakor, P.; Nambiar, A. G.; Singh, M.; Agrawal, A. K.; Shastri, N. R.; Kumar, D. Co-Crystallization Approach to Enhance the Stability of Moisture-Sensitive Drugs. *Pharmaceutics* **2023**, *15* (1), 189.

(16) Báthori, N. B.; Lemmerer, A.; Venter, G. A.; Bourne, S. A.; Caira, M. R. Pharmaceutical Co-Crystals with Isonicotinamide-Vitamin B3, Clofibric Acid, and Diclofenac-and Two Isonicotinamide Hydrates. *Cryst. Growth Des* **2011**, *11* (1), 75–87.

(17) Tothadi, S.; Desiraju, G. R. Unusual Co-Crystal of Isonicotinamide: The Structural Landscape in Crystal Engineering. *Philosophical Transactions of the Royal Society A: Mathematical, Physical and Engineering Sciences* **2012**, *370* (1969), 2900–2915.

(18) Eccles, K. S.; Deasy, R. E.; Fábián, L.; Braun, D. E.; Maguire, A. R.; Lawrence, S. E. Expanding the Crystal Landscape of Isonicotinamide: Concomitant Polymorphism and Co-Crystallisation. *CrystEngComm* **2011**, *13* (23), 6923–6925.

(19) Bhogala, B. R.; Basavoju, S.; Nangia, A. Tape and Layer Structures in Cocrystals of Some Di- and Tricarboxylic Acids with 4,4′-Bipyridines and Isonicotinamide. From Binary to Ternary Cocrystals. *CrystEngComm* **2005**, *7*, 551–562.

(20) Manin, A. N.; Boycov, D. E.; Simonova, O. R.; Volkova, T. V.; Churakov, A. V.; Perlovich, G. L. Formation Thermodynamics of Carbamazepine with Benzamide, Para-Hydroxybenzamide and Isonicotinamide Cocrystals: Experimental and Theoretical Study. *Pharmaceutics* **2022**, *14* (9), 1881.

(21) Jiang, J.; Wang, A.; Zhang, X.; Wang, Y.; Wang, Q.; Zhai, M.; Huang, Y.; Qi, R. The Isonicotinamide Cocrystal Promotes Inhibitory Effects of Naringenin on Nonalcoholic Fatty Liver Disease in Mice. *J. Drug Deliv Sci. Technol.* **2020**, *59* (May), No. 101874.

(22) Li, J.; Bourne, S. A.; Caira, M. R. New Polymorphs of Isonicotinamide and Nicotinamide. *Chem. Commun.* **2011**, *47* (5), 1530–1532.

(23) Aakeröy, C. B.; Beatty, A. M.; Helfrich, B. A.; Nieuwenhuyzen, M. Do Polymorphic Compounds Make Good Cocrystallizing Agents? A Structural Case Study That Demonstrates the Importance of Synthon Flexibility. *Cryst. Growth Des* **2003**, *3* (2), 159–165.

(24) Vicatos, A. I.; Caira, M. R. A New Polymorph of the Common Coformer Isonicotinamide. *CrystEngComm* **2019**, *21* (5), 843–849.

(25) Semjonova, A.; Bērziņš, A. Crystallization of Metastable Isonicotinamide Polymorphs and Prevention of Concomitant Crystallization by Additives. *Cryst. Growth Des.* **2023**, *23* (12), 8584–8596.

(26) Fellah, N.; Zhang, C. J.; Chen, C.; Hu, C. T.; Kahr, B.; Ward, M. D.; Shtukenberg, A. G. Highly Polymorphous Nicotinamide and Isonicotinamide: Solution versus Melt Crystallization. *Cryst. Growth Des* **2021**, *21* (8), 4713–4724.

(27) Oswald, I. D. H. *Rationalisation and Design of Hydrogen Bonding Patterns in Co-Crystals and Polymorphs*; University of Edinburgh, 2004. http://hdl.handle.net/1842/15564.

(28) Oswald, I. D. H.; Motherwell, W. D. S.; Parsons, S. A 1:2 Co-Crystal of Isonicotinamide and Propionic Acid. *Acta Crystallogr. Sect E Struct Rep. Online* **2004**, *60* (12), o2380–o2383.

(29) Oswald, I. D. H.; Motherwell, W. D. S.; Parsons, S. Isonicotinamide - Formamide (1/1). *Acta Crystallogr. E Struct. Rep. Online* **2005**, *61* (10), 3161–3163.

(30) Vishweshwar, P.; Nangia, A.; Lynch, V. M. Molecular Complexes of Homologous Alkanedicarboxylic Acids with Isonicotinamide: X-Ray Crystal Structures, Hydrogen Bond Synthons, and Melting Point Alternation. *Cryst. Growth Des* **2003**, *3* (5), 783–790.

(31) Thompson, L. J.; Voguri, R. S.; Male, L.; Tremayne, M. The Crystal Structures and Melting Point Properties of Isonicotinamide Cocrystals with Alkanediacids $HO_2C(CH_2)N-2CO_2H$ n = 7–9. *CrystEngComm* **2011**, *13* (12), 4188.

(32) International Council for Harmonisation. *Impurities: Guideline for Residual Solvents Q3C(R6)*, 2016. https://database.ich.org/sites/

default/files/Q3C-R6_Guideline_ErrorCorrection_2019_0410_0.pdf.

(33) Council of Europe. Residual Solvents. In *European Pharmacopoeia*, Supplement 11.2; Council of Europe: Strasbourg, 2023; pp 753−760.

(34) Altomare, A.; Cuocci, C.; Giacovazzo, C.; Moliterni, A.; Rizzi, R.; Corriero, N.; Falcicchio, A. EXPO2013: A Kit of Tools for Phasing Crystal Structures from Powder Data. *J. Appl. Crystallogr.* **2013**, *46* (4), 1231−1235.

(35) Altomare, A.; Campi, G.; Cuocci, C.; Eriksson, L.; Giacovazzo, C.; Moliterni, A.; Rizzi, R.; Werner, P.-E. Advances in Powder Diffraction Pattern Indexing: N-TREOR09. *J. Appl. Crystallogr.* **2009**, *42* (5), 768−775.

(36) Boultif, A.; Louër, D. Powder Pattern Indexing with the Dichotomy Method. *J. Appl. Crystallogr.* **2004**, *37* (5), 724−731.

(37) le Bail, A.; Duroy, H.; Fourquet, J. L. Ab-Initio Structure Determination of LiSbWO6 by X-Ray Powder Diffraction. *Mater. Res. Bull.* **1988**, *23* (3), 447−452.

(38) Wahl, H.; Haynes, D. A.; le Roex, T. Porous Salts Based on the Pamoate Ion. *Chem. Commun.* **2012**, *48* (12), 1775−1777.

(39) Kons, A.; Bērziņš, A.; Actiņš, A.; Rekis, T.; van Smaalen, S.; Mishnev, A. Polymorphism of R-Encenicline Hydrochloride: Access to the Highest Number of Structurally Characterized Polymorphs Using Desolvation of Various Solvates. *Cryst. Growth Des.* **2019**, *19* (8), 4765−4773.

(40) Coelho, A. A. TOPAS and TOPAS-Academic: An Optimization Program Integrating Computer Algebra and Crystallographic Objects Written in C++. *J. Appl. Crystallogr.* **2018**, *51* (1), 210−218.

(41) Mason, J. C.; Handscom, D. C. *Chebyshev Polynomials*, 1st ed.; Chapman and Hall/CRC, 2002.

(42) Thompson, P.; Cox, D. E.; Hastings, J. B. Rietveld Refinement of Debye−Scherrer Synchrotron X-Ray Data from Al2O3. *J. Appl. Crystallogr.* **1987**, *20* (2), 79−83.

(43) Sheldrick, G. M. SHELXT - Integrated Space-Group and Crystal-Structure Determination. *Acta Crystallogr. A* **2015**, *71* (1), 3−8.

(44) Bruno, I. J.; Cole, J. C.; Edgington, P. R.; Kessler, M.; Macrae, C. F.; McCabe, P.; Pearson, J.; Taylor, R. New Software for Searching the Cambridge Structural Database and Visualizing Crystal Structures. *Acta Crystallogr. B* **2002**, *58* (3), 389−397.

(45) Groom, C. R.; Bruno, I. J.; Lightfoot, M. P.; Ward, S. C. The Cambridge Structural Database. *Acta Crystallogr. B Struct Sci. Cryst. Eng. Mater.* **2016**, *72* (2), 171−179.

(46) Macrae, C. F.; Sovago, I.; Cottrell, S. J.; Galek, P. T. A.; McCabe, P.; Pidcock, E.; Platings, M.; Shields, G. P.; Stevens, J. S.; Towler, M.; Wood, P. A. Mercury 4.0: From Visualization to Analysis, Design and Prediction. *J. Appl. Crystallogr.* **2020**, *53* (1), 226−235.

(47) Giannozzi, P.; Baroni, S.; Bonini, N.; Calandra, M.; Car, R.; Cavazzoni, C.; Ceresoli, D.; Chiarotti, G. L.; Cococcioni, M.; Dabo, I.; Dal Corso, A.; de Gironcoli, S.; Fabris, S.; Fratesi, G.; Gebauer, R.; Gerstmann, U.; Gougoussis, C.; Kokalj, A.; Lazzeri, M.; Martin-Samos, L.; Marzari, N.; Mauri, F.; Mazzarello, R.; Paolini, S.; Pasquarello, A.; Paulatto, L.; Sbraccia, C.; Scandolo, S.; Sclauzero, G.; Seitsonen, A. P.; Smogunov, A.; Umari, P.; Wentzcovitch, R. M. QUANTUM ESPRESSO: A Modular and Open-Source Software Project for Quantum Simulations of Materials. *J. Phys.: Condens. Matter* **2009**, *21* (39), No. 395502.

(48) Giannozzi, P.; Andreussi, O.; Brumme, T.; Bunau, O.; Buongiorno Nardelli, M.; Calandra, M.; Car, R.; Cavazzoni, C.; Ceresoli, D.; Cococcioni, M.; Colonna, N.; Carnimeo, I.; Dal Corso, A.; de Gironcoli, S.; Delugas, P.; Distasio, R. A.; Ferretti, A.; Floris, A.; Fratesi, G.; Fugallo, G.; Gebauer, R.; Gerstmann, U.; Giustino, F.; Gorni, T.; Jia, J.; Kawamura, M.; Ko, H. Y.; Kokalj, A.; Kücükbenli, E.; Lazzeri, M.; Marsili, M.; Marzari, N.; Mauri, F.; Nguyen, N. L.; Nguyen, H. V.; Otero-De-La-Roza, A.; Paulatto, L.; Poncé, S.; Rocca, D.; Sabatini, R.; Santra, B.; Schlipf, M.; Seitsonen, A. P.; Smogunov, A.; Timrov, I.; Thonhauser, T.; Umari, P.; Vast, N.; Wu, X.; Baroni, S. Advanced Capabilities for Materials Modelling with Quantum ESPRESSO. *J. Phys.: Condens. Matter* **2017**, *29* (46), 465901.

(49) Grimme, S.; Antony, J.; Ehrlich, S.; Krieg, H. A Consistent and Accurate Ab Initio Parametrization of Density Functional Dispersion Correction (DFT-D) for the 94 Elements H-Pu. *J. Chem. Phys.* **2010**, *132* (15), 154104.

(50) Spackman, P. R.; Turner, M. J.; McKinnon, J. J.; Wolff, S. K.; Grimwood, D. J.; Jayatilaka, D.; Spackman, M. A. CrystalExplorer: A Program for Hirshfeld Surface Analysis, Visualization and Quantitative Analysis of Molecular Crystals. *J. Appl. Crystallogr.* **2021**, *54* (3), 1006−1011.

(51) Tothadi, S.; Phadkule, A. Does Stoichiometry Matter? Cocrystals of Aliphatic Dicarboxylic Acids with Isonicotinamide: Odd−Even Alternation in Melting Points. *CrystEngComm* **2019**, *21* (15), 2481−2484.